

Biomimetic Synthesis of Ag and ZnO Nanoparticles and their Potential Applications

THESIS

Submitted in partial fulfilment
of the requirements for the degree of
DOCTOR OF PHILOSOPHY

by

NAVIN JAIN

Under the Supervision of
Prof. Jitendra Panwar



BITS Pilani
Pilani | Dubai | Goa | Hyderabad

BIRLA INSTITUTE OF TECHNOLOGY AND SCIENCE, PILANI

2014

BIRLA INSTITUTE OF TECHNOLOGY AND SCIENCE, PILANI

CERTIFICATE

This is to certify that the thesis entitled "**Biomimetic Synthesis of Ag and ZnO Nanoparticles and their Potential Applications**" submitted by **Navin Jain, ID.No. 2009PHXF004P** for award of Ph.D. Degree of the Institute embodies original work done by him under my supervision.



Signature of the Supervisor

Date: 30/06/2014

Name : **JITENDRA PANWAR**
Designation: **Associate Professor**

*Dedicated to
My
Beloved Parents
&
Respected Teachers*

Acknowledgements

My PhD journey has been a wonderful and overwhelming experience and I am indebted to countless people, who supported me during this grueling event. I would like to acknowledge all of them for their unstinting support and assistance throughout this experience.

First of all, I am obliged to the Lord almighty, merciful, gracious and passionate, for providing me the support to proceed patiently and the capability to complete my thesis.

I am thankful to the Vice Chancellor, Directors, Deputy Directors and Deans of Birla Institute of Technology & Science (BITS), Pilani for providing necessary facilities and financial support. Special thanks to Prof. Sanjay Kumar Verma, Dean, Academic Research Division (ARD), BITS Pilani, Pilani Campus and Dr. Lalita Gupta, Convenor, Departmental Research Committee (DRC), Department of Biological Sciences, BITS Pilani, Pilani Campus for their official support and encouragement. I overwhelmingly acknowledge Prof. Hemanth Jadav, Associate Dean, ARD and his office staff for their cooperation and constant assistance for submitting the various evaluation documents in time. A special thanks to all staff members of CPU and SRCDD division, BITS Pilani, in particular, Mr. Mahipal and Mr. Virendra.

I would like to express my sincere gratitude to Prof. Jitendra Panwar, my supervisor, without whom, this thesis would not have been materialized. He has taught me more about research and life in general than I could have ever thought possible. I am grateful to him for giving me the liberty to carry out my research work independently throughout the tenure. I will always be indebted for his utmost patience, unceasing encouragement, unending support and constructive criticisms. He has truly been an amazing mentor throughout my PhD venture.

Along with my research supervisor, I am thankful to my Doctoral Advisory Committee (DAC) members Dr. Prabhat N. Jha and Dr. Pankaj K. Sharma who were always there to support me and spared their valuable time to proof-read this thesis. Their honest criticisms and valuable suggestions have immensely helped in enrichment of this thesis. A special thanks to Dr. Rajesh Mehrotra and Prof. Shibasish Chowdhury for their kind assistance throughout the thesis.

I would also like to thank my co-scholars Arpit, Priyanka, Purva, Garima, Parwez, Kamesh, Manoj, Sonu and laboratory staff Sanjay, Manoj and Naresh. Without

their help and assistance in the laboratory, I would not have accomplished so many tasks. I am also thankful to my senior labmates, Dr. Pankaj, Dr. Ashwin Dr. Deepak, Dr. Narayan, Dr. Pradeep, Dr. Shachi, Dr. Prameela, Amit, Boopathi, Prakash, Swarna for their valuable advices and my co-scholars, Parva, Gagan, Zarna, Kuldeep, Rajnish, Senthil, Jyothi, Gurpreet, Panchsheela, Monika, Vidushi and all others for their timely help. All of you possess unique personalities which allowed me to learn a lot and I will always treasure the friendship we shared during the course of my PhD. A special acknowledgement and gratitude to project students, Mohit, Debabrat, Aditi, Sonali, Manju and Ramya who assisted me with my experiments at various timepoints.

Special words of indebtedness are due to our collaborators, Dr. J.C. Tarafdar, CAZRI, Jodhpur and Dr. S.S. Mukhopadhyay, PAU, Ludhiana along with their research teams for sharing their expertise in the field of soil science and electron microscopy, respectively. Thank you all for sharing your knowledge and support throughout the years. I am also indebted to Dr. M.S. Akhtar, Dr. S.K. Singh, Prof. Y.S. Yun for acquiring some experimental data presented in this thesis. I thank AIRF, JNU, New Delhi and Sandor Proteomics Pvt Ltd., CDFD Instrumentation Facility, Hyderabad for their technical support for TEM and proteomics, respectively.

None of this would have been possible without the everlasting support and innumerable blessings of my family. Special indebtedness to my parents, Mr. C. S. Jain and Ms. Pushpa for their indeterminate love, unflinching support, tremendous patience, trust and encouragement regardless of not knowing the field of scientific research. They have been a constant source of strength and inspiration for me. My due thanks to my siblings and their kids who spared so much love to me.

I convey my obligation to CSIR, NAIP-ICAR and DST-Nanomission, New Delhi for their valuable financial support during my research tenure.

Lastly, I wish to apologize if I forgot to acknowledge anyone who had helped me in any way.

(Navin Jain)

Abstract

Since several decades, biological systems serve as a prominent source of inspiration due to their remarkable variety of complex structures and functions which confer a huge impact on material science. In the present thesis, taking inspiration from natural phenomenon of metal resistance among microorganisms, a “biomimetic” eco-friendly and low-cost protocol for nanoparticles synthesis has been demonstrated. The motivation behind the biomimetic approach is the fact that fungi inhabitant in metal rich regions could alter their normal physiological activities which leads to development of “unusual” metabolic processes to exhibit metal resistance. The rationale of using fungi as a model organism was their economical cultivation, ease in handling, secretion of enormous amount of proteins as well as easy downstream processing.

Soil samples were collected from zinc mines of Zawar, Udaipur, India in order to isolate efficient metal-tolerant fungal isolates and subsequently identified using the standard morphological and molecular techniques. Metal tolerance ability of fungal isolates was tested against various concentrations of silver and zinc ions. Isolates exhibiting prominent metal tolerance were further evaluated for their potential of nanoparticles synthesis using a “biomimetic” approach which utilizes secreted fungal proteins for synthesis of nanoparticles. Two indigenous fungi, *Aspergillus flavus* isolate NJP08 and *Aspergillus* sp. isolate NJP02 were found to possess the potential to execute extracellular synthesis of silver nanoparticles. The protocol was optimized and found to possess numerous advantages such as enormous secretion of fungal proteins, convenient handling as well as ease in downstream processing.

The curiosity to understand “How the fungal proteins can “synthesize” and “stabilize” nanoparticles?” has motivated further studies to decipher the “bioactive molecules” involved in the synthesis of silver nanoparticles by fungus *Aspergillus flavus* isolate NJP08. Protein profiling, systematic separation and subsequent screening of individual protein for their potential towards synthesis of silver nanoparticles has been carried out. A protein with a molecular mass of ca. 33kDa was found to execute “dual function” of silver reduction as well as stabilization and identified as “alkaline protease”. The effect of silver nanoparticle binding on the structure and function of alkaline protease was investigated. Further, based on homology approach, the three dimensional structure was constructed to decipher the binding site of silver nanoparticle on protease and related protein-nanoparticle interactions. Brownian dynamics simulations of the protease-Ag(111) complex showed that the protease binding to silver nanoparticles is highly specific with involvement of four amino acid residues viz. Tyr59, Ser107, Asp111 and Asn 118. To the best of our knowledge, this is the first attempt which identifies a structural configuration among aspartic residues and silver nanoparticles.

The antibacterial studies of silver nanoparticles with special emphasis to the role of protein shell were also investigated. Comparative antibacterial studies of protein-capped and bare silver nanoparticles were executed against representative Gram positive and Gram negative bacterial pathogens. Preliminary findings based on minimum inhibitory concentration and disk diffusion assays revealed that bare nanoparticles were

more effective than protein-capped silver nanoparticles with varying antibacterial potential against tested bacterial strains. Further, mechanistic studies based on ROS generation and membrane damage suggested that protein-capped and bare silver nanoparticles demonstrate distinct mode of actions. TEM micrographs in conjunction with silver ion release measurements further strengthened these findings. The obtained results clearly indicated that surface modifications of nanoparticles with proteins allow modulation of their functional properties.

Similar to synthesis of silver nanoparticles, two indigenous fungi, *Aspergillus aeneus* isolate NJP12 and *Aspergillus* sp. isolate NJP02 were utilized for extracellular synthesis of ZnO nanoparticles under ambient conditions. The as-synthesized nanoparticles were spherical/quasi-spherical in shape with presence of proteins on the surface of individual nanoparticles. Various parameters such as reactant concentration (salt and proteins) and pH of the solution were found to influence the process of nanoparticle synthesis. Attempts toward understanding of the synthesis mechanism indicated that the process is non-enzymatic in nature but involves amino acids present in the protein chains. The low cost, simplicity and eco-friendly nature of the present protocol for “one-pot” synthesis and modification of ZnO nanoparticles could be extended to synthesize other metal nanoparticles thus expanding its applicability in various fields. The photocatalytic performance of protein-capped ZnO nanoparticles towards the degradation of methylene blue dye was also investigated. Owing to the presence of surface proteins, ZnO nanoparticles exhibited excellent enhancement of photocatalysis towards methylene blue dye suggesting their potential applications in catalysis, waste water treatment etc. The remarkable photocatalytic performance was attributed to the presence of surface proteins that act as effectual host for methylene blue dye and facilitates absorption of dye along with low recombination rate of the e^-/h^+ pairs.

Lastly, we investigated the potential of ZnO nanoparticles as future “nano-fertilizers”. A systematic comparison of chemically synthesized and biologically synthesized zinc oxide (ZnO) nanoparticles with Zn^{+2} ions and its bulk counterpart was carried out using chili plant as a model system. The physico-chemical characteristics of various zinc salts in aqueous medium were determined followed by their effect on chili plants in terms of plant growth and biomass. Studies on stress and zinc related enzymes were carried out to determine the extent of plant damage after zinc exposure. In addition, the plant zinc content was determined to compare the efficacy of various tested zinc salts to deliver zinc in plants.

In a nutshell, the present thesis demonstrated the extracellular biosynthesis silver and zinc oxide nanoparticles along with their potential applications. The work demonstrates the utilization of secreted fungal proteins to synthesize nanoparticles in a simple, eco-friendly and low-cost protocol manner at ambient conditions. Studies on understanding of synthesis mechanism and related protein-nanoparticle interactions can contribute significantly in designing rationale approaches to achieve mass scale production of nanoparticles. Further diverse applications of silver and zinc oxide nanoparticles in the vital areas of antibacterial, photocatalytic and nano-fertilizers have been demonstrated.

Table of Contents

<i>Certificate</i>	
<i>Dedication</i>	
<i>Acknowledgements</i>	
<i>Abstract</i>	
<i>Table of Contents</i>	
<i>List of Tables</i>	
<i>List of Figures</i>	
<i>List of Abbreviations</i>	
Chapter I. General Introduction	1-10
1.1 Nanotechnology: a gentle introduction	2
1.2 Nanoparticles: properties and their significance	2
1.3 Characterization of nanoparticles	4
1.4 Applications of nanoparticles	5
1.5 Objectives of the thesis	6
1.6 Outline of the thesis	6
1.7 References	8
Chapter II. Isolation, Characterization and Metal Tolerance Profile of Fungi Isolated from Metal Rich Region	11-23
2.1 Introduction	12
2.2 Materials and methods	13
2.2.1 Sampling site and isolation of fungi	13
2.2.2 Physico-chemical characteristics of rhizosphere soil	1
	4
2.2.3 Molecular characterization of fungal isolates	14
2.2.4 Phylogeny analysis	15
2.2.5 Metal tolerance profiles of fungal isolates	15
2.3 Results and discussion	15
2.3.1 Physico-chemical characteristics of soil samples	15
2.3.2 Identification of fungal isolates	16
2.3.2.1 Morphological identification	
2.3.2.2 Molecular identification	
2.3.3 Metal tolerance profile of fungal isolates	20
2.4 Conclusions	21
2.5 References	22
Chapter III. Biosynthesis of silver nanoparticles and optimization studies	24-49
3.1 Introduction	25
3.2 Materials and methods	26
3.2.1 Extracellular synthesis of silver nanoparticles	26

3.2.2	Characterization of nanoparticles	27
3.2.2.1	UV-visible spectroscopy	
3.2.2.2	Transmission electron microscopy	
3.2.2.3	Energy dispersive spectroscopy	
3.2.2.4	Selected area diffraction pattern	
3.2.2.5	X-ray diffraction	
3.2.2.6	Dynamic light scattering	
3.2.3	Characterization of capping molecules	28
3.2.3.1	Fourier transform infrared spectroscopy	
3.2.3.2	Photoluminescence spectroscopy	
3.2.3.3	Sodium dodecyl sulphate polyacrylamide gel electrophoresis	
3.2.4	Optimization of nanoparticle synthesis	29
3.2.4.1	Effect of pH	
3.2.4.2	Effect of salt concentration	
3.2.4.3	Effect of biomass	
3.3	Results and discussion	29
3.3.1	Extracellular synthesis of silver nanoparticles using <i>Aspergillus flavus</i> isolate NJP08	29
3.3.1.1	Characterization of silver nanoparticles	
3.3.1.2	Characterization of capping molecule	
3.3.2	Optimization of silver nanoparticles using <i>Aspergillus flavus</i> isolate NJP08	36
3.3.2.1	Effect of pH	
3.3.2.2	Effect of Salt concentration	
3.3.2.3	Effect of Biomass	
3.3.3	Synthesis of silver nanoparticles using <i>Aspergillus</i> sp. isolate NJP02	39
3.3.3.1	Characterization of silver nanoparticles	
3.3.3.2	Characterization of capping molecule	
3.3.4	Optimization of silver nanoparticles using <i>Aspergillus</i> sp. isolate NJP02	43
3.3.4.1	Effect of pH	
3.3.4.2	Effect of Salt concentration	
3.3.4.3	Effect of Biomass	
3.4	Conclusions	45
3.5	References	45
Chapter IV. Understanding Mechanism of Silver Nanoparticles Biosynthesis and Associated Protein-Nanoparticle Interactions		50-97
4.1	Introduction	51
4.2	Materials and methods	54
4.2.1	Preparation of fungal cell-free filtrate	54

4.2.2	Protein estimation in fungal cell-free filtrate	54
4.2.3	Protein profiling of fungal cell-free filtrate	54
4.2.3.1	Ammonium sulphate precipitation	
4.2.3.2	One dimensional gel electrophoresis	
4.2.3.3	Peptide mass fingerprinting by matrix-assisted laser desorption/ionization (MALDI) mass spectrometry	
4.2.4	Protein depletion studies	56
4.2.4.1	Gel filtration chromatography	
4.2.4.2	Ion exchange chromatography	
4.2.5	Characterization of purified protein	56
4.2.5.1	<i>De novo</i> sequencing	
4.2.5.2	N-terminal sequencing	
4.2.6	Physico-chemical characteristics	57
4.2.7	Effect of salt - protein ratio on nanoparticle synthesis	57
4.2.8	Protein-nanoparticle interactions	57
4.2.8.1	Effect on protease activity	
4.2.8.2	<i>In silico</i> studies	
4.3	Results and Discussion	59
4.3.1	Protein profiling of fungal cell filtrate	59
4.3.2	One dimensional gel electrophoresis	59
4.3.3	Peptide mass fingerprinting	60
4.3.4	Protein depletion and nanoparticle synthesis	63
4.3.5	Detailed characterization of alkaline protease	68
4.3.5.1	<i>De novo</i> sequencing	
4.3.5.2	N-terminal sequencing	
4.3.5.3	Physico-chemical characteristics	
4.3.6	Effect of protein - salt ratio on nanoparticle synthesis	73
4.3.7	Protein-nanoparticle interactions	74
4.3.7.1	Effect of silver nanoparticles on protease activity	
4.3.7.2	Homology modelling and structure validation	
4.3.7.3	Brownian dynamics simulation	
4.4	Conclusions	86
4.5	References	87
Chapter V. Silver Nanoparticles: Antibacterial Activity and Mode of Action		98-120
5.1	Introduction	99
5.2	Materials and methods	101
5.2.1	Synthesis of protein-capped and bare silver nanoparticles	101
5.2.2	Test bacterial strains	101
5.2.3	Minimum inhibitory concentration assay	102
5.2.4	Disk diffusion assay	102
5.2.5	Bacterial growth curve	102

5.2.6	Reactive oxygen species formation	102
5.2.6.1	2',7'-dichlorofluorescein-diacetate quantitative assay	
5.2.6.2	Anti-oxidative enzyme assay	
5.2.7	Effect on bacterial membrane integrity	103
5.2.7.1	Malondialdehyde content	
5.2.7.2	Membrane leakage analysis	
5.2.8	Silver ion measurement	104
5.2.9	Transmission electron microscopy	105
5.3	Results and discussion	105
5.3.1	Bactericidal assay	105
5.3.2	Bactericidal mechanism of protein-capped and bare silver nanoparticles	108
5.4	Conclusions	115
5.5	References	116

Chapter VI. Biosynthesis of Zinc Oxide Nanoparticles and their Photocatalysis Applications 121-144

6.1	Introduction	122
6.2	Materials and methods	124
6.2.1	Extracellular synthesis of ZnO nanoparticles	124
6.2.2	Characterization of ZnO nanoparticles	125
6.2.3	Role of proteins in ZnO nanoparticle synthesis	125
6.2.4	Photocatalytic studies of ZnO nanoparticles	125
6.2.5	Optimization of ZnO nanoparticle synthesis	126
6.3	Results and discussion	
6.3.1	Synthesis of ZnO nanoparticles using <i>Aspergillus aeneus</i> isolate NJP12	126
6.3.1.1	Characterization of zinc oxide nanoparticles	
6.3.1.2	Characterization of capping molecule	
6.3.1.3	Role of proteins in ZnO nanoparticle synthesis	
6.3.2	Optimization of ZnO nanoparticle synthesis using <i>Aspergillus aeneus</i> isolate NJP12	130
6.3.3	Synthesis of zinc oxide nanoparticles using <i>Aspergillus</i> sp. isolate NJP02	131
6.3.3.1	Characterization of zinc oxide nanoparticles	
6.3.3.2	Characterization of capping molecule	
6.3.4	Optimization of zinc oxide nanoparticle synthesis using <i>Aspergillus</i> sp. isolate NJP02	134
6.3.5	Photocatalytic activity of "protein-capped" ZnO nanoparticles	135
6.4	Conclusions	138
6.5	References	138

Chapter VII. Zinc oxide nanoparticles as Potential “Nano-fertilizers”	145-172
7.1 Introduction	146
7.2 Materials and methods	148
7.2.1 Characterization of ZnO nanoparticles and their stability in aqueous solution	148
7.2.2 Effect of ZnO nanoparticles on chili plants (pot studies)	149
7.2.2.1 Site description and plant growth conditions	
7.2.2.2 Effect on plant growth	
7.2.2.3 Effect on plant metabolism	
7.2.2.4 Effect on stress related enzymes and plant damage	
7.2.2.5 Effect on zinc related enzymes	
7.2.2.6 Effect on zinc content	
7.3 Results and discussion	152
7.3.1 Characterization of ZnO nanoparticles and their stability in aqueous solution	
7.3.2 Effect of ZnO nanoparticles on chilli plants	154
7.3.2.1 Phenotypic assessment of plants	
7.3.2.2 Effect on plant growth	
7.3.2.3 Effect on plant biomass	
7.3.2.4 Effect on plant metabolism	
7.3.2.5 Effect on plant defence	
7.3.2.6 Effect on zinc related enzymes	
7.3.2.7 Effect on zinc content	
7.4 Conclusion	164
7.5 References	165
Chapter-VIII Summary and Future Scope	173-176
Appendices	177-196
Appendix I: List of Publications	178
Appendix II: Brief Biography of the Supervisor	180
Appendix III: Brief Biography of the Candidate	181
Appendix IV: MTCC Certificate for Culture Deposition	182
Appendix V: Supplementary Information	183

List of Tables

S. No.	Title	Page No.
2.1	Physico-chemical characteristics of rhizospheric soil samples collected from the Zawar mines, India.	16
2.2	Morphology of axenic fungal isolates derived from Zawar mines, Udaipur, India.	17
2.3	Analysis of ITS1-5.8S-ITS2 complex sequences of fungal isolates with their reference organisms.	19
3.1	Effect of pH on particle size of silver nanoparticles synthesized using <i>Aspergillus flavus</i> isolate NJP08.	37
3.2	Effect of salt concentration on particle size of silver nanoparticles synthesized using <i>Aspergillus flavus</i> isolate NJP08.	38
3.3	Effect of biomass on particle size of silver nanoparticles synthesized using <i>Aspergillus flavus</i> isolate NJP08.	38
3.4	Effect of pH on particle size of silver nanoparticles synthesized using <i>Aspergillus</i> sp. isolate NJP02.	44
3.5	Effect of salt concentration on particle size of silver nanoparticles synthesized using <i>Aspergillus</i> sp. isolate NJP02.	44
3.6	Effect of biomass on particle size of silver nanoparticles synthesized using <i>Aspergillus</i> sp. isolate NJP02.	45
4.1	Identification of proteins present in the cell-free filtrate of fungus <i>Aspergillus flavus</i> isolate NJP08. The obtained mass spectrum, identified peptides and deduced sequences are summarized in Appendix 4.1-4.8.	62
4.2	Particle size distribution and stability profile of silver nanoparticles synthesized using various protein groups of <i>Aspergillus flavus</i> isolate NJP08. The protein groups were prepared by subjecting crude fungal cell-free filtrate on a pre-equilibrated size exclusion column (Sephadex G-75, Tris-Cl pH=8.0).	65
4.3	Particle size distribution and stability profile of silver nanoparticles synthesized using group II proteins separated on a pre-equilibrated anion exchange column (DEAE cellulose, KCl = 0.0 - 0.5M).	67
4.4	Homology analysis of N-terminal amino acid sequence of alkaline protease from <i>Aspergillus flavus</i> isolate NJP08 with closely related proteases reported in NCBI database.	72
4.5	<i>In silico</i> characterization of alkaline protease from <i>Aspergillus flavus</i> isolate NJP08.	72
4.6	Comparison of Ramachandran plot values for homology model of alkaline protease.	78
4.7	Validation results obtained for homology model of alkaline protease.	78
4.8	Summary of the most abundant encounter complex from Brownian dynamics simulation of the protease-Ag(111) system.	84
5.1	Mean zone of inhibition (mm) of protein-capped and bare silver nanoparticles as determined using disk diffusion method.	106
5.2	Magnitude of membrane leakage from bacterial cells after exposure to silver nanoparticles.	112

S. No.	Title	Page No.
6.1	Kinetic parameters for the photocatalytic degradation of methylene blue (MB) dye with protein-capped and bare ZnO nanoparticles catalysts.	137
7.1	Selected physico-chemical characteristics of the ZnO nanoparticles, bulk ZnO and zinc sulphate at a concentration of 1000 mg L ⁻¹ .	154
7.2	Effect on metabolism of chili plants sprayed with water (control) and various zinc salt treatments.	158
7.3	Zinc concentration in chili plants sprayed with distilled water (control) and various zinc treatments.	164

List of Figures

Fig. No.	Figure caption	Page No.
2.1	Agarose gel electrophoresis of amplified internal transcribed spacer (ITS) rDNA products.	17
2.2	Pie chart depicting species richness among fungal isolates: relative proportions of various (A) Genera and (B) <i>Aspergillus</i> species. (C) Molecular phylogenetic analysis of internal transcribed spacer (ITS) gene sequences of fungal isolates from zinc rich regions of Zawar mines, India.	20
2.3	Metal tolerance profile of fungal isolates towards (a) zinc and (b) silver.	21
3.1	Erlenmeyer flasks containing cell-free filtrate of <i>Aspergillus flavus</i> isolate NJP08 without (a) and with (b) silver nitrate solution (1mM) after 72 h of reaction.	30
3.2	UV-visible spectra recorded as a function of time after addition of fungal cell-free filtrate to silver nitrate solution (1.0 mM). The arrow represents the time of reaction with respective curves at 0, 3, 6, 12, 24, 48 and 72 hrs. Inset graph shows saturation curve of silver nanoparticles synthesis with function of time.	31
3.3.	UV-visible spectra showing presence of proteins in the fungal cell-free filtrate. An absorption maximum at 280 nm arises due to electronic excitations in tyrosine and tryptophan residues of proteins.	31
3.4	TEM micrographs showing uniformly distributed silver nano-particles. (a) Low magnification image and (b) high magnification image.	32
3.5	Particle size distribution histogram of silver nanoparticles as determined using (a) transmission electron micrographs and (b) dynamic light scattering measurements. X-axis represents diameter of nanoparticles in nanometer (d.nm).	32
3.6	High resolution - transmission electron micrograph showing spherical shape of silver nanoparticle. Inset shows SAD pattern recorded from silver nanoparticle; the spot array is from [111] beam direction for fcc pattern of a silver nanoparticle.	33
3.7	X-ray diffraction pattern showing crystalline nature of silver nanoparticles.	33
3.8	Energy dispersive spectrum showing the presence of elemental silver in silver nanoparticles.	33
3.9	Fourier transform infrared spectroscopy spectrum of freeze-dried samples showing the presence of proteins on the surface of silver nanoparticles.	34
3.10	Dynamic light scattering spectra showing the difference in particle size of protein-capped and silver nanoparticles.	35
3.11	SDS-PAGE depicting the removal of capping proteins. Lane 1, standard molecular weight marker; lane 2, protein-capped silver nanoparticles; lane 3, separated capping proteins present on the surface of silver nanoparticles.	36
3.12	(a) Visual assessment showing change in color of the fungal cell-free filtrate without (left) and with (right) silver nitrate solution after 72 h of reaction. (b) UV-visible spectrum of silver nanoparticles recorded from the reaction medium as a function of time. Inset showing saturation curve of silver nanoparticle synthesis with function of time.	39

Fig. No.	Figure caption	Page No.
3.13	(a) A representative transmission electron micrograph showing spherical shaped silver nanoparticles (<i>scale bar</i> equivalent to 50 nm). Inset showing SAD pattern recorded from a single nanoparticle. Particle size distribution histogram of silver nanoparticles as determined using (b) transmission electron microscope and (c) dynamic light scattering measurements.	40
3.14	XRD spectrum of as-synthesized protein-capped silver nanoparticles recorded in the 2θ range of 30° - 80° (* indicates peaks due to the capping molecules).	40
3.15	Energy dispersive spectrum showing the elemental composition of silver nanoparticles.	41
3.16	(a) FTIR spectra and (b) photoluminescence spectra of protein-capped and bare silver nanoparticles.	42
3.17	(a) UV visible spectra and (b) particle size distribution of protein-capped and bare silver nanoparticles.	43
3.18	SDS-PAGE showing the capping proteins present on the surface of silver nanoparticles synthesized using fungus <i>Aspergillus</i> sp. isolate NJP02. Lane 1: standard protein molecular weight marker; Lane 2: capping proteins obtained after treating silver nanoparticles with SDS solution.	43
4.1	One-dimensional SDS-PAGE of secreted proteins from fungus <i>Aspergillus flavus</i> . Lanes 1 and 2 contain standard marker and secreted proteins, respectively. The number adjacent to the protein bands represents their molecular mass (in kDa).	60
4.2	Size exclusion chromatography profile of proteins present in fungal cell-free filtrate of <i>Aspergillus flavus</i> isolate NJP08. The eluted fractions were classified into four groups viz. I, II, III and IV (separated with dot lines).	63
4.3	Silver nanoparticle synthesis profile of protein fractions obtained after size exclusion chromatography. Dotted line (λ_{\max} 420 nm) was used as a reference to represent "Red shift" of peaks in various groups.	64
4.4	(a) SDS-PAGE of group II proteins (lane 2) illustrating two proteins with molecular mass of ca. 33.0 and 31.0 kDa. (b) Elution profile of group II proteins when subjected on a pre-equilibrated anion exchange column (DEAE cellulose, KCl = 0.0 - 0.5M).	66
4.5	UV-visible spectroscopy measurements depicting the role of group II proteins in synthesis of silver nanoparticles.	66
4.6	<i>De novo</i> sequencing of the peptide sequence SAPWGLGSISHK of alkaline protease. (a) peptide ion values (b) error graph (c) MS/MS spectrum (d) Extracted ion chromatogram with deduced sequence.	69
4.7	<i>De novo</i> sequencing of the peptide sequence AAINMSLGGYSK of alkaline protease. (a) peptide ion values (b) error graph (c) MS/MS spectrum (d) Extracted ion chromatogram with deduced sequence.	70
4.8	Effect of salt - protein ratio on silver nanoparticle synthesis The ratio was varied by increasing Ag^+ concentrations (0-50 mM) at a constant protease concentration (50 μM).	73
4.9	Azocasein assay showing the effect of increasing concentration of silver nanoparticles on residual proteolytic activity of alkaline protease.	75
4.10	A ribbon diagram depicting the three dimensional structure of alkaline protease predicted using 3F70 as the template.	76

Fig. No.	Figure caption	Page No.
4.11	Ramachandran plot of predicted structure of alkaline protease after energy minimization steps. The quadrangle describes the classification of amino acid residues according to their Φ and Ψ torsion angles.	77
4.12	Plot depicting Z-score of predicted model for alkaline protease.	79
4.13	Superposition of template (green) with the predicted model of alkaline protease (red). The picture has been captured using the software Swiss PDB viewer.	80
4.14	Snapshot depicting the Brownian dynamics simulation of the protease-Ag(111) complex.	82
4.15	A representative image showing the predicted binding sites of protease on Ag(111) surface after performing Brownian dynamics simulation.	83
4.16	Close-up view depicting the orientation of Asp111 in the predicted binding site of protease on Ag(111) surface.	86
5.1	Dehydrogenase assay demonstrating MIC profiles of (a) protein-capped and (b) bare silver nanoparticles against selected Gram positive and Gram negative bacteria.	106
5.2	Growth dynamics of tested bacterial species in presence of protein-capped or bare silver nanoparticles as compared to controls. The nutrient medium with bacterial inoculation (no nanoparticles) and silver nanoparticles (no bacterial inoculation) were used as positive and negative control, respectively.	107
5.3	Relative fluorescence intensity (with respect to H_2O_2) showing the cellular ROS formation capability of protein-capped and bare silver nanoparticles as compare to control. Vertical bars represent standard errors. Significant differences from control ($p \leq 0.05$) are marked with asterisk.	109
5.4	Levels of (a) peroxidase and (b) superoxide dismutase in untreated (control: not treated with silver nanoparticles) and treated (with protein-capped and bare silver nanoparticles) bacteria cells. The data are expressed as mean \pm standard error of three independent experiments ($p < 0.05$).	110
5.5	Malondialdehyde (MDA) assay demonstrating the difference in membrane damage capability of protein-capped and bare silver nanoparticles. Vertical bars represent standard errors. Significant differences from control ($p \leq 0.05$) are marked with asterisk.	111
5.6	Silver dissolution profiles of protein-capped and bare silver nanoparticles.	113
5.7	Transmission electron micrographs depicting the morphological changes in Gram positive <i>B. cereus</i> and Gram negative <i>E. coli</i> after exposure to protein-capped and bare silver nanoparticles.	114
5.8	Cartoon representation of antibacterial potential of protein-capped and bare silver nanoparticles.	115
6.1	UV-visible spectrum representing gradual synthesis of ZnO nanoparticles with respect to time.	127
6.2	(a) A representative transmission electron micrograph showing the spherical shape of ZnO nanoparticles. (scale bar = 500 nm) (b) EDS spectrum representing the elemental composition of ZnO nanoparticles.	127
6.3	X-ray diffraction spectrum of ZnO nanoparticles with Bragg's diffraction values shown in parentheses. The absorbance is expressed in terms of arbitrary unit (a.u.).	128

Fig. No.	Figure caption	Page No.
6.4	FTIR spectrum of freeze-dried samples of ZnO nanoparticles depicting the presence of proteins on the surface of ZnO nanoparticles. The absorbance is expressed in terms of arbitrary unit (a.u.).	128
6.5	Effect of denaturation of proteins on synthesis of ZnO nanoparticles. The absorbance is expressed in terms of arbitrary unit (a.u.)	129
6.6	Optimization of process parameters for synthesis of ZnO nanoparticles using fungus <i>Aspergillus aeneus</i> isolate NJP12 with respect to (a) pH, (b) salt concentration and (c) biomass.	130
6.6	UV-visible spectra showing gradual synthesis of ZnO nanoparticles with respect to time.	132
6.8	X-ray Diffraction pattern recorded for freeze-dried ZnO nanoparticles synthesized using fungus <i>Aspergillus</i> sp. isolate NJP02. Bragg's diffraction values are shown in parentheses.	132
6.9	Characterization of as-synthesized "protein-capped" ZnO nanoparticles. (a) A representative TEM micrograph depicting quasi-spherical shape. (b) Histogram showing the size distribution analysis. (c) Optically transparent solution under daylight. (d) EDX spectrum showing elemental composition.	133
6.10	(a) Intrinsic fluorescence spectra of protein-capped ZnO nanoparticles excited at a wavelength of 280 nm (black) and 325 nm (red). (b) FTIR spectrum of freeze-dried ZnO nanoparticles with inset showing the amide I band of the proteins.	134
6.11	Optimization of various process parameters for synthesis of ZnO nanoparticles using fungus <i>Aspergillus</i> sp. isolate NJP02 (a) pH, (b) salt concentration and (c) biomass.	135
6.12	Photodegradation of methylene blue dye solution under UV-light irradiation by (a) as-prepared protein-capped ZnO nanoparticles and (b) bare ZnO nanoparticles. (c) The extent of MB dye decomposition with respect to time intervals over a period of 30 min UV irradiation. (catalyst concentration: 10 mg/mL; initial dye concentration: 10 μ M).	136
7.1	Transmission electron micrographs of ZnO nanoparticles depicting agglomeration in aqueous suspension. Bars show the scale in nanometers.	152
7.2	Comparative phenotypic assessment of chili plants sprayed with distilled water (control) and various zinc treatments. 50 and 100 represent mg L ⁻¹ concentrations of respective salt.	155
7.3	Variation in shoot and root length of chili plants sprayed with distilled water (control) and various zinc treatments. Vertical bars represent standard deviation. Significant differences from control ($p \leq 0.05$) are marked with asterisk.	156
7.4	(a) Fresh weight and (b) dry weight of chili plants sprayed with distilled water (control) and various zinc treatments. Vertical bars represent standard deviation. No significant differences were observed between control and treatments ($p \leq 0.05$).	157
7.5	SOD activity in leaves of chili plants sprayed with distilled water (control) and various zinc treatments. Vertical bars represent standard errors. Significant differences from control ($p \leq 0.05$) are marked with asterisk.	159
7.6	(a) Peroxidase and (b) Polyphenol oxidase activity in leaves of chili plants	160

Fig. No.	Figure caption	Page No.
	sprayed with distilled water (control) and various zinc treatments. Vertical bars represent standard errors. Significant differences from control ($p \leq 0.05$) are marked with asterisk.	
7.7	TBARS concentration in leaves of chili plants sprayed with distilled water (control) and various zinc treatments. Vertical bars represent standard errors. Significant differences from control ($p \leq 0.05$) are marked with asterisk.	161
7.8	Carbonic anhydrase (CA) activity in leaves of chili plants sprayed with distilled water (control) and various zinc treatments. Vertical bars represent standard errors. Significant differences from control ($p \leq 0.05$) are marked with asterisk.	162
7.9	Changes in acid phosphatase (AP) activity in roots of chili plants sprayed with distilled water (control) and various zinc treatments. Vertical bars represent standard errors. Significant differences from control ($p \leq 0.05$) are marked with asterisk.	163

List of Abbreviations

Symbol	Abbreviation
α -Cyano	alpha-cyano-4-hydroxycinnamic acid
AAS	Atomic absorption spectrophotometry
AMBER	Assisted model building with energy refinement
BCA	Bicinchoninic acid
BD	Brownian dynamics
BLAST	Basic local alignment search tool
BSA	Bovine serum albumin
bZN	Protein-capped biologically synthesized zinc oxide nanoparticles
CA	Carbonic anhydrase
CBB	Coomassie brilliant blue
CFU	Colony forming unit
cZN	Chemically synthesized bare zinc oxide nanoparticles
DCFH-DA	2',7'-Dichlorodihydrofluorescein diacetate
DEAE	Diethylaminoethyl cellulose
DLS	Dynamic light scattering
DTT	Dithiothreitol
EDS	Energy dispersive spectroscopy
EDTA	Ethylenediaminetetraacetic acid
EtBr	Ethidium bromide
ESI	Electrospray ionization
FTIR	Fourier transform infrared
ICP-AES	Inductively coupled plasma atomic emission spectroscopy
IEF	Iso electric focusing
IPG	Immobilized pH gradient
ITS	Internal transcribed space
LC	Liquid chromatography
MALDI-TOF	Matrix assisted laser desorption ionization-time of flight
MB	Methylene blue
MDA	Malondialdehyde
MIC	Minimum inhibitory concentration
MS	Mass spectrometry
MTC	Maximum tolerable concentration
MTCC	Microbial type culture collection
NB	Nutrient broth
NBT	Nitro blue tetrazolium
NCBI	National Center for Biotechnology Information
pI	Isoelectric point
PBS	Phosphate buffer saline
PCR	Polymerase chain reaction
PDA	Potato dextrose agar
PDB	Protein structure data bank
PL	Photoluminescence
PMSF	Phenylmethanesulfonyl fluoride
POD	Peroxidase

Symbol	Abbreviation
PPO	Polyphenol oxidase
PVDF	Polyvinylidene fluoride
Q-TOF	Quadripole- time of flight
ROS	Reactive oxygen species
SDS PAGE	Sodium dodecyl sulphate polyacrylamide gel electrophoresis
SEM	Scanning electron microscopy
SOD	Superoxide dismutase
TAE	Tris acetate EDTA
TBARS	Thiobarbituric acid reactive substances
TCA	Tri-chloro acetic acid
TTC	Triphenyl tetrazolium chloride
TEM	Transmission electron microscopy
UPLC	Ultra-performance liquid chromatography
XRD	X-ray diffraction
ZB	Bulk zinc oxide
ZS	Zinc sulphate.

Chapter I

General Introduction

This chapter is an introduction to the research work presented in this thesis and gives a brief overview of nanotechnology. A brief discussion on unique and interesting physico-chemical properties observed in nanometer regime is provided. Further, an account of potential applications of nanoparticles has been described with special emphasis on biological context. Finally, a brief outline of the thesis is presented.

1.1. Nanotechnology: a gentle introduction

Nanotechnology is a new field, but not a new word. The word 'Nano' originated from the Greek word “nanos”, which means dwarf or extremely small. It can be used as a prefix for any unit to mean a billionth of that unit. In context to nanoparticles, it refers to particles ranging on a billionth scale. What actually is "nanotechnology"? Doing things on a small scale. It can be chemistry, physics, biology or engineering. It can be materials, or medicine, and so forth. It's just a human quest to utilize the concept and knowledge of various disciplines to generate products at billionth scale for improvement of humankind. In simpler terms, nanotechnology is an essentially modern scientific field that is constantly evolving as commercial and academic interest continues to increase and as new research is presented to the scientific community. The appropriate scientific definition can be obtained from the National Nanotechnology Initiative, which defines nanotechnology as "the understanding and control of matter at dimensions of roughly 1 to 100 nanometers (nm), where unique phenomena enable novel applications" (www.nano.gov/html/facts/whatIsNano.html).

The field's simplest roots can be traced, albeit arguably, to 1959 when the physicist Richard Feynman at the California Institute of Technology, presented his lecture entitled “There is plenty of room at the bottom”. The lecture has become an integral part of the nanotechnology community's founding liturgy and now considered as one of 20th century science's classic lectures. The word “nanotechnology” entered into the general and scientific vocabulary only recently but has been introduced at least as early as 1974 by Taniguchi, then a professor of Tokyo Science University (Taniguchi 1974).

The era of nanomaterials and nanotechnologies promises to be one of major scientific developments and breakthroughs that in the not too distant future will permanently affect our everyday lives. In the last decade, nanotechnology has crossed several billions of dollars of investment especially in research and development. As a result, several nano-based products are already being used and countless products are in pipelines which foresee annual world markets in the order of one trillion USD by the beginning of 2015 (Roco 2005). The fact that nanotechnology embraces and attracts many different disciplines, encompassing both researchers and business leaders, has also inspired huge number of industries to come in this sector.

1.2. Nanoparticles: properties and their significance

Nanoparticles are a subset of nanotechnology and consist of thousands of atoms in them, making them larger than atoms and most molecules. However, nanoparticles are smaller than their bulk counterparts due to size confinement and size restriction between 1-100 nm, the only conserved and unique feature of nanoparticles. Among nanoparticles, a plethora of entities are present having variables like size, shape and composition which determine their physical and chemical properties and subsequently, their behaviour in the environment.

Nanoparticles possess several distinctive physico-chemical characteristics which are normally not encountered in the corresponding bulk material. The first scientific description of the properties of nanoparticles was provided in 1857 by Michael Faraday in his famous paper “Experimental relations of gold (and other metals) to light” (Faraday, 1857). Many of these properties are found to be dependent on the unique structural features of nanoparticles like the particle size, dispersity, surface features, shape, organization of the nanoparticles into nanomaterials and their dispensability. From both theoretical and practical aspects, monodispersity of nanoparticles is a very critical feature which indicates the uniformity in distribution in terms of both size and shape (Rao et al. 2002).

Nanoparticles have an exceptionally high surface area to volume ratio owing to their nanoscale dimensions. This high value confers profound changes in the catalytic, thermal and mechanical properties of the substance. It has been observed that as this ratio increases the dominant behaviour of atoms on the surface of nanoparticles becomes more than the ones present in the particle interior which is the contributing factor behind their unique properties (Jain et al. 2007). The high surface area to volume ratio also provides sufficient sites for binding of substrates during a reaction which confer remarkable chemical reactivity (Cuenya 2010). In this case, particle size plays a role which sometimes can be compared to its chemical constitution. Hence, this adds another factor towards the control and design of nanoparticles. Surface plasmon resonance in certain metal nanoparticles, superparamagnetism in magnetic nanoparticles and quantum confinement in case of semiconductors are some of the significant size dependent properties of nanoparticles.

Certain metal nanoparticles like gold, silver and copper possess remarkable optical properties which is due to their distinctive interaction with light and is highlighted by their intense and vibrant colours (Kelly et al. 2002). A collective consistent electron mediated oscillation with respect to the positive metallic lattice is observed when free electron containing metal nanoparticles are placed in the electromagnetic field of light (Kelly et al. 2002, Jain et al. 2006). At a particular frequency this oscillation exhibits resonance termed as local surface plasmon resonance (LSPR) oscillation. For ease of understanding this electron mediated oscillation can be considered as confinement of an electron inside a nanostructure which constitutes an intense electric field around it. Two possible ways by which the surface plasmon resonance oscillations can decay are scattering of light or conversion of absorbed light to heat (Jain et al. 2007). At the corresponding LSPR frequency the intensity of the electric field and cross-sectional area of scattering and absorption are significantly enhanced. For gold, silver and copper the LSPR frequency lies within the visible range of the electromagnetic spectrum. Due to its high affinity for oxygen copper easily gets oxidized thus, gold and silver nanomaterials are more preferable candidates with respect to optical applications (Jain et al. 2008).

Besides size, the shape of nanoparticles is also a very important parameter which contributes to the physico-chemical properties of the nanoparticles. Nanoparticles possessing different geometric shapes will lead to formation of enveloping planes which are differently oriented in a different number resulting in variations in density of surface atoms, electronic structure, adsorption, bonding and catalytic abilities. For example, different crystallographic planes have different surface energies which can be generally sequenced as: $\gamma_{(111)} < \gamma_{(100)} < \gamma_{(110)}$. This fact has been observed in case of platinum nanoparticles where the structures which remain enclosed by (111) facets are usually more stable than the structures enclosed by (100) facets (Wang et al. 1998). Catalytic activities of platinum nanoparticles of varied shapes have also been investigated since catalytic reaction is a surface related phenomenon. Thus, two different surfaces will exhibit different catalytic attributes due to the difference in crystallographic planes. In addition, species which are strongly adsorbed can act negatively to decrease the rate of reaction by acting as a poison for the reaction; hence, a low coordination number vertex and edge atoms which are found on the surface of particles and are generally variable with the shape of particle exhibit high catalytic activity (Narayanan and El-Sayed 2004).

1.3. Characterization of nanoparticles

Nanoparticle characterization is necessary to establish understanding and control of nanoparticle synthesis and applications. The synthesized nanoparticles are routinely characterized for their size, shape, surface area, phase constitution and microstructural features. Importantly, the synthesis methods are not 100% accurate which results in presence of bulk-sized particles as contamination. The extent of bulk-sized particles may vary from synthesis method and the crystal growth conditions. The development of novel tools and instruments is one of the greatest challenges in nanotechnology.

Common techniques employed for characterization of nanoparticles are electron microscopy (TEM, SEM), atomic force microscopy (AFM), dynamic light scattering (DLS), x-ray photoelectron spectroscopy (XPS), powder X-ray diffraction (XRD), Fourier transform infrared spectroscopy (FTIR), ultraviolet-visible spectroscopy and nuclear magnetic resonance (NMR). Recently, a new method nanoparticle tracking analysis (NTA) allows direct tracking of the Brownian motion and therefore allows the sizing of individual nanoparticles in solution. Also, Isoelectric focusing electrophoresis in a polyacrylamide pH gradient gel has been used to analyze the size distribution of gold nanoparticles synthesized by mercapto-succinic acid as a ligand (Arnaud et al. 2005). The description of principle and handling of all the instruments has well been reported (Rao and Biswas 2009).

1.4. Applications of nanoparticles

In recent years, nanotechnology has become one of the most important and exciting forefront fields. The fast growing field of nanotechnology has influenced various sectors such as energy, environment, agriculture, healthcare, etc. Integration of nanoparticles in daily life style has already underway through fast-moving consumer goods such as shampoos, soaps, detergents, shoes and toothpaste products. Over 300 nanotechnology-based products are already in commerce including over 70 healthcare related products (Ray et al. 2013, Seal and Karn 2014). In addition, nanoparticles have been expanding their horizons and nano-products are coming to market rapidly in the diverse areas ranging from catalysis, sensing, coatings, materials, electronics, imaging to biomedical applications. To date, silver is used in most manufacturer-identified consumer products than any other nanomaterial. Hundreds of silver nanoparticles based products are currently available in the market and their number is growing rapidly (www.nanotechproject.org/inventories/consumer). Integration of other nanoparticles such as ZnO, quantum dots in various cosmetic-based products can also be seen easily in the market (Nohynek et al. 2007, Kokura et al. 2010).

The potential use of nanoparticles in the biological applications has been perceived and resulted in the development of a new subject “nanobiotechnology”. The subject is the convergence of nanotechnology and molecular biology that leads to development at the atomic, molecular or macromolecular size range to create and use structures, devices and systems that have novel properties (Seetharam 2006). Nanotechnology has permeated into majority of biological disciplines such as bioprocessing, molecular medicine and medical diagnostic, nanodrugs, drug delivery systems, biosensors, body implants, environmental improvement, food and agricultural systems, cosmetics, etc (De et al. 2008, Chan and Don 2011).

Nanomedicine is an important cutting-edge area of research that combines the concepts of nanotechnology and medicine and providing new hopes for research in both areas (Moghimi et al. 2005). Some of the earliest applications are in molecular diagnostics as it does not require introduction of nanoparticles in the human body and thereby the safety concerns associated with their fate are not important. Quantum dots and gold nanoparticles have shown important roles in *in vitro* diagnostics owing to their high extent of sensitivity and bio-compatibility (Wilson 2008). Recently, nanomedicine research has extended its wings in the areas such as biological mimetics (e.g. functionalized carbon nanotubes), nanomachines (DNA origami), tissue engineering (polymeric nanoparticles as biomaterials) and nanoscale devices (e.g. silicon microchips). Efforts have also been commenced to implement nanotechnology at all stages of drug development - from formulations for optimal delivery to diagnostic applications in clinical trials (Han et al. 2007, Ghosh et al. 2008, Bao et al. 2013).

Enormous efforts have been placed to gauge the potential impact of nanotechnology in agricultural and food industry. New nano-based tools for rapid detection and treatment of diseases, enhancing the ability of plants to absorb nutrients etc. are being developed to improve the crop productivity (Cifuentes et al. 2010). Studies are on-going to explore the possibilities to implement nanoparticles to enhance photosynthesis, biomass production and soil fertility (Lin et al. 2009, Kole et al. 2013). An important area of research is the controlled release and site targeted delivery of agrochemicals and various other macromolecules needed for improved plant disease resistance and efficient nutrient management (Nair et al. 2010).

1.5. Objectives of the thesis

With the overgrowing consumption of nanoparticles in various applications as discussed above, there is a constant need to develop new synthesis methods. Conventional synthesis of nanoparticles involves a number of chemical and physical methods which can offer synthesis of various size, shape and compositions. However, these methods are energy and capital intensive, employ toxic chemicals, and often yield particles in non-polar organic solutions, thus precluding their biological applications. Thus the need to develop a clean, reliable, bio-compatible and low cost process to synthesize nanoparticles motivated us to exploit biological systems as possible future “nano-factories”. Based on these considerations, the present thesis aims to achieve following objectives:

1. Isolation, screening and identification of microorganisms possessing the potential of metal/metal oxide nanoparticle synthesis.
2. To develop an eco-friendly protocol for biosynthesis of metal/metal oxide nanoparticles and its optimization.
3. Purification and characterization of bioactive molecules involved in nanoparticle synthesis and elucidation of possible mechanism.
4. To study the potential of nanoparticles as antimicrobial agents along with their possible modes of action.
5. To evaluate the effect of nanoparticles on plant metabolism.

1.6. Outline of the thesis

The work presented in this thesis focuses mainly on two broad aspects of nanotechnology research viz. synthesis and application. This thesis encompasses two different metallic nanoparticles, the results and discussion chapters are systematically split in to two halves. Initial part (Chapters III-V) deals with silver nanoparticles and remaining part (Chapters VI- VIII) comprised of the work related to zinc oxide nanoparticles. The details of individual chapter are as follows:

Chapter II highlights molecular characterization and metal tolerance profiles of fungi isolated from metal rich regions. The chapter mainly describes isolation and characterization of

fungus isolates from natural zinc mines of Zawar, Udaipur, India. Furthermore, zinc and silver metal tolerance profiles were prepared by subjecting all fungal isolates to various concentrations of Zn^{+2} and Ag^+ ions, respectively.

Chapter III demonstrates the ability of two metal tolerant fungal (*Aspergillus flavus* isolate NJP08 and *Aspergillus* sp. isolate NJP02) towards extracellular synthesis of silver nanoparticles. Interestingly, as-synthesized silver nanoparticles were found to be individually capped with protein molecules. The effect of variation in physico-chemical environment such as pH, salt concentration and protein content on nanoparticle synthesis is also demonstrated.

Chapter IV deals with the elucidation of mechanism involved in extracellular synthesis of silver nanoparticles by fungus *Aspergillus flavus* isolate NJP08. The complete extracellular proteomic profile was developed followed by protein depletion studies using chromatographic methods. Subsequently, screening of individual protein for potential of nanoparticle synthesis and stabilization has been commenced. The chapter also discussed the prediction of plausible nanoparticle binding site on protein surface and associated protein-nanoparticle interactions.

Chapter V highlights the potential application of silver nanoparticles as future “antibacterial” agents. The study deeply investigate the role of protein shell present on the surface of as-synthesized silver nanoparticles in controlling the antibacterial activity in comparison with bare silver nanoparticles.

Chapter VI demonstrates the extracellular synthesis of zinc oxide nanoparticles using two zinc tolerant fungal isolates (*Aspergillus aeneus* isolate NJP12 and *Aspergillus* sp. isolate NJP02) and their detailed characterization using standard techniques. Similar to silver nanoparticles, zinc oxide nanoparticles were also synthesized at ambient conditions with presence of protein coat on the nanoparticles surface. Furthermore, role of physico-chemical environment (pH, salt concentration and protein content) in controlling the rate of nanoparticle synthesis has been investigated. Last section of this chapter demonstrates the higher efficacy of protein-capped ZnO nanoparticles in comparison to bare ZnO nanoparticles for removal of organic pollutants.

Chapter VII deals with the possibility of implementing zinc oxide nanoparticles as potential “nano-fertilizers” for agricultural applications. A systematic comparison of ZnO nanoparticles (protein-capped and bare) with Zn^{+2} ions and their bulk counterpart were performed using chilli plant as a model system. Physico-chemical characteristics of ZnO nanoparticles in aqueous medium were also calculated to determine their stability and surface characteristics. Our results showed that ZnO nanoparticles were more effective as compared to zinc sulphate and bulk ZnO indicating their potential scope as a promising alternative to conventional zinc fertilizers. Moreover, we noticed a superior growth response in case of

protein-capped ZnO nanoparticles as compared to bare ZnO nanoparticles signifying the importance of surface modification with protein shell.

Chapter VIII provides a summary of the research work presented in the thesis and offers a scope for future work in the area studied.

1.7. References

- Arnaud, I., Abid, J.-P., Roussel, C. and Girault, H. H. (2005). Size-selective separation of gold nanoparticles using isoelectric focusing electrophoresis (IEF). *Chemical Communications*: 787-788.
- Bao, G., Mitragotri, S. and Tong, S. (2013). Multifunctional nanoparticles for drug delivery and molecular imaging. *Annual Review of Biomedical Engineering* **15**: 253-282.
- Chan, Y. and Don, M. (2011). A macro view of bionanotechnology: Application and implications in the near future. *Journal of Bionanoscience* **5**: 97-106.
- Cifuentes, Z., Custardoy, L., de la Fuente, J. M., Marquina, C., Ibarra, M. R., Rubiales, D. and Perez-de-Luque, A. (2010). Absorption and translocation to the aerial part of magnetic carbon-coated nanoparticles through the root of different crop plants. *J Nanobiotechnology* **8**: 26.
- Cuenya, B. R. (2010). Synthesis and catalytic properties of metal nanoparticles: Size, shape, support, composition, and oxidation state effects. *Thin Solid Films* **518**: 3127-3150.
- De, M., Ghosh, P. S. and Rotello, V. M. (2008). Applications of nanoparticles in biology. *Advanced Materials* **20**: 4225-4241.
- Ghosh, P., Han, G., De, M., Kim, C. K. and Rotello, V. M. (2008). Gold nanoparticles in delivery applications. *Advanced Drug Delivery Reviews* **60**: 1307-1315.
- Han, G., Ghosh, P. and Rotello, V. M. (2007). Functionalized gold nanoparticles for drug delivery. *Nanomedicine* **2**: 113-123.
- Jain, P. K., Huang, X., El-Sayed, I. and El-Sayed, M. (2007). Review of some interesting surface plasmon resonance-enhanced properties of noble metal nanoparticles and their applications to biosystems. *Plasmonics* **2**: 107-118.
- Jain, P. K., Huang, X., El-Sayed, I. H. and El-Sayed, M. A. (2008). Noble metals on the nanoscale: optical and photothermal properties and some applications in imaging, sensing, biology, and medicine. *Accounts of Chemical Research* **41**: 1578-1586.
- Jain, P. K., Lee, K. S., El-Sayed, I. H. and El-Sayed, M. A. (2006). Calculated absorption and scattering properties of gold nanoparticles of different size, shape, and composition: applications in biological imaging and biomedicine. *Journal of Physical Chemistry B* **110**: 7238-7248.

- Kelly, K. L., Coronado, E., Zhao, L. L. and Schatz, G. C. (2002). The optical properties of metal nanoparticles: the influence of size, shape, and dielectric environment. *Journal of Physical Chemistry B* **107**: 668-677.
- Kokura, S., Handa, O., Takagi, T., Ishikawa, T., Naito, Y. and Yoshikawa, T. (2010). Silver nanoparticles as a safe preservative for use in cosmetics. *Nanomedicine: Nanotechnology, Biology and Medicine* **6**: 570-574.
- Kole, C., Kole, P., Randunu, K. M., Choudhary, P., Podila, R., Ke, P. C., Rao, A. and Marcus, R. (2013). Nanobiotechnology can boost crop production and quality: first evidence from increased plant biomass, fruit yield and phytomedicine content in bitter melon (*Momordica charantia*). *BMC Biotechnology* **13**: 37-46.
- Lin, S., Bhattacharya, P., Rajapakse, N. C., Brune, D. E. and Ke, P. C. (2009). Effects of quantum dots adsorption on algal photosynthesis. *The Journal of Physical Chemistry C* **113**: 10962-10966.
- Moghimi, S. M., Hunter, A. C. and Murray, J. C. (2005). Nanomedicine: current status and future prospects. *The FASEB Journal* **19**: 311-330.
- Nair, R., Varghese, S. H., Nair, B. G., Maekawa, T., Yoshida, Y. and Kumar, D. S. (2010). Nanoparticulate material delivery to plants. *Plant Science* **179**: 154-163.
- Narayanan, R. and El-Sayed, M. A. (2004). Shape-dependent catalytic activity of platinum nanoparticles in colloidal solution. *Nano Letters* **4**: 1343-1348.
- Nohynek, G. J., Lademann, J., Ribaud, C. and Roberts, M. S. (2007). Grey goo on the skin? Nanotechnology, cosmetic and sunscreen safety. *Critical Reviews in Toxicology* **37**: 251-277.
- Rao, C. N. R. and Biswas, K. (2009). Characterization of nanomaterials by physical methods. *Annual Review of Analytical Chemistry* **2**: 435-462.
- Rao, C. N. R., Kulkarni, G. U., Thomas, P. J. and Edwards, P. P. (2002). Size-dependent chemistry: properties of nanocrystals. *Chemistry--A European Journal* **8**: 28-35.
- Ray, P. C., Singh, A. K., Senapati, D., Fan, Z. and Yu, H. (2013). Toxicity and environmental risks of nanomaterials: an update. *Bio-Nanotechnology: A Revolution in Food, Biomedical and Health Sciences*: 733-748.
- Roco, M. C. (2005). International perspective on government nanotechnology funding in 2005. *Journal of Nanoparticle Research* **7**: 707-712.
- Seal, S. and Kam, B. (2014). Safety aspects of nanotechnology based activity. *Safety Science* **63**: 217-225.
- Seetharam, R. N. (2006). Nanomedicine-emerging area of nanobiotechnology research. *Current Science* **91**: 260.

- Taniguchi, N. (1974). On the basic concept of 'Nano-Technology'. Proceedings of the international conference on production engineering. Tokyo, Japan Society of Precision Engineering (JSPE): 18-23.
- Wang, Z. L., Petroski, J. M., Green, T. C. and El-Sayed, M. A. (1998). Shape transformation and surface melting of cubic and tetrahedral platinum nanocrystals. *Journal of Physical Chemistry B* **102**: 6145-6151.
- Wilson, R. (2008). The use of gold nanoparticles in diagnostics and detection. *Chemical Society Reviews* **37**: 2028-2045.

Chapter II

Isolation, Characterization and Metal Tolerance Profile of Fungi Isolated from Metal Rich Region

Since several decades, biological systems have served as prominent source of inspiration for novel material synthesis and created a huge impact on science. Taking inspiration from phenomenon of metal resistance, the present chapter demonstrates isolation and identification of metal tolerant fungal isolates. The motivation behind the study is the fact that fungi inhabitant in metal rich regions alter their normal physiological activities which leads to development of “unusual” metabolic processes to exhibit metal resistance. Hence, well adapted microbes isolated from native metal rich soil conditions with “unusual” and extreme properties could be an appropriate source for bio-inspired synthesis of metal nanoparticles. The rationale of using fungus as a model organism were economical cultivation, ease in handling and secretion of enormous amount of proteins.

Part of the work presented in this chapter has been published as per the following details:
Jain et al. (2013) *Appl. Microbiol. Biotechnol.* 97:859-869.

2.1 Introduction

Nature is considered as a school for material science and its associated disciplines such as chemistry, biology, physics or engineering. During the development of science, various biological entities serve as the fundamental base for solving a variety of challenges in the field of architecture, aerodynamics and mechanical engineering, as well as in material science (Bensaude-Vincent et al. 2002, Fratzl 2007). Biology is considered as the master of so-called ‘bottom-up’ fabrication which includes building up nanostructures starting from basic atoms or molecules (Naik and Stone 2005). Biological systems serve as prominent source of inspiration due to their remarkable variety of complex structures and functions which confer a huge impact on material science since several decades. Some examples of natural amalgams include crustacean’s carapaces, mollusc shells and vertebrate bone and tooth tissues (Sanchez et al. 2005). A number of single-celled organisms also produce inorganic materials of nanometer range intra- and/or extra-cellularly. Common examples include magnetotactic bacteria which synthesize magnetite (Lovley et al. 1987); diatoms which synthesize siliceous materials (Kröger et al. 1999), S-layer forming bacteria (Pum and Sleytr 1999), etc. These structures are highly controlled, range from macroscopic to nanometer scale and result in intricate architectures that provide multifunctional properties.

Taking inspiration from these natural biological systems, recently, biologists were able to develop an alternative strategy for nanoparticle synthesis using micro-organisms. A landmark study by Klaus et al. (1999) established an interface between material science and biological systems. Their findings demonstrated the synthesis of crystalline silver nanoparticles of well-defined composition and shapes using *Pseudomonas stutzeri* isolated from a silver mine. The nanoparticles were observed on the surface of bacterium with sizes ranging from a few to 200 nanometers. A similar approach by Nangia et al. (2009) demonstrated the intracellular synthesis of gold nanoparticles by *Stenotrophomonas maltophilia* isolated from soil samples of the Singhbhum gold mines, India. The study also proposed a mechanism of production which suggests the involvement of a NADPH-dependent enzyme that reduces Au^{+3} to Au^0 through an electron shuttle pathway for the synthesis of gold nanoparticles. In contrast, synthesis of ZnO nanoparticles using *Lactobacillus sporogens* hypothesized the role of pH-dependent membrane-localized oxidoreductases (Prasad and Jha 2009). Labrenz et al. (2000) had shown the synthesis of spherical aggregates of sphalerite (ZnS) particles (2-5 nm) within the natural biofilms dominated by sulphate-reducing bacteria of the family *Desulfobacteriaceae*. These observations lead to the emergence of a new branch of science called “Biomimetics”, which is defined as application of biological principles for material synthesis (Sarikaya et al. 2003). Biomimetics is sometimes also coined as material bionics or bio-inspired material research (Fratzl 2007). The subject involves an observation of naturally occurring structures and their secret complex biochemical and physiological processes which might play an important role in the formation of structures in nanometer range.

Microorganisms present in metal rich regions exhibit high metal resistance which is mostly due to absorption or adsorption of metals and their chelation by extra- or intracellular proteins (Pócsi 2011). Moreover, it is well demonstrated that high metal stress may affect various microbial activities (Giller et al. 2009). Hence, well adapted microbes isolated from native metal rich soil conditions with extreme properties could be an appropriate source for bio-inspired synthesis of metal nanoparticles as an indigenous ecotype resulting from the long term adaption to soil with extreme conditions. The aim of the present study was to select metal tolerant fungal isolates that can be used for controlled and efficient synthesis of nanoparticles. The rationale of using fungus as a model organism were economical cultivation, ease in handling and secretion of enormous amount of proteins (Jain et al. 2011).

The study was carried out in two phases. The first step involved the isolation and molecular characterization of fungi from metal rich regions of Zawar mines, India and secondly, investigation of the metal tolerance profile of fungal isolates.

2.2 Materials and methods

2.2.1 Sampling site and isolation of fungi

Soil samples were collected in February and July 2009 from the Zawar mines area (24°21' N, 73°44' E) which is located on the bank of the River Tiri, about 38 km south of Udaipur town in the Aravalli hill regions of Rajasthan, India. The mine is historically well known for zinc deposits and is owned by Hindustan Zinc Limited (HZL), Udaipur, India; the world's second largest producer of zinc. The deposits have estimated ore reserves of 28.7 million tonnes (Mt) containing 4.76% zinc with an annual ore production capacity of 1.50 Mt as in the year 2013 (<http://www.hzlindia.com/zawar.aspx>). The mine also contains silver deposits which are extracted in form of zinc or lead contaminant and varies from 171.4 gm to 774.5 gm per tonnes of zinc and lead contaminant, respectively (Sharma 2007). The region has a seasonally tropical climate and minimum & maximum temperatures of 5.0 and 38.4 °C, respectively with a total annual rainfall of 637 mm as recorded by the Agro-Meteorological Department, Udaipur, India.

A total of five sampling sites were studied. Rhizosphere soil samples were collected from naturally growing plants (*Calotropis procera* and *Tephrosia purpurea*) from three spatially separated points at each site, with a minimum of 5 m distance between each sampling point. The upper layers of soil were scraped off to remove foreign particles and litter before taking samples. Soil firmly adhering to the root, designated as rhizosphere soil, was collected by brushing the root part of the plants. The soil samples were stored in self-sealing polyethylene bags, placed in an insulated carrier for transport and then immediately refrigerated at 4 °C. Before processing (in most cases within 2 days), soil samples were passed through a sieve (2 mm mesh size) to remove stones and coarse roots. A subsample of each soil was air dried and used for estimation of various physico-chemical properties as mentioned below. In order to rule out the possibility of seasonal variation, an additional set of

soil samples was also collected after a 6-month interval from the subsets of sites and processed separately.

Isolation of fungi was carried out for each sampling site by plating the inoculum on Martin rose bengal agar medium (HiMedia, India, pH 7.2) after serial dilutions of pooled soil samples (homogenized soils of three samples taken per sampling site) during both first and second collection of soils. Bacterial contamination was inhibited by supplementing the medium with chloramphenicol (Sigma-Aldrich, USA) at a concentration of $10 \mu\text{g mL}^{-1}$ after autoclaving. Petri plates were incubated at 28°C for 4 days under dark conditions. Individual fungal colonies were selected and further purified by repeated sub-culturing on potato dextrose agar (PDA) medium (HiMedia, India, pH 5.6). Preliminary identification of fungal isolates was performed on the basis of morphological characteristics (colour, texture of mycelia, spore formation pattern, etc).

2.2.2 Physico-chemical characteristics of rhizosphere soil

Rhizospheric soil samples were analysed for pH and electrical conductivity on 1:2.5 soil: water suspension using digital pH and EC meter, respectively. Organic carbon was estimated by the method of Walkley and Black (1934) using 1.0 N potassium dichromate for titration and 0.5 N ferrous ammonium sulphate for back titration. Available phosphorus (Olsen P) in soil samples was determined by chlorostannus-reduced molybdophosphoric blue colour method (Olsen et al. 1954) after extraction with 0.5 M sodium bicarbonate for 30 min. Available N, K and micronutrients (Cu, Fe, Pb, Zn) in soil samples were estimated as described by Jackson (1967).

2.2.3 Molecular characterization of fungal isolates

Liquid cultures of fungal isolates were prepared using 25 mL of mineralic Czapek's dox broth medium (HiMedia, India, pH 7.3) in 100 mL Erlenmeyer flasks to obtain fresh mycelia. Separation of mycelia was carried out by centrifugation at 8000 rpm at 4°C for 10 min. The obtained mycelia were mechanically crushed in liquid nitrogen. The genomic DNA was extracted from 100 mg of fungal mycelia using HiPurA Plant Genomic DNA Miniprep Purification Kit (HiMedia, India) according to the manufacturer's instructions.

Polymerase chain reaction (PCR) primers namely ITS-1 (5' TCC GTA GGT GAA CCT GCG G 3') and ITS-4 (5' TCC TCC GCT TAT TGA TAT GC 3') developed by White et al. (1990) were used to amplify the internal transcribed spacer (ITS) region of ribosomal DNA, which encompasses the 5.8S gene and the ITS1 and ITS2 regions. PCR amplification was performed in a total volume of 50 μL containing: 1U Taq DNA polymerase (Promega, Germany), 2.5 mM MgCl_2 , 160 μM dNTP mix (MBI Fermentas, Germany), 50 pmol of each of the ITS-1 and ITS-4 primers (Sigma-Aldrich, USA) and 50 ng genomic DNA in dH_2O . The reactions were performed in a gradient thermal cycler with the following conditions: 1 min denaturation at 95°C , 30 s annealing at 50°C , 90 s elongation at 72°C , for 34 cycles with a final elongation step of 72°C for 10 min. Electrophoresis of amplified PCR products was carried out on 1% agarose gel prepared in 1X Tris Acetate EDTA (TAE) buffer and

electrophoresed with 1X TAE buffer in the gel tank at a constant voltage of 90 V for 1h. The resolved gels were visualized and documented with a Syngene Genesnap gel documentation system. Sequencing of PCR products were carried out with an ABI prism DNA sequencer (Applied Biosystems, USA) using either the ITS-1 and/or the ITS-4 primer for DNA labelling by the BigDye terminator method (Applied Biosystems, USA). The sequenced data obtained from the ITS-4 primer was inversed and clubbed with the sequence data obtained with the ITS-1 primer, to obtain the complete sequence of the ITS region using GeneDoc software (Nicholas et al. 1997). Comparison of nucleotide sequences was performed using the Basic Local Alignment Search Tool (BLAST) network services of the National Centre for Biotechnology Information (NCBI) (<http://www.ncbi.nlm.nih.gov>). Molecular characterization of fungal isolates was based on 96% minimum sequence similarity with the existing type stains entries from the GenBank database. The ITS1-5.8S-ITS2 gene complex sequences of obtained fungal isolates were submitted to the GenBank database of NCBI.

2.2.4 Phylogeny analysis

A multiple alignment of obtained ITS1-5.8S-ITS2 gene complex sequences of the fungal isolates was built using CLUSTAL_X online server (Larkin et al. 2007). The phylogeny tree was constructed using neighbor joining method in Mega 4.0 software (Kumar et al. 2008). The substitution model was based on Jukes and Cantor (1969).

2.2.5 Metal tolerance profiles of fungal isolates

A maximum tolerable concentration (MTC) assay was performed to determine the zinc and silver metal tolerance ability of all the fungal isolates. To determine the zinc metal tolerance ability, experimental plates were prepared by supplementing PDA medium with varying amounts of zinc sulphate (ZnSO_4 ; Merck Inc., India) to obtain final concentration of Zn^{+2} ions in the ranges of 200, 400, 800, 1600 and 3200 $\mu\text{g mL}^{-1}$. Plates without Zn^{+2} ions were used as control. Each plate was subdivided into four equal sectors and an inoculum of test fungi (10^6 cfu mL^{-1}) was spotted on the media surface. After inoculation, the plates were incubated at 28 °C for 4 days under dark conditions to examine the fungal growth. The experiment was done in triplicate. The maximum concentration of Zn^{+2} ions in the medium which allowed the growth of a fungus was taken as the MTC value. To determine the silver metal tolerance ability of all fungal isolates, similar set of experiments were carried out except that silver nitrate (Sigma Chemicals, India) was used instead of zinc sulphate.

2.3 Results and discussion

2.3.1 Physico-chemical characteristics of soil samples

The Zawar mines, Udaipur were opted as sample collection site which is a natural metal-enriched region. The rhizospheric soil samples of naturally growing plants were used as a source for isolation of fungi. It is well known that rhizosphere regions exhibit high microbial populations due to presence of more organic contents (Griffiths et al. 2001). Analysis of physico-chemical properties of soil samples is a pre-requisite for a better understanding of microbial population. Physico-chemical characteristics of rhizospheric soils

of naturally grown plants collected from the Zawar mines, Udaipur, India are shown in Table 2.1. The soil was slightly alkaline in nature. Nitrogen, phosphorus and potassium contents of the soil samples were calculated as 63.4, 30.0 and 150.0 mg kg⁻¹, respectively. Determination of micronutrient content revealed an abundance of Zn in the rhizosphere soil with a mean value of 121.0 mg kg⁻¹ along with moderate concentrations of Cu, Fe and Pb.

Table 2.1 Physico-chemical characteristics of rhizospheric soil samples collected from the Zawar mines, India.

Parameter	Value
pH	7.72 ± 0.02
EC	0.48 ± 0.01 dS m ⁻¹
Available N	63.39 ± 4.5 mg kg ⁻¹
Available P	30.0 ± 1.2 mg kg ⁻¹
Available K	150.0 ± 10.9 mg kg ⁻¹
Zn	121.0 ± 14.3 mg kg ⁻¹
Cu	0.02 ± 0.001 mg kg ⁻¹
Fe	10.0 ± 0.61 mg kg ⁻¹
Pb	3.4 ± 0.08 mg kg ⁻¹

n=30; 15 samples from the first and 15 samples from the second collection of soils

2.3.2 Identification of fungal isolates

2.3.2.1 Morphological identification

Preliminary identification of fungal isolates was performed on the basis of morphological and microscopic observations such as colour, spore shape, arrangement and hyphal branching pattern after staining with cotton blue. A total of 19 fungal isolates were discriminated on the basis of distinct morphological characteristics. The morphology and texture details were recorded as listed in Table 2.2.

2.3.2.2 Molecular identification

Molecular characterization of fungal isolates was carried out using the universal primers for the amplification of the internal transcribed spacer (ITS) regions of the fungal rRNA operon as described by White et al. (1990). The nuclear ribosomal nucleotide sequences evolve very slowly and serve as promising candidate for studying distantly related microorganisms. Amplification of the ITS regions of obtained fungal isolates using polymerase chain reaction resulted in products of 458-619 bp with considerably varying ITS region length (Figure 2.1). The amplified products were subjected to sequencing and the derived sequences were submitted to NCBI with PopSet ID: 329755747.

Table 2.2 Morphology of axenic fungal isolates derived from Zawar mines, Udaipur, India.

Fungal isolate	Morphology	Texture
NJP01	Olive green with a cream reverse	Woolly
NJP02	Drab olive after conidia formation.	Velvety
NJP03	Green colour conidia with wheel pattern; reverse remains brown in colour	Granular
NJP04	Yellow-gold coloured conidia	Cottony
NJP05	Olive green with black reverse	Velvety
NJP06	Olive green with a cream reverse	Cottony
NJP07	Pale green colour conidia with wheel pattern	Granular
NJP08	Yellow-green conidia	Woolly
NJP09	Initially white, transforms to black after maturation; reverse remains white in colour	Granular
NJP10	Dark green with a cream reverse	Cottony
NJP11	Green shaded pattern with reverse brown in colour	Velvety
NJP12	Drab grey with wheel pattern and white border	Cottony
NJP13	Yellow- green conidia	Cottony
NJP14	Pale yellow patches	Velvety
NJP15	Dark olive green with a cream reverse	Woolly
NJP16	Grey shade with white border	Cottony
NJP17	Drab brownish with white border	Woolly
NJP18	Dark green with a cream reverse	Woolly
NJP19	Olivaceous green with black in reverse	Velvety

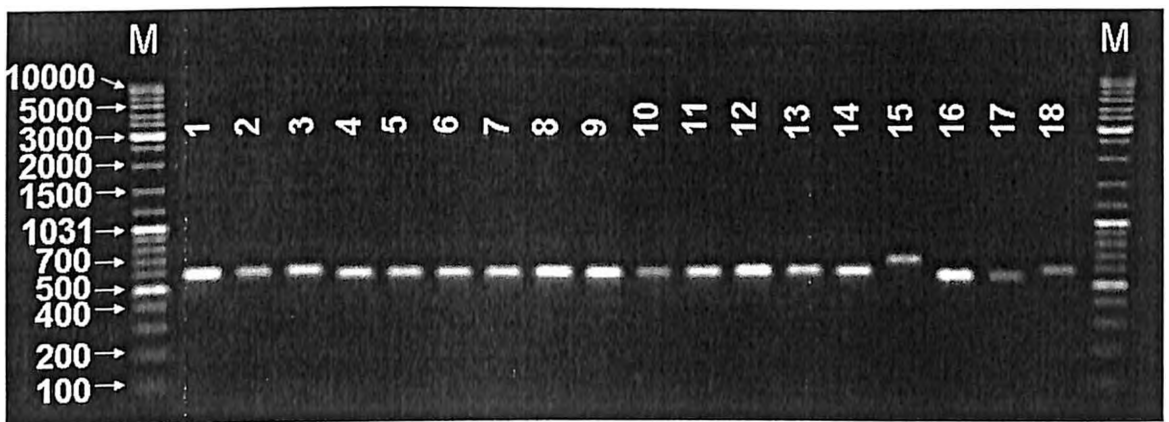


Figure 2.1 Agarose gel electrophoresis of amplified internal transcribed spacer (ITS) rDNA products of 18 fungal isolates.

BLAST analysis of the obtained sequences was performed against the nucleotide sequences of the type strains available in NCBI database. It has been advisable to designate a “species” if sequence identity was above 98% with standard type strains (Rokas et al. 2007). Among all 19 fungal isolates, 15 isolates exhibited high sequence similarity with type strains and were identified conveniently up to species level (Table 2.3). The four to which species could not be assigned were: NJP02, NJP05, NJP14 and NJP19. Fungal isolate NJP02 showed 99% sequence similarity with two fungal type strains *A. minutus* NRRL 279 and *A. insuetus* NRRL 1974 (both possess identical sequences). This ambiguity in database prevents the identification of isolate NJP02 on the basis of ITS nucleotide sequences and thus it was named as *Aspergillus* sp. isolate NJP02. For isolate NJP05, BLAST results showed that the fungus is indeed a new species and not yet present in the GenBank database (Simon et al. 2009). BLAST result of fungal isolate NJP14 showed a low 96% similarity with available type strain *Mortierialla alpina*. However, as per the accepted rules in molecular characterization of fungi, a low 96% similarity from ITS data clearly suggests that it was a different species and hence named as *Mortierialla* sp. NJP14. Similarly, fungal isolate NJP19 had shown less similarity with type strains of *Cladosporium* and hence named as *Cladosporium* sp. NJP19.

Clustering of obtained nucleotide sequences resulted in the distribution of 19 morphological distinct fungal isolates into 12 different species from 5 different genera (Table 2.3). All identified fungal isolates belong to the phylum *Ascomycota* except *Mortierella alpina* which belongs to the phylum *Zygomycota*. An abundance of the genus *Aspergillus* (in total 11 isolates from 6 different species representing 58% of all isolated species) was observed (Figure 2.2a). *Aspergillus oryzae* was found to be the predominant species (46%) followed by *A. ochraceus* among the six *Aspergillus* species found in rhizosphere soils (Figure 2.2b). In order to investigate the evolutionary relationship among the fungal isolates, phylogenetic analysis of nucleotide sequences of ITS region was carried out. Phylogenetic tree revealed a close evolutionary association among obtained fungal isolates owing to the presence of two major clusters belonging to genus *Aspergillus* and *Penicillium* (Figure 2.2c).

Table 2.3 Analysis of ITS1-5.8S-ITS2 complex sequences of fungal isolates with their reference organisms.

Fungus	Isolate	Accession Number	Sequence length			BLAST results				Reference
			ITS1	5.8S	ITS2	Maximum Score	Query Coverage	Maximum Identity	Closest match	
<i>Aspergillus oryzae</i>	NJP01	HQ710532	181	157	170	1061	98 %	99 %	AY373857 ^T	Haugland et al.
<i>Aspergillus</i> sp.	NJP02	HM222932	154	156	170	983	99 %	99 %	EF652481	Peterson (2008)
<i>Penicillium commune</i>	NJP03	HQ710533	175	156	169	1044	100 %	99 %	AY373905 ^T	Haugland et al.
<i>Aspergillus ochraceus</i>	NJP04	HQ710534	169	157	100*	837	98 %	100 %	AY373856 ^T	Haugland et al.
<i>Cladosporium</i> sp.	NJP05	HQ710535	157	157	148*	845	99 %	95 %	EU167574	Simon et al. (2009)
<i>Aspergillus oryzae</i>	NJP06	HQ710536	181	157	170	1053	98 %	99 %	AY373857 ^T	Haugland et al.
<i>Penicillium commune</i>	NJP07	HQ710537	175	156	168	1029	100 %	99 %	AY373905 ^T	Haugland et al.
<i>Aspergillus flavus</i>	NJP08	HM222933	180	158	168	1037	100 %	99 %	AF027863 ^T	Haugland et al.
<i>Aspergillus niger</i>	NJP09	HQ710538	185	157	170	1018	94 %	99 %	EF661191 ^T	Peterson (2008)
<i>Aspergillus oryzae</i>	NJP10	HQ710539	183	157	169	1051	99 %	99 %	AY373857 ^T	Haugland et al.
<i>Penicillium commune</i>	NJP11	HQ710540	175	156	168	1051	100 %	99 %	AY373905 ^T	Haugland et al.
<i>Aspergillus aeneus</i>	NJP12	HM222934	152	157	164	891	100 %	99 %	EF652474 ^T	Peterson (2008)
<i>Aspergillus ochraceus</i>	NJP13	HQ710541	142*	157	176	957	100 %	100 %	EF661419 ^T	Peterson (2008)
<i>Mortierella</i> sp.	NJP14	HQ710542	173	158	258	1000	100 %	96 %	HQ630345	Nagy et al. (2011)
<i>Aspergillus oryzae</i>	NJP15	HQ710543	181	157	168	1064	100 %	99 %	AY373857 ^T	Haugland et al.
<i>Penicillium crustosum</i>	NJP16	HQ710544	175	156	168	1035	99 %	99 %	AY373907 ^T	Haugland et al.
<i>Eupenicillium</i>	NJP17	HQ710545	175	157	169	931	94 %	97 %	GU981613 ^T	Houbraken et al.
<i>Aspergillus oryzae</i>	NJP18	HQ710546	181	157	170	1077	99 %	99 %	AY373857 ^T	Haugland et al.
<i>Cladosporium</i> sp.	NJP19	JF298825	154	157	152	952	97 %	99 %	FJ936159	Schubert et al.

* Incomplete ITS sequence

^T Type strain

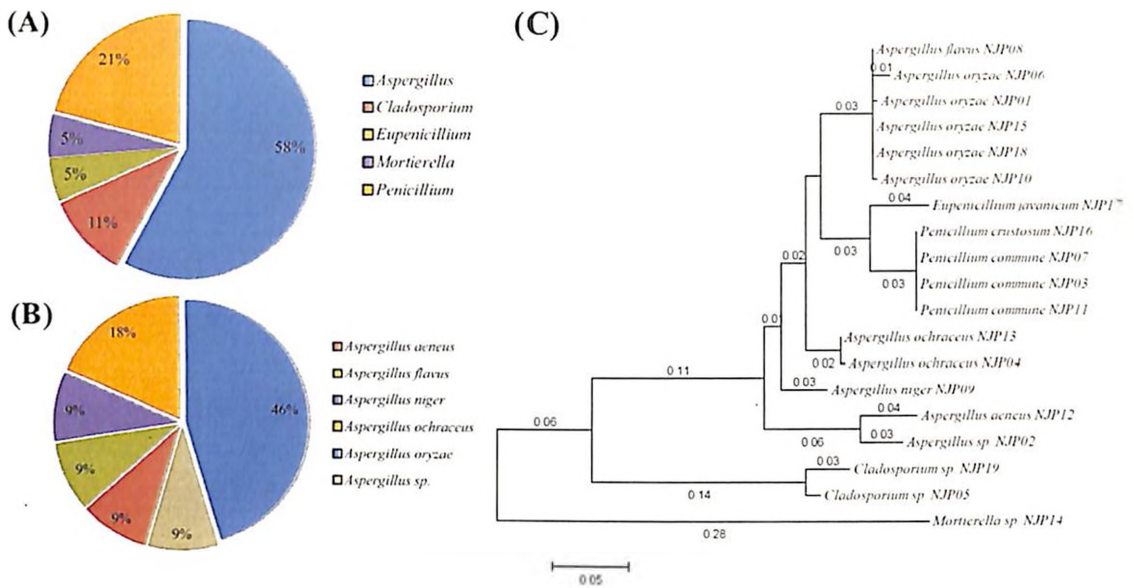


Figure 2.2 Pie chart depicting species richness among fungal isolates: relative proportions of various (a) Genera and (b) *Aspergillus* species. (c) Molecular phylogenetic analysis of internal transcribed spacer (ITS) gene sequences of fungal isolates from zinc rich regions of Zawar mines, India.

2.3.3 Metal tolerance profile of fungal isolates

All the 19 fungal isolates were subjected to a screening for metal tolerance towards zinc and silver ions, and the results were expressed in terms of maximum tolerable concentration (MTC). A high proportion (90 %) of fungal isolates showed significant tolerance to Zn^{+2} ions with a varying degree of magnitude (Figure 2.3a). The genus *Aspergillus* exhibited a more prominent level of metal tolerance towards both silver and zinc as compared to other fungal isolates. It is evident from the results that *A. aeneus* isolate NJP12 and *Aspergillus sp.* isolate NJP02 have very high zinc metal tolerances with MTC values of 2800 and 2400 $\mu g Zn mL^{-1}$ respectively (Figure 2.3a). In contrast, fungus *Aspergillus flavus* isolate NJP08 and *Aspergillus sp.* isolate NJP02 exhibited high silver ion tolerance with MTC value of 1600 $\mu g Ag mL^{-1}$ among all tested isolates (Figure 2.3b). The fungal isolates exhibiting high MTC values were further subjected to screening for their potential towards zinc and silver nanoparticle synthesis.

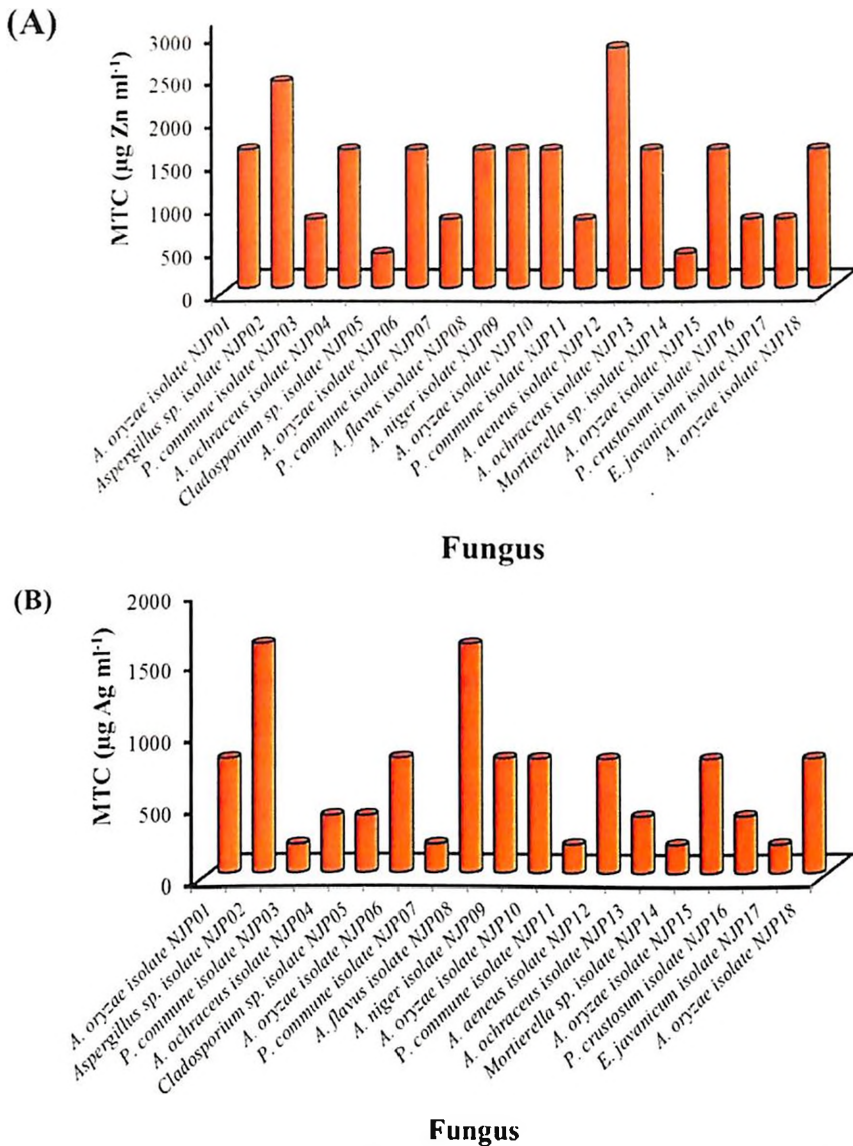


Figure 2.3. Metal tolerance profile of fungal isolates towards (a) zinc and (b) silver.

2.4 Conclusions

This chapter provides a brief overview of sampling and isolation of fungi from metal rich regions of Zawar mines, India. Characterization of physico-chemical properties of collected soil samples showed the alkaline nature of the soil with abundant Zn content. Cluster analysis of ITS nucleotide sequences of fungal isolates revealed a total of 12 distinct species from 5 genera. Species richness analysis showed higher proportions of genus *Aspergillus* with “*oryzae*” as dominant species. Screening of all the obtained fungal isolates towards zinc metal tolerance demonstrated *Aspergillus aeneus* isolate NJP12 and *Aspergillus flavus* isolate NJP08 as high zinc tolerant isolates. Similarly, *Aspergillus* sp. isolate NJP02 and *Aspergillus flavus* isolate NJP08 exhibited highest silver metal tolerance. Hence, these fungal isolates can be utilized as potential candidates for respective nanoparticle (zinc or silver) synthesis.

2.5 References

- Bensaude-Vincent, B., Arribart, H., Bouligand, Y. and Sanchez, C. (2002). Chemists and the school of nature. *New Journal of Chemistry* **26**: 1-5.
- Fratzl, P. (2007). Biomimetic materials research: what can we really learn from nature's structural materials? *Journal of the Royal Society Interface* **4**: 637-642.
- Griffiths, B. S., Ritz, K., Wheatley, R., Kuan, H. L., Boag, B., Christensen, S., Ekelund, F., Sørensen, S. J., Muller, S. and Bloem, J. (2001). An examination of the biodiversity-ecosystem function relationship in arable soil microbial communities. *Soil Biology and Biochemistry* **33**: 1713-1722.
- Haugland, R. A., Varma, M., Wymer, L. J. and Vesper, S. J. (2004). Quantitative PCR analysis of selected *Aspergillus*, *Penicillium* and *Paecilomyces* species. *Systematic and Applied Microbiology* **27**: 198-210.
- Houbraken, J., López-Quintero, C. A., Frisvad, J. C., Boekhout, T., Theelen, B., Franco-Molano, A. E. and Samson, R. A. (2011). *Penicillium araracuarensense* sp. nov., *Penicillium elleniae* sp. nov., *Penicillium penarojense* sp. nov., *Penicillium vanderhammenii* sp. nov. and *Penicillium wotroi* sp. nov., isolated from leaf litter. *International Journal of Systematic and Evolutionary Microbiology* **61**: 1462-1475.
- Jackson, M. L. (1967). Soil Chemical Analysis. New Delhi, Prentice Hall of Indian Private Limited.
- Jain, N., Bhargava, A., Majumdar, S., Tarafdar, J. C. and Panwar, J. (2011). Extracellular biosynthesis and characterization of silver nanoparticles using *Aspergillus flavus* NJP08: A mechanism perspective. *Nanoscale* **3**: 635-641.
- Jukes, T. H. and Cantor, C. R. (1969). Evolution of protein molecules. New York, Academic Press.
- Klaus, T., Joerger, R., Olsson, E. and Granqvist, C. G. (1999). Silver-based crystalline nanoparticles, microbially fabricated. *Proceedings of the National Academy of Sciences of the United States of America* **96**: 13611-13614.
- Kröger, N., Deutzmann, R. and Sumper, M. (1999). Polycationic Peptides from Diatom Biosilica That Direct Silica Nanosphere Formation. *Science* **286**: 1129-1132.
- Kumar, S., Nei, M., Dudley, J. and Tamura, K. (2008). MEGA: A biologist-centric software for evolutionary analysis of DNA and protein sequences. *Briefings in Bioinformatics* **9**: 299-306.
- Labrenz, M., Druschel, G. K., Thomsen-Ebert, T., Gilbert, B., Welch, S. A., Kemner, K. M., Logan, G. A., Summons, R. E., Stasio, G. D., Bond, P. L., Lai, B., Kelly, S. D. and Banfield, J. F. (2000). Formation of sphalerite (ZnS) deposits in natural biofilms of sulfate-reducing bacteria. *Science* **290**: 1744-1747.
- Larkin, M., Blackshields, G., Brown, N., Chenna, R., McGettigan, P. A., McWilliam, H., Valentin, F., Wallace, I. M., Wilm, A. and Lopez, R. (2007). Clustal W and Clustal X version 2.0. *Bioinformatics* **23**: 2947-2948.

- Lovley, D. R., Stolz, J. F., Nord, G. L. and Phillips, E. J. P. (1987). Anaerobic production of magnetite by a dissimilatory iron-reducing microorganism. *Nature* **330**: 252-254.
- Nagy, L. G., Petkovits, T., Kovács, G. M., Voigt, K., Vágvölgyi, C. and Papp, T. (2011). Where is the unseen fungal diversity hidden? A study of *Mortierella* reveals a large contribution of reference collections to the identification of fungal environmental sequences. *New Phytologist* **191**: 789-794.
- Naik, R. R. and Stone, M. O. (2005). Integrating biomimetics. *Materials Today* **8**: 18-26.
- Nangia, Y., Wangoo, N., Sharma, S., Wu, J.-S., Dravid, V., Shekhawat, G. S. and Suri, C. R. (2009). Facile biosynthesis of phosphate capped gold nanoparticles by a bacterial isolate *Stenotrophomonas maltophilia*. *Applied Physics Letters* **94**: 233901-233903.
- Nicholas, K. B., Nicholas, H. and Deerfield, D. (1997). GeneDoc: analysis and visualization of genetic variation. *EMBNEWNEWS* **4**: 14.
- Olsen, S. R., Cole, C. V., Watanabe, F. S. and Dean, L. A. (1954). Estimation of available phosphorus in soils by extraction with sodium bicarbonate. *Circular 939, US Department of Agriculture: Washington, DC, USA*: 1-19.
- Peterson, S. W. (2008). Phylogenetic analysis of *Aspergillus* species using DNA sequences from four loci. *Mycologia* **100**: 205-226.
- Prasad, K. and Jha, A. K. (2009). ZnO nanoparticles: synthesis and adsorption study. *Natural Sciences* **1**: 129-135.
- Pum, D. and Sleytr, U. B. (1999). The application of bacterial S-layers in molecular nanotechnology. *Trends in Biotechnology* **17**: 8-12.
- Rokas, A., Payne, G., Fedorova, N., Baker, S., Machida, M., Yu, J., Georgianna, D. R., Dean, R. A., Bhatnagar, D. and Cleveland, T. (2007). What can comparative genomics tell us about species concepts in the genus *Aspergillus*? *Studies in Mycology* **59**: 11-17.
- Sanchez, C., Arribart, H. and Guille, M. M. G. (2005). Biomimetism and bioinspiration as tools for the design of innovative materials and systems. *Nature Materials* **4**: 277-288.
- Sarikaya, M., Tamerler, C., Jen, A. K. Y., Schulten, K. and Baneyx, F. (2003). Molecular biomimetics: nanotechnology through biology. *Nature Materials* **2**: 577-585.
- Schubert, K., Greslebin, A., Groenewald, J. and Crous, P. (2009). New foliicolous species of *Cladosporium* from South America. *Persoonia* **22**: 111.
- Sharma, P. (2007). *Human Geography: Energy Resources*, Discovery Publishing House.
- Simon, U., Groenewald, J. and Crous, P. (2009). *Cymadothea trifolii*, an obligate biotrophic leaf parasite of *Trifolium*, belongs to *Mycosphaerellaceae* as shown by nuclear ribosomal DNA analyses. *Persoonia* **22**: 49.
- Walkley, A. J. and Black, I. A. (1934). Estimation of soil organic carbon by the chromic acid titration method. *Soil Science* **37**: 29-38.
- White, T., Bruns, T., Lee, S. and Taylor, J. (1990). *Amplification and direct sequencing of fungal ribosomal rna genes for phylogenetics*. San Diego, Academic Press.

Chapter III

Biosynthesis of Silver Nanoparticles and Optimization Studies

This chapter demonstrates the use of indigenous metal tolerant fungal isolates to develop an eco-friendly and low cost protocol for synthesis of silver nanoparticles. The study investigates the potential of soil born fungal isolates *Aspergillus flavus* isolate NJP08 and *Aspergillus* sp. isolate NJP02 towards extra-cellular synthesis of silver nanoparticles. The protocol involves collection of cell-free filtrate and its subsequent exposure to precursor silver ions. The as-synthesized nanoparticles were characterized using standard techniques viz. UV-visible spectroscopy, TEM, DLS, SAD, XRD and EDS. Capping molecules surrounding nanoparticles were characterized using FTIR and photoluminescence spectroscopy measurements. Optimization studies were performed to test the effect of various factors (pH, salt concentration and biomass) on particle size of silver nanoparticles synthesized using both the fungal isolates.

Part of the work presented in this chapter has been published as per the following details:
Jain et al. (2011) *Nanoscale* 3:635-641.

3.1 Introduction

Nanotechnology has now started leaving the confines of laboratories; and is conquering new applications to change our lives. According to estimates, the worldwide nano product market is estimated to reach \$1 trillion by the year 2015 (Roco 2005). The project on Emerging Nanotechnologies at the Woodrow Wilson International Center for Scholars had compiled a list of more than 1600 manufacturer-identified nanotechnology-based consumer products introduced to the market as in 2013 that claim to contain engineered nanomaterials (Scholars 2013). Among these, about 25% of the consumer products contain silver nanoparticles with majority of them targeted as antimicrobial agents.

The role of silver as an antimicrobial agent has been known since ancient times and particularly recognized by clinicians for over 100 years. Historically, silver compounds and ions have been extensively used for both hygienic and healing purposes (Chen and Schluesener 2008). However, over time, the use of silver compounds and ions has faded as an antimicrobial agent due to the emergence of antibiotics with various disinfectants and the poorly understood mechanisms of their toxic effects. In recent decades, silver has regained considerable attention due to the rising need for antimicrobial compounds because bacterial resistance is increasing to most of the commonly used antibiotics. With the advent of nanotechnology, scientists and academicians become interested in silver nanoparticles as in nano regime, silver exhibits unusually enhanced physicochemical and biological properties compared to the bulk parent materials. Silver nanoparticles have many important commercial applications that include spectrally selective coating for solar energy absorption and intercalation material for electrical batteries, optical receptors, polarizing filters, catalysts in chemical reaction and bio-labelling agents in disinfecting medical devices and home appliances to water treatment (Ghorbani et al. 2011). Hence, silver nanoparticles could be considered as an attractive choice among nanomaterials to encompass broad applications ranging from electronics to medicine to food technology.

To compete with the tremendous demand of silver nanoparticles, novel strategies to produce mass scale of nanoparticles are highly desirable. Moreover, the synthesis of nanoparticles with desired composition, shape and size make the task more challenging. Conventional synthesis of nanoparticles involves a plethora of chemical and physical methods resulting in different shapes and sizes for use in numerous applications. Broadly, the synthesis methods are categorized into two approaches: top-down and bottom-up (Bhushan 2004). The top-down approach uses bulk form of silver as a precursor, then, reducing its size using specialized methods such as lithography, laser ablation and precisely mechanical tools (Mafune et al. 2000, Amendola and Meneghetti 2009). The bottom-up approach seeks the means and tools to build things by combining smaller components such as single molecules and atoms, which are held together by covalent forces. The method is also commonly known as “self-assembly” and involves three steps: (i) dissolution of silver salt into a solvent system;

(ii) addition of a reducing agent, and (iii) use of stabilizing agents to prevent agglomeration of nanoparticles (Tolaymat et al. 2010). The typical methods based on bottom-up approach are: chemical reduction in aqueous or non-aqueous solution (Petit et al. 1993), micro-emulsion (Solanki and Murthy 2010), solution-phase (Chen and Carroll 2002), sono-chemical (Pol et al. 2002) and microwave-assisted (Li et al. 2010) methods. However, all these methods are energy and capital intensive, employ toxic chemicals, and often yield particles in non-polar organic solutions, thus precluding their biomedical applications. Thus the need for the development of clean, reliable, bio-compatible and benign process to synthesize nanoparticles has turned more and more researchers to exploit biological systems as possible eco-friendly “nano-factories”.

As outlined in Chapter I, a wide array of biological entities ranging from bacteria, fungi, plants, algae, and yeast has been explored towards biosynthesis of metal, metal oxide and metal sulfide nanoparticles (Ahmad et al. 2003, Sharma et al. 2009, Duran et al. 2011, Peter Amaladhas et al. 2012). Moreover, various biomolecules such as proteins, DNA, viral capsid proteins, etc. have been utilized to achieve controlled synthesis of nanoparticles (Blum et al. 2004, Sweeney et al. 2004, Colombo et al. 2012, Taajamaa et al. 2013). The simplicity and miniaturization of biomolecules and biological systems as well as ambient conditions (temperature, pressure and pH) for the synthesis reaction makes this biosynthesis process very attractive. The formation of nanoparticles by various biological entities in the natural way is highly inspirational. Even more fascinating is the fact that microorganisms that had encountered high metal stress in their natural habitat could exhibit high potential to synthesize nanoparticles in an efficient manner (Nangia et al. 2009).

In the present study, learning from nature’s own sustainable way of interacting with metal ions, indigenous metal tolerant soil fungal isolates were utilized to develop an eco-friendly and low cost protocol for the extracellular synthesis of silver nanoparticles. Although, intracellular as well as cell-surface mediated synthesis of nanoparticles has been reported by many workers (Mukherjee et al. 2001, Zhang 2013), the recovery of nanoparticles from biomass and subsequent purification needs additional steps which confer additional time, cost and labour. The extracellular synthesis protocol possesses numerous advantages over intracellular as well as cell-surface mediated synthesis protocols such as enormous secretion of fungal proteins, convenient handling as well as ease in downstream processing (Kowshik et al. 2003, Bhainsa and D’Souza 2006, Gericke and Pinches 2006). Hence, simplicity and versatility of the extracellular biosynthesis makes it attractive and could be implemented for various metal nanoparticles synthesis leading to future “nano-factories”.

3.2 Materials and methods

3.2.1 Extracellular synthesis of silver nanoparticles

The fungal isolate exhibiting the highest MTC value was selected for extracellular synthesis of silver nanoparticles. For this, the fungal isolate was maintained at 28 °C with

regular sub-culturing on fresh PDA medium slants. The stock culture (4 days old) was inoculated in 100 mL of MGYP medium (0.3% malt extract, 1.0% glucose, 0.3% yeast extract, 0.5% peptone; pH 7.0) in 250 mL Erlenmeyer flasks. Inoculated flasks were incubated at 28 °C for 72 h on a rotary shaker (150 rpm) under dark conditions. Fungal mycelia were separated from culture medium by centrifugation (8000 rpm, 10 min and 4 °C) and washed thrice with sterile water in order to remove all traces of media. Typically, 10 g of biomass (fresh weight) was re-suspended in 100 mL of sterile deionized Milli-Q water and further incubated for 72 h under the same conditions as described above. After incubation, biomass was separated by filtration using Whatman filter paper no. 1 (Whatman Inc., USA) and the fungal cell-free filtrate containing extracellular secretions was collected. For synthesis of nanoparticles, aqueous silver nitrate solution (Sigma-Aldrich, USA) at a final concentration of 1.0 mM was added to flasks containing 100 mL of fungal cell-free filtrate and incubated for 72 h under the same conditions as described above. Controls containing fungal cell-free filtrate (without silver nitrate) and pure silver nitrate solution (without fungal cell-free filtrate) were also run simultaneously along with experimental flasks in three replicates.

3.2.2 Characterization of nanoparticles

3.2.2.1 UV-visible spectroscopy

Synthesis of nanoparticles was monitored using UV-visible spectroscopy by sampling of aliquots (1 mL) at different time intervals. Absorption spectra were measured using a Jasco V-630 UV-visible spectrophotometer (Jasco Corporation, Japan) operated within the range of 200-900 nm at a resolution of 1 nm.

3.2.2.2 Transmission electron microscopy

Samples for transmission electron microscopy (TEM) were prepared by drop coating the as-synthesized nanoparticle solution onto carbon coated copper grids. After about a minute, extra solution was removed using a blotting paper and the grids were kept in a vacuum desiccator, prior to measurement. TEM micrographs were taken by analysing the prepared grids on a Hitachi H-7650 TEM instrument (Hitachi High-Technologies Corporation, Japan) at an acceleration voltage of 100 kV.

3.2.2.3 Energy dispersive spectroscopy

Energy dispersive spectroscopy (EDS) of drop coated grids of samples was carried out using Bruker attachment (Bruker AXS Ltd., UK) with a TEM instrument. The X-ray beam of TEM was used as an electron source and energy emitted from the samples was converted into voltage signals using a Si(Li) detector which was cooled to cryogenic temperature with liquid nitrogen. The data was recorded using a pulse processor, which measures the signals and passes them onto an analyser for data display and analysis.

3.2.2.4 Selected area diffraction pattern

The method is also termed as selected area electron diffraction (SAD) pattern and was captured in parallel to TEM imaging by inserting selected area aperture, which is located

below the sample holder on the TEM column. The aperture is a thin strip of metal containing several different sized holes that block the beam and can be adjusted by the user to obtain optimal SAD patterns. The aperture blocks majority of the electron beam except for the small fraction passing through one of the holes which contributes to the formation of SAD pattern.

3.2.2.5 X-ray diffraction

X-ray diffraction (XRD) measurements of the freeze dried samples were carried out using a Rigaku MiniFlex II Bench top XRD System (Rigaku Company, USA) operated at a voltage of 20 kV and current of 15 mA with CuK_α radiation. Phase analysis was carried out by comparing the calculated values of interplanar spacing and corresponding intensities of diffraction peaks with theoretical values from the Powder Diffraction File database (PCPDF-WIN; JCPDS-ICDD 2008).

3.2.2.6 Dynamic light scattering

Particle size distribution of as-synthesized nanoparticles was measured using dynamic light scattering (DLS) on a Malvern Zetasizer Nano-ZS spectrometer (Malvern Instruments, UK). Measurements were recorded at $25\text{ }^\circ\text{C} \pm 1\text{ }^\circ\text{C}$, in triplicates; each measurement was the average of 20 data sets acquired for 10 seconds each. Hydrodynamic diameter and polydispersity index (PDI) have been calculated using the internal software analysis from the DLS intensity-weighted particle size distribution.

3.2.3 Characterization of capping molecules

3.2.3.1 Fourier transform infrared spectroscopy

For Fourier transform infrared spectroscopy (FTIR) measurements, as-synthesized nanoparticles present in the fungal cell-free filtrate were freeze-dried and diluted with potassium bromide in a ratio of 1:100. FTIR spectra of samples were recorded on a Shimadzu IR Prestige-21 FTIR spectrometer (Shimadzu, Japan) with a diffuse reflectance mode (DRS-8000) attachment (Shimadzu Corporation, Japan). All measurements were carried out in the range of $400\text{--}4000\text{ cm}^{-1}$ at a resolution of 4 cm^{-1} .

3.2.3.2 Photoluminescence spectroscopy

Photoluminescence spectroscopy (PL) measurements were performed on a Horiba spectrofluorometer (Horiba, Japan) with an excitation wavelength of 280 nm using a 90° illumination. In order to achieve maximal signal-to-noise ratio, excitation and emission slit width values were set to 2.5 and 3.0 nm, respectively.

3.2.3.3 Sodium dodecyl sulphate polyacrylamide gel electrophoresis

In order to investigate the proteins present on the surface of silver nanoparticles, as-synthesized silver nanoparticles were boiled with 1% SDS solution for 10 min followed by centrifugation at 8000 rpm for 10 min to collect capping proteins as supernatant. Sodium dodecyl sulphate polyacrylamide gel electrophoresis (SDS-PAGE) was carried out to determine the molecular weight of capping molecules as described by Laemmli (1970). Samples (capping proteins) were mixed in a 1:1 ratio with Laemmli sample buffer containing

0.5 M Tris-HCl (pH 6.8), 0.5% bromophenol blue, 10% glycerol, 5% β -mercaptoethanol and 2% SDS and incubated for 5 min at 100 °C in a boiling water bath. The preparations were centrifuged at 10,000 g for 5 min at 4 °C and the supernatant was used for electrophoresis on a Mini Protean gel system (Bio-Rad, USA) at a constant voltage of 120 V at room temperature. A 12% separation gel and 5% stacking gel were used for polyacrylamide gel electrophoresis. After electrophoresis, gels were stained with 0.25% Coomassie brilliant blue (CBB) R-250 in 45% methanol-10% acetic acid solution for 3 h and de-stained overnight with 45% methanol-10% acetic acid solution. The molecular mass of the protein bands were determined by interpolation from a semi- logarithmic plot of relative molecular mass versus the R_f value (relative mobility).

3.2.4 Optimization of nanoparticle synthesis

3.2.4.1 Effect of pH

Effect of pH on nanoparticle synthesis was studied by varying the initial pH of fungal cell-free filtrate in the range of 2 to 10 before addition of precursor salt solution. The pH of the solution was gradually adjusted by addition of 0.1 N HCl or 0.1 N NaOH under constant stirring conditions. The silver nanoparticles synthesized thereby were subjected to further characterization as mentioned above.

3.2.4.2 Effect of salt concentration

The effect of salt concentration on efficacy of silver nanoparticle synthesis was carried out by varying the initial concentration of precursor ions in the range of 0.5-5.0 mM. The optimal concentration was determined by the comparison of DLS measurements and absorbance at 420 nm using UV-visible spectroscopy.

3.2.4.3 Effect of biomass

Effect of biomass on nanoparticle synthesis was studied by varying the amount of fungal biomass suspended in 100 ml of Milli-Q water. The experiments were conducted with the biomass range of 4 to 20 g and the protein content was also determined by the method of Lowry et al. (1951) using bovine serum albumin (BSA) as standard.

3.3 Results and discussion

3.3.1 Extracellular synthesis of silver nanoparticles using *Aspergillus flavus* isolate NJP08

3.3.1.1 Characterization of silver nanoparticles

The extracellular synthesis of silver nanoparticles using cell-filtrate of fungus *Aspergillus flavus* isolate NJP08 was monitored by change in colour of the reaction medium. Figure 3.1 shows Erlenmeyer flasks containing the fungal cell-free filtrate without and with silver nitrate after completion of reaction at 72h. The flask containing silver nitrate solution and fungal cell-free filtrate showed gradual change in colour of reaction mixture from colourless to brown with intensity increasing during the incubation period. In contrast, no change in colour was observed in flask containing only the fungal cell-free filtrate. Moreover, the negative control (pure silver nitrate solution without cell-free filtrate) did not show the

characteristic change in colour suggesting the importance of fungal cell-free filtrate in nanoparticle synthesis.

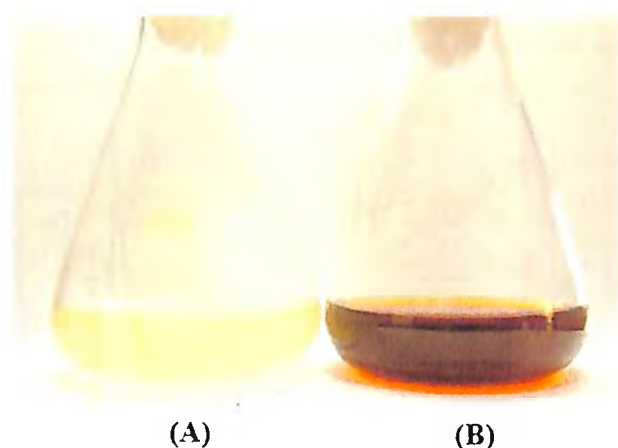


Figure 3.1 Erlenmeyer flasks containing cell-free filtrate of *Aspergillus flavus* isolate NJP08 without (a) and with (b) silver nitrate solution (1mM) after 72 h of reaction.

The rate of nanoparticle synthesis was monitored using UV-visible spectroscopy which has been considered as most commonly employed technique for characterization of silver nanoparticles. The absorption spectra of nanoparticles showed single-band absorption with peak maxima at *ca.* 421 nm with steady increase in intensity as a function of time of reaction without any shift in the peak (Figure 3.2). This indicates the presence of silver nanoparticles which is due to the excitation of surface plasmons; a typical phenomenon of noble nanoparticles (Gurunathan et al. 2009). Inset to Figure 3.2 represent the plot of absorbance at 420 nm at different time intervals of reaction. After 72 h of incubation, no further increase in intensity was recorded indicating complete reduction of precursor silver ions. It is observed that the graph follows the sigmoid kinetics which is characteristic of enzyme catalysis reactions. The kinetics of silver nanoparticles formation showed that more than 85% of the particles were formed within the 48 h of the reaction which suggests that the formation of silver nanoparticles is exponential in nature.

Figure 3.3 shows the UV-visible spectrum recorded from the reaction vessel after 72 h of reaction. An absorption peak at *ca.* 280 nm was observed which corresponds to aromatic amino acids of proteins. It is well known that the absorbance peak at 280 nm arises due to electronic excitations in tyrosine and tryptophan residues of proteins (Xie et al. 2007, Saifuddin et al. 2009). This observation indicates the presence of proteins secreted by fungus in the cell-free filtrate. The particles in the solution are thus stabilized by the capping agent that is likely to be proteins present in the cell-free filtrate. Stability of as-synthesized silver nanoparticles was monitored regularly for more than four months of completion of reaction. It was observed that the nanoparticle solution was extremely stable at room temperature, with no evidence of flocculation of particles as determined by UV-visible spectroscopy measurements. This indicates that the nanoparticles were well dispersed in the solution

without aggregation. Monodispersity and chemical stability are highly desirable characteristics of the nanoparticles (Bhainsa and D'Souza 2006). This is an important aspect of synthesis of nanoparticles, since the lack of sufficient stability of many nanoparticle preparations has to some extent impeded the development of the real world applications of nanomaterials (Shankar et al. 2003).

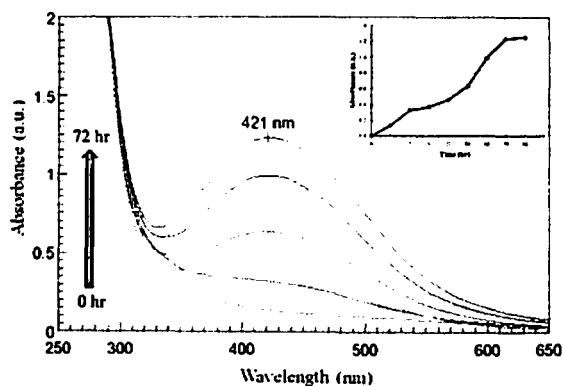


Figure 3.2 UV-visible spectra recorded as a function of time after addition of fungal cell-free filtrate to silver nitrate solution (1.0 mM). The arrow represents the time of reaction with respective curves at 0, 3, 6, 12, 24, 48 and 72 hrs. Inset graph shows saturation curve of silver nanoparticles synthesis with function of time.

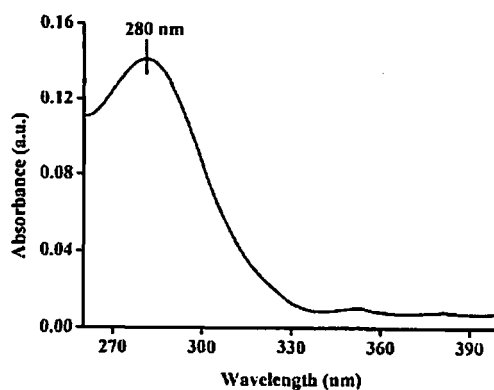


Figure 3.3 UV-visible spectra showing presence of proteins in the fungal cell-free filtrate. An absorption maximum at 280 nm arises due to electronic excitations in tyrosine and tryptophan residues of proteins.

Transmission electron microscopy (TEM) measurements were used to determine the morphology and shape of nanoparticles. TEM micrographs (Figure 3.4a and b) revealed that the as-synthesized nanoparticles were somewhat spherical in shape and uniformly distributed (mono-dispersed) without significant agglomeration. As illustrated in Figure 3.5a, particle size histogram of silver nanoparticles shows size ranging from 10 to 35 nm with an average size of 17 ± 5.9 nm. The frequency distribution observed from the histogram showed that almost 80% of the particles were in the 10 to 25 nm range. Although, very tiny particles (ca.

5-10 nm) have also been observed that may be due to vigorous shaking. These results were in agreement with the values obtained by DLS measurements as shown in Figure 3.5b.

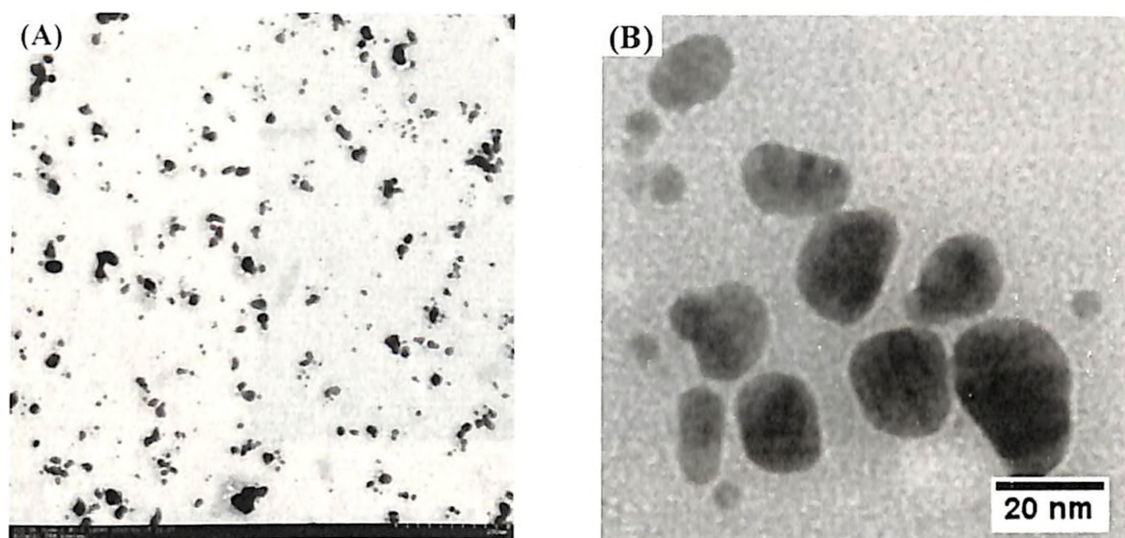


Figure 3.4 TEM micrographs showing uniformly distributed silver nano-particles. (a) Low magnification image and (b) high magnification image.

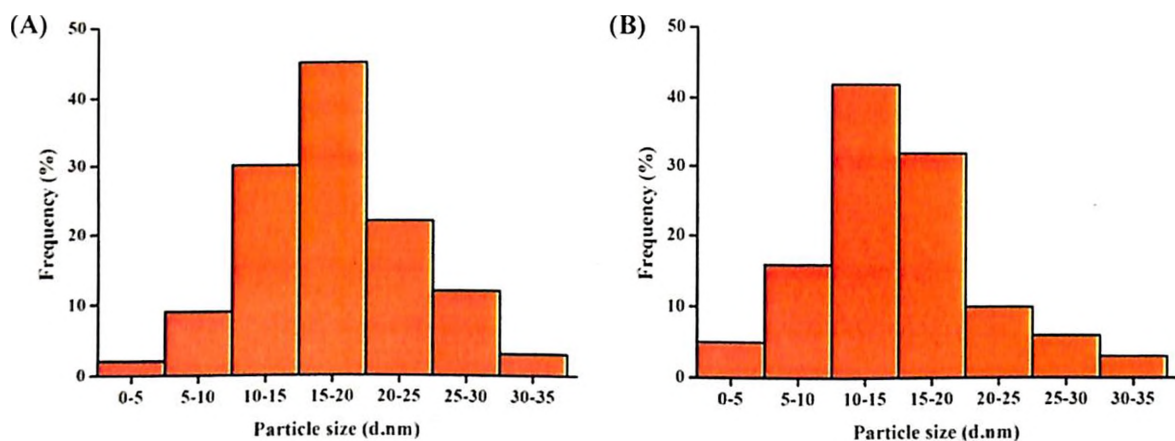


Figure 3.5 Particle size distribution histogram of silver nanoparticles as determined using (a) transmission electron micrographs and (b) dynamic light scattering measurements. X-axis represents diameter of nanoparticles in nanometer (d.nm).

The structural features of the individual silver nanoparticles can be observed more clearly in the HR-TEM images (Figure 3.6). The particles are predominantly spherical with round edges and with no sign of crystal defects. Inset to Figure 3.6 shows the selected area diffraction pattern from one of the silver nanoparticles which confirmed the plane (111) of silver nanoparticles. The lattice fringes observed in micrograph also supports the crystalline nature of silver nanoparticles. The crystalline nature of silver nanoparticles was further validated with powder diffraction studies. As shown in Figure 3.7, diffraction pattern of drop-coated film of as-synthesized nanoparticles showed well-defined peaks at 2θ values of 38.16° , 44.31° , 64.36° , and 77.50° which corresponds to (111), (200), (220) and (311) planes

of silver, respectively. These values were in agreement with the face-centered cubic (fcc) lattice structure of crystalline silver (JCPDS file no. 04-0783).

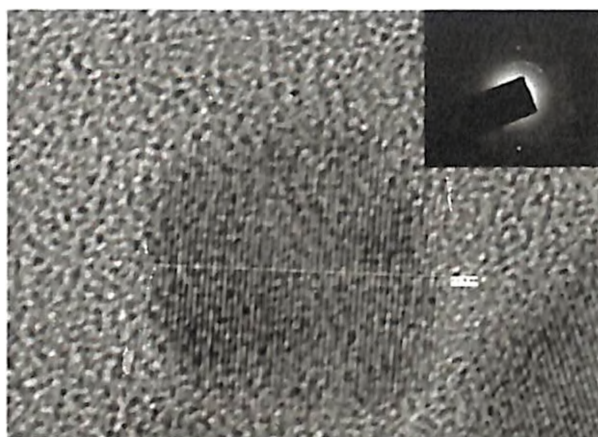


Figure 3.6 High resolution - transmission electron micrograph showing spherical shape of silver nanoparticle. Inset shows SAD pattern recorded from silver nanoparticle: the spot array is from [111] beam direction for fcc pattern of a silver nanoparticle.

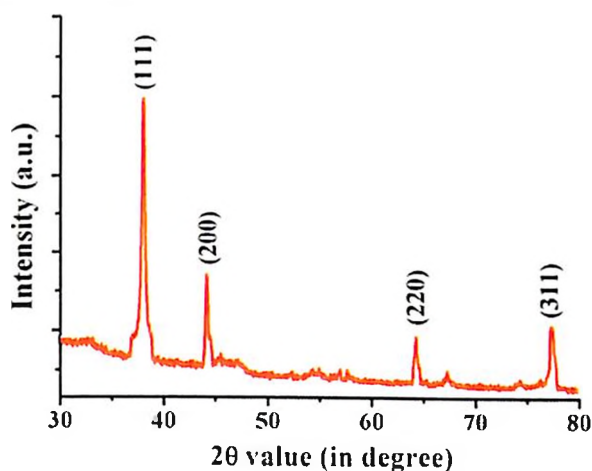


Figure 3.7 X-ray diffraction pattern showing crystalline nature of silver nanoparticles.

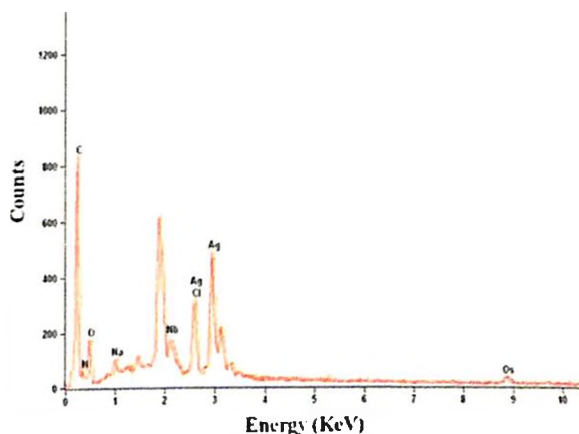


Figure 3.8 Energy dispersive spectrum showing the presence of elemental silver in silver nanoparticles.

An energy dispersive spectrum of drop coated film of silver nanoparticles is shown in Figure 3.8. The presence of an optical absorption band at ~ 3 eV reveals the presence of pure metallic silver nanoparticles (Magudapathy et al. 2001). The spectrum showed mainly Ag (59 atom %) and only minor amounts of other elements with Nb (8.99 atom %) being the largest. Apart from this, the signals for C, N and O indicated the presence of proteins as a capping material on the surface of silver nanoparticles.

3.3.1.2 Characterization of capping molecules

Fourier transform infrared spectroscopy (FTIR) measurements of the freeze-dried samples were carried out to characterize the capping molecules (stabilization material) present on the surface of silver nanoparticles. FTIR spectrum reveals two bands at wave number 1647 and 1543 cm^{-1} that corresponds to the bending vibrations of the amide I and amide II bands of the proteins respectively; while their corresponding stretching vibrations were seen at wave number 3302 and 2926 cm^{-1} respectively (Figure 3.9). The amide linkages between amino acid residues in proteins give rise to well-known signatures in the infrared region of the electromagnetic spectrum. The presence of the signature peaks of amino acids supports the presence of proteins in cell-free filtrate as observed in UV-visible spectrum (Figure 3.3).

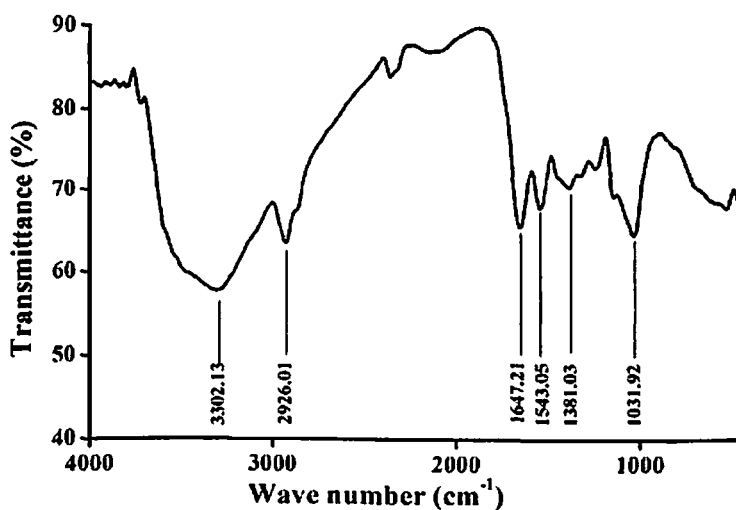


Figure 3.9 Fourier transform infrared spectroscopy spectrum of freeze-dried samples showing the presence of proteins on the surface of silver nanoparticles.

It has been very well demonstrated that interactions of proteins with nanoparticles can occur either through free amine groups or cysteine residues in proteins and via the electrostatic attraction of negatively charged carboxylate groups in enzymes (Gole et al. 2001). The two bands observed at wave number 1381 and 1032 cm^{-1} could be assigned to the C-N stretching vibrations of the aromatic and aliphatic amines, respectively (Vigneshwaran et al. 2006). These observations indicate the presence and binding of proteins with silver nanoparticles which could lead to their possible stabilization. Moreover, presence of intact

bands indicates that secondary structure of proteins has not been affected as a consequence of reaction with silver ions or binding with silver nanoparticles.

In order to remove the proteins bound to the surface of silver nanoparticles, the as-synthesized silver nanoparticles were treated with 1% SDS solution in boiling water bath for 10 min. SDS act as a widely used denaturing agent and its treatment results in detachment of the surface bounded proteins from nanoparticles (Wigginton et al. 2010). The treated and untreated silver nanoparticles were analysed by dynamic light scattering to confirm the successful removal of proteins from the surface of silver nanoparticles. A decrease in the mean particle size from 24.36 nm (before SDS treatment) to 21.04 nm (after SDS treatment) indicated the successful removal of protein corona from the surface of silver nanoparticles (Figure 3.10). The maximum number of protein molecules present on the surface of individual silver nanoparticles were calculated on the basis of simple steric considerations using the following equation (Calzolari et al. 2010):

$$N_{\max} = 0.65 \left(\frac{R_{\text{protein-capped NP}}^3 - R_{\text{bare NP}}^3}{R_{\text{protein}}^3} \right)$$

where, $R_{\text{protein-capped NP}}$ was taken as radius of protein capped nanoparticle, $R_{\text{bare NP}}$ as the radius of bare nanoparticle, and R_{protein} as the radius of capping protein molecule (http://www.calctool.org/CALC/prof/bio/protein_size).

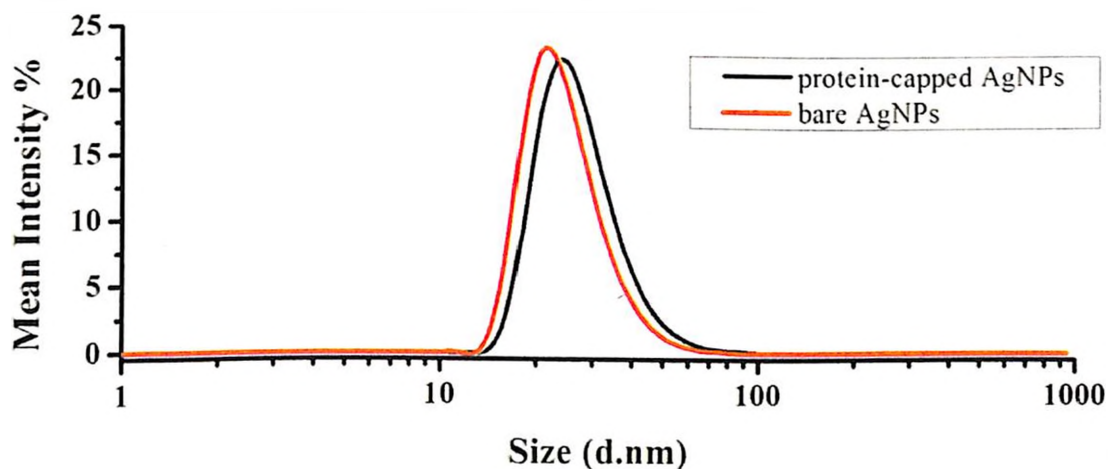


Figure 3.10 Dynamic light scattering spectra showing the difference in particle size of protein-capped and silver nanoparticles.

In the present case, a theoretical maximum number of ~120 protein molecules per nanoparticle were calculated. However, the actual number of protein molecules per nanoparticle is more likely to be lower as this calculation assumes a close packing of proteins on the nanoparticle surface. The observed difference between the mean diameter of protein-capped and bare silver nanoparticles was approximately 3.0 nm which is equivalent to diameter of a protein molecule. The observation suggests the formation of a single-layer protein corona over the surface of silver nanoparticles.

The proteins separated from the surface of silver nanoparticles were further resolved on SDS-PAGE using a 12% resolving gel (Figure 3.11). Lane 2, containing the untreated silver nanoparticles, showed an intense band at the transition of stacking and resolving gel showing the silver deposition (Figure 3.11, lane 2). It suggests that the strong interactions between protein and nanoparticles prevent the migration of proteins into resolving gel. Interestingly, when the proteins were separated from nanoparticles using SDS treatment and subjected to SDS-PAGE, a single band of ca. 35 kDa was observed (Figure 3.11, lane 3). Therefore, it can be proposed that the observed protein (35 kDa) acts as a capping material and confers stability to silver nanoparticles.

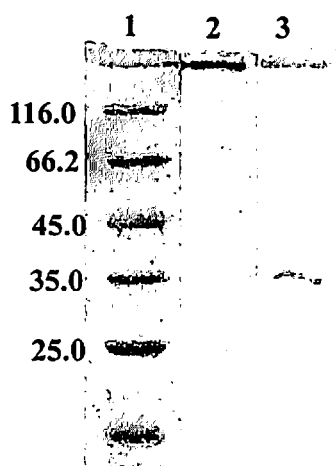


Figure 3.11 SDS-PAGE depicting the removal of capping proteins. Lane 1, standard molecular weight marker; lane 2, protein-capped silver nanoparticles; lane 3, separated capping proteins present on the surface of silver nanoparticles.

3.3.2 Optimization of silver nanoparticle synthesis using *Aspergillus flavus* isolate NJP08

The synthesis of nanoparticles of various sizes, shapes and composition in a controlled manner has been considered as one of the foremost challenging tasks in the areas of nanotechnology research. It has been realised that for most of the applications, well-defined size and shape of nanoparticles is a pre-requisite. Moreover, it has been observed that the rate of nanoparticle formation and therefore the size of the nanoparticles could, to an extent, be manipulated by controlling parameters such as pH, temperature, substrate concentration and exposure time to substrate. Also, the optimization studies could contribute significantly in designing strategies for attaining mass scale synthesis of nanoparticles using biological systems.

The effect of pH on the silver nanoparticle synthesis was studied in the pH range of 2 to 10. Table 3.1 shows the effect of initial pH of reaction mixture on size of silver nanoparticles as determined using dynamic light scattering measurements. The size of nanoparticles ranged between 42.8 to 44.3 nm. The smallest particles (42.8 nm) were formed at neutral pH (pH = 7) with minimum polydispersity index (PDI = 0.194) indicating

nanoparticles of similar sizes. The plausible reason for this may be the higher stability of secreted proteins at neutral pH. It has been proposed that reducing groups such as hydroxyl (OH⁻) are more reactive near neutral pH as compared to acidic or alkaline conditions (Binupriya et al. 2010). In alkaline conditions, size of nanoparticles was found to be consistently increasing with increase in pH, with formation of larger aggregates (119.5 nm) at pH 10. In alkaline conditions, O-H bands of hydroxyl groups possess certain acid character and reacts with basic ions which may halt the rate of nanoparticle synthesis leading to high particle size (Mata et al. 2009). Similar pattern of rate of nanoparticle synthesis was observed in acidic medium with particle size growing with more acidic conditions. The observation can be explained by the fact that in acidic conditions, hydroxyl groups behave as weak bases due to the unshared pairs of electrons in the oxygen atom and subsequently protonated. Protonated hydroxyl groups can be transformed into carbo-cations which decrease the reducing ability and hence rate of nanoparticle synthesis (Davis et al. 2003). The presence of other reducing groups on protein molecules such as sulfhydryl (-SH) may also be involved in nanoparticle synthesis and generally follows a similar chemical behaviour in various pH environments (Grzelczak et al. 2008).

Table 3.1 Effect of pH on particle size of silver nanoparticles synthesized using *Aspergillus flavus* isolate NJP08.

pH	Particle size (d.nm)	Polydispersity index (PDI)
2.0	353.8 ± 15.2	0.216 ± 0.04
4.0	444.3 ± 10.5	0.479 ± 0.08
5.0	253.1 ± 11.9	0.504 ± 0.04
6.0	92.4 ± 7.9	0.348 ± 0.07
7.0	42.8 ± 6.4	0.194 ± 0.02
8.0	73.8 ± 3.7	0.250 ± 0.11
10.0	119.5 ± 5.1	0.226 ± 0.06

The effect of salt concentration on particle size of silver nanoparticles synthesized using *Aspergillus flavus* isolate NJP08 was also investigated. The salt concentration was studied in the range of 0.5 to 5.0 mM by varying the initial concentration of precursor silver ions. As shown in Table 3.2, salt concentration played an important role in controlling the size of silver nanoparticles. The smallest nanoparticles (49.5 nm) were observed at an initial salt concentration of 1.0 mM while higher salt concentrations tend to promote aggregates formation resulting in particle size above >100 nm. The PDI index was found to be consistently lower than 0.5 indicating high mono-dispersity. These observations were consistent with the previous reports which demonstrated a change in particle size of gold nanoparticles with different concentrations of HAuCl₄ solution (Grzelczak et al. 2008, Pimprikar et al. 2009).

Various amount of biomass were suspended in 100 mL of de-ionized water to evaluate the effect of the secretory protein content on nanoparticle synthesis. A positive correlation was observed between the suspended biomass and obtained protein content. At low protein content in reaction medium (4:100, biomass: water ratio), the particle size obtained was found to be maximum (321.8 nm) which suggests the significant role of secretory proteins in stabilization of nanoparticles (Table 3.3). The optimum ratio was found to be 10:100 (biomass: water) at which minimum size (48.4 nm) of nanoparticles was obtained. With the increase in concentration of protein content, particle size was also found to be increased which may be due to the higher deposition of protein layers on nanoparticle surface (Nel et al. 2009, Monopoli et al. 2010, Walkey and Chan 2012). The role of proteins for stabilization of nanoparticles during biological synthesis process has been well documented (Shaligram et al. 2009, Suresh et al. 2010, Duran et al. 2011). Moreover, it has been demonstrated that the size of nanoparticles can be consistently controlled by keeping the varying amount of seed (protein in the present case) and salt concentration constant (Perez-Juste et al. 2005).

Table 3.2 Effect of salt concentration on particle size of silver nanoparticles synthesized using *Aspergillus flavus* isolate NJP08.

Salt concentration (mM)	Particle size (d.nm)	Polydispersity index (PDI)
0.5	87.6 ± 7.2	0.248 ± 0.04
1.0	49.5 ± 6.7	0.224 ± 0.06
2.0	115.1 ± 5.9	0.236 ± 0.03
3.0	117.3 ± 6.8	0.214 ± 0.01
4.0	136.9 ± 8.4	0.286 ± 0.04
5.0	155.7 ± 9.6	0.224 ± 0.08

Table 3.3 Effect of biomass on particle size of silver nanoparticles synthesized using *Aspergillus flavus* isolate NJP08.

Biomass (g) to water (ml) ratio	Protein content ($\mu\text{g mL}^{-1}$)	Particle size (d.nm)	Polydispersity index (PDI)
4:100	184.4 ± 5.7	321.8 ± 13.2	0.326 ± 0.04
6:100	284.7 ± 2.4	148.5 ± 9.8	0.294 ± 0.05
8:100	403.4 ± 4.6	84.4 ± 6.6	0.198 ± 0.04
10:100	513.4 ± 1.2	48.4 ± 3.8	0.126 ± 0.04
12:100	521.4 ± 6.4	54.5 ± 4.9	0.254 ± 0.02
15:100	544.2 ± 4.8	59.7 ± 5.1	0.292 ± 0.07
20:100	587.9 ± 5.9	61.5 ± 3.7	0.341 ± 0.08

3.3.3 Extracellular synthesis of silver nanoparticles using *Aspergillus* sp. isolate NJP02

3.3.3.1 Characterization of silver nanoparticles

Similar to fungus *Aspergillus flavus* isolate NJP08, the extracellular synthesis of silver nanoparticles using cell-free filtrate of fungus *Aspergillus* sp. isolate NJP02 was performed. A gradual change in colour of reaction medium (containing fungal cell-free filtrate and precursor silver ions) from colourless to reddish brown provided a visual evidence for formation of silver nanoparticles (Figure 3.12a). UV-visible spectra (Figure 3.12b) showed a gradual increase in absorbance at ca. 429 nm with respect to time of reaction. The absorption maxima at 429 nm can be attributed to the surface plasmon resonance vibrations of synthesized silver nanoparticles (Lu et al. 2009). No further increase in absorbance was observed after 72 h of reaction, which indicated the complete reduction of precursor silver ions in reaction medium (Inset to figure 3.12b). Stability of as-synthesized silver nanoparticles was monitored periodically for more than three months of completion of reaction.

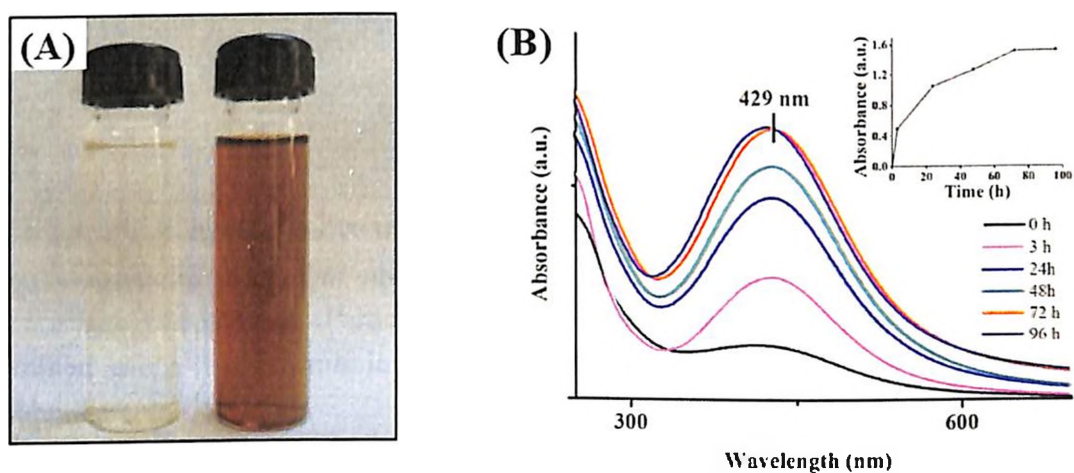


Figure 3.12 (a) Visual assessment showing change in color of the fungal cell-free filtrate without (left) and with (right) silver nitrate solution after 72 h of reaction. (b) UV-visible spectrum of silver nanoparticles recorded from the reaction medium as a function of time. Inset showing saturation curve of silver nanoparticle synthesis with function of time.

Transmission electron microscopy measurements were carried out to determine the size and morphology of silver nanoparticles. TEM micrograph (Figure 3.13a) revealed the presence of homogenous, nearly mono-dispersed and predominantly spherical shaped particles with individual nanoparticles surrounded by a thick protein layer. Inset to Figure 3.13a shows selected area electron diffraction (SAD) pattern recorded from a single silver nanoparticle which indicated the crystalline phase (111) of silver nanoparticles. The calculated particle size distribution based on TEM micrographs revealed particle size in the range of 40-80 nm with a mean diameter of 54 ± 2.3 nm (Figure 3.13b) which were consistent with the results obtained in dynamic light scattering measurements (Figure 3.13c). The particles were found to be bigger in size as compared to those obtained with fungus *Aspergillus flavus* isolate NJP08. Previous reports also demonstrated that different fungi

synthesize nanoparticles of varied sizes and shapes which may be due to the differences in their extracellular protein profiles (Shankar et al. 2003, Gericke and Pinches 2006, Vigneshwaran et al. 2006).

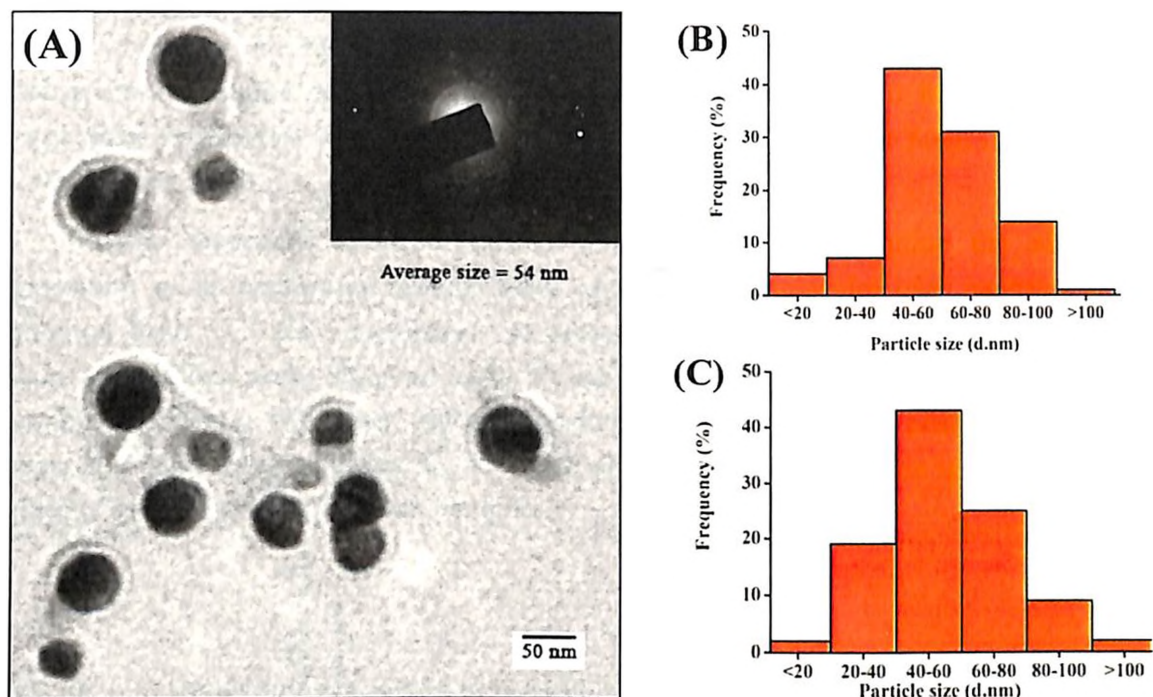


Figure 3.13 (a) A representative transmission electron micrograph showing spherical shaped silver nanoparticles (*scale bar* equivalent to 50 nm). Inset showing SAD pattern recorded from a single nanoparticle. Particle size distribution histogram of silver nanoparticles as determined using (b) transmission electron microscope and (c) dynamic light scattering measurements.

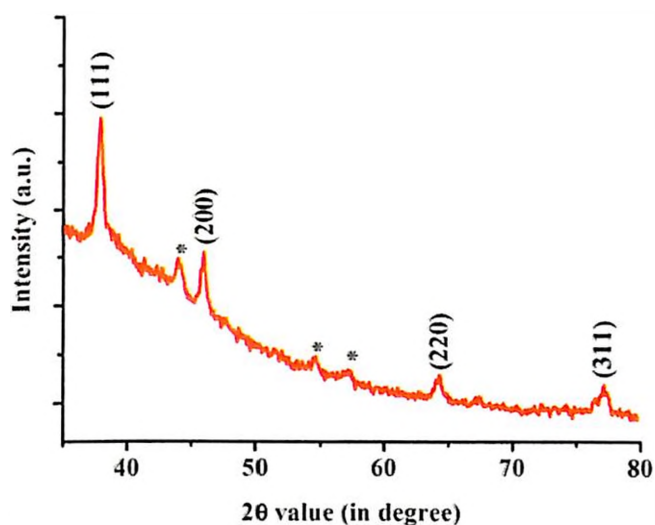


Figure 3.14 XRD spectrum of as-synthesized protein-capped silver nanoparticles recorded in the 2θ range of 30° - 80° (* indicates peaks due to the capping molecules).

X-ray diffraction pattern recorded by preparing drop-coated films of protein-capped silver nanoparticles further validated the crystalline nature of as-synthesized silver

nanoparticles. The well-defined peaks at 2θ values of 38.03° , 46.18° , 64.60° , and 77.18° corresponds to (111), (200), (220) and (311) planes of silver, respectively (Figure 3.14). These values were in complete agreement with the face-centered cubic (fcc) lattice structure of crystalline silver (JCPDS file no. 04-0783). The presence of other peaks (marked with asterisk) could be attributed to protein molecules present on the surface of silver nanoparticles. A similar pattern of XRD spectrum has been observed for metallic silver nanoparticles synthesized by *Aspergillus flavus* isolate NJP08 and other fungi (Shaligram et al. 2009, Jain et al. 2011).

Energy dispersive spectrum (EDS) was recorded to determine the elemental composition of as-synthesized nanoparticles and capping molecules. An intense optical absorption band at 3 KeV confirmed the presence of pure metallic silver nanoparticles (Figure 3.15). Other peaks observed for C, N and O atoms indicated the presence of proteins as capping molecules. Moreover, higher intensities of protein attributed peaks (C and O) as compared to silver peak indicated the presence of large number of protein molecules on the surface of as-synthesized silver nanoparticles.

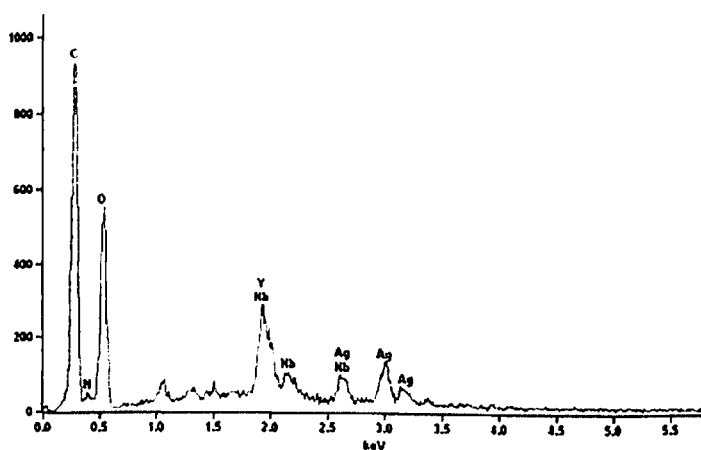


Figure 3.15 Energy dispersive spectrum showing the elemental composition of silver nanoparticles.

3.3.3.2 Characterization of capping molecules

The as-synthesized silver nanoparticles were boiled in 1% SDS solution to remove thick protein shell resulting in preparation of bare silver nanoparticles (no protein shell). FTIR and photoluminescence (PL) measurements of protein-capped and bare silver nanoparticles were carried out to confirm the removal of capping proteins from the surface of silver nanoparticles. FTIR spectrum of protein-capped silver nanoparticles (Figure 3.16a) exhibits characteristic bands of amide I and amide II at wavenumbers 1651 and 1539 cm^{-1} , respectively. These band positions were found to be similar to silver nanoparticle synthesized using *Aspergillus flavus* isolate NJP08. (Jain et al. 2011). The disappearance of these characteristic protein bands in the FTIR spectrum of bare silver nanoparticles indicated the removal of proteins from the surface of silver nanoparticles. With an excitation wavelength of 280 nm , the PL spectrum of bare silver nanoparticles (Figure 3.16b) showed no fluorescence

(emission peak) which clearly indicated the complete removal of protein molecules in case of bare silver nanoparticles. In contrast, PL spectrum of protein-capped silver nanoparticles showed a distinct emission peak at 340 nm under similar conditions, which could be attributed to the tyrosine residues of capping proteins.

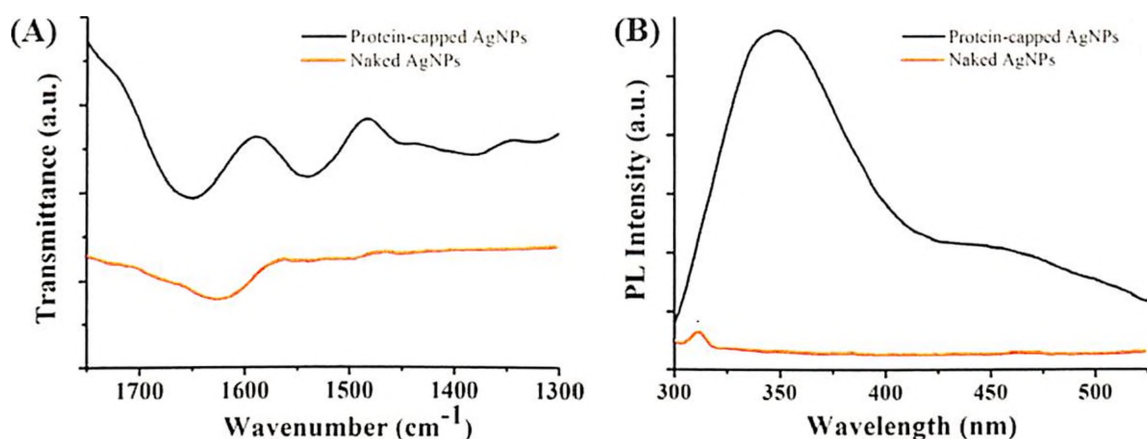


Figure 3.16 (a) FTIR spectra and (b) photoluminescence spectra of protein-capped and bare silver nanoparticles.

As the values of surface plasmon resonance vibration depends on the size of nanoparticles, UV-visible spectroscopy measurements were performed to evaluate the change in size of nanoparticles occurring due to removal of protein corona after SDS treatment. Comparison of UV-visible spectra showed a blue shift from 429 to 425 nm in case of bare silver nanoparticle spectrum which confirmed the reduction in size of silver nanoparticles after the SDS treatment (Figure 3.17a). This observation was in agreement with the absorbance shift observed during the ubiquitin-gold nanoparticle binding studies (Calzolari et al. 2010). Furthermore, hydrodynamic particle size distribution analysis was carried out to investigate the occupancy of protein corona on protein-capped silver nanoparticles. Protein-capped silver nanoparticles showed a mean particle size of 90.53 nm which decreased to 58.39 nm indicating the successful removal of protein corona from the surface of silver nanoparticles (Figure 3.17b). Based on the equation mentioned earlier, a maximum number of ~4300 protein molecules per nanoparticle were calculated which may form a multi-layered protein corona (32 nm thick) on the surface of silver nanoparticles. The plausible reason for multi-layered corona could be the non-specific and non-competitive binding of proteins present in the surrounding environment (reaction medium). The persistence of thick protein corona on biogenic silver nanoparticles has attracted our attention to compare the antibacterial efficacy of protein-capped silver nanoparticles in comparison to bare silver nanoparticles. The detailed description is presented in Chapter V of the present thesis.

The proteins separated from the surface of silver nanoparticles synthesized using *Aspergillus* sp. isolate NJP02 were further resolved on a 12% resolving SDS-PAGE gel (Figure 3.18). The capping proteins obtained after SDS treatment on as-synthesized silver nanoparticles are shown in Figure 3.18, lane 2. A number of protein bands were observed

with high abundance (thick nature of bands) suggesting the presence of thick protein corona on the surface of silver nanoparticles. The results are in complete agreement with DLS measurements which also indicated the presence of multi-layered protein corona on the surface of silver nanoparticles. The observation suggest that the recognition and binding of secreted proteins of fungus *Aspergillus* sp. isolate NJP02 on the surface of nanoparticles were non-specific in nature. Previous studies also demonstrated that the amount and presentation of proteins largely define the protein-nanoparticle interactions which plays a key role in formation of protein shell on the nanoparticle surface (Lynch and Dawson 2008, Lynch et al. 2009, Calzolari et al. 2010, Mahmoudi et al. 2011).

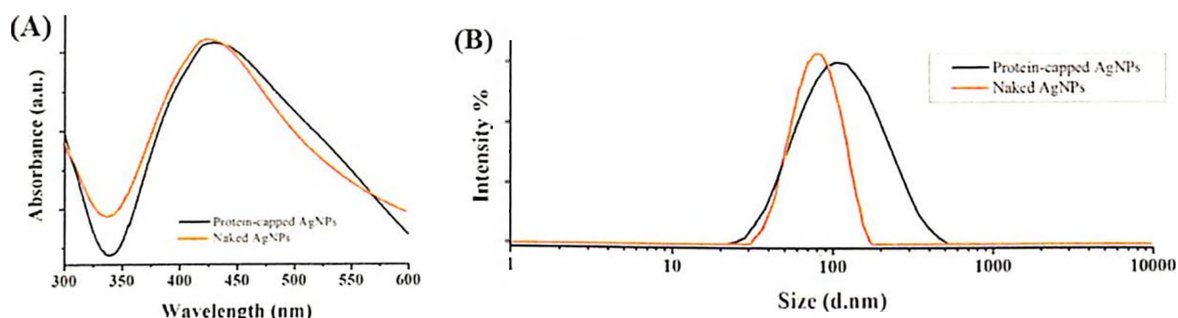


Figure 3.17 (a) UV visible spectra and (b) particle size distribution of protein-capped and bare silver nanoparticles.

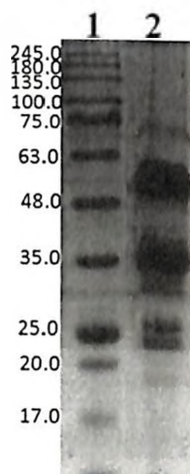


Figure 3.18 SDS-PAGE showing the capping proteins present on the surface of silver nanoparticles synthesized using fungus *Aspergillus* sp. isolate NJP02. Lane 1: standard protein molecular weight marker; Lane 2: capping proteins obtained after treating silver nanoparticles with SDS solution.

3.3.4 Optimization of silver nanoparticles using *Aspergillus* sp. isolate NJP02

To achieve strict control over size of nanoparticles during synthesis process, the initial pH of the reaction medium was varied in the range of 2-10. It has been observed that silver nanoparticle synthesis near neutral pH value (pH 7-8) had minimum nanoparticle size (64.3 - 87.9 nm). In contrast, the synthesis of nanoparticles was highly unfavourable at acidic pH conditions which may be due to instability of proteins which are responsible for nanoparticle

synthesis and stabilization (Table 3.4). Studies using fungus *Aspergillus oryzae* var. *viridis* also demonstrated that acidic pH was unfavourable for production of gold nanoparticles (Binupriya et al. 2010). A similar effect of pH variation on synthesis of silver nanoparticles was also observed using fungus *Aspergillus flavus* isolate NJP08 as mentioned earlier (section 3.3.2).

Table 3.4 Effect of pH on particle size of silver nanoparticles synthesized using *Aspergillus* sp. isolate NJP02.

pH	Particle size (d.nm)	PDI
2.0	1653.5 ± 31.4	0.875 ± 0.09
4.0	1688.1 ± 27.2	0.639 ± 0.10
5.0	793.7 ± 13.7	0.414 ± 0.05
6.0	312.2 ± 7.8	0.359 ± 0.03
7.0	87.9 ± 4.1	0.203 ± 0.02
8.0	64.3 ± 5.4	0.148 ± 0.04
10.0	144.0 ± 9.8	0.215 ± 0.03

Similar to pH studies, varying salt concentration in the reaction medium influenced the size of silver nanoparticles. The salt concentration in the range of 1.0 to 2.0 mM resulted in small size of nanoparticles while higher salt concentrations led to the formation of aggregates (Table 3.5). However, no significant variation in PDI values was noted suggesting that salt concentration does not play an important role in controlling mono-dispersity of nanoparticles.

Table 3.5 Effect of salt concentration on particle size of silver nanoparticles synthesized using *Aspergillus* sp. isolate NJP02.

Salt concentration (mM)	Particle size (d.nm)	PDI
0.5	235.8 ± 41.9	0.479 ± 0.03
1.0	82.0 ± 9.8	0.385 ± 0.03
2.0	98.2 ± 6.9	0.380 ± 0.08
3.0	162.3 ± 12.6	0.404 ± 0.02
4.0	282.5 ± 13.5	0.310 ± 0.05
5.0	380.7 ± 22.6	0.393 ± 0.07

In a biological synthesis process, the role of proteins in synthesis and stabilization of nanoparticles is well characterized. Hence, variation in initial biomass content was tested to attain various protein concentrations and to investigate their effect on size of silver nanoparticles. As shown in Table 3.6, at lowest protein concentration (179.6 µg mL⁻¹), the particle size of silver nanoparticles was found to be maximum (784.6 nm). However, increase in protein content makes the nanoparticle synthesis process more controlled which results in mono-dispersed silver nanoparticles of uniform size. This observation clearly suggests that the process of nanoparticle synthesis is controlled by the proteins present in the reaction

medium. A deeper understanding of the nanoparticle synthesis mechanism is presented in the chapter IV of the thesis.

Table 3.6 Effect of biomass on particle size of silver nanoparticles synthesized using *Aspergillus* sp. isolate NJP02.

Biomass (g) to water (ml) ratio	Protein content ($\mu\text{g mL}^{-1}$)	Particle size (d.nm)	PDI
4:100	179.6 \pm 3.4	784.6 \pm 38.3	0.465 \pm 0.07
6:100	251.8 \pm 0.8	485.4 \pm 21.5	0.387 \pm 0.04
8:100	347.1 \pm 4.1	113.2 \pm 9.6	0.148 \pm 0.08
10:100	458.2 \pm 2.8	84.6 \pm 5.8	0.239 \pm 0.06
12:100	471.7 \pm 5.4	85.7 \pm 3.2	0.254 \pm 0.03
15:100	497.4 \pm 8.7	86.9 \pm 1.9	0.266 \pm 0.04
20:100	512.1 \pm 6.9	89.1 \pm 3.4	0.231 \pm 0.07

3.4 Conclusions

The present chapter demonstrates a biomimetic approach to utilize indigenous metal tolerant fungi for synthesis of silver nanoparticles. An eco-friendly and low cost protocol for extra-cellular biosynthesis of silver nanoparticles has been demonstrated by two metal tolerant fungal isolates namely *Aspergillus flavus* isolate NJP08 and *Aspergillus* sp. isolate NJP02. The extra-cellular proteins of both the fungal isolates could be able to reduce the precursor silver ions and synthesize silver nanoparticles. The particles were found to be homogenous, pre-dominantly spherical and monodispersed in both the cases. Smaller size of nanoparticles (17 ± 5.9 nm) was observed in case of *Aspergillus flavus* NJP08, while comparatively bigger particles (54 ± 2.3 nm) were observed in case of *Aspergillus* sp. NJP02. The particles were found to be covered by a thick protein corona in the latter case. The possibility of proteins as stabilizing agents in silver nanoparticles as well as their subsequent removal was revealed by UV-visible spectroscopy, fourier transform infrared spectroscopy (FTIR) and photoluminescence (PL) analysis. A theoretically calculated number of ~ 120 protein molecules per nanoparticle were present on nanoparticles synthesized by *Aspergillus flavus* NJP08, while this number was ~ 4300 on nanoparticles synthesized by *Aspergillus* sp. NJP02. These results revealed that the larger size of nanoparticles was due to the presence of multi-layered protein corona in the latter case.

3.5 References

- Ahmad, A., Mukherjee, P., Senapati, S., Mandal, D., Khan, M. I., Kumar, R. and Sastry, M. (2003). Extracellular biosynthesis of silver nanoparticles using the fungus *Fusarium oxysporum*. *Colloids and Surfaces, B: Biointerfaces* **28**: 313-318.
- Amendola, V. and Meneghetti, M. (2009). Laser ablation synthesis in solution and size manipulation of noble metal nanoparticles. *Physical Chemistry Chemical Physics* **11**: 3805-3821.

- Bhainsa, K. C. and D'Souza, S. (2006). Extracellular biosynthesis of silver nanoparticles using the fungus *Aspergillus fumigatus*. *Colloids and Surfaces B: Biointerfaces* **47**: 160-164.
- Bhushan, B., Ed. (2004). Springer Handbook of Nanotechnology. Berlin, Heidelberg, Spinger-Verlag.
- Binupriya, A. R., Sathishkumar, M., Vijayaraghavan, K. and Yun, S. I. (2010). Bioreduction of trivalent aurum to nano-crystalline gold particles by active and inactive cells and cell-free extract of *Aspergillus oryzae* var. *viridis*. *Journal of Hazardous Materials* **177**: 539-545.
- Blum, A. S., Soto, C. M., Wilson, C. D., Cole, J. D., Kim, M., Gnade, B., Chatterji, A., Ochoa, W. F., Lin, T. and Johnson, J. E. (2004). Cowpea mosaic virus as a scaffold for 3-D patterning of gold nanoparticles. *Nano Letters* **4**: 867-870.
- Calzolari, L., Franchini, F., Gilliland, D. and Rossi, F. (2010). Protein-nanoparticle interaction: identification of the ubiquitin-gold nanoparticle interaction site. *Nano Letters* **10**: 3101-3105.
- Chen, S. and Carroll, D. L. (2002). Synthesis and characterization of truncated triangular silver nanoplates. *Nano Letters* **2**: 1003-1007.
- Chen, X. and Schluesener, H. (2008). Nanosilver: A nanoproduct in medical application. *Toxicology Letters* **176**: 1-12.
- Colombo, M., Mazzucchelli, S., Collico, V., Avvakumova, S., Pandolfi, L., Corsi, F., Porta, F. and Prosperi, D. (2012). Protein-assisted one-pot synthesis and biofunctionalization of spherical gold nanoparticles for selective targeting of cancer cells. *Angewandte Chemie* **124**: 9406-9409.
- Davis, T. A., Volesky, B. and Mucci, A. (2003). A review of the biochemistry of heavy metal biosorption by brown algae. *Water Research* **37**: 4311-4330.
- Duran, N., Marcato, P. D., Duran, M., Yadav, A., Gade, A. and Rai, M. (2011). Mechanistic aspects in the biogenic synthesis of extracellular metal nanoparticles by peptides, bacteria, fungi, and plants. *Applied Microbiology and Biotechnology* **90**: 1609-1624.
- Gericke, M. and Pinches, A. (2006). Biological synthesis of metal nanoparticles. *Hydrometallurgy* **83**: 132-140.
- Ghorbani, H. R., Safekordi, A. A., Attar, H. and Sorkhabadi, S. (2011). Biological and non-biological methods for silver nanoparticles synthesis. *Chemical and Biochemical Engineering Quarterly* **25**: 317-326.
- Gole, A., Dash, C., Ramakrishnan, V., Sainkar, S., Mandale, A., Rao, M. and Sastry, M. (2001). Pepsin-gold colloid conjugates: preparation, characterization, and enzymatic activity. *Langmuir* **17**: 1674-1679.
- Grzelczak, M., Pérez-Juste, J., Mulvaney, P. and Liz-Marzán, L. M. (2008). Shape control in gold nanoparticle synthesis. *Chemical Society Reviews* **37**: 1783-1791.
- Gurunathan, S., Kalishwaralal, K., Vaidyanathan, R., Deepak, V., Pandian, S. R. K., Muniyandi, J., Hariharan, N. and Eom, S. H. (2009). Biosynthesis, purification and

- characterization of silver nanoparticles using *Escherichia coli*. *Colloids and Surfaces, B: Biointerfaces* **74**: 328-335.
- Jain, N., Bhargava, A., Majumdar, S., Tarafdar, J. C. and Panwar, J. (2011). Extracellular biosynthesis and characterization of silver nanoparticles using *Aspergillus flavus* NJP08: A mechanism perspective. *Nanoscale* **3**: 635-641.
- Kowshik, M., Ashtaputre, S., Kharrazi, S., Vogel, W., Urban, J., Kulkarni, S. K. and Paknikar, K. M. (2003). Extracellular synthesis of silver nanoparticles by a silver-tolerant yeast strain MKY3. *Nanotechnology* **14**: 95-100.
- Laemmli, U. K. (1970). Cleavage of structural proteins during the assembly of the head of bacteriophage T4. *Nature* **227**: 680-685.
- Li, X., Wang, L. and Lu, X. (2010). Preparation of silver-modified TiO₂ via microwave-assisted method and its photocatalytic activity for toluene degradation. *Journal of Hazardous Materials* **177**: 639-647.
- Lowry, O. H., Rosebrough, N. J., Farr, A. L. and Randall, R. J. (1951). Protein measurement with the Folin phenol reagent. *Journal of Biological Chemistry* **193**: 265-275.
- Lu, X., Rycenga, M., Skrabalak, S. E., Wiley, B. and Xia, Y. (2009). Chemical synthesis of novel plasmonic nanoparticles. *Annual Review of Physical Chemistry* **60**: 167-192.
- Lynch, I. and Dawson, K. (2008). Protein-nanoparticle interactions. *Nano Today* **3**: 40-47.
- Lynch, I., Salvati, A. and Dawson, K. A. (2009). Protein-nanoparticle interactions: what does the cell see? *Nature Nanotechnology* **4**: 546-547.
- Mafune, F., Kohno, J., Takeda, Y., Kondow, T. and Sawabe, H. (2000). Structure and stability of silver nanoparticles in aqueous solution produced by laser ablation. *Journal of Physical Chemistry B* **104**: 8333-8337.
- Magudapathy, P., Gangopadhyay, P., Panigrahi, B., Nair, K. and Dhara, S. (2001). Electrical transport studies of Ag nanoclusters embedded in glass matrix. *Physica B: Condensed Matter* **299**: 142-146.
- Mahmoudi, M., Lynch, I., Ejtehadi, M. R., Monopoli, M. P., Bombelli, F. B. and Laurent, S. (2011). Protein-nanoparticle interactions: opportunities and challenges. *Chemical Reviews* **111**: 5610-5637.
- Mata, Y., Torres, E., Blazquez, M., Ballester, A., González, F. and Muñoz, J. (2009). Gold (III) biosorption and bioreduction with the brown alga *Fucus vesiculosus*. *Journal of Hazardous Materials* **166**: 612-618.
- Monopoli, M. P., Bombelli, F. B. and Dawson, K. A. (2010). Nanobiotechnology: nanoparticle coronas take shape. *Nature Nanotechnology* **6**: 11-12.
- Mukherjee, P., Ahmad, A., Mandal, D., Senapati, S., Sainkar, S. R., Khan, M. I., Parishcha, R., Ajaykumar, P., Alam, M. and Kumar, R. (2001). Fungus-mediated synthesis of silver nanoparticles and their immobilization in the mycelial matrix: a novel biological approach to nanoparticle synthesis. *Nano Letters* **1**: 515-519.

- Nangia, Y., Wangoo, N., Sharma, S., Wu, J.-S., Dravid, V., Shekhawat, G. S. and Suri, C. R. (2009). Facile biosynthesis of phosphate capped gold nanoparticles by a bacterial isolate *Stenotrophomonas maltophilia*. *Applied Physics Letters* **94**: 233901-233903.
- Nel, A. E., Madler, L., Velegol, D., Xia, T., Hoek, E. M., Somasundaran, P., Klaessig, F., Castranova, V. and Thompson, M. (2009). Understanding biophysicochemical interactions at the nano-bio interface. *Nature Materials* **8**: 543-557.
- Perez-Juste, J., Pastoriza-Santos, I., Liz-Marzan, L. M. and Mulvaney, P. (2005). Gold nanorods: synthesis, characterization and applications. *Coordination Chemistry Reviews* **249**: 1870-1901.
- Peter Amaladhas, T., Sivagami, S., Akkini Devi, T., Ananthi, N. and Priya Velammal, S. (2012). Biogenic synthesis of silver nanoparticles by leaf extract of *Cassia angustifolia*. *Advances in Natural Sciences: Nanoscience and Nanotechnology* **3**: 045006.
- Petit, C., Lixon, P. and Pileni, M. P. (1993). *In situ* synthesis of silver nanocluster in AOT reverse micelles. *The Journal of Physical Chemistry* **97**: 12974-12983.
- Pimprikar, P., Joshi, S., Kumar, A., Zinjarde, S. and Kulkarni, S. (2009). Influence of biomass and gold salt concentration on nanoparticle synthesis by the tropical marine yeast *Yarrowia lipolytica* NCIM 3589. *Colloids and Surfaces B: Biointerfaces* **74**: 309-316.
- Pol, V. G., Srivastava, D., Palchik, O., Palchik, V., Slifkin, M., Weiss, A. and Gedanken, A. (2002). Sonochemical deposition of silver nanoparticles on silica spheres. *Langmuir* **18**: 3352-3357.
- Roco, M. C. (2005). Environmentally responsible development of nanotechnology. *Environmental Science & Technology* **39**: 106-112.
- Saifuddin, N., Wong, C. and Yasumira, A. (2009). Rapid biosynthesis of silver nanoparticles using culture supernatant of bacteria with microwave irradiation. *Journal of Chemistry* **6**: 61-70.
- Scholars, W. W. I. C. f. (2013). Nanotechnology consumer products inventory. Retrieved 25-10-2013, from <http://www.nanotechproject.org/cpi/>.
- Shaligram, N., Bule, M., Bhambure, R., Singhal, R., Singh, S., Szakacs, G. and Pandey, A. (2009). Biosynthesis of silver nanoparticles using aqueous extract from the compactin producing fungal strain. *Process Biochemistry* **44**: 939-943.
- Shaligram, N. S., Bule, M., Bhambure, R., Singhal, R. S., Singh, S. K., Szakacs, G. and Pandey, A. (2009). Biosynthesis of silver nanoparticles using aqueous extract from the compactin producing fungal strain. *Process Biochemistry* **44**: 939-943.
- Shankar, S. S., Ahmad, A., Pasricha, R. and Sastry, M. (2003). Bioreduction of chloroaurate ions by geranium leaves and its endophytic fungus yields gold nanoparticles of different shapes. *Journal of Materials Chemistry* **13**: 1822-1826.
- Sharma, V. K., Yngard, R. A. and Lin, Y. (2009). Silver nanoparticles: green synthesis and their antimicrobial activities. *Advances in Colloid and Interface Science* **145**: 83-96.

- Solanki, J. N. and Murthy, Z. (2010). Highly monodisperse and sub-nano silver particles synthesis via microemulsion technique. *Colloids and Surfaces A: Physicochemical and Engineering Aspects* **359**: 31-38.
- Suresh, A. K., Pelletier, D. A., Wang, W., Moon, J. W., Gu, B. H., Mortensen, N. P., Allison, D. P., Joy, D. C., Phelps, T. J. and Doktycz, M. J. (2010). Silver nanocrystallites: biofabrication using *Shewanella oneidensis*, and an evaluation of their comparative toxicity on gram-negative and gram-positive bacteria. *Environmental Science & Technology* **44**: 5210-5215.
- Sweeney, R. Y., Mao, C. B., Gao, X. X., Burt, J. L., Belcher, A. M., Georgiou, G. and Iverson, B. L. (2004). Bacterial biosynthesis of cadmium sulfide nanocrystals. *Chemistry & Biology* **11**: 1553-1559.
- Taajamaa, L., Rojas, O. J., Laine, J., Yliniemi, K. and Kontturi, E. (2013). Protein-assisted 2D assembly of gold nanoparticles on a polysaccharide surface. *Chemical Communications* **49**: 1318-1320.
- Tolaymat, T. M., El Badawy, A. M., Genaidy, A., Scheckel, K. G., Luxton, T. P. and Suidan, M. (2010). An evidence-based environmental perspective of manufactured silver nanoparticle in syntheses and applications: A systematic review and critical appraisal of peer-reviewed scientific papers. *Science of the Total Environment* **408**: 999-1006.
- Vigneshwaran, N., Kathe, A. A., Varadarajan, P., Nachane, R. P. and Balasubramanya, R. (2006). Biomimetics of silver nanoparticles by white rot fungus, *Phaenerochaete chrysosporium*. *Colloids and Surfaces B: Biointerfaces* **53**: 55-59.
- Walkey, C. D. and Chan, W. C. W. (2012). Understanding and controlling the interaction of nanomaterials with proteins in a physiological environment. *Chemical Society Reviews* **41**: 2780-2799.
- Wigginton, N. S., Titta, A. d., Piccapietra, F., Dobias, J., Nesatyy, V. J., Suter, M. J. and Bernier-Latmani, R. (2010). Binding of silver nanoparticles to bacterial proteins depends on surface modifications and inhibits enzymatic activity. *Environmental Science & Technology* **44**: 2163-2168.
- Xie, J., Lee, J. Y., Wang, D. I. C. and Ting, Y. P. (2007). Silver nanoplates: from biological to biomimetic synthesis. *ACS Nano* **1**: 429-439.
- Zhang, M. (2013). Fungus-based nanoparticles: inspiration from nature for cancer therapy. *Nanomedicine* **8**: 313-316.

Chapter IV

Understanding Mechanism of Silver Nanoparticles Biosynthesis and Associated Protein-Nanoparticle Interactions

The present chapter deals with studies attempted to decipher the “bioactive molecules” involved in the synthesis of silver nanoparticles by fungus *Aspergillus flavus* isolate NJP08. Protein profiling, systematic separation and subsequent screening of individual protein for their potential towards synthesis of silver nanoparticles has been carried out. A protein with a molecular mass of ca. 33kDa was found to execute the “dual function” of silver reduction as well as stabilization and identified as “alkaline protease”. The effect of silver nanoparticle binding on the structure and function of alkaline protease was investigated. Further, based on homology approach, the three dimensional structure was constructed to decipher the binding site of silver nanoparticle on protease and related protein-nanoparticle interactions. Brownian dynamics simulations of the protease-Ag(111) complex showed that the protease binding to silver nanoparticles is highly specific with involvement of four amino acid residues viz. Tyr59, Ser107, Asp111 and Asn118. To the best of our knowledge, this is the first attempt which identifies a structural configuration among aspartic residues and silver nanoparticles. The obtained knowledge of protein-nanoparticle interactions can be exploited for the design and development of future bio-scaffolds to achieve mass scale production of nanoparticles.

4.1 Introduction

From a scientific point of view, the potential of biological synthesis of nanoparticles is yet to realize its full potential and is limited only by our imagination. It has been experimentally demonstrated that various biological entities such as cells, enzymes and peptides can reduce the metal ions leading to the formation of nanoparticles. The detailed mechanisms of the processes are not well understood, however, it has been predicted that the conformation, overall charge, and functional groups of biomolecules may all contribute to biological reduction (Nam et al. 2008). A large proportion of efforts have explored the use of microorganisms to synthesize nanoparticles under conditions similar to those encountered in nature. As mentioned earlier in the Chapter III, fungi have emerged as potential candidates for biosynthesis of nanoparticles because of their ease in handling, low cost of maintenance as well as easy downstream processing. Being eukaryote, fungi have been reported to secrete a versatile range of extracellular components in higher amounts as compared to prokaryotic organisms. This might be helpful in achieving significantly higher and desired productivity of various nanoparticles (Dhillon et al. 2012).

Despite of the realization as well as establishment of the importance of fungus-mediated nanoparticle synthesis, the progress to uplift the process for mass scale synthesis of nanoparticles is still in its infancy. The major lacuna is lack of understanding of plausible mechanism(s) which includes identification and characterization of “bioactive” molecules that control the shape and crystal structure of nanoparticles as well as their stabilization behaviour. The extraction of these so-called “nucleating biomolecules” and the identification of materials specific biomolecules followed by elucidation of mechanism are of immense interest in the field of nano-biotechnology. The underlying mechanism can be applied to the synthesis of technologically important materials beyond those few existing biominerals in nature (Thakkar et al. 2010). Moreover, the pursuit to find molecules which can regulate self-assembly of nanoparticles with appropriate surface modification has been recently considered as an attractive area of research in the field of nanotechnology (Colombo et al. 2012).

An appreciable work has been attempted to elucidate the actual mechanism of nanoparticle synthesis by microorganisms. For instance, an elegant study by Klaus et al. (1999) on interactions of silver ions with bacterium *Pseudomonas stutzeri* demonstrated that the defensive mechanism for silver detoxification resulted in the synthesis of silver nanoparticles. Ahmad et al. (2003) had predicted the role of NADH-dependent enzymes for biosynthesis of nanoparticles using the fungus *Fusarium oxysporum*. The reduction mechanism was expected to be initiated by electron transfer from the NADH by NADH-dependent reductase as electron carrier. Further investigations with *Fusarium oxysporum* demonstrated that reduction of silver ions occurred by a nitrate-dependent reductase and a shuttle quinone extracellular process (Durán et al. 2005). It has been further validated that nitrate reductase enzyme system can be responsible for the bioreduction of silver ions which subsequently leads to formation of silver nanoparticles (Kumar et al. 2007). Studies on

biosynthesis of zirconia nanoparticles using fungus *Fusarium oxysporum* showed involvement of two cationic proteins of molecular masses around 24 and 28 kDa, which are rather similar in nature to silicatein (Bansal et al. 2004). Studies on a filamentous cyanobacterium, *Plectonema boryanum* UTEX 485 suggested that silver ions could be reduced by an intracellular electron donor or exported by a membrane transporter system (Lengke et al. 2007). The involvement of various proteins of oxido-reductive system and nuclear histone protein of *Chlamydomonas reinhardtii* in the biosynthesis and capping of silver nanoparticles has also been reported (Barwal et al. 2011). In Chapter III, we have also showed the possible role of fungal secreted proteins in bio-molecular reduction and stabilization of silver nanoparticles. Collectively, all the above mentioned reports suggest that proteins are the most likely “bioactive” molecules involved in nanoparticle synthesis using microbiological approach.

The use of proteins as a suitable template has been motivated in part by the desire to develop environmentally benign routes of nanoparticle synthesis as well as to exploit the highly specific binding interactions of peptides with nanoparticles (Smith et al. 2009). Synthesis of nanoparticles using proteins is very ideal because of their potential to perform “dual” function of reduction and stabilization. The approach offers an environmental footprint of carrying out the “green” synthesis at room temperature and at or near neutral pH in aqueous solution. Due to the biological origin of proteins, their presence on nanoparticle surface assures high bio-compatibility of synthesized nanoparticles. Additionally, natural occurrence of the large diversity of proteins and/or peptides available for use and exploration offers a new opportunity to organize, interact, and direct the shape, size, and structure evolution of the metal nanoparticles in more varied and innovative ways (Tan et al. 2010). Moreover, the prospect of executing modifications at biological (gene) and chemical level makes it a more attractive alternative.

Recent advances in biotechnology and proteomic approaches have made it possible to isolate and characterize specific proteins from natural organisms that are responsible for catalyzing inorganic reactions. Notable examples are the use of phage display to isolate peptides capable of mediating the formation of gold, silver, germanium, CoPt and TiO₂ nanoparticles (Naik et al. 2002a, 2002b, 2004, Dickerson et al. 2004, 2008, Naik and Stone 2005, Slocik et al. 2005, Crookes-Goodson et al. 2008, Shrinivas and Naik 2011). A similar interesting example is the use of RNA *in vitro* selection to isolate RNA sequences for the assembly of particles containing Pt and Pd (Gugliotti et al. 2005, Smith et al. 2009). The use of protein cavity (cage) for the growth of nanoparticles has also been considered as a suitable method for obtaining mono-dispersed nanoparticles (Kramer et al. 2004). The use of cowpea chlorotic mottle virus (CCMV) protein cage to fabricate polyoxometalate particles has been much appreciated (Douglas and Young 1998, 2006). As we learn more about the exquisite control that biomolecule templates can afford over the synthesis and placement of materials their applications are sure to expand.

Protein cages have been widely explored as a prominent platform to direct the synthesis of various inorganic nanomaterials. Protein cages are three-dimensional self-assemblies of highly similar or identical subunits, almost spherical in shape, which enclose a central cavity that is used for the physiological deposition of different materials (e.g., nucleic acids in viral capsids or ferric hydroxide micelles in ferritins) (Uchida et al. 2007). Ferritin is one of the most widely studied proteins with a cage-like structure. A variety of materials such as Fe_3O_4 , Co_3O_4 , Mn_3O_4 , Pt, CoPt, Pd, CdS, CdSe, ZnSe, CaCO_3 , SrCO_3 or BaCO_3 have been produced and characterized in different ferritin templates (Dickerson et al. 2008). The utilization of ferritin for synthesis of noble metal nanoparticles such as gold and silver nanoparticles has also been attempted. However, very low yields (~20-40%) in terms of a metal incorporated/added ratio were achieved (Kramer et al. 2004, Yoshizawa et al. 2006). Ferritin variants such as recombinant HuHFt and HuLFt have also been prepared, but efficient synthesis of silver nanoparticles was not achieved with these variants (Kasyutich et al. 2010). Hence, there is a need to search for novel proteins which can achieve synthesis of noble nanoparticles.

Another important interesting aspect of nanoparticle synthesis using proteins is the adsorption of proteins on the nanoparticles as a post-synthesis process resulting in the formation of “protein-capped” nanoparticles. Due to their relatively large surface-to-volume ratio, nanoparticles have tremendous adsorption capacity; therefore, they can adsorb protein molecules in greater capacity as compared to their bulk counterpart (Walkey and Chan 2012). The interaction of proteins with nanoparticles is not only a fundamental phenomenon but is also vital to several important and novel applications. In fact, protein-nanoparticle interactions have been considered as an integral part of the nanotechnology-based applications in biological systems and have been studied extensively.

In biological applications, nanoparticles tend to reduce their large surface energy by interaction with the medium components in which they are dispersed (Monopoli et al. 2010, 2011, 2012). Interestingly, it has been demonstrated that nanoparticles could facilitate the protein fibrillation process (Mahmoudi et al. 2013). An astute study by Linse et al. (2007) showed that nanoparticles such as cerium oxide, carbon nanotubes and poly(ethylene glycol)-coated quantum dots can enhance the rate of fibrillation of the amyloidogenic protein β -2-microglobulin under controlled conditions. Moreover, it has been observed that when a nanoparticle enters a physiological environment, its surface is immediately covered by a layer of proteins, forming what is known as the protein ‘corona’ (Lynch and Dawson 2008, Lynch et al. 2009). Formation of the protein corona on nanoparticle surface is a dynamic, competitive process and involves a competition among the proteins present in surrounding environment for the nanoparticle surface. The nano-protein interface evolves rapidly due to exchange of low-affinity high-abundance proteins (that bind immediately) by lower abundance proteins with a higher affinity for the nanoparticle surface, which is very similar to “Vroman effect” (Scott 1991). This Vroman-like effect has been well-studied by molecular

dynamics simulations to demonstrate the competitive protein adsorption on a nanoparticle surface (Vilaseca et al. 2013). A detailed mechanistic understanding of the protein-nanoparticle interactions would be of immense value to design novel biomedical applications. Moreover, the ability to tailor specific protein-surface interactions would benefit nanoscale materials and bio-nano-assembly technologies. We have attempted identification of “bioactive molecules” involved in the synthesis and stabilization of silver nanoparticles by fungus *Aspergillus flavus* isolate NJP08. Studies on associated protein-nanoparticle interactions were also performed.

4.2 Materials and methods

4.2.1 Preparation of fungal cell-free filtrate

The fungus *Aspergillus flavus* isolate NJP08 was inoculated in an Erlenmeyer flask containing 80 mL of MGY medium (0.3% malt extract, 1% glucose, 0.3% yeast extract, 0.5% peptone; pH 7.0) and incubated at 28 °C in an orbital shaker (150 rpm) under dark conditions. After 72 h, fungal mycelia were separated from the culture medium by centrifugation (8000 rpm, 10 min and 4 °C) and washed thrice with sterile water to remove all traces of media components. Typically, 10 g fungal biomass (fresh weight) was suspended to Erlenmeyer flasks containing 100 mL of sterile de-ionized water and further incubated for 72 h under the similar conditions as described above. After incubation, biomass was separated by filtration using filter paper No. 1 (Whatman; Merck Inc, Germany) and the fungal cell-free filtrate containing extracellular secretions was collected and stored at 4 °C until further use.

4.2.2 Protein estimation in fungal cell-free filtrate

Protein concentration was determined using bicinchoninic acid (BCA) method of Smith et al. (1985) using bovine serum albumin as standard. Briefly, fungal cell-free filtrate (100 µL) was added to 2 mL of BCA reagent and incubated at 37 °C for 10 min. Subsequently, absorbance was measured at 562 nm on a Jasco V-630 UV-visible spectrophotometer (Jasco Corporation, Japan) and the concentration of protein in sample was determined against a standard curve prepared using BSA.

4.2.3 Protein profiling of fungal cell-free filtrate

4.2.3.1 Ammonium sulphate precipitation

The protein precipitation was achieved by gradual addition of solid ammonium sulphate to the crude fungal cell-free filtrate containing extracellular secretions at a final concentration of 80% (w/v). The mixture was gently stirred overnight at 4 °C and the resulting precipitate was collected after centrifugation at 12000 rpm for 10 min at 4 °C. The protein pellet obtained thereafter was suspended in copious amount of sterile Milli-Q water and placed in a dialysis bag (12 kDa cut off) made up of cellulose acetate membrane. The bag containing proteins was immersed in 50 mM phosphate buffer (pH 7.2) and dialyzed gently for 24 h at 4 °C by repeated changing of the buffer. The dialysate was concentrated with Amicon centrifugal filter units and stored at -70 °C in aliquots.

4.2.3.2 One dimensional gel electrophoresis

One dimensional gel electrophoresis (SDS-PAGE) was carried out as per the standard protocol of Laemmli (1970). The electrophoresis was performed on a Mini Protean gel system (Bio-Rad, USA) by supplying a constant voltage of 120 V at room temperature. A 5% stacking gel and 12% separation gel were used for polyacrylamide gel electrophoresis. After electrophoresis, silver staining of the gels were carried out using ProteoSilver™ silver stain kit (Sigma-Aldrich, USA) and visualized under a Gel Doc XR System (BioRad, USA). The molecular mass of the protein bands were determined by interpolation from a linear logarithmic plot of relative molecular mass versus the R_f value (relative mobility).

4.2.3.3 Peptide mass fingerprinting by matrix-assisted laser desorption/ionization (MALDI) mass spectrometry

In-gel tryptic digestion was carried out as per standard procedure of Shevchenko et al. (1996) as follows. For this, protein-containing bands observed on SDS-PAGE were excised precisely using a scalpel to minimize the amount of polyacrylamide matrix. Blank gel pieces served as control for auto-digestion by trypsin and processed in parallel with the protein spots of interest. The gel pieces were incubated for at least 24 h in double distilled water with frequent water changes. Subsequently, bands were gently diced but not grounded and were dehydrated repeatedly with changes of acetonitrile (50% followed by 100%). The gel pieces were dried by lyophilisation for 30 min and incubated in digestion buffer containing 50 mM NH_4CO_3 , 5 mM CaCl_2 and trypsin in an ice-cold bath. The amount of trypsin added was 25 $\text{ng } \mu\text{l}^{-1}$ of buffer or $\sim 1 \mu\text{g}$ per band. A minimum reaction volume, sufficient for rehydration of the gel pieces was used. The tryptic cleavage fragments were eluted by centrifugation at 14,000 rpm for 5 min, extracted twice with 5% formic acid in 50% acetonitrile, dried by vacuum centrifugation, and stored at -20°C until further analysis.

The resultant tryptic digests were analysed using an Ultraflex MALDI/TOF instrument (Bruker Daltonics, Germany). For this, matrix α -Cyano-4-hydroxycinnamic acid (α -Cyano) was prepared using the following steps: a saturated solution of α -Cyano was prepared in 50% (v/v) acetonitrile and 0.1% (v/v) trifluoroacetic acid (TFA) in deionized water. The solution was then centrifuged to separate remaining insoluble α -Cyano at the bottom of tube. A thin layer of matrix was prepared by immediately transferring 2 μl of the supernatant (saturated α -Cyano solution) onto 600 μm anchors of an AnchorChip target plate (Bruker Daltonics, USA). The tryptic digest sample (0.5 μl) was then embedded onto the thin layered matrix with 2.5 μl of 0.1% (v/v) TFA for 1 min and further dried on a stainless steel target for analysis. The apparatus was set up with following parameters: nitrogen laser wavelength, 337 nm; linear-flight distance, 1.2 m; acceleration voltage, 20 kV; detector voltage, 25 kV. Internal and external calibrations were performed using 10 pmoles CytoC and a standard peptide mix (Bruker Daltonics, USA), respectively.

The mass spectrum was analysed and sequence homologies were searched against the NCBI database using the peptide mass fingerprint algorithm available on MASCOT server

(Matrix Science Ltd.). The following parameters were applied during analysis: trypsin digestion (up to one missed cleavage), peptide mass tolerance of ± 100 ppm, peptide charge state of +1, carbamidomethyl on cysteine (C) and oxidation of methionine (M) as fixed and variable modifications, respectively.

4.2.4 Protein depletion studies

4.2.4.1 Gel filtration chromatography

The concentrated protein solution obtained after dialysis step was subjected to gel filtration chromatography on a Sephadex G-75 column (1 cm \times 50 cm) equilibrated with 50 mM Tris-HCl (pH 8.0) buffer. Fractions of 10 mL each were collected at a flow rate of 30 mL h⁻¹ with the same buffer and subsequently analysed for presence of proteins by measuring the absorbance at 280 nm. All the purification steps were conducted at temperatures not exceeding 4 °C unless stated.

4.2.4.2 Ion exchange chromatography

Ion exchange chromatography was carried out on a DEAE cellulose column (1.5 cm \times 20 cm) equilibrated with 50 mM Tris-HCl buffer (pH 8.0). After washing the column with equilibration buffer, elution was carried out with a linear gradient of potassium chloride in the range of 0-0.5 M in the same buffer. Fractions (2 mL) were collected at a continuous flow rate of 20 mL h⁻¹ and analysed for presence of proteins (280 nm Abs). Fractions showing presence of proteins were pooled and concentrated by lyophilisation after desalting using Amicon centrifugal filter units and subsequently evaluated for synthesis of silver nanoparticles. All the purification steps were conducted at temperatures not exceeding 4 °C unless stated.

4.2.5 Characterization of purified protein

4.2.5.1 *De novo* sequencing

The tryptic digestion of protein sample was performed as per the protocol used for peptide mass fingerprinting (section 4.2.3.3). *De novo* sequencing was carried out by introducing tryptic digests (5 μ L) into an ultra-performance liquid chromatography (UPLC) system coupled to a Q-TOF micro tandem mass spectrometer (MS/MS) (Waters, USA) with a nano-ESI source. Mass spectrometer settings for spectra measurements were as follows: capillary voltage of 2.8 kV, cone voltage of 20 V, collision energy of 5.0 V and source temperature of 80 °C. The mass spectra were recorded over the mass range of 200-2000 Da. Insulin was used as an internal standard; while an oxidized β -chain of insulin served as an external standard.

The obtained mass spectra were analysed by performing sequence homologies search against curated *Aspergillus flavus* proteins database using the MS/MS ion search algorithms available on MASCOT software (Matrix Science Ltd.) The following parameters were applied: trypsin digestion (up to one missed cleavage), peptide mass tolerance of ± 1.2 Da, a fragment mass tolerance of ± 0.6 Da, peptide charges of +2 and +3 and carbamidomethyl on

cysteine (C) and oxidation of methionine (O) as fixed and variable modifications, respectively.

4.2.5.2 N-terminal sequencing

For N-terminal sequencing, the purified protein was subjected to SDS-PAGE and electrophoretically transferred to a PVDF membrane. After brief staining with CBB R-250, the PVDF band corresponding to the protease was excised and N-terminal amino acid sequence was determined by the Edman degradation method (Edman 1950) on a Procise protein sequencing system (Applied Biosystems, France).

4.2.6 Physico-chemical characteristics

The amino acid sequence of the purified protein (assembled) based on mass spectroscopic investigations was converted to FASTA format prior to subsequent analysis. To compute various physico-chemical properties of purified protein, the sequence was submitted to ProtParam tool at the Expasy server (<http://web.expasy.org/protparam>). The pI of enzyme was calculated using pK values of amino acids according to Bjellqvist et al. (1993). The instability index and GRAVY were estimated by Guruprasad et al. (1990) and Kyte and Doolittle (1982), respectively.

4.2.7 Effect of salt - protein ratio on nanoparticle synthesis

To test the effect of salt - protein ratio on nanoparticle synthesis, we used a constant concentration (50 μ M) of protein, to which silver nitrate was added in varying concentration (0-50 mM) to achieve a series of molar ratio (10^2) in the range of 0, 0.02, 0.04 5.0 and 10.0. The samples were gently mixed and incubated for 72 h at 28 °C in dark conditions. After completion of reaction, 200 μ L of aliquots of the reaction mixtures were transferred into a microtiter plate and images were captured using a DSLR camera (Olympus, Japan) in macro mode.

4.2.8 Protein-nanoparticle interactions

4.2.8.1 Effect on protease activity

Protease assay was carried out using a chromogenic azocasein as substrate which comprises of casein conjugated to an azo-dye. Degradation of the casein by protease liberates free azo-dye into the supernatant that can be quantitatively analyzed (Deng et al. 2010). Briefly, the reaction mixture was prepared by incubating protease enzyme (50 μ M) with varying concentrations of silver nanoparticles (0-100 mM) in a 1:1 ratio. The reaction mixture was incubated for 15 min at room temperature. Subsequently, 300 μ l of azocasein (5 mg/ml in 0.1 M Tris-HCl buffer, pH 8.0) was added, mixed gently and incubated at 37 °C for 20 min. The reaction was terminated with 500 μ l of 20% (w/v) TCA, thoroughly mixed and incubated at 37 °C for 20 min. The tubes were centrifuged at 10,000 rpm for 5 min at ambient conditions to separate unutilized azocasein. Supernatant (800 μ l) was collected and diluted with 1 N sodium hydroxide solution in a 1:1 ratio and absorbance of the samples was measured at 440 nm using a JASCO V-630 UV-Visible spectrophotometer (Jasco Corporation, Japan).

4.2.8.2 *In silico* studies

Homology modelling and structure refinement: The three dimensional structure of alkaline protease protein was predicted using comparative modelling based on homology approach. The approach predicts protein models on the basis of available homologous template structures in Protein structure Data Bank (PDB) (<http://www.rcsb.org>). Template selection was performed by protein BLAST search against PDB database. The structure with highest sequence similarity was selected and alignment was made as per the requirement of MODELLER software (<http://salilab.org/modeller>). Auto model module of modeler 9v10 was used to generate 1000 initial models with a GA431 score of 1 and the models were ranked based on their DOPE scores. (Fiser and Šali 2003, Eswar et al. 2006). The model with the lowest DOPE score was selected and subjected to energy minimization using SANDER program of AMBER package, which is recognized as one of the widely-used and highly effective programs for energy optimization (Weiner and Kollman 1981, Pearlman et al. 1995).

The refined protein structure was analysed online by various structure validation servers. PROCHECK is a versatile protein structure analysis program available at the Joint Centre for Structural Genomics, Bioinformatics core, University of California, San Diego (Laskowski et al. 1993). The program was used for validation of protein structure and models by verifying the parameters like Ramachandran plot quality, peptide bond planarity, bad non-bonded interactions, main chain hydrogen bond energy, C alpha chirality and over-all G factor (Ramachandran et al. 1963). The statistics of non-bonded interactions between different atom types were analyzed by ERRAT program which gives a measure of the structural error at each residue in the protein (Colovos and Yeates 1993). The compatibility of the atomic model (3D) with its own amino acid sequence was determined by VERIFY3D (Liithy et al. 1992, Eisenberg et al. 1997). DFIRE values were calculated using the server provided by Zhou and Zhou (2002). QMEAN and Z-score values were deduced using structure assessment tools of Swiss model workspace (Arnold et al. 2006, Bordoli et al. 2008). The RMSD value between the template and model structure was calculated using PYMOL software.

Brownian dynamics simulations: Brownian dynamics (BD) simulations were carried out with the ProMetCS continuum solvent model originally developed for protein gold surface interactions (Kokh et al. 2010). The calculations were performed using the SDA version 6 software. The Ag(111) surface was constructed with a surface area of $100 \text{ \AA} \times 100 \text{ \AA}$ and three atomic layers (Iori et al. 2009). An experimental salt concentration of 1.0 mM was included as a non-specific screening effect on the electrostatic potential of the protein which was calculated using the APBS program (Baker et al. 2001). All titratable protein side chains, were assigned their standard protonation state corresponding to the experimental pH with H⁺⁺ (Gordon et al. 2005). Subsequently, 1000 BD trajectories were computed starting with the protein positioned randomly with its center at a distance of 70 Å from the surface

where the protein surface interaction energy is negligible. The specified number of docked complexes was extracted directly from the runs and clustered with a clustering algorithm. The simulation time step was set to 0.50 ps. At each BD step, the protein surface interaction energy and forces acting on the protein were computed using the implicit-solvent ProMetCS force field, originally developed and parameterised for protein-gold surface interactions (Kokh et al. 2010).

4.3 Results and Discussion

4.3.1 Protein profiling of fungal cell-free filtrate

Recent advances in proteomic analysis based on one- and two-dimensional electrophoresis and mass spectrometry have led to a progressive increase in understanding the proteomics of organisms. In spite of economic importance and immense benefits to mankind, fungal proteomics studies are still at a relatively early stage of development due in part to the lack of available genome sequence data. Understanding of fungal proteins seems more valuable considering the role of protein secretion, particularly in nutrition and infection (Peberdy 1994, Iwashita 2002). Among fungal proteomic studies, filamentous fungi like *Aspergillus* have received particular attention owing to their valuable protein-based products, the majority of which are hydrolytic enzymes (amylases, cellulases, and proteases). Proteomic studies on *Aspergillus flavus* were pioneered by Francisco and colleagues who performed two detailed studies which collectively identified a total of 73 proteins which were documented in two research articles (Medina et al. 2004, 2005). Majority of these proteins were hydrolytic enzymes, metabolic proteins or proteins involved in electron/proton transport. It is important to note that a substantial number of identified proteins (27%) were labelled 'hypothetical' due to the incomplete annotation of the genome. Another detailed comparative proteomic analysis for the filamentous fungus *Aspergillus oryzae* has also been reported (Oda et al. 2006).

The “bottom-up” proteomics is the most widely employed strategy to identify proteins and characterize their amino acid sequences (Aebersold and Mann 2003, Chait 2006). The method comprises of separation of crude proteins by a method such as gel electrophoresis followed by a proteolytic digestion prior to analysis by mass spectrometry. By comparing the masses of proteolytic peptides (mass spectra) with those predicted from a sequence database or annotated peptide spectral library, the obtained peptides can be identified. The multiple peptide identifications can be assembled leading to an identification of the protein.

4.3.2 One dimensional gel electrophoresis

To differentiate secreted proteins of fungus *Aspergillus flavus* isolate NJP08, the fungal cell-free filtrate was salted out overnight at 4 °C using ammonium sulfate precipitation method. The precipitated protein in the form of pellet was collected by centrifugation and subsequently dialyzed using a 12.0 kDa cut-off cellulose membrane. Further, protein sample was resolved on a one dimensional SDS-PAGE gel using silver staining (Figure 4.1). The protein fraction showed presence of numerous proteins of varying molecular masses ranging

from 80.0 to 26.0 kDa. Among these proteins, three bands of molecular masses 48.0, 33.0 and 28.0 kDa were more prominent implying their abundance in fungal cell-free filtrate as compared to remaining proteins. At this point, it is important to emphasize that our method does not claim to have extracted all extracellular proteins but only those that were being released and remain survived (not degraded) under conditions of nanoparticle synthesis protocol. For instance, the incubation of fungal mycelium in nutrient deprived conditions (only Milli-Q water) for three days to collect extracellular proteins might have resulted in the liberation of proteins from fungal mycelium. It could also be possible that the presence of secreted hydrolytic enzymes may lead to degradation of proteins in substantial amounts. Similarly, studies with *Fusarium oxysporum* and *Verticillium* sp. showed presence of extracellular proteins responsible for the synthesis of metal nanoparticles (Bansal et al. 2004, Bharde et al. 2006, Parikh et al. 2008). Viability study was also conducted after 72 h incubation of fungus in milli-Q water. The fungus was found to be viable (data not shown) signifying that intracellular proteins (cytoplasmic) were not released in the fungal cell-free filtrate.

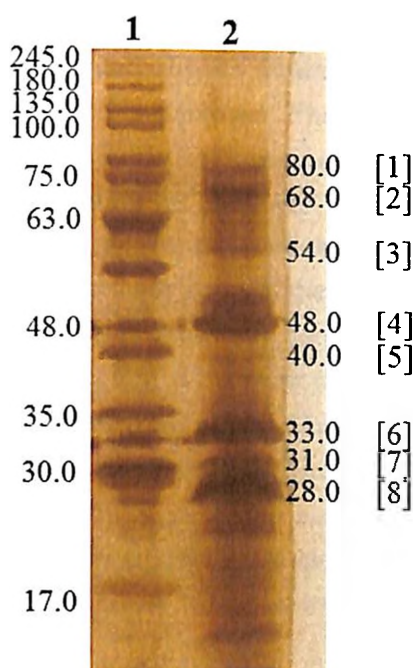


Figure 4.1 One-dimensional SDS-PAGE of secreted proteins from fungus *Aspergillus flavus*. Lanes 1 and 2 contain standard marker and secreted proteins, respectively. The number adjacent to the protein bands represents their molecular mass (in kDa).

4.3.3 Peptide mass fingerprinting

The identification of the obtained protein bands was carried out using peptide mass fingerprinting method. It is an analytical technique that offers a “fingerprint” unique for a particular protein or protein mixtures. The approach is paramount for well characterized organisms (for which entire genome is known) as well as can be used for organisms where only a part of the genome is known or for which homologous sequences are available. In our study, the method was well suited due to the available genome sequence of fungus

Aspergillus oryzae, a very closely related organism to our experimental fungus *Aspergillus flavus* isolate NJP08. Moreover, the availability of genome sequence for *Aspergillus flavus* strain NRRL 3357 to the level of 5 fold sequence coverage (Payne et al. 2006) also facilitated the identification of proteins using peptide mass fingerprinting.

Individual protein bands were excised from SDS-PAGE gel and proteolytic digestion with trypsin was carried out. The extracted peptides were analysed by liquid chromatography coupled with MALDI-TOF mass spectrometry to obtain peptide mass spectra of individual protein. The obtained mass spectrum were subjected to MASCOT search against the sequences documented in NCBI database and literature reports (Medina et al. 2004, 2005, Machida et al. 2005, Mellon et al. 2007, Kim et al. 2008, Chen et al. 2009, Hernández-Martínez et al. 2011). The search resulted in the identification of all proteins with sequence coverage percentage ranging between 20 and 42 (Table 4.1). The "sequence coverage" represents the percentage of the protein's sequence represented by the peptides identified in the mass spectroscopy run and has been considered as an important criterion to evaluate mass spectroscopy data (Ong and Mann 2005).

Since a protein can be identified based on the detection of as few as 2 peptides (Aebersold and Mann 2003), our submitted queries resulted in identification of at least one protein. The list of proteins is summarised in Table 4.1. The maximum and minimum number of peptides was matched for catalase and alkaline serine protease protein with values of 16 and 5, respectively. Another consideration is how well the mass spectrum matches the expected spectrum for a given peptide can be assessed on the basis of "MOWSE" protein score (Cottrell and London 1999). The protein score is the sum of the highest ions score for each distinct sequence, however, a small correction is applied to reduce the contribution of low-scoring random matches. This correction is a function of the total number of molecular mass matches for each query. A large MOWSE score value indicates a close fit between the experimental tandem mass spectrum and the model tandem mass spectrum constructed from the sequence. Based on mass spectra analysis, MOWSE score value of 66 was determined as minimum score to assign protein at 95% significant value. As shown in Table 4.1, all the identified proteins exhibited MOWSE score values above 66 with maximum values for catalase and FG-GAP repeat proteins.

To predict the secretory nature of the identified proteins, the assembled sequences were analysed using SignalP server. Majority of the proteins present in fungal cell-free filtrate were considered to be either secreted or loosely bound to cell wall of fungal mycelium, and therefore were readily released into the extracellular environment. Of the eight identified proteins, five had a signal peptide which explains the high rate of propensity of secretory proteins in fungal cell-free filtrate. The data validates our prospect to collect extracellular proteins by incubating fungus in Milli-Q water for 3 days. Shinano et al. (2011) also reported that the method of collection of proteins was critical in determining the ratio of secretory proteins i.e. proteins containing signal peptides.

Table 4.1 Identification of proteins present in the cell-free filtrate of fungus *Aspergillus flavus* isolate NJP08. The obtained mass spectrum, identified peptides and deduced sequences are summarized in Appendix 4.1-4.8.

Band	Match ^a	Sequence coverage ^b	MOWSE Score ^c	Accession number ^d	Identification ^d	Number of amino acids	Theoretical pI/mass (kDa) ^e	Signal peptide ^f
1.	16	26.76	118	XP_002380889	Catalase Cat1	725	5.34/ 79839.1	+(16)
2.	11	20.58	71	XP_002383995	Glutaminase A	690	4.81/ 76165.1	+(21)
3.	8	40.10	68	XP_002377316	Elastinolytic metalloproteinase Mep	634	5.07/ 69301.6	+(20)
4.	15	42.44	67	XP_002377954	Protein kinase (NpkA), putative	466	7.09/ 52575.7	-
5.	7	22.15	72	XP_002382479	DNA repair protein (RadR), putative	429	6.30/48050.0	-
6.	5	39.01	75	XP_002374291	Alkaline serine protease Alpl	403	5.95/ 42571.4	+(21)
7.	9	39.61	102	XP_002374393	FG-GAP repeat protein, putative	308	5.08/33983.5	+(28)
8.	10	37.81	68	XP_002372877	Acyl-CoA:6-aminopenicillanic-acid-acyltransferase, putative	365	5.85/39958.8	-

^a number of peptides matched from protein in mass spectroscopy query.

^b percentage of amino acid sequence of protein covered in mass spectroscopy analysis.

^c MOWSE score > 66 indicates identity or extensive homology ($p < 0.05$).

^d based on *Aspergillus flavus* genome database.

^e theoretical isoelectric point and molecular mass calculated based on Protparam server.

^f indicates presence of signal peptides as predicted by SignalP software.

4.3.4 Protein depletion and nanoparticle synthesis

The utilization of cavities formed by proteins as a template to fabricate and regulate growth of homogenous nanoparticles is well reported. For instance, cavities of proteins such as ferritin, apo-ferritin, Dps (DNA-binding proteins from starved cells) from *Escherichia coli*) served as a template to restrain particle growth as well as coating to prevent coagulation between nanoparticles (Wong and Mann 1996, Ilari et al. 2002, Liu et al. 2007, Todd et al. 2013, Zhen et al. 2013). In the present study, protein depletion experiments were performed to identify the protein(s) which are responsible for synthesis and stabilization of silver nanoparticles. The concentrated fungal cell-free filtrate was subjected to pre-equilibrated gel-filtration column (Sephadex-75) at pH 7.4 to maintain the functional and physiological condition of cellular proteins. The elution profile was prepared by plotting the A_{280} of eluted fractions against the elution time. As illustrated in Figure 4.2, the crude fungal cell-free filtrate was resolved into four distinct fractions viz. fraction numbers 4-6, 7-10, 11-14 and 15-20 which were classified as group I, II, III and IV, respectively. The protein present in flow through fractions of individual groups were mixed and then incubated with precursor silver ions (1 mM final concentration) for 72 h in dark conditions. The kinetics of silver nanoparticle synthesis was measured by UV-visible spectroscopy after the completion of the reaction.

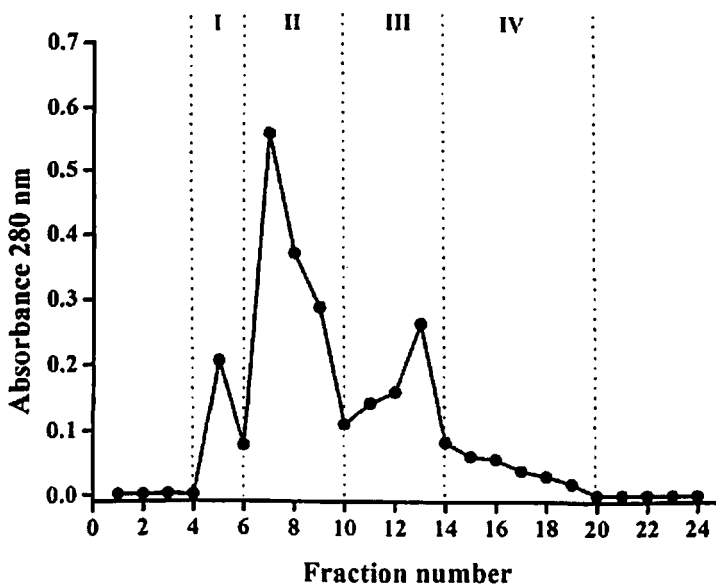


Figure 4.2 Size exclusion chromatography profile of proteins present in fungal cell-free filtrate of *Aspergillus flavus* isolate NJP08. The eluted fractions were classified into four groups viz. I, II, III and IV (separated with dot lines).

The results of silver nanoparticle synthesis after the exposure of silver ions to individual protein groups (I to IV) are shown in Figure 4.3. All the protein groups exhibited the synthesis of silver nanoparticles which could be due to the presence of proteins which can perform reduction and subsequent nucleation reactions. However, the magnitude of

nanoparticle synthesis varied significantly with maximum and minimum rate of synthesis observed in group II and group IV, respectively. The variation in the rate of nanoparticle synthesis can be explained by the fact that rate of nanoparticle synthesis is directly proportional to the nature and concentration of “seed”. The seed-mediated nanoparticle synthesis is a useful way to make gold and silver nanoparticles of controllable aspect ratio (Brown et al. 2000). “Seed” is a single crystalline particle which can be capped with several surface groups, such as citrate, surfactants, etc. In our study, the capping molecules could be functional groups present on the surface amino acids of protein molecules. The controlled aging of seed particles result in formation of nanoparticles which is often monitored by the reducing agent (amino acids in our case). The observed low rate of nanoparticle synthesis in Group I, III and especially Group IV indicates the lack of formation of “seed” particles. It may be due to the absence of specific molecules which may act as capping molecules. The absence of capping molecules probably allows the uncontrolled growth on the surface of seed, thus producing large sized particles. It is supported by the observed “red shift” in the UV-visible spectrum indicating formation of large-sized particles (Figure 4.3).

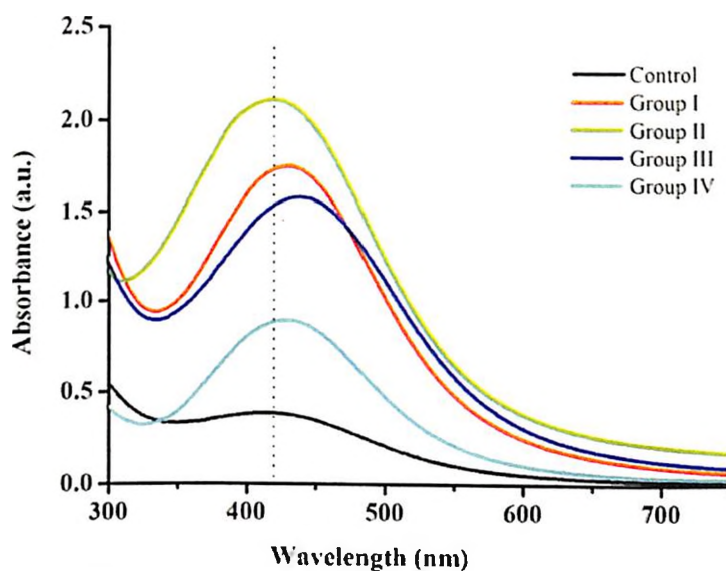


Figure 4.3 Silver nanoparticle synthesis profile of protein fractions obtained after size exclusion chromatography. Dotted line (λ_{\max} 420 nm) was used as a reference to represent “Red shift” of peaks in various groups.

Further analysis with DLS measurements confirmed a significant variation in particle size distribution of silver nanoparticles synthesized with various protein groups. As shown in Table 4.2, the smallest size (20.5 ± 1.3 nm) of silver nanoparticles was observed for group II proteins whilst, largest particle size (76.4 ± 7.9 nm) was determined for group IV proteins. The particle size of silver nanoparticles synthesized using group I and III proteins were almost similar with average size around 50 nm. These observations were in complete agreement with the results observed with absorption measurements indicating a “red shift” in the peaks for large-sized silver nanoparticles.

The variation in the particle size as well as their correlation on homogeneity and stability prompted us to further investigate the stability of as-synthesized silver nanoparticles. Stability and homogeneity are two key issues which are inter-related and play a vital role for several applications of silver nanoparticles (Nair and Laurencin 2007). Stability studies were performed by measuring the magnitude of Abs 420 nm. The obtained results explicitly showed that silver nanoparticles synthesized with Group II proteins were stable at room temperature for over a period of 3 months as compared to other groups (Table 4.2). This observation indicated that Group II contains protein(s) which can accomplish synthesis as well as stabilization of silver nanoparticles. The observed controlled and miniature size (20.5 ± 1.3) of silver nanoparticles also supports the “dual” role of proteins in synthesis as well as stabilization of nanoparticles. It is noteworthy to mention that although remaining group of proteins (I, III and IV) were able to synthesize silver nanoparticles, very feeble stability was observed with these groups (Table 4.2). Hence, it can be inferred that these proteins (specific amino acids) react with silver ions to generate nanoparticles but the lack of specific cavities (domains) on proteins restrict them to stabilize nanoparticles. It may also be possible that the protein-nanoparticle interactions occur in a non-specific manner resulting in loosely bound proteins on silver nanoparticles. This type of protein binding on nanoparticles is often classified as “soft corona” (Lynch and Dawson 2008).

Table 4.2 Particle size distribution and stability profile of silver nanoparticles synthesized using various protein groups of *Aspergillus flavus* isolate NJP08. The protein groups were prepared by subjecting crude fungal cell-free filtrate on a pre-equilibrated size exclusion column (Sephadex G-75, Tris-Cl pH=8.0).

Fractions	Particle size (nm) ^a	Stability ^b
Group I	53.4 ± 6.2	4 days
Group II	20.5 ± 1.3	> 3 months
Group III	48.7 ± 5.8	5-6 days
Group IV	76.4 ± 7.9	2 days

^aas determined using DLS measurements

^bmeasured using UV-visible spectroscopy

Due to the “dual” role of nanoparticle synthesis and stabilization observed in case of group II proteins; this group was selected for further studies. The group II proteins were discriminated using a 12% SDS-PAGE gel which indicated the presence of two proteins with molecular masses of ca. 33 and 31 kDa viz. alkaline protease and FG-GAP binding protein, respectively (Figure 4.4a). These two proteins were separated by subjecting on to a DEAE cellulose column with salt gradient which eluted both these proteins in different fractions (Figure 4.4b). The protein alkaline protease (33.0 kDa) was eluted in fractions 4-11 while the FG-GAP binding protein (31.0 kDa) was eluted in fractions 12-23.

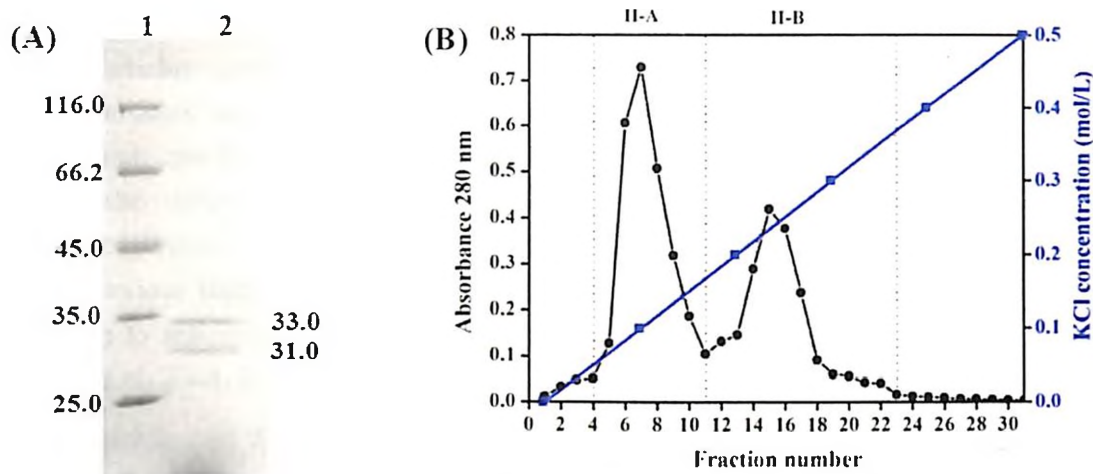


Figure 4.4 (a) SDS-PAGE of group II proteins (lane 2) illustrating two proteins with molecular mass of ca. 33.0 and 31.0 kDa. (b) Elution profile of group II proteins when subjected on a pre-equilibrated anion exchange column (DEAE cellulose, KCl = 0.0 - 0.5M).

Fractions of individual protein sub-group were pooled and incubated with precursor silver ions for 72 h as mentioned earlier. The kinetics of silver nanoparticle synthesis was measured by UV-visible spectroscopy after the completion of the reaction and illustrated in Figure 4.5. The results astonished us with the observation that synthesis of silver nanoparticles was exclusively observed when fractions containing purified alkaline protease (Group II-A) were exposed to silver ions. Moreover, the intensity and sharpness of the absorbance peak indicated the homogeneity and monodispersity of silver nanoparticles. In contrast, very minute sign of silver nanoparticle synthesis was observed with purified FG-GAP binding protein and silver ions (Group II-B). The broad vicinity of absorption band further implies polydispersity and uncontrolled size of silver nanoparticles.

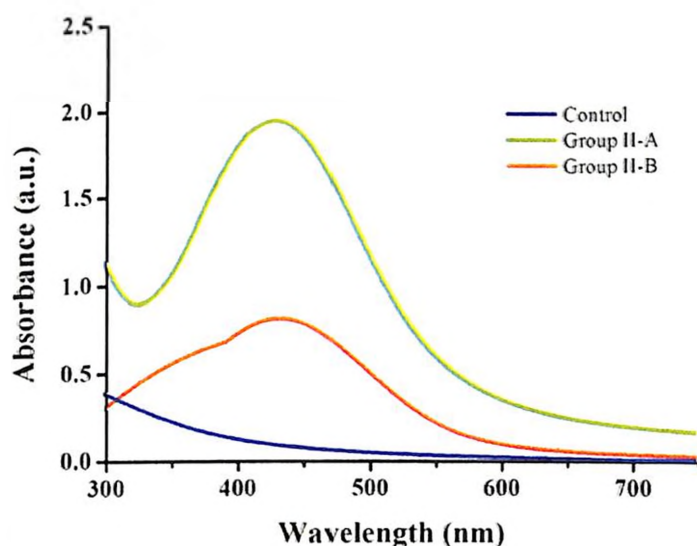


Figure 4.5 UV-visible spectroscopy measurements depicting the role of group II proteins in synthesis of silver nanoparticles.

Dynamic light measurements further substantiate the synthesis of mono-dispersed silver nanoparticles using protein alkaline protease. A narrow particle size distribution of silver nanoparticles with stability over a period of 3 months at ambient conditions was observed which can be considered as highly significant (Table 4.3). The observed high stability is also indispensable considering the fact that the synthesis was performed at millimolar concentration level (1 mM) of silver ions which often can hinder nanoparticle solubility. Previous studies have demonstrated that at millimolar levels, silver nanoparticles are incapable to maintain adequate solution stability which is observed at sub-micromolar levels (Lok et al. 2006, 2007).

Table 4.3 Particle size distribution and stability profile of silver nanoparticles synthesized using group II proteins separated on a pre-equilibrated anion exchange column (DEAE cellulose, KCl = 0.0 - 0.5M).

Fractions	Particle size (nm)^a	Stability^b
Group II-A	17.2 ± 0.8	> 3 months
Group II-B	83.4 ± 9.2	1 day

^aas determined using DLS measurements

^bmeasured using UV-visible spectroscopy

In view of need of molecules which can regulate self-assembly of nanoparticles with appropriate surface modification, the observed “dual function” of alkaline protease to synthesize and stabilize silver nanoparticles could be considered as highly indispensable. This “one-pot” synthesis protocol embodies immense importance considering the integrated surface modification of nanoparticles with protein molecules, which confer stability and “biocompatibility”. In addition, the proteinaceous shell provides a platform for surface modifications on functional groups of exposed amino acids for the attachment of a variety of ligands. To the best of our knowledge, no reports of alkaline protease-mediated synthesis of silver nanoparticles are available so far in literature. Indeed, the present study could be considered as a first systematic investigation to elucidate the mechanism of fungi-mediated nanoparticle synthesis. Bansal et al. (2004) demonstrated the synthesis of crystalline zirconia nanoparticles at room temperature by the cationic proteins secreted by the fungus *Fusarium oxysporum*. These proteins were capable of hydrolyzing aqueous ZrF_6^{2-} ions extracellularly and belong to protease-like family. Another fascinating example of a protease-family protein is silica-binding silicatein, which is an axial protein extracted from a marine demosponge *Tethya aurantia* (known colloquially as the orange puffball sponge) marine sponge (Sarikaya et al. 2003, Brutchey and Morse 2008). Silicatein proteins belong to cathepsin-L protein family and contain serine, tyrosine, and threonine clusters.

As discussed in the introduction section earlier, various protein molecules such as phage display peptides, protein cages, silicateins, etc are very well demonstrated for

nanoparticle synthesis. However, feeble understanding of molecular mechanism(s) that mediate the process of nanoparticle synthesis has prevented their up gradation for mass scale production of nanoparticles. Hence, we focused our further studies to characterize the alkaline protease in order to elucidate molecular mechanism for silver nanoparticle synthesis and subsequent protein-nanoparticle interactions. The obtained knowledge could be rationally abstracted into innovative synthetic methodologies for the mass scale fabrication of nanoparticles at ambient conditions.

4.3.5 Detailed characterization of alkaline protease

4.3.5.1 *De novo* sequencing

De novo sequencing (commonly known as “tandem mass spectrometry” or MS/MS or MS²) involves multiple steps of mass spectrometry selection, with some form of fragmentation occurring in between the stages. *De novo* sequencing is a widely utilized method to characterize proteins of microorganisms whose genome sequences are unavailable or annotation is incomplete. In general, the strategy is to identify, align and merge short fragments (amino acids) derived from a much longer sequence (peptides) in order to construct the complete sequence (protein). More precisely, a mixture of peptides (different sequences) obtained after proteolytic cleavage of a protein was ionized followed by measurement of their respective parent mass/charge ratios (mass spectrum of peptides). Subsequently, selective fragmentation of each peptide into pieces (amino acids) was carried out with measurement of the mass/charge ratios of the fragment ions (MS/MS spectra of peptides).

The tryptic digest products of alkaline protease protein were subjected to nano-ESI-MS–MS analysis and amino acid sequences of the two most prominent internal peptides of molecular masses 1239.65 and 1268.63 Da were deduced. The ion chromatograms demonstrating the fragmentation pattern (b and y ions) for peptides I and II are illustrated in Figures 4.6 and 4.7, respectively. The b ions appear to originate from the amino terminus (N-terminus) whereas y ions appear to extend from the carboxyl terminus (C-terminus) of the peptide chain. It can be readily observed that frequency and abundance for y ions is higher in comparison to b ions. The first peptide with a molecular mass of 1239.65 Da was found to be composed of the 12 amino acids (SAPWGLGSISHK) whereas, the other peptide fragment (1268.63 Da) subjected to analysis was found to be composed of 13 amino acid residues (AAINMSLGGYSK). Both the peptide sequences were searched against the protein database using MASCOT MS/MS search tool. The results revealed 100% identity with “alkaline protease” protein of fungus *Aspergillus oryzae*, suggesting that the protein is well conserved among the *Aspergillus* isolates.

(A)	#	b	b-H ₂ O	b-NH ₃	b(2+)	Seq	y	y-H ₂ O	y-NH ₃	y(2+)	#
	1	88.04	70.03	71.01	44.52	S					12
	2	159.08	141.07	142.05	80.04	A	1152.62	1134.61	1135.59	576.81	11
	3	256.13	238.12	239.10	128.56	P	1081.58	1063.54	1064.55	541.29	10
	4	442.21	424.20	425.18	221.60	W	984.57	966.67	967.51	492.76	9
	5	499.23	481.24	482.20	250.12	G	798.45	780.40	781.42	399.72	8
	6	612.31	594.30	595.29	306.66	L	741.45	723.43	724.40	371.21	7
	7	669.34	651.33	652.33	335.17	G	628.34	610.37	611.31	314.67	6
	8	756.37	738.36	739.34	378.68	S	571.30	553.31	554.29	286.16	5
	9	869.45	851.44	852.43	435.23	I	484.46	466.28	467.26	242.64	4
	10	956.48	938.47	939.47	478.74	S	371.20	353.19	354.18	186.10	3
	11	1093.54	1075.53	1076.52	547.27	H	284.17	266.16	267.14	142.59	2
	12					K	147.11	129.10	130.09	74.06	1

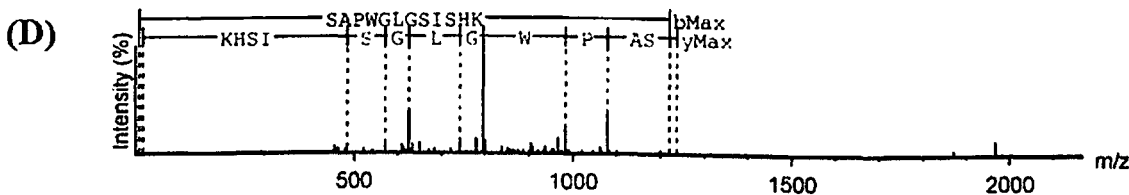
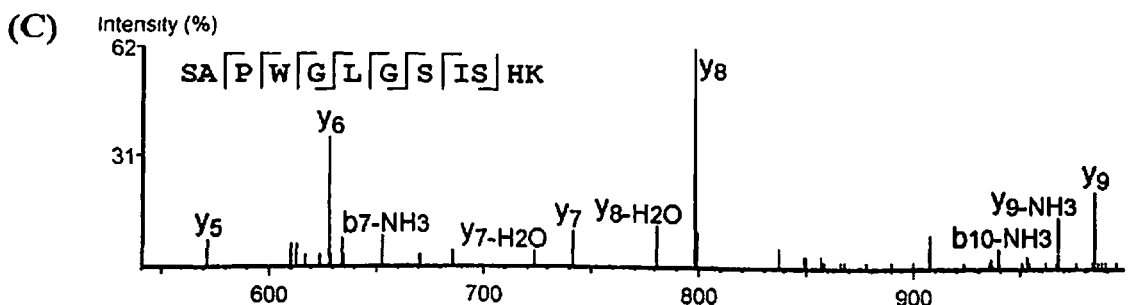
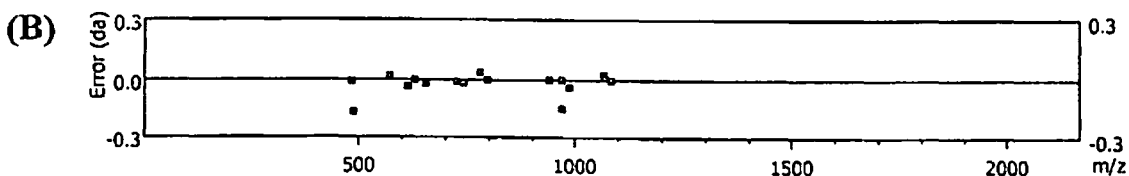


Figure 4.6 *De novo* sequencing of the peptide sequence SAPWGLGSISHK of alkaline protease. (a) peptide ion values (b) error graph (c) MS/MS spectrum (d) Extracted ion chromatogram with deduced sequence.

(A)

#	b	b-H ₂ O	b-NH ₃	b (2+)	Seq	y	y-H ₂ O	y-NH ₃	y (2+)	#
1	72.04	54.03	55.02	36.52	A					13
2	143.08	125.07	126.06	72.04	A	1197.59	1179.58	1180.57	599.30	12
3	256.17	238.16	239.14	128.58	I	1126.56	1108.55	1109.53	563.78	11
4	370.21	352.20	353.18	185.60	N	1013.47	995.46	996.42	507.24	10
5	501.25	483.24	484.22	251.12	M	899.43	881.42	882.40	450.21	9
6	588.28	570.27	571.25	294.64	S	768.34	750.37	751.35	384.69	8
7	701.37	683.36	684.34	351.18	L	681.36	663.31	664.30	341.18	7
8	758.39	740.38	741.36	379.69	G	568.27	550.26	551.25	284.64	6
9	815.41	797.40	798.38	408.20	G	511.24	493.23	494.22	256.13	5
10	872.43	854.42	855.40	436.71	G	454.24	436.22	437.20	227.61	4
11	1035.49	1017.48	1018.47	518.25	Y	397.21	379.20	380.18	199.10	3
12	1122.53	1104.51	1105.50	561.76	S	234.14	216.13	217.12	117.57	2
13					K	147.11	129.10	130.09	74.06	1

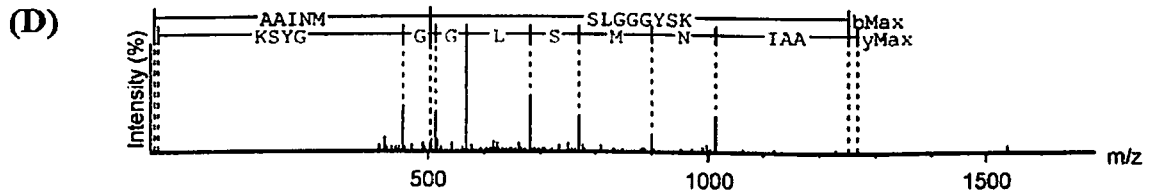
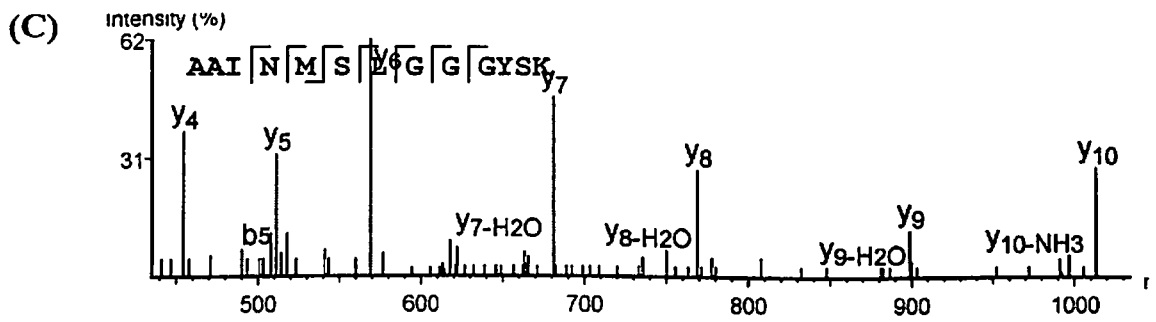
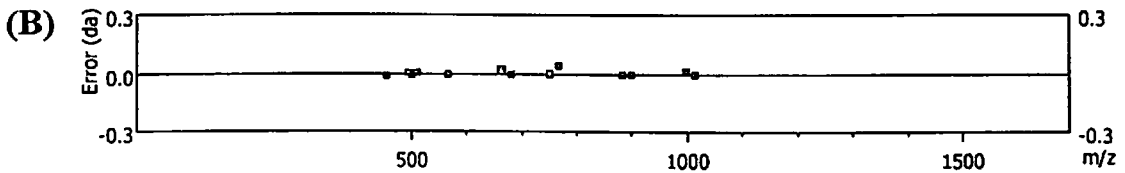


Figure 4.7 *De novo* sequencing of the peptide sequence AAINMSLGGYISK of alkaline protease. (a) peptide ion values (b) error graph (c) MS/MS spectrum (d) Extracted ion chromatogram with deduced sequence.

4.3.5.2 N-terminal sequencing

The N-terminal sequence of the first 13 amino acid residues of the purified protein was determined by the automated Edman method and found to be GLTTQKSAPWGLG. The deduced amino acid sequence was analysed and further aligned with other closest proteases as shown in Table 4.4. The obtained amino acid sequence exhibited maximum homology with alkaline proteases from *Aspergillus flavus* (Yu et al. 1999) and *Aspergillus oryzae* (Tatsumi et al. 1989, 1991). The N-terminal amino acid sequence was found to match against the alkaline protease sequences from *Aspergillus flavus* reported by various groups (Mikeš et al. 1980, Ramesh et al. 1995, Chen et al. 2009). A difference of only one amino acid was found between the sequenced alkaline protease protein and the serine proteases from *Aspergillus viridinutans* (Katz et al. 2005) and *Aspergillus fumigatus* (Kolattukudy et al. 1993). Comparison with alkaline serine protease of *Streptomyces avermitilis* (Ikeda et al. 2003) depicted relatively low identity with the 13 N-terminal amino acids as the sequenced protein differ by 4 residues from the reported one. It is evident from these findings that the purified protease from *Aspergillus flavus* isolate NJP08 is a serine protease and amino acid sequence of N-terminal domain is highly conserved among *Aspergillus* species.

4.3.5.3 Physico-chemical characteristics

Various biochemical features of the purified alkaline protease were calculated (Table 4.5). The theoretical pI value of the alkaline protease protein was calculated as 6.08 and found to be consistent with previous experimental observations (Yu et al. 1999, Muthulakshmi et al. 2011). The calculated pI value is slightly lower than neutral which can be justified based on the fact that the protein comprises of more number of negatively charged residues (Asp + Glu; 25 residues) in comparison to positively charged residues (Arg + Lys; 22 residues). The aliphatic index is a measure of the relative volume occupied by aliphatic side chain of amino acids (Ala, Val, Leu and Ile) which indicate the thermo stability of a protein molecule. The aliphatic index of alkaline protease was found to be 79.65, indicating admirable thermo stability, a highly desirable feature for industrial applications. The instability index, based on the occurrence of dipeptides of certain instability, was calculated to determine the *in vivo* half-life of the protease (Guruprasad et al. 1990). It has been postulated that proteins with instability index of more than 40 are unstable, whereas those having instability index of less than 40 are often stable (Rogers et al. 1986). The instability index of the alkaline protease was calculated as 24.09 which indicated its high stability with an *in vivo* half-life of more than 20 hours. The observed negative GRAVY index value (-0.161) indicates hydrophilic nature which substantiates secretory nature of the alkaline protease (Kyte and Doolittle 1982).

Table 4.4 Homology analysis of N-terminal amino acid sequence of alkaline protease from *Aspergillus flavus* isolate NJP08 with closely related proteases reported in NCBI database.

Description	N-terminal sequence											Accession No.	Reference		
	*	*			*	*	*	*	*						
<i>Aspergillus flavus</i> isolate NJP08	G	L	T	T	Q	K	S	A	P	W	G	L	G		Present study
<i>Aspergillus flavus</i> (Asp fl 1)	G	L	T	T	Q	K	S	A	P	W	G	L	G	AAD47202	Yu et al. 1999
<i>Aspergillus oryzae</i>	G	L	T	T	Q	K	S	A	P	W	G	L	G	BAA00258	Tatsumi et al. 1989, 1991
<i>Aspergillus viridinutans</i>	-	L	T	T	Q	K	G	A	P	W	G	L	G	AAT85627	Katz et al. 2005
<i>Aspergillus fumigatus</i>	-	L	T	T	Q	K	G	A	P	W	G	L	G	AAB07672	Kolattukudy et al. 1990
<i>Metarhizium acridum</i> CQMa 102	-	L	K	T	Q	K	S	A	P	W	G	L	R	EFY89488	Gao et al. 2011
<i>Trichoderma reesei</i> QM6a	-	L	K	T	Q	T	G	A	P	W	G	L	G	EGR49466	Martinez et al. 2008
<i>Streptomyces avermitilis</i> MA-4680	-	-	T	T	Q	S	S	A	P	W	G	L	D	NP_827752	Ikeda et al. 2003

The asterisks (*) indicate identical amino acid residues.

Table 4.5 *In silico* characterization of alkaline protease from *Aspergillus flavus* isolate NJP08.

Physico-chemical characteristics	Value
Theoretical pI	6.08
Aliphatic index	79.65
Instability index	24.09
GRAVY index	-0.161
Theoretical Ml. wt.	28997.0 Da
Estimated half-life	>20 hours
Total number of negatively charged residues (Asp+Glu)	25
Total number of positively charged residues (Arg+Lys)	22

4.3.6 Effect of salt - protein ratio on nanoparticle synthesis

To demonstrate the utility of protease as an ideal platform for the efficient synthesis of mono-dispersed silver nanoparticles, we assessed the extent of nanoparticle synthesis by varying Ag^+ : protease molar ratio. The ratio was varied by increasing Ag^+ concentrations (0-50 mM) with a constant protease concentration (50 μM). In this experiment, the appearance of brown colour, which is an indicator for nanoparticle synthesis as well as size, was found to be dependent upon Ag^+ concentration. At Ag^+ /protease molar ratio of less than 4.0, no noticeable change in colour was observed indicating lack of silver nanoparticle synthesis. In contrast, higher Ag^+ /protease molar ratio (above 4.0) facilitated the silver nanoparticle synthesis in a dose-dependent manner (Figure 4.8). Moreover, at moderate Ag^+ /protease molar ratios (8.0 to 62.0), the particles were smaller and more mono-dispersed than nanoparticles formed at the higher ratio (above 62.0) (Figure 4.8). We noticed that this observation is consistent with other nanoparticle synthesis reactions in which an increase in metal precursor: capping ligand ratio yields larger diameter particles. For example, at lower Ag^+ /lysozyme molar ratios, particles were smaller and more mono-dispersed than nanoparticles formed at the higher Ag^+ /lysozyme molar ratio (Eby et al. 2009). Another study on TiO_2 nanoparticle synthesis using enzyme papain with titanium (IV) bis-ammoniumlactato-dihydroxide as precursor demonstrated that nanoparticle synthesis was dependent upon precursor concentration (Smith et al. 2009).

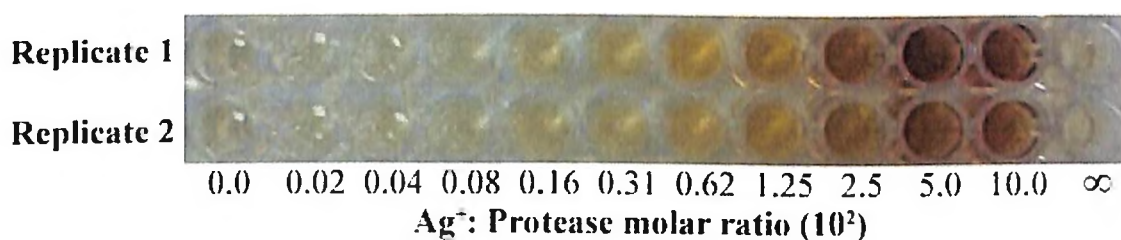


Figure 4.8 Effect of salt - protein ratio on silver nanoparticle synthesis The ratio was varied by increasing Ag^+ concentrations (0-50 mM) at a constant protease concentration (50 μM).

It is interesting to note that increase in Ag^+ /protease molar ratio value to 500.0 showed a saturation of silver nanoparticle synthesis (Figure 4.8), which suggests that higher Ag^+ concentration could either disorder the protease structure or alter the course of nucleation and growth of the nanoparticle. It could be possible that in presence of high Ag^+ concentration, protein may undergo conformational changes resulting in unfolding, aggregation, the formation of intermediate state, or the loss of activity (Lynch et al. 2007, Lundqvist et al. 2008). The interaction between protein and metals (especially nanoparticles) is a topic of immense interest in the area of nano-biotechnology. A plethora of studies has revealed the plausible protein-nanoparticle interactions and the extent of conformation changes in proteins due to the presence of nanoparticles. It has been observed that exposure of nanoparticles to proteins resulted in adsorption of proteins at nanoparticles surface leading to the “corona” formation (Lynch and

Dawson 2008, Nel et al. 2009, Walkey and Chan 2012). Moreover, the extent of corona formation depends on both the nature of protein as well as the surface properties of nanoparticle (De et al. 2007, Rana et al. 2010).

4.3.7 Protein-nanoparticle interactions

4.3.7.1 Effect of silver nanoparticles on protease activity

The adsorption of proteins on nanoparticle i.e. corona formation may result in altered structure and activity of protein. For instance, the binding of ZnO nanoparticles led to the unfolding of the periplasmic domain of ToxR protein of *Vibrio cholera* (Chatterjee et al. 2010). In contrast, proteins lysozyme and bovine serum albumin were found to retain their structure on adsorption to ZnO nanoparticles and gold-chloroquine nanoconjugates, respectively (Joshi et al. 2011, Bhunia et al. 2013). On the other hand, hydroxyapatite nanoparticles were found to act as a chaperone (by imparting thermostability) as well as a synthetic enhancer of activity of an isolated extracellular pectate lyase (APL) with low native state activity (Dutta et al. 2013). This research group reported that the purified enzyme from an attenuated strain of *Macrophomina phaseolina* showed feeble activity at 50 °C and pH 5.6. However, on addition of hydroxyapatite nanoparticles (10.5 µg ml⁻¹), enzyme activity increased 27.7 fold with a 51 fold increase in half-life at a temperature of 90 °C as compared to untreated APL. The chaperone like activity of nanoparticles was evident from entropy-enthalpy compensation profile of APL. Moreover, the upper critical temperature for such compensation was elevated from 50 °C to 90 °C in presence of nanoparticles (Dutta et al. 2013).

To investigate the effect of silver nanoparticles on structure and corresponding activity of alkaline protease, we determined variation in protease activity in presence of silver nanoparticles using azocasein assay. We observed no or less inhibition of enzyme activity when alkaline protease (50 µM) was incubated with low (0-50 mM) concentration range of silver nanoparticles. In contrast, an increase in concentration of silver nanoparticles to 100 mM resulted in a decrease in the proteolytic activity by 35% indicating loss in protease structure (Figure 4.9). No inhibition in proteolytic activity at lower silver nanoparticle concentration suggests that the nanoparticle binding site of alkaline protease is different from its catalytic site. At higher concentration of silver nanoparticles, high degree of silver ion release could make non-specific interactions with the functional groups present in the side chain amino acid residues of the active site. Previous study on titania nanoparticles (150 mM) showed a relatively slow transition from full protease activity to near complete inhibition of papain activity (Smith et al. 2009). Recently, dose-dependent inhibition of firefly luciferase activity has been observed after the exposure of the enzyme to citrate-coated silver nanoparticles (Käkinen et al. 2013). The study postulated that the binding of the enzyme induced an increase in zeta potential from -22 to +6 mV for the silver nanoparticles and rendered a 'protein corona' of 20 nm in thickness on the nanoparticle surface.

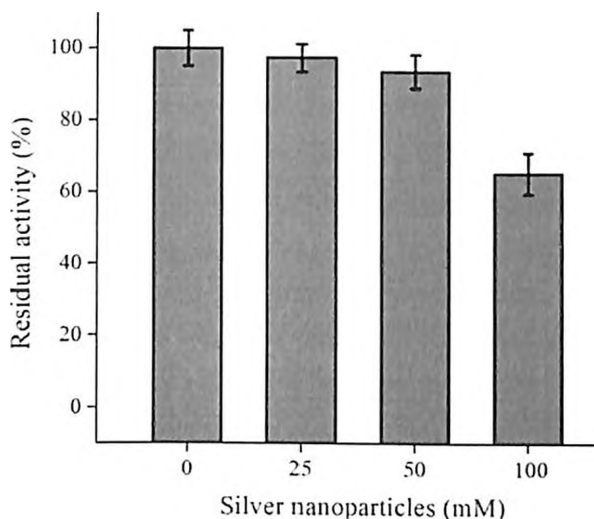


Figure 4.9 Azocasein assay showing the effect of increasing concentration of silver nanoparticles on residual proteolytic activity of alkaline protease.

4.3.7.2 Homology modelling and structure validation

The observed variation in the alkaline protease activity after binding of silver nanoparticles prompted us to further determine the associated protein-nanoparticle interactions. In order to achieve this, the knowledge of three dimensional structure of protein “alkaline protease” is a pre-requisite step. The structure is of immense interest not only because it provides a novel template to study protein-nanoparticle interactions but also provides essential information to elucidate the mechanism of silver nanoparticle synthesis mediated by secreted fungal proteins. The protein structure prediction remains an extremely difficult and unresolved undertaking. Experimental methods such as X-ray crystallography and NMR spectroscopy are methods of choice but often face two main problems: (a) calculation of protein free energy and (b) finding the global minimum of this energy. In contrast, protein structure prediction using *in silico* methods partially bypass these problems by the assumption that the protein in question adopts a structure that is close to the experimentally determined structure of another homologous protein. This would allow users to generate considerably reliable structures in a rapid time with an accuracy that is comparable to the best results achieved experimentally.

Protein modelling based on homology approach is the most commonly employed approach for *in silico* protein structure prediction. The approach utilizes experimentally determined protein structures to predict the three dimensional structure of another protein that has a similar amino acid sequence. The principle lies in the fact that during evolution, the structure is more stable and changes in them are much slower than the associated sequence, so that similar sequences adopt practically identical structures, and distantly related sequences still fold into similar structures (Krieger et al. 2003). This approach to modelling is possible since a

small change in the protein sequence usually results in a small change in its 3D structure (Hubbard and Blundell 1987). Moreover, homology modelling remains the only modelling method that can provide models with a root mean square error lower than 2 Å (Kherraz et al. 2011).

We built a three-dimensional model of our protein “alkaline protease” during the present study using homology modelling approach based on an alignment with a high-resolution X-ray crystallography structure of the cuticle-degrading protease from *Paecilomyces lilacinus* (PDB ID: 3F70). The choice of using 3F70 as the template was based on the BLAST analysis which showed highest sequence similarity (52.13%) between the sequence pair of 3F70 (template) and “alkaline protease” (target). It is noteworthy that homology modelling approach is well-suited to protein sequences (targets) that share 30% or more sequence identity to an experimentally solved protein structure template. A template-target sequence identity of 30-55% tends to have nearly 85% of their C- α atoms within 3.5 Å of the correct position resulting into medium accuracy models which should be treated with attention (Marsden and Orengo 2008). An important concern is that alignment obtained from automatic programs such as Clustal W, Modeler, Swiss model etc. has been considered unsatisfactory. This is because, automatic programs tend to introduce breaks in the middle of regular secondary structural elements, or align hydrophobic residues in the target with solvent exposed residues in the template among other reasons (Rakshambikai et al. 2013). Therefore, a manual intervention was exercised to obtain a high quality alignment suitable for the homology modelling. The curated alignment obtained has been provided in Appendix 4.9. The obtained three dimensional structure of alkaline protease protein after energy refinement has been illustrated in Figure 4.10.

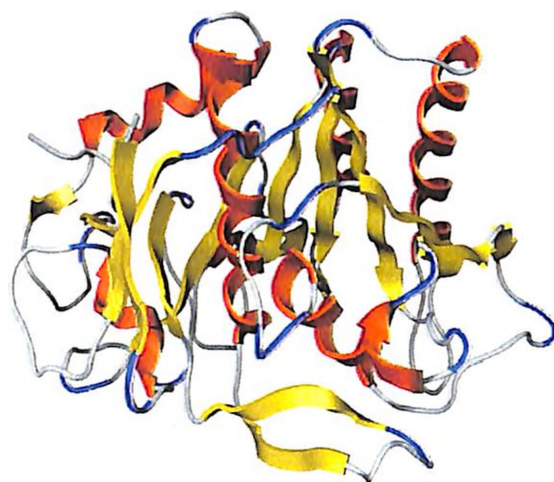


Figure 4.10 A ribbon diagram depicting the three dimensional structure of alkaline protease predicted using 3F70 as the template.

Structure validation is an important pre-requisite step to assess the accuracy and quality of the predicted protein structures. It is an essential quality control method to avoid errors creeping in Ramachandran plot, packing scores, torsion angle analysis, etc. Several methods are available for the detection of errors in protein models. One of them, PROCHECK, is a package that checks the stereo-chemical quality of the model, a requirement for a good structural prediction. PROCHECK is a versatile protein structure analysis program available at the Joint Centre for Structural Genomics, Bioinformatics core, University of California, San Diego (Laskowski et al. 1993). The aim of PROCHECK is to assess how normal, or conversely how unusual, the geometry of the residues in a given protein structure is, as compared with stereo-chemical parameters derived from well-refined, high-resolution structures. The program validates protein structures by verifying the parameters like Ramachandran plot quality, peptide bond planarity, bad non-bonded interactions, main chain hydrogen bond energy, C alpha chirality and over-all G factor. The description of all the above mentioned parameters can be found in Morris et al. (1992). As shown in Figure 4.11, Ramachandran plot analysis describes the classification of amino acid residues according to their Φ and Ψ torsion angles in the quadrangle. The corresponding plot statistics (Table 4.6) showed that main-chain conformations for 87.7% of amino acid residues were within the most favoured region, 11.5 % in the allowed and 0.4% in both the generously allowed and the disallowed regions. The observed values were significantly similar to the values observed for experimentally driven template structure (3F7O) indicating that predicted protease structure was of good quality. The details of Ramachandran plot of template structure and protease structure before minimization have been provided in appendix A4.10 and A4.11, respectively.

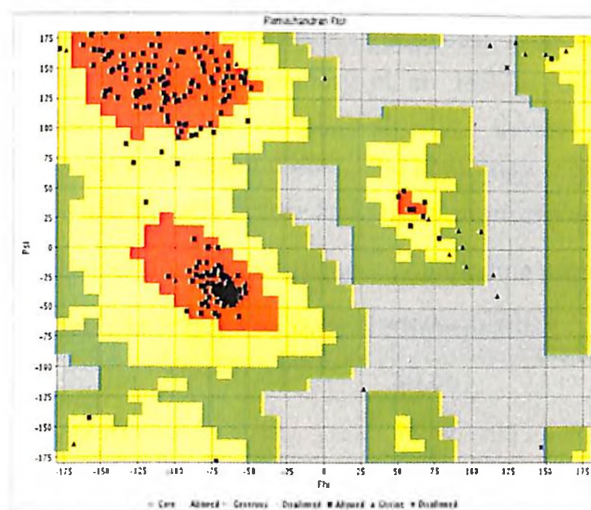


Figure 4.11 Ramachandran plot of predicted structure of alkaline protease after energy minimization steps. The quadrangle describes the classification of amino acid residues according to their Φ and Ψ torsion angles.

Table 4.6 Comparison of Ramachandran plot values for homology model of alkaline protease.

Residues in quadrangle	Template (3F7O)	Before Minimization	After Minimization
Most favoured regions [A, B, L]	88.2%	92.2%	87.7%
Additional allowed regions [a,b,l,p]	10.9%	6.6%	11.5%
Generously allowed regions [~a,~b,~l,~p]	0.9%	0.4%	0.4%
Disallowed regions [XX]	0.0%	0.8%	0.4%
Non-glycine and non-proline residues	88.2%	92.2%	87.7%

ERRAT is another protein structure verification algorithm that is especially well-suited for evaluating the progress of protein model building and refinement (Colovos and Yeates 1993). The program works by analyzing the statistics of non-bonded interactions between different atom types. ERRAT plots for the template structure and protease structure (before and after energy minimization) have been illustrated in Appendix A4.12. In general, ERRAT score is expressed as the percentage of the protein for which the calculated error value falls below the 95% rejection limit. Good high resolution structures generally produce values around 95% or higher. For lower resolutions (2.5 to 3Å) the average overall quality factor is around 91%. We observed an ERRAT score of 80.66 for the structure obtained from homology modelling which suggested a lower resolution of the obtained structure. Energy minimization steps increased the ERRAT score of the structure to 91.83 which was similar to the ERRAT score of 92.75 as determined for the experimentally derived template structure (3F7O). VERIFY3D plot determines the compatibility of an atomic model (3D) with its own amino acid sequence (1D) by assigning a structural class based on its location and environment (alpha, beta, loop, polar, nonpolar etc) and comparing the results to good structures (Eisenberg et al. 1997). All the evaluated models revealed high score values (Table 4.7). The template structure showed very high score value (99.65%) indicating its origin from experimental data. The homology model of alkaline protease showed score values of 96.47% and 91.34% before and after minimization steps, respectively.

Table 4.7 Validation results obtained for homology model of alkaline protease.

Validation tool	Template (3F7O)	Before Minimization	After Minimization
ERRAT	92.75	80.66	91.83
VERIFY3D (%)	99.65	96.47	91.34
DFIRE	-375.73	-354.52	-360.77
QMEAN Score	0.76	0.69	0.67
Z-Score	-0.11	-0.88	-1.09

DFIRE was used to assess non-bonded atomic interactions in the protein model. It is an all-atom statistical potential based on a distance-scaled finite ideal-gas reference state (Zhou and Zhou 2002). The method provides pseudo energy for the entire model which reflects the quality of the model and can be used for ranking alternative predictions of the same target. A lower energy score indicates that a model is closer to the native conformation. The observed scores for template and predicted models before & after minimization were found to be -375.73, -354.52 and -360.77, respectively (Table 4.7). The observed negative values indicate that the predicted model is reliable and very close to the experimentally determined structures. QMEAN is a composite scoring function for the estimation of global model quality (Benkert et al. 2008, Benkert et al. 2009). QMEAN provides pseudo energy of the whole model which can be used in order to compare and rank the alternative models of the same target. The lower the predicted energy, the better model it is. The QMEAN score of the predicted model before minimization steps was 0.69 which was decreased to 0.67 indicating that minimization steps effectively improved the structure quality (Table 4.7). Moreover, the score of predicted model is very close to the QMEAN score of the template (0.76) reflecting the predicted model as a reliable structure. The observed graphs and associated details are mentioned in Appendix A4.13.

The Z-score indicates overall model quality and measures the deviation of the total energy of structure with respect to an energy distribution derived from random conformations (Benkert et al. 2011). The results display the Z-score of predicted model in a plot that contains Z-scores of all the experimentally determined protein chains in current PDB database. As illustrated in Figure 4.12, Z-score value of the predicted model of alkaline protease was located within the space of experimentally derived structures. As expected, Z-score of the template structure was also found within the same space (Appendix A4.14).

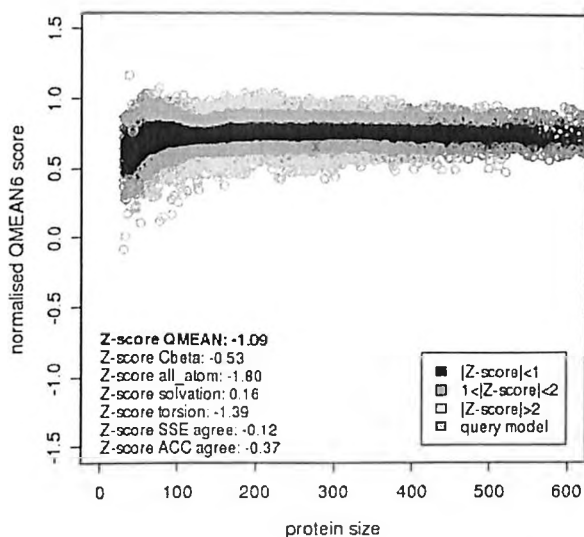


Figure 4.12 Plot depicting Z-score of predicted model for alkaline protease.

The ultimate aim of homology modelling is to generate structure similar to the experimentally derived structures. Backbone superimposition using SPDB viewer was carried out to determine the overall general similarities and subtle differences among the three dimensional structure of template (3F7O) and predicted model. As shown in Figure 4.13, general folding topology of the structure is similar; however, some structural differences appeared between the predicted model and template especially in the loop regions. The RMSD (Root Mean Square Deviation) between predicted model and template was calculated as 0.26 Å. The low RMSD between the target and template reflects the presence of strong homology (the lower the value, the more similar the structures are).

Based on the validation results, the predicted model can be considered as a reliable structure which is quite similar to the experimentally derived structures. The obtained model was further used to perform Brownian dynamics simulation to decipher the possible nanoparticle binding site on the alkaline protease and related protein-nanoparticle interactions.



Figure 4.13 Superposition of template (green) with the predicted model of alkaline protease (red). The picture has been captured using the software Swiss PDB viewer.

4.3.7.3 Brownian dynamics simulation

The interactions between “alkaline protease” protein and silver nanoparticles were further studied using *in silico* simulations. It is well evident that the functional dynamics of proteins typically take place on a picosecond to millisecond timescale. As the field on nanobiotechnology is in its infant stage, there are hardly any experimental techniques available which can deliver sufficient time and spatial resolution to follow the atomistic motions step by step, in order to be able to view proteins "in real time action", like under a microscope. Moreover,

atomic-detail insights into protein-nanoparticle complexes are difficult to obtain because the high surface-to-volume ratio of nanoparticles makes them physically and chemically different from the bulk, requiring unconventional methods to probe the interface (Mahmoudi et al. 2011, Mout and Rotello 2013). Therefore, *in silico* simulations were opted as methods of choice to monitor the atomic motions of the proteins. The observations would not only determine protein dynamics but also help in understanding protein-nanoparticle interactions.

Molecular simulation is a powerful and modern “predictive” tool for solving scientific problems as numerical experiments can be performed for new materials without synthesizing them (Rapaport 2004, Dodson et al. 2008). Moreover, molecular simulations owing to their unique property of probing the space and timescales simultaneously can serve as a promising avenue for the significantly detailed characterization of many biological reactions. The most widely used simulation methods for molecular systems are Monte Carlo, Molecular dynamics and Brownian dynamics. The Monte Carlo method is a stochastic strategy that relies on probabilities (Martí-Renom et al. 2000). The Monte Carlo sampling technique generates large numbers of configurations or microstates of equilibrated systems by stepping from one microstate to the next in a particular statistical ensemble. Random changes are made to the positions of the species present, together with their orientations and conformations where appropriate. In contrast, molecular dynamics is the most detailed molecular simulation method which computes the motions of individual molecules (Karplus and McCammon 2002). Molecular dynamics efficiently evaluates different configuration properties and dynamic quantities which generally cannot be obtained by Monte Carlo (Haile 1992).

Brownian dynamics (BD) simulation is a variation of molecular dynamics in which the use of approximations makes possible long timescale calculations. It is an efficient approach for simulation of large polymer molecules or colloidal particles in a small molecule solvent. In this approach, the solvent is treated as a viscous continuum which dissipates energy as macromolecules or particles move through it. The Brownian motion of the macromolecules produced by random collisions with solvent molecules is mimicked by a stochastic force generated by pseudo-random numbers. BD simulations have been widely employed to investigate the protein-nanoparticle interactions. Based on three-dimensional Brownian dynamics, Noguchi and Takasu (2001) developed a model of amphiphilic molecules to investigate the shape transformations with topological change with molecular resolution. A similar model was further modified to study the interaction of bilayer vesicles and adhesive nanoparticles using a Brownian dynamics simulation (Noguchi and Takasu 2002). Similarly, BD simulation was utilized to investigate the initial stages of hen egg-white lysozyme (HEWL) adsorption at a charged solid interface (Ravichandran et al. 2001). The protein was modelled at the atomistic level and the adsorption surface was represented by a planar array of positively

charged sites. Recently, Brancolini et al. (2012) used BD simulations to investigate the interaction between gold nanoparticles and ubiquitin protein.

The BD simulations of alkaline protease protein and silver nanoparticles were performed using PrometCS protein-metal continuum solvent model. The model has been well demonstrated for studying protein-nanoparticle interactions for an uncharged surface such as bare gold surface (Kokh et al. 2010). In this model, the interaction energy of a protein molecule with a metal surface is described by three main terms: van der Waals energy (which accounts for weak chemical binding of aromatic residues, sulphur and histidine nitrogen atoms to metal), adsorbate-metal electrostatic interaction energy (contributed by binding of the charged side chains), and desolvation energy of the protein, $U_{ds p}$, and that of the metal surface, $U_{ds M}$.

Our studies were based on the assumption that a nanoparticle exposing an Ag(111) face larger than the protein diameter (3 nm), can be approximated as a large crystalline surface. As shown in Chapter III, the silver nanoparticles used have an approximate mean diameter of 17 nm; therefore the space available on the surface of a single NP is approximately 150 times that occupied by a single protein. Thus, it is reasonable to assume that protease sees the nanoparticle locally as a flat Ag surface. The structures of protein surface encounter complexes were generated by running Brownian dynamics simulations during which the internal structure of the protein is kept rigid (Figure 4.14). The interaction (free) energy of protein with the surface and adsorption free energies of protease on the Ag(111) surface were computed for the obtained structures. Moreover, the protein surface encounter complexes obtained during a BD simulation trajectory were clustered to identify genuinely different protein orientations. For each of the most populated complexes, which were ranked by size, a representative structure was selected.

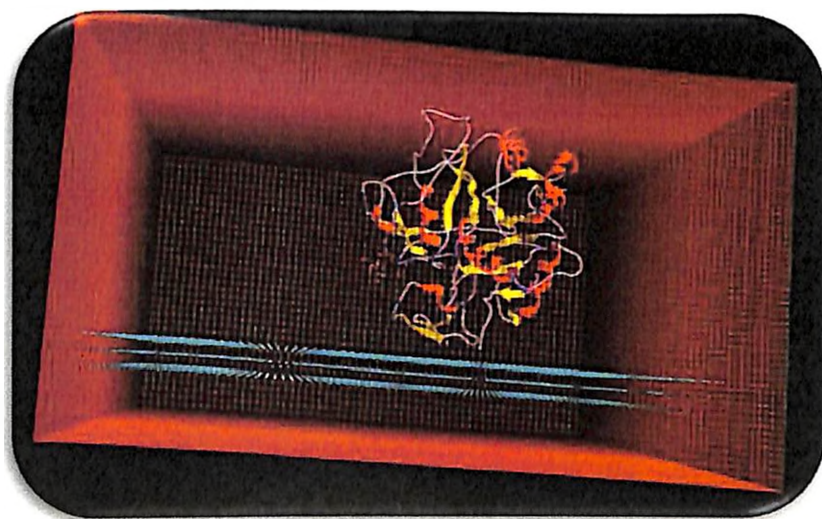


Figure 4.14 Snapshot depicting the Brownian dynamics simulation of the protease-Ag(111) complex.

BD simulations of protease-Ag(111) complex yielded one orientation which accounted for more than 70% of all the obtained encounter orientations. A representative structure of computed protease-Ag(111) complex is shown in Figure 4.15. It can be observed that the most abundant orientation comprises of four binding residues viz. TYR59, SER107, ASP111 and ASN118. The involvement of these four residues indicated strong binding of protease with Ag(111) surface. The observation is in agreement with a previous report which associated the nanoparticle binding with the total amount of residues contacting the surface (Brancolini et al. 2012). Moreover, polypeptides containing a higher number of residues were found to be more effective in controlling nanoparticle growth. The energy values of the interactions between abundant protein orientation and Ag(111) surface have been mentioned in Table 4.8. The binding in protease-Ag(111) complex is mostly driven by the Lennard-Jones potential which can be justified based on the presence of aromatic tyrosine amino acid in the predicted binding site. A significant contribution of electrostatic interactions was also observed which could be contributed by the presence of aspartic acid residue in the binding site. The spread value was calculated by measuring the average distance between the backbone atoms after superimposition of all the observed structures of abundant encounter complex. An observed low spread value (0.22) indicated minute deviation of the atoms at binding site suggesting stable interactions between protease and Ag(111) surface.

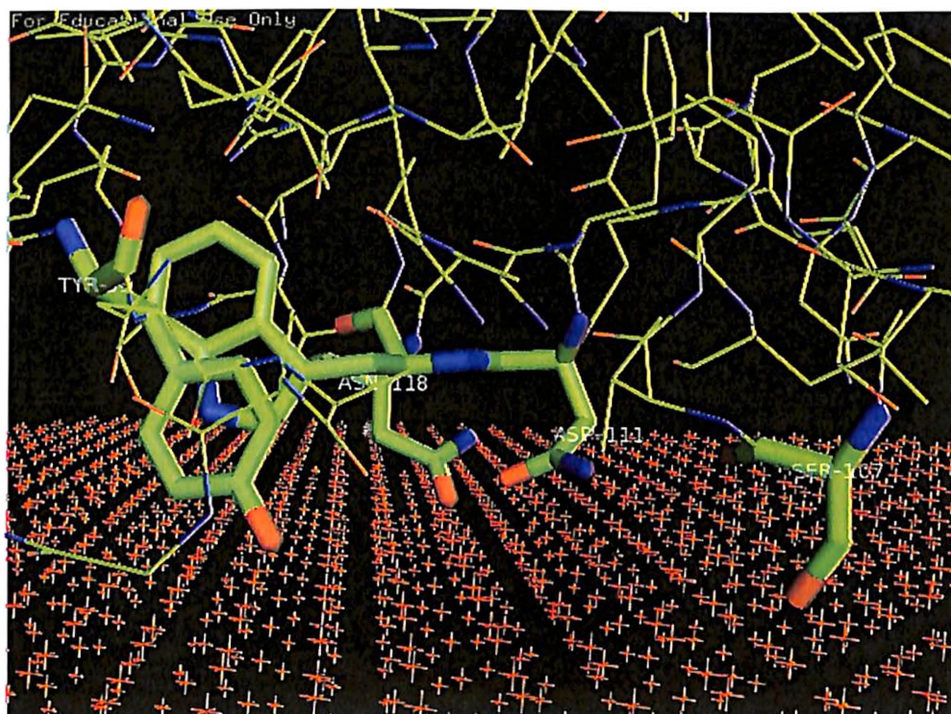


Figure 4.15 A representative image showing the predicted binding sites of protease on Ag(111) surface after performing Brownian dynamics simulation.

Table 4.8 Summary of the most abundant encounter complex from Brownian dynamics simulation of the protease-Ag(111) system.

Parameter	Value
U_{repr}	-30.12
$E_{LJ} + U_{ds}^p$	-89.45
$E_{LJ} + U_{ds}^p + U_{ds}^m$	-29.14
U_{EP}	-5.79
spread	0.22

U_{repr} = total interaction energy; E_{LJ} = Lennard-Jones energy; U_{ds}^p = nonpolar desolvation energy; U_{ds}^m = surface desolvation energy; U_{EP} = total electrostatic energy and spread = RMSD of the structures within the cluster

The occurrence of negatively charged amino acid (Asp111) in the predicted binding site was found to be very interesting. Aspartic acid can bear a negative charge due to the negatively charged carboxylate ion which can attract silver ions and serve as prominent nucleation site. The binding of silver ions with the carboxylate group of different molecules has been previously well-documented (Joly et al. 2000). In general, negatively charged amino acid residues sequester positively charged silver ions resulting in their reduction and nucleation to form silver nanoparticles (Rafey et al. 2011).

After the incorporation of silver ions, the next step of silver nanoparticle synthesis involves the reduction of silver ions. As shown in Figure 4.15, our predicted binding site comprised of terminal -COOH group of ASP111 and -OH groups of TYR59 and SER107 residues. The importance of terminal -COOH, -OH and -SH groups of proteins and/or peptides in the synthesis of different size and shape of advanced silver nanomaterials has been well recognized. Tyrosine has been long considered as a key molecule in nanoparticle synthesis and the interactions between tyrosine residues and metal ions are well characterized (Selvakannan et al. 2004). The amino acid contains three very polar functional groups viz. carboxyl, primary amine and hydroxyl which can easily transfer their electron to perform reduction reactions. Zhou and co-workers prepared gold-silk fibroin core-shell nanoparticles by using silk fibroin containing tyrosine residues as both reducing and stabilizing agents (Zhou et al. 2001). An elegant study by Naik et al. (2002) demonstrated the prominent role of tyrosine in nanoparticle synthesis. By combinatorial approaches using a phage display peptide library; they identified three dodecapeptides (AG3, AG4, and AG5) which can bind silver. Interestingly, only AG3 (AYSSGAPMPPF) and AG4 (NPSSLFRYLPSD) peptides were active for the reduction of Ag^+ ions to Ag nanoparticles. In contrast, the Ag-binding peptide without the Tyr residue (AG5

(SLATQPRTTPPV)) could not reduce Ag^+ ions. Si et al. (2006) also reported the reduction of silver ions with tyrosine at alkaline conditions leading to formation of silver nanoparticles. They predicted the involvement of tyrosine side chains (indole-, hydroxyl-, carboxyl-, and sulfur-side chain residues) in the reduction process. A tyrosine-containing short peptide was also designed to execute self-assembly of gold nanoparticles (Bhattacharjee et al. 2005).

Serine, an amino acid with a hydroxyl group, has also been reported to perform important role in nanoparticle synthesis such as biosilicification process (Shimizu et al. 1998). Moreover, it has been postulated that hydroxyl-rich residues in addition to cationic residues can accelerate silica polymerization (Brutchey and Morse 2008). Similarly, there are sufficient evidences in the literature which indicates the role of aspartic acid in the reduction of metal ions. Aspartic acid has been reported to reduce aqueous chloroaurate ions leading to the formation of stable gold nanoparticles (Shao et al. 2004). Moreover, after the reduction process, aspartic acid can make electrostatic interaction and thereby stabilize nanoparticles. This ability of aspartic acid to bind to nanoparticle surface has been exploited to modulate the size of gold nanoparticles by simple variation in the chloroaurate ion: aspartic acid molar ratio in the reaction medium (Mandal et al. 2002). Peptides and proteins with aspartic acids in their sequences allowed the reduction of silver or titanium and formation of nanoparticles in many different studies (Naik et al. 2002, 2004, Sano et al. 2005). While studying the synthesis of silver nanoparticles using algae *Chlorella vulgaris*, Xie et al. (2007) observed the important role of aspartate residues in an algal protein to direct the anisotropic growth of silver nanoparticles. Similarly, a yeast was modified to display the aspartic or glutamic hexamer peptides on its surface to allow the formation of a coat of silver nanoparticles (Nam et al. 2008). More recently, Carreño-Fuentes et al. (2013) proposed that the spatial arrangement of aspartate is fundamental for silver ion nucleation.

In the present study, involvement of Asp111 residue has been observed which indicates its role in reduction of silver ions. It is noteworthy that in the predicted binding site, Asp111 is oriented in such a way that the carboxylate group of their side chains faces towards the solvent, which allows nucleation and stabilization of silver nanoparticles in the center by the side chains (Figure 4.16). Our studies on protein-nanoparticle interactions predict a peculiar arrangement of amino acids that execute the synthesis and stabilization of silver nanoparticles. We propose that Asp111 served as site for binding of silver ions based on electrostatic attraction. Subsequently, $-\text{COOH}$ group of Asp111 and $-\text{OH}$ groups of Tyr59 and Ser107 residues reduced the silver ions to generate Ag^0 state and allowed nucleation. Lastly, the spatial arrangement of carboxylate group of the Asp111 residue towards the solvent allowed the stabilization of silver nanoparticles in the center by the side chains. Hence, our results indicate that the sequence and charge of amino acids in a protein alone are not sufficient, but a specific tri-dimensional configuration is also required to achieve “dual function” of nanoparticle synthesis and stabilization.

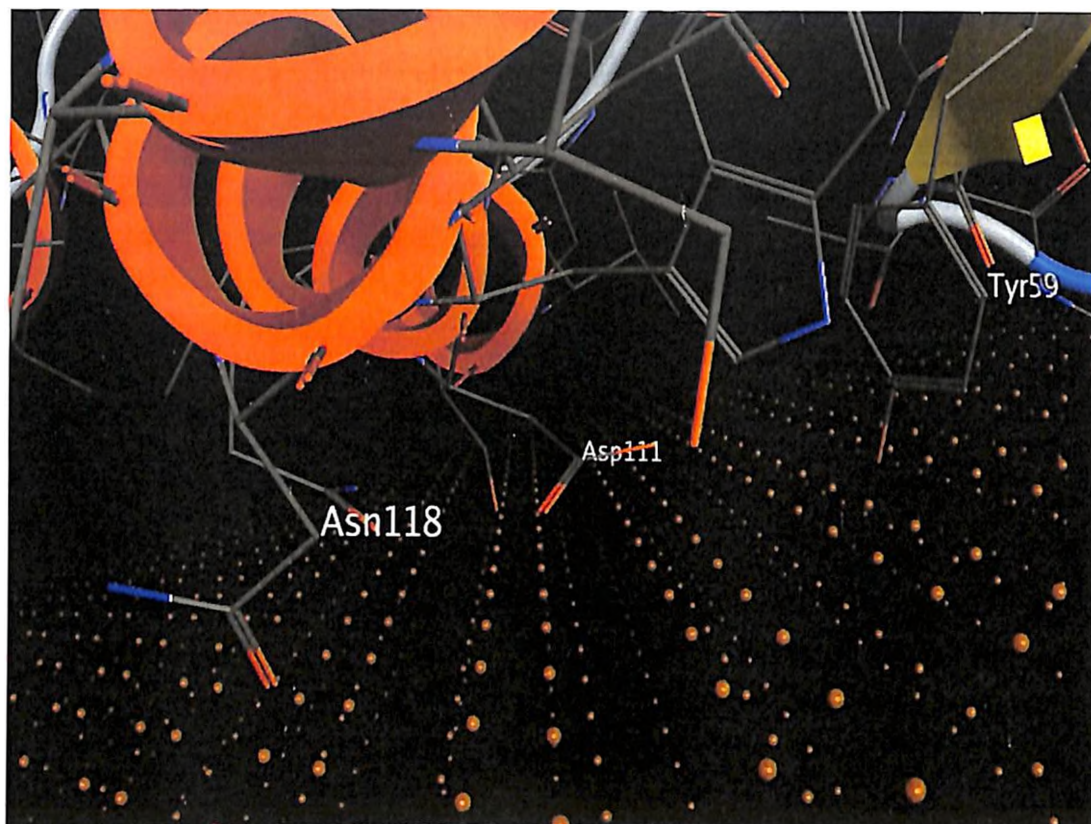


Figure 4.16 Close-up view depicting the orientation of Asp111 in the predicted binding site of protease on Ag(111) surface.

4.4 Conclusions

The present chapter attempted to decipher the secret “bioactive molecules” involved in the synthesis of silver nanoparticles by fungus *Aspergillus flavus* isolate NJP08. Our investigations commenced with the profiling of secreted proteins present in the fungal cell-free filtrate. We observed eight prominent proteins which were systematically separated and screened for silver nanoparticle synthesis using chromatographic methods. A protein with a molecular mass of ca. 33 kDa was found to execute the “dual function” of silver reduction and stabilization. Characterization of the purified protein using SDS-PAGE, LC-MS/MS and N-terminal sequencing revealed its identity as “alkaline protease”. We further investigated the effect of silver nanoparticle binding on the structure and function of alkaline protease. A dose-dependent response was observed with no or minute loss of proteolytic activity up to the nanoparticle concentration of 50 mM. This clearly indicated that the site of nanoparticle binding is distinct from the protease catalytic site and prompted us to perform further investigations to reveal the binding site of nanoparticles. To achieve this, we constructed the three dimensional structure of alkaline protease using homology modelling tools. The structure refinement and subsequent validation using various softwares validated the constructed homology model as a reliable

structure. Brownian dynamics simulations of the protease-Ag(111) complex showed that the protease binding to silver nanoparticles is highly specific with binding site involving four amino acid residues viz. Tyr59, Ser107, Asp111 and Asn 118. Energy calculations revealed the involvement of electrostatic as well as Lennard-Jones energy potential. To the best of our knowledge, this is the first attempt to identify such a structural configuration among aspartic residues and silver nanoparticles in the enzyme alkaline protease. The obtained knowledge of protein-nanoparticle interactions can be exploited for the design and development of future bio-scaffolds to achieve mass scale production of nanoparticles.

4.5 References

- Aebersold, R. and Mann, M. (2003). Mass spectrometry-based proteomics. *Nature* **422**: 198-207.
- Ahmad, A., Mukherjee, P., Senapati, S., Mandal, D., Khan, M. I., Kumar, R. and Sastry, M. (2003). Extracellular biosynthesis of silver nanoparticles using the fungus *Fusarium oxysporum*. *Colloids and Surfaces, B: Biointerfaces* **28**: 313-318.
- Arnold, K., Bordoli, L., Kopp, J. and Schwede, T. (2006). The SWISS-MODEL workspace: a web-based environment for protein structure homology modelling. *Bioinformatics* **22**: 195-201.
- Baker, N. A., Sept, D., Joseph, S., Holst, M. J. and McCammon, J. A. (2001). Electrostatics of nanosystems: application to microtubules and the ribosome. *Proceedings of the National Academy of Sciences* **98**: 10037-10041.
- Bansal, V., Rautaray, D., Ahmad, A. and Sastry, M. (2004). Biosynthesis of zirconia nanoparticles using the fungus *Fusarium oxysporum*. *Journal of Materials Chemistry* **14**: 3303-3305.
- Barwal, I., Ranjan, P., Kateriya, S. and Yadav, S. C. (2011). Cellular oxido-reductive proteins of *Chlamydomonas reinhardtii* control the biosynthesis of silver nanoparticles. *Journal of Nanobiotechnology* **9**: 1-12.
- Benkert, P., Biasini, M. and Schwede, T. (2011). Toward the estimation of the absolute quality of individual protein structure models. *Bioinformatics* **27**: 343-350.
- Benkert, P., Schwede, T. and Tosatto, S. C. (2009). QMEANclust: estimation of protein model quality by combining a composite scoring function with structural density information. *BMC Structural Biology* **9**: 35.
- Benkert, P., Tosatto, S. C. and Schomburg, D. (2008). QMEAN: A comprehensive scoring function for model quality assessment. *Proteins: Structure, Function, and Bioinformatics* **71**: 261-277.
- Bharde, A., Rautaray, D., Bansal, V., Ahmad, A., Sarkar, I., Yusuf, S. M., Sanyal, M. and Sastry, M. (2006). Extracellular biosynthesis of magnetite using fungi. *Small* **2**: 135-141.

- Bhattacharjee, R. R., Das, A. K., Haldar, D., Si, S., Banerjee, A. and Mandal, T. K. (2005). Peptide-assisted synthesis of gold nanoparticles and their self-assembly. *Journal of Nanoscience and Nanotechnology* **5**: 1141-1147.
- Bhunia, A., Samanta, P., Saha, S. and Kamilya, T. (2013). ZnO nanoparticle-protein interaction: Corona formation with associated unfolding. *Applied Physics Letters* **103**: 143701.
- Bjellqvist, B., Pasquali, C., Ravier, F., Sanchez, J. C. and Hochstrasser, D. (1993). A nonlinear wide-range immobilized pH gradient for two-dimensional electrophoresis and its definition in a relevant pH scale. *Electrophoresis* **14**: 1357-1365.
- Bordoli, L., Kiefer, F., Arnold, K., Benkert, P., Battey, J. and Schwede, T. (2008). Protein structure homology modeling using SWISS-MODEL workspace. *Nature Protocols* **4**: 1-13.
- Brancolini, G., Kokh, D. B., Calzolari, L., Wade, R. C. and Corni, S. (2012). Docking of ubiquitin to gold nanoparticles. *ACS Nano* **6**: 9863-9878.
- Brown, K. R., Walter, D. G. and Natan, M. J. (2000). Seeding of colloidal Au nanoparticle solutions. 2. Improved control of particle size and shape. *Chemistry of Materials* **12**: 306-313.
- Brutchey, R. L. and Morse, D. E. (2008). Silicatein and the translation of its molecular mechanism of biosilicification into low temperature nanomaterial synthesis. *Chemical Reviews* **108**: 4915-4934.
- Carreño-Fuentes, L., Ascencio, J. A., Medina, A., Aguila, S., Palomares, L. A. and Ramírez, O. T. (2013). Strategies for specifically directing metal functionalization of protein nanotubes: constructing protein coated silver nanowires. *Nanotechnology* **24**: 235602.
- Chait, B. T. (2006). Mass spectrometry: Bottom-up or top-down? *Science* **314**: 65-66.
- Chatterjee, T., Chakraborti, S., Joshi, P., Singh, S. P., Gupta, V. and Chakrabarti, P. (2010). The effect of zinc oxide nanoparticles on the structure of the periplasmic domain of the *Vibrio cholerae* ToxR protein. *FEBS Journal* **277**: 4184-4194.
- Chen, Z. Y., Brown, R. L., Cary, J. W., Damann, K. E. and Cleveland, T. E. (2009). Characterization of an *Aspergillus flavus* alkaline protease and its role in the infection of maize kernels. *Toxin Reviews* **28**: 187-197.
- Colombo, M., Mazzucchelli, S., Collico, V., Avvakumova, S., Pandolfi, L., Corsi, F., Porta, F. and Prospero, D. (2012). Protein-assisted one-pot synthesis and biofunctionalization of spherical gold nanoparticles for selective targeting of cancer cells. *Angewandte Chemie* **124**: 9406-9409.
- Colovos, C. and Yeates, T. O. (1993). Verification of protein structures: patterns of nonbonded atomic interactions. *Protein Science* **2**: 1511-1519.
- Cottrell, J. S. and London, U. (1999). Probability-based protein identification by searching sequence databases using mass spectrometry data. *Electrophoresis* **20**: 3551-3567.

- Crookes-Goodson, W. J., Slocik, J. M. and Naik, R. R. (2008). Bio-directed synthesis and assembly of nanomaterials. *Chemical Society Reviews* **37**: 2403-2412.
- De, M., You, C.-C., Srivastava, S. and Rotello, V. M. (2007). Biomimetic interactions of proteins with functionalized nanoparticles: a thermodynamic study. *Journal of the American Chemical Society* **129**: 10747-10753.
- Deng, Z., Wang, S., Li, Q., Ji, X., Zhang, L. and Hong, M. (2010). Purification and characterization of a novel fibrinolytic enzyme from the polychaete, *Neanthes japonica* (Iznka). *Bioresource Technology* **101**: 1954-1960.
- Dhillon, G. S., Brar, S. K., Kaur, S. and Verma, M. (2012). Green approach for nanoparticle biosynthesis by fungi: current trends and applications. *Critical Reviews in Biotechnology* **32**: 49-73.
- Dickerson, M. B., Naik, R. R., Stone, M. O., Cai, Y. and Sandhage, K. H. (2004). Identification of peptides that promote the rapid precipitation of germania nanoparticle networks via use of a peptide display library. *Chemical Communications*: 1776-1777.
- Dickerson, M. B., Sandhage, K. H. and Naik, R. R. (2008). Protein- and peptide-directed syntheses of inorganic materials. *Chemical Reviews* **108**: 4935.
- Dodson, G. G., Lane, D. P. and Verma, C. S. (2008). Molecular simulations of protein dynamics: new windows on mechanisms in biology. *EMBO Reports* **9**: 144-150.
- Douglas, T. and Young, M. (1998). Host-guest encapsulation of materials by assembled virus protein cages. *Nature* **393**: 152-155.
- Douglas, T. and Young, M. (2006). Viruses: making friends with old foes. *Science* **312**: 873-875.
- Durán, N., Marcato, P. D., Alves, O. L., De Souza, G. I. and Esposito, E. (2005). Mechanistic aspects of biosynthesis of silver nanoparticles by several *Fusarium oxysporum* strains. *Journal of Nanobiotechnology* **3**: 1-7.
- Dutta, N., Mukhopadhyay, A., Dasgupta, A. K. and Chakrabarti, K. (2013). Nanotechnology enabled enhancement of enzyme activity and thermostability: Study on impaired pectate lyase from attenuated *Macrophomina phaseolina* in presence of hydroxyapatite nanoparticle. *PLoS One* **8**: e63567.
- Eby, D. M., Schaeublin, N. M., Farrington, K. E., Hussain, S. M. and Johnson, G. R. (2009). Lysozyme catalyzes the formation of antimicrobial silver nanoparticles. *ACS Nano* **3**: 984-994.
- Edman, P. (1950). Method for determination of the amino acid sequence in peptides. *Acta Chemica Scandinavica* **4**: 283-293.
- Eisenberg, D., Lüthy, R. and Bowie, J. U. (1997). VERIFY3D: Assessment of protein models with three-dimensional profiles. *Methods in Enzymology* **277**: 396-404.

- Eswar, N., Webb, B., Marti-Renom, M. A., Madhusudhan, M., Eramian, D., Shen, M. y., Pieper, U. and Sali, A. (2006). Comparative protein structure modeling using Modeller. *Current protocols in bioinformatics*: 5.6. 1-5.6. 30.
- Fiser, A. and Šali, A. (2003). Modeller: generation and refinement of homology-based protein structure models. *Methods in Enzymology* 374: 461-491.
- Gao, Q., Jin, K., Ying, S.-H., Zhang, Y., Xiao, G., Shang, Y., Duan, Z., Hu, X., Xie, X.-Q. and Zhou, G. (2011). Genome sequencing and comparative transcriptomics of the model entomopathogenic fungi *Metarhizium anisopliae* and *M. acridum*. *PLoS Genetics* 7: e1001264.
- Gordon, J. C., Myers, J. B., Folta, T., Shoja, V., Heath, L. S. and Onufriev, A. (2005). H⁺⁺: a server for estimating pK_as and adding missing hydrogens to macromolecules. *Nucleic Acids Research* 33: W368-W371.
- Gugliotti, L. A., Feldheim, D. L. and Eaton, B. E. (2005). RNA-mediated control of metal nanoparticle shape. *Journal of the American Chemical Society* 127: 17814-17818.
- Guruprasad, K., Reddy, B. B. and Pandit, M. W. (1990). Correlation between stability of a protein and its dipeptide composition: a novel approach for predicting *in vivo* stability of a protein from its primary sequence. *Protein Engineering* 4: 155-161.
- Haile, J. M. (1992). *Molecular Dynamics Simulation: Elementary Methods*, Wiley.
- Hernández-Martínez, R., Gutiérrez-Sánchez, G., Bergmann, C., Loera-Corral, O., Rojo-Domínguez, A., Huerta-Ochoa, S., Regalado-González, C. and Prado-Barragán, L. (2011). Purification and characterization of a thermodynamic stable serine protease from *Aspergillus fumigatus*. *Process Biochemistry* 46: 2001-2006.
- Hubbard, T. and Blundell, T. (1987). Comparison of solvent-inaccessible cores of homologous proteins: definitions useful for protein modelling. *Protein Engineering* 1: 159-171.
- Ikeda, H., Ishikawa, J., Hanamoto, A., Shinose, M., Kikuchi, H., Shiba, T., Sakaki, Y. and Hattori, M. (2003). Complete genome sequence and comparative analysis of the industrial microorganism *Streptomyces avermitilis*. *Nature Biotechnology* 21: 526-531.
- Ilari, A., Ceci, P., Ferrari, D., Rossi, G. L. and Chiancone, E. (2002). Iron incorporation into *Escherichia coli* Dps gives rise to a ferritin-like microcrystalline core. *Journal of Biological Chemistry* 277: 37619-37623.
- Iori, F., Di Felice, R., Molinari, E. and Corni, S. (2009). GolP: An atomistic force-field to describe the interaction of proteins with Au (111) surfaces in water. *Journal of Computational Chemistry* 30: 1465-1476.
- Iwashita, K. (2002). Recent studies of protein secretion by filamentous fungi. *Journal of Bioscience and Bioengineering* 94: 530-535.

- Joly, S., Kane, R., Radzilowski, L., Wang, T., Wu, A., Cohen, R., Thomas, E. and Rubner, M. (2000). Multilayer nanoreactors for metallic and semiconducting particles. *Langmuir* **16**: 1354-1359.
- Joshi, P., Chakraborty, S., Dey, S., Shanker, V., Ansari, Z., Singh, S. P. and Chakrabarti, P. (2011). Binding of chloroquine-conjugated gold nanoparticles with bovine serum albumin. *Journal of Colloid and Interface Science* **355**: 402-409.
- Käkinen, A., Ding, F., Chen, P., Mortimer, M., Kahru, A. and Ke, P. C. (2013). Interaction of firefly luciferase and silver nanoparticles and its impact on enzyme activity. *Nanotechnology* **24**: 345101.
- Karplus, M. and McCammon, J. A. (2002). Molecular dynamics simulations of biomolecules. *Nature Structural & Molecular Biology* **9**: 646-652.
- Kasyutich, O., Ilari, A., Fiorillo, A., Tatchev, D., Hoell, A. and Ceci, P. (2010). Silver ion incorporation and nanoparticle formation inside the cavity of *Pyrococcus furiosus* ferritin: structural and size-distribution analyses. *Journal of the American Chemical Society* **132**: 3621-3627.
- Katz, M. E., Dougall, A. M., Weeks, K. and Cheetham, B. F. (2005). Multiple genetically distinct groups revealed among clinical isolates identified as atypical *Aspergillus fumigatus*. *Journal of Clinical Microbiology* **43**: 551-555.
- Kherraz, K., Kherraz, K. and Kameli, A. (2011). Homology modeling of Ferredoxin-nitrite reductase from *Arabidopsis thaliana*. *Bioinformation* **6**: 115.
- Kim, Y., Nandakumar, M. P. and Marten, M. R. (2008). The state of proteome profiling in the fungal genus *Aspergillus*. *Briefings in Functional Genomics and Proteomics* **7**: 87-94.
- Klaus, T., Joerger, R., Olsson, E. and Granqvist, C. G. (1999). Silver-based crystalline nanoparticles, microbially fabricated. *Proceedings of the National Academy of Sciences of the United States of America* **96**: 13611-13614.
- Kokh, D. B., Corni, S., Winn, P. J., Hoefling, M., Gottschalk, K. E. and Wade, R. C. (2010). ProMetCS: an atomistic force field for modeling protein - metal surface interactions in a continuum aqueous solvent. *Journal of Chemical Theory and Computation* **6**: 1753-1768.
- Kolattukudy, P., Lee, J., Rogers, L., Zimmerman, P., Ceselski, S., Fox, B., Stein, B. and Copelan, E. (1993). Evidence for possible involvement of an elastolytic serine protease in aspergillosis. *Infection and Immunity* **61**: 2357-2368.
- Kramer, R. M., Li, C., Carter, D. C., Stone, M. O. and Naik, R. R. (2004). Engineered protein cages for nanomaterial synthesis. *Journal of the American Chemical Society* **126**: 13282-13286.
- Krieger, E., Nabuurs, S. B. and Vriend, G. (2003). Homology modeling. *Methods of Biochemical Analysis* **44**: 509-524.

- Kumar, S. A., Abyaneh, M. K., Gosavi, S., Kulkarni, S. K., Pasricha, R., Ahmad, A. and Khan, M. (2007). Nitrate reductase-mediated synthesis of silver nanoparticles from AgNO₃. *Biotechnology Letters* **29**: 439-445.
- Kyte, J. and Doolittle, R. F. (1982). A simple method for displaying the hydrophobic character of a protein. *Journal of Molecular Biology* **157**: 105-132.
- Laemmli, U. K. (1970). Cleavage of structural proteins during the assembly of the head of bacteriophage T4. *Nature* **227**: 680-685.
- Laskowski, R. A., MacArthur, M. W., Moss, D. S. and Thornton, J. M. (1993). PROCHECK: a program to check the stereochemical quality of protein structures. *Journal of Applied Crystallography* **26**: 283-291.
- Lengke, M. F., Fleet, M. E. and Southam, G. (2007). Biosynthesis of silver nanoparticles by filamentous cyanobacteria from a silver (I) nitrate complex. *Langmuir* **23**: 2694-2699.
- Liithy, R., Bowie, J. U. and Eisenberg, D. (1992). Assessment of protein models with three-dimensional profiles. *Nature* **356**: 83-85.
- Linse, S., Cabaleiro-Lago, C., Xue, W.-F., Lynch, I., Lindman, S., Thulin, E., Radford, S. E. and Dawson, K. A. (2007). Nucleation of protein fibrillation by nanoparticles. *Proceedings of the National Academy of Sciences* **104**: 8691-8696.
- Liu, G., Wu, H., Dohnalkova, A. and Lin, Y. (2007). Apoferritin-templated synthesis of encoded metallic phosphate nanoparticle tags. *Analytical Chemistry* **79**: 5614-5619.
- Lok, C.-N., Ho, C.-M., Chen, R., He, Q.-Y., Yu, W.-Y., Sun, H., Tam, P. K.-H., Chiu, J.-F. and Che, C.-M. (2007). Silver nanoparticles: partial oxidation and antibacterial activities. *Journal of Biological Inorganic Chemistry* **12**: 527-534.
- Lok, C. N., Ho, C. M., Chen, R., He, Q. Y., Yu, W. Y., Sun, H. Z., Tam, P. K. H., Chiu, J. F. and Che, C. M. (2006). Proteomic analysis of the mode of antibacterial action of silver nanoparticles. *Journal of Proteome Research* **5**: 916-924.
- Lundqvist, M., Stigler, J., Elia, G., Lynch, I., Cedervall, T. and Dawson, K. A. (2008). Nanoparticle size and surface properties determine the protein corona with possible implications for biological impacts. *Proceedings of the National Academy of Sciences of the United States of America* **105**: 14265-14270.
- Lynch, I., Cedervall, T., Lundqvist, M., Cabaleiro-Lago, C., Linse, S. and Dawson, K. A. (2007). The nanoparticle - protein complex as a biological entity; a complex fluids and surface science challenge for the 21st century. *Advances in Colloid and Interface Science* **134-35**: 167-174.
- Lynch, I. and Dawson, K. A. (2008). Protein-nanoparticle interactions. *Nano Today* **3**: 40-47.
- Lynch, I., Salvati, A. and Dawson, K. A. (2009). Protein-nanoparticle interactions: what does the cell see? *Nature Nanotechnology* **4**: 546-547.

- Machida, M., Asai, K., Sano, M., Tanaka, T., Kumagai, T., Terai, G., Kusumoto, K.-I., Arima, T., Akita, O. and Kashiwagi, Y. (2005). Genome sequencing and analysis of *Aspergillus oryzae*. *Nature* **438**: 1157-1161.
- Mahmoudi, M., Kalhor, H. R., Laurent, S. and Lynch, I. (2013). Protein fibrillation and nanoparticle interactions: opportunities and challenges. *Nanoscale* **5**: 2570-2588.
- Mahmoudi, M., Lynch, I., Ejtehadi, M. R., Monopoli, M. P., Bombelli, F. B. and Laurent, S. (2011). Protein-nanoparticle interactions: opportunities and challenges. *Chemical Reviews* **111**: 5610-5637.
- Mandal, S., Selvakannan, P., Phadtare, S., Pasricha, R. and Sastry, M. (2002). Synthesis of a stable gold hydrosol by the reduction of chloroaurate ions by the amino acid, aspartic acid. *Journal of Chemical Sciences* **114**: 513-520.
- Marsden, R. L. and Orengo, C. A. (2008). Target selection for structural genomics: an overview. *Structural Proteomics*, Springer: 3-25.
- Martí-Renom, M. A., Stuart, A. C., Fiser, A., Sánchez, R., Melo, F. and Šali, A. (2000). Comparative protein structure modeling of genes and genomes. *Annual Review of Biophysics and Biomolecular Structure* **29**: 291-325.
- Martinez, D., Berka, R. M., Henrissat, B., Saloheimo, M., Arvas, M., Baker, S. E., Chapman, J., Chertkov, O., Coutinho, P. M. and Cullen, D. (2008). Genome sequencing and analysis of the biomass-degrading fungus *Trichoderma reesei* (syn. *Hypocrea jecorina*). *Nature Biotechnology* **26**: 553-560.
- Medina, M. L., Haynes, P. A., Brecci, L. and Francisco, W. A. (2005). Analysis of secreted proteins from *Aspergillus flavus*. *Proteomics* **5**: 3153-3161.
- Medina, M. L., Kiernan, U. A. and Francisco, W. A. (2004). Proteomic analysis of rutin-induced secreted proteins from *Aspergillus flavus*. *Fungal Genetics and Biology* **41**: 327-335.
- Mellon, J. E., Cotty, P. J. and Dowd, M. K. (2007). *Aspergillus flavus* hydrolases: their roles in pathogenesis and substrate utilization. *Applied Microbiology and Biotechnology* **77**: 497-504.
- Mikeš, O., Turková, J. and Allen, G. (1980). Isolation and structure determination of the peptides from the chymotryptic hydrolysate of the alkaline protease from *Aspergillus flavus*. *Collection of Czechoslovak Chemical Communications* **45**: 1996-2028.
- Monopoli, M. P., Åberg, C., Salvati, A. and Dawson, K. A. (2012). Biomolecular coronas provide the biological identity of nanosized materials. *Nature Nanotechnology* **7**: 779-786.
- Monopoli, M. P., Bombelli, F. B. and Dawson, K. A. (2010). Nanobiotechnology: nanoparticle coronas take shape. *Nature Nanotechnology* **6**: 11-12.
- Monopoli, M. P., Walczyk, D., Campbell, A., Elia, G., Lynch, I., Baldelli Bombelli, F. and Dawson, K. A. (2011). Physical- chemical aspects of protein corona: relevance to *in vitro*

- and *in vivo* biological impacts of nanoparticles. *Journal of the American Chemical Society* **133**: 2525-2534.
- Morris, A. L., MacArthur, M. W., Hutchinson, E. G. and Thornton, J. M. (1992). Stereochemical quality of protein structure coordinates. *Proteins: Structure, Function, and Bioinformatics* **12**: 345-364.
- Mout, R. and Rotello, V. M. (2013). Bio and nano working together: engineering the protein-nanoparticle interface. *Israel Journal of Chemistry* **53**: 521-529.
- Muthulakshmi, C., Gomathi, D., Kumar, D. G., Ravikumar, G., Kalaiselvi, M. and Uma, C. (2011). Production, purification and characterization of protease by *Aspergillus flavus* under solid state fermentation. *Jordan Journal of Biological Sciences* **4**: 137-148.
- Naik, R. R., Brott, L. L., Clarson, S. J. and Stone, M. O. (2002a). Silica-precipitating peptides isolated from a combinatorial phage display peptide library. *Journal of Nanoscience and Nanotechnology* **2**: 95-100.
- Naik, R. R., Jones, S. E., Murray, C. J., McAuliffe, J. C., Vaia, R. A. and Stone, M. O. (2004). Peptide templates for nanoparticle synthesis derived from polymerase chain reaction-driven phage display. *Advanced Functional Materials* **14**: 25-30.
- Naik, R. R. and Stone, M. O. (2005). Integrating biomimetics. *Materials Today* **8**: 18-26.
- Naik, R. R., Stringer, S. J., Agarwal, G., Jones, S. E. and Stone, M. O. (2002b). Biomimetic synthesis and patterning of silver nanoparticles. *Nature Materials* **1**: 169-172.
- Nair, L. S. and Laurencin, C. T. (2007). Silver nanoparticles: synthesis and therapeutic applications. *Journal of Biomedical Nanotechnology* **3**: 301-316.
- Nam, K. T., Lee, Y. J., Krauland, E. M., Kottmann, S. T. and Belcher, A. M. (2008). Peptide-mediated reduction of silver ions on engineered biological scaffolds. *ACS Nano* **2**: 1480-1486.
- Nel, A. E., Madler, L., Velegol, D., Xia, T., Hoek, E. M., Somasundaran, P., Klaessig, F., Castranova, V. and Thompson, M. (2009). Understanding biophysicochemical interactions at the nano-bio interface. *Nature Materials* **8**: 543-557.
- Noguchi, H. and Takasu, M. (2001). Self-assembly of amphiphiles into vesicles: A Brownian dynamics simulation. *Physical Review E* **64**: 041913.
- Noguchi, H. and Takasu, M. (2002). Adhesion of nanoparticles to vesicles: a Brownian dynamics simulation. *Biophysical Journal* **83**: 299-308.
- Oda, K., Kakizono, D., Yamada, O., Iefuji, H., Akita, O. and Iwashita, K. (2006). Proteomic analysis of extracellular proteins from *Aspergillus oryzae* grown under submerged and solid-state culture conditions. *Applied and Environmental Microbiology* **72**: 3448-3457.
- Ong, S.-E. and Mann, M. (2005). Mass spectrometry-based proteomics turns quantitative. *Nature Chemical Biology* **1**: 252-262.

- Parikh, R. Y., Singh, S., Prasad, B. L. V., Patole, M. S., Sastry, M. and Shouche, Y. S. (2008). Extracellular synthesis of crystalline silver nanoparticles and molecular evidence of silver resistance from *Morganella* sp.: towards understanding biochemical synthesis mechanism. *ChemBioChem* **9**: 1415-1422.
- Payne, G., Nierman, W., Wortman, J., Pritchard, B., Brown, D., Dean, R., Bhatnagar, D., Cleveland, T., Machida, M. and Yu, J. (2006). Whole genome comparison of *Aspergillus flavus* and *A. oryzae*. *Medical Mycology* **44**: 9-11.
- Pearlman, D. A., Case, D. A., Caldwell, J. W., Ross, W. S., Cheatham III, T. E., DeBolt, S., Ferguson, D., Seibel, G. and Kollman, P. (1995). AMBER, a package of computer programs for applying molecular mechanics, normal mode analysis, molecular dynamics and free energy calculations to simulate the structural and energetic properties of molecules. *Computer Physics Communications* **91**: 1-41.
- Peberdy, J. F. (1994). Protein secretion in filamentous fungi-trying to understand a highly productive black box. *Trends in Biotechnology* **12**: 50-57.
- Rafey, A., Shrivastava, K., Iqbal, S. A. and Khan, Z. (2011). Growth of Ag-nanoparticles using aspartic acid in aqueous solutions. *Journal of Colloid and Interface Science* **354**: 190-195.
- Rakshambikai, R., Srinivasan, N. and Nishant, K. T. (2013). Structural insights into *Saccharomyces cerevisiae* Msh4-Msh5 complex function using homology modeling. *PLoS One* **8**: e78753.
- Ramachandran, G. N., Ramakrishnan, C. and Sasisekharan, V. (1963). Stereochemistry of polypeptide chain configurations. *Journal of Molecular Biology* **7**: 95-99.
- Ramesh, M. V., Sirakova, T. D. and Kolattukudy, P. E. (1995). Cloning and characterization of the cDNAs and genes (*mep20*) encoding homologous metalloproteinases from *Aspergillus flavus* and *A. fumigatus*. *Gene* **165**: 121-125.
- Rana, S., Yeh, Y. C. and Rotello, V. M. (2010). Engineering the nanoparticle-protein interface: applications and possibilities. *Current Opinion in Chemical Biology* **14**: 828-834.
- Rapaport, D. C. (2004). The art of molecular dynamics simulation, Cambridge university press.
- Ravichandran, S., Madura, J. D. and Talbot, J. (2001). A Brownian dynamics study of the initial stages of hen egg-white lysozyme adsorption at a solid interface. *The Journal of Physical Chemistry B* **105**: 3610-3613.
- Rogers, S., Wells, R. and Rechsteiner, M. (1986). Amino acid sequences common to rapidly degraded proteins: the PEST hypothesis. *Science* **234**: 364-368.
- Sano, K.-I., Sasaki, H. and Shiba, K. (2005). Specificity and biomineralization activities of Ti-binding peptide-1 (TBP-1). *Langmuir* **21**: 3090-3095.
- Sarikaya, M., Tamerler, C., Jen, A. K. Y., Schulten, K. and Baneyx, F. (2003). Molecular biomimetics: nanotechnology through biology. *Nature Materials* **2**: 577-585.

- Scott, C. F. (1991). Mechanism of the participation of the contact system in the Vroman effect. Review and summary. *Journal of Biomaterials Science, Polymer Edition* **2**: 173-181.
- Selvakannan, P., Swami, A., Srisathiyarayanan, D., Shirude, P. S., Pasricha, R., Mandale, A. B. and Sastry, M. (2004). Synthesis of aqueous Au core-Ag shell nanoparticles using tyrosine as a pH-dependent reducing agent and assembling phase-transferred silver nanoparticles at the air-water interface. *Langmuir* **20**: 7825-7836.
- Shao, Y., Jin, Y. and Dong, S. (2004). Synthesis of gold nanoplates by aspartate reduction of gold chloride. *Chemical Communications*: 1104-1105.
- Shevchenko, A., Wilm, M., Vorm, O. and Mann, M. (1996). Mass spectrometric sequencing of proteins from silver-stained polyacrylamide gels. *Analytical Chemistry* **68**: 850-858.
- Shimizu, K., Cha, J., Stucky, G. D. and Morse, D. E. (1998). Silicatein α : cathepsin L-like protein in sponge biosilica. *Proceedings of the National Academy of Sciences* **95**: 6234-6238.
- Shinano, T., Komatsu, S., Yoshimura, T., Tokutake, S., Kong, F.-J., Watanabe, T., Wasaki, J. and Osaki, M. (2011). Proteomic analysis of secreted proteins from aseptically grown rice. *Phytochemistry* **72**: 312-320.
- Shrinivas, D. and Naik, G. R. (2011). Characterization of alkaline thermostable keratinolytic protease from thermoalkalophilic *Bacillus halodurans* JB 99 exhibiting dehairing activity. *International Biodeterioration & Biodegradation* **65**: 29-35.
- Si, S., Bhattacharjee, R. R., Banerjee, A. and Mandal, T. K. (2006). A mechanistic and kinetic study of the formation of metal nanoparticles by using synthetic tyrosine-based oligopeptides. *Chemistry-A European Journal* **12**: 1256-1265.
- Slocik, J. M., Stone, M. O. and Naik, R. R. (2005). Synthesis of gold nanoparticles using multifunctional peptides. *Small* **1**: 1048-1052.
- Smith, G. P., Baustian, K. J., Ackerson, C. J. and Feldheim, D. L. (2009). Metal oxide formation by serine and cysteine proteases. *Journal of Materials Chemistry* **19**: 8299.
- Smith, P., Krohn, R. I., Hermanson, G., Mallia, A., Gartner, F., Provenzano, M., Fujimoto, E., Goeke, N., Olson, B. and Klenk, D. (1985). Measurement of protein using bicinchoninic acid. *Analytical Biochemistry* **150**: 76-85.
- Tan, Y. N., Lee, J. Y. and Wang, D. I. (2010). Uncovering the design rules for peptide synthesis of metal nanoparticles. *Journal of the American Chemical Society* **132**: 5677-5686.
- Tatsumi, H., Murakami, S., Tsuji, R. F., Ishida, Y., Murakami, K., Masaki, A., Kawabe, H., Arimura, H., Nakano, E. and Motaf, H. (1991). Cloning and expression in yeast of a cDNA clone encoding *Aspergillus oryzae* neutral protease II, a unique metalloprotease. *Molecular and General Genetics* **228**: 97-103.
- Tatsumi, H., Ogawa, Y., Murakami, S., Ishida, Y., Murakami, K., Masaki, A., Kawabe, H., Arimura, H., Nakano, E. and Motai, H. (1989). A full length cDNA clone for the alkaline

- protease from *Aspergillus oryzae*: structural analysis and expression in *Saccharomyces cerevisiae*. *Molecular and General Genetics* **219**: 33-38.
- Thakkar, K. N., Mhatre, S. S. and Parikh, R. Y. (2010). Biological synthesis of metallic nanoparticles. *Nanomedicine-Nanotechnology Biology and Medicine* **6**: 257-262.
- Todd, T. J., Zhen, Z. and Xie, J. (2013). Ferritin nanocages: great potential as clinically translatable drug delivery vehicles? *Nanomedicine* **8**: 1555-1557.
- Uchida, M., Klem, M. T., Allen, M., Suci, P., Flenniken, M., Gillitzer, E., Varpness, Z., Liepold, L. O., Young, M. and Douglas, T. (2007). Biological containers: protein cages as multifunctional nanoplatfoms. *Advanced Materials* **19**: 1025-1042.
- Vilaseca, P., Dawson, K. A. and Franzese, G. (2013). Understanding and modulating the competitive surface-adsorption of proteins through coarse-grained molecular dynamics simulations. *Soft Matter* **9**: 6978-6985.
- Walkey, C. D. and Chan, W. C. W. (2012). Understanding and controlling the interaction of nanomaterials with proteins in a physiological environment. *Chemical Society Reviews* **41**: 2780-2799.
- Weiner, P. K. and Kollman, P. A. (1981). AMBER: Assisted model building with energy refinement. A general program for modeling molecules and their interactions. *Journal of Computational Chemistry* **2**: 287-303.
- Wong, K. K. and Mann, S. (1996). Biomimetic synthesis of cadmium sulfide-ferritin nanocomposites. *Advanced Materials* **8**: 928-932.
- Xie, J., Lee, J. Y., Wang, D. I. C. and Ting, Y. P. (2007). Silver nanoplates: from biological to biomimetic synthesis. *ACS Nano* **1**: 429-439.
- Yoshizawa, K., Iwahori, K., Sugimoto, K. and Yamashita, I. (2006). Fabrication of gold sulfide nanoparticles using the protein cage of apoferritin. *Chemistry Letters* **35**: 1192.
- Yu, C.-J., Chiou, S.-H., Lai, W.-Y., Chiang, B.-L. and Chow, L.-P. (1999). Characterization of a novel allergen, a major IgE-binding protein from *Aspergillus flavus*, as an alkaline serine protease. *Biochemical and Biophysical Research Communications* **261**: 669-675.
- Zhen, Z., Tang, W., Chen, H., Lin, X., Todd, T., Wang, G., Cowger, T., Chen, X. and Xie, J. (2013). RGD-modified apoferritin nanoparticles for efficient drug delivery to tumors. *ACS Nano* **7**: 4830-4837.
- Zhou, H. and Zhou, Y. (2002). Distance-scaled, finite ideal-gas reference state improves structure-derived potentials of mean force for structure selection and stability prediction. *Protein Science* **11**: 2714-2726.
- Zhou, Y., Chen, W., Itoh, H., Naka, K., Ni, Q., Yamane, H. and Chujo, Y. (2001). Preparation of a novel core-shell nanostructured gold colloid-silk fibroin bioconjugate by the protein *in situ* redox technique at room temperature. *Chemical Communications*: 2518-2519.

Chapter V

Silver Nanoparticles: Antibacterial Activity and Mode of Action

The present chapter herein details pertaining to the antibacterial studies of biologically synthesized silver nanoparticles with special emphasis to the role of protein shell. To achieve this, comparative antibacterial studies of protein-capped and bare silver nanoparticles were executed against representative Gram positive and Gram negative bacterial pathogens. Preliminary findings based on minimum inhibitory concentration and disk diffusion assays revealed that bare nanoparticles were more effective than protein-capped silver nanoparticles with varying antibacterial potential against tested bacterial strains. Further, mechanistic studies based on ROS generation and membrane damage suggested that protein-capped and bare silver nanoparticles demonstrate distinct mode of actions. TEM micrographs in conjunction with silver ion release measurements further strengthened these findings. The obtained results clearly indicated that surface modifications of nanoparticles with proteins allow modulation of their functional properties.

5.1 Introduction

Since the ancient times, silver has been popular for domestic use especially as an antibacterial agent. In fact, before the introduction of antibiotics in 1940s, silver was considered as the most effective antimicrobial compound and has been traditionally used for treatment of ulcers, to stimulate wound healing and as food preservative (Alexander 2009). The fabrication of utensils with silver coating and their use for the preservation of perishable items as well as for disinfection of water has been observed since ancient times. Evidences for the use of silver nitrate as an anti-bacterial agent has been traced back to the Roman pharmacopeia. In fact, silver was globally used as a disinfectant and anti-spoilage agent across many civilizations (Greece, Rome, Phoenicia, Macedonia). The writings of Herodotus suggested the use of silver as a precious booty, during the time of Pausanias (Sparta, 5th century BC). The account also reports that Hippocrates, the Father of medicine, promoted the use of silver for early healing of wounds (Lansdown 2002, Lansdown 2006). Alexander the Great (335 BC) was advised by Aristotle to store water in silver vessels and boil prior to use (Russell and Hugo 1994). Silver preparations have been found in a variety of medical applications such as topical cream for wound healing, optical preservatives, dental amalgams and importantly as coating agent for catheters. However, the use of silver has been limited due to its higher cost and emergence of equivalent effective antibiotics as an economic and efficient alternative. Moreover, lack of proper understanding of mechanism of their toxic effects also prevented the modifications and development of new silver-based formulations (Reidy et al. 2013).

Over the past few years, worldwide escalation and augmentation of multi-drug resistance in microorganisms, along with the rise of healthcare costs has been a serious concern for modern medicine (Neu 1992, Stewart and William Costerton 2001, Ruden et al. 2009, Allen et al. 2010, Andersson and Hughes 2010, 2011). Hence, there is a growing need to develop new and effective antimicrobial agents which are free of bacterial-resistance and exhibit low cost. Therefore, interest in the antimicrobial properties of silver has been revived. A variety of new silver formulations such as silver sulfadiazine, silver citrate, silver lactate, etc. has been developed and numerous silver integrated formulations (Katadyn, Argyrol, Movidyn, Tetrasil, Alagon, etc.) have been also commercialized (Pradeep and Anshup 2009). However, cost concern and reports of silver-resistant bacterial isolates has limited the use of silver as potential alternative to antibiotics.

Recent advances in the field of metal nanoparticles have opened avenues to use silver with nanometer dimensions as an effective antimicrobial agent. Since, most of the biological processes take place at the nanoscale level, a combined application of biology and nanotechnology can perhaps meet this challenge (Curtis and Wilkinson 2001). Silver nanoparticles are particularly advantageous in comparison to their bulk counterpart as former manifest high surface area to volume ratio which may provide better contact with microorganisms. It has been also demonstrated that silver nanoparticles restrict

microorganisms to develop resistance (Morones et al. 2005). Additionally, at low concentrations, silver nanoparticles are non-toxic to human cells, and hence considered as an environmental friendly antimicrobial agent (Arora et al. 2008). Thus, an enormous increase in applications of silver nanoparticles for a wide range of medical and commercial products has been observed which includes household antiseptic sprays and antimicrobial coatings for medical devices that sterilize air and surfaces (Rai et al. 2009). Silver nanoparticles are also widely used in textiles, cosmetics, air cleaners, food packaging, coating for refrigerators, water disinfection; in fact, in every application where bacteria may exert a harmful effect (Bartłomiejczyk et al. 2013).

The mechanism of bactericidal effects of silver nanoparticles has not been yet completely elucidated. In particular, there is debate as to whether toxicity is due to the effects of silver ions released from silver nanoparticles or specifically confined only to the nanoparticles. A plethora of studies has confirmed that the release of silver ions from the crystalline core of silver nanoparticles contribute to the bactericidal effects (Neal 2008, Xu et al. 2012). In aerobic conditions, silver nanoparticles get oxidised and release high concentrations of silver ions in solution, which interacts with proteins, giving rise to bactericidal effects. Moreover, micromolar levels of silver ions have been reported to uncouple respiratory electron transport from oxidative phosphorylation (Holt and Bard 2005), inhibit respiratory chain enzymes or interfere with the membrane permeability (Li et al. 2010) or interact with cytoplasmic components and nucleic acids (Feng et al. 2000). Thus, molecular mechanism of the bactericidal effect of much lower, i.e., micromolar, concentrations of silver ions is still not clear. In contrast, whether the bactericidal effects are “particle-specific” and exerted by crystalline nanoparticles is an elusive question. A recent study by Xiu et al. (2012), attempted to decipher this challenge by performing antibacterial studies under strict anaerobic conditions which allows precluding silver oxidation and Ag^+ release. Their findings completely ruled out the direct particle-specific bactericidal effects of silver nanoparticles and inferred Ag^+ ions as the definitive molecular toxicant for bactericidal effects.

Based on the above mentioned literature, release of silver ions can be considered as primary determinant for bactericidal effects. Thus, a strict control over the release of silver ions is a pre-requisite to modulate and control antibacterial activity of silver nanoparticles. Manipulation at various levels such as oxygen availability, particle size and morphology, surface charge and coating have been considered as important parameters to control and modulate antibacterial activity of silver nanoparticles. Among these parameters, surface coating (or functionalization) is more important as it determines aggregation and solubility in the environment which governs nanoparticle-microbe interactions. It has been observed that coating of silver nanoparticles with surfactants resulted in greater damage to microorganisms in comparison to similar-sized bare silver nanoparticles (Panáček et al. 2006, Kvitek et al. 2008). Similarly, comparative studies of polysaccharide coated silver nanoparticles and bare

silver nanoparticles showed that presence of polysaccharide molecules on nanoparticle surface facilitates the damage to mammalian cell-lines (Ahamed et al. 2008). Conversely, zero-valent iron oxide nanoparticles were found to be less toxic to microorganisms when coated with polymers or natural organic matter (Li et al. 2010). Variegated effects of surface chemistry on silver nanoparticle uptake and toxicity have been also reported. For instance, presence of molecules such as albumin, lecithin, polysorbital 80 or peptide on nanoparticle surface have facilitated nanoparticle uptake and toxicity, while polyethylene glycol interfered with nanoparticle uptake in the liver cells (Somasundaran et al. 2004). In contrast, a systematic sub-chronic reproduction toxicity assessment of silver nanoparticles coated with polyvinylpyrrolidone (hydrophilic) or oleic acid (amphiphilic) on soil earthworms (*Eisenia fetida*) showed no significant differences in Ag accumulation or toxicity (Shoults-Wilson et al. 2011). Hence, studies targeted to understand dynamic behaviour of nanoparticle coatings (inorganic or organic) could be highly informative for designing efficient antibacterial formulations of silver nanoparticles.

The presence of capping proteins on the surface of silver nanoparticles synthesized using biological method (Chapter IV) motivated us to evaluate their role in determining bactericidal effects. Systematic comparative investigations of protein-capped silver nanoparticles with bare nanoparticles were carried out against common clinical pathogenic microorganisms. The present findings would help in determining the effect of capping proteins on bactericidal effects of silver nanoparticles.

5.2 Materials and methods

5.2.1 Synthesis of protein-capped and bare silver nanoparticles

Aspergillus sp. NJP02 was used for the synthesis of protein-capped silver nanoparticles as per the protocol mentioned in Chapter III of the thesis. The fungus was used as it synthesizes silver nanoparticles with relatively thick protein shell on their surface. For preparation of bare silver nanoparticles, the as-synthesized protein-capped silver nanoparticle solution was centrifuged at 10,000 rpm for 20 min. The pellet was suspended in 1 % (w/v) Sodium dodecyl sulphate (SDS) solution and boiled in a water bath for 30 min in order to detach the protein corona from the surface of nanoparticles followed by centrifugation at 10,000 rpm for 20 min. The supernatant containing the unreacted SDS and SDS-protein complex was discarded and the pellet was boiled with 1 mL of Tris-Cl (pH 8.0) in a water bath for 10 min to eliminate the possibility of SDS binding to the nanoparticles, if any. For complete removal of SDS from the solution, dialysis was carried out against Milli-Q water with four changes of water. The bare silver nanoparticles thus obtained were characterized using standard techniques prior to their use in further experiments.

5.2.2 Test bacterial strains

In vitro bactericidal effects of protein-capped and bare silver nanoparticles were evaluated against common clinically-important bacterial pathogens. All strains were procured from the Microbial Type Culture Collection (MTCC) and Gene Bank, Institute of Microbial Technology, India. The tested strains were Gram-positive *Bacillus cereus* (MTCC 430) and

Pseudomonas putida (MTCC 102); and Gram-negative *Escherichia coli* (MTCC 1652) and *Klebsiella pneumoniae* (MTCC 432).

5.2.3 Minimum inhibitory concentration assay

Minimum inhibitory concentration (MIC) values of protein-capped and bare silver nanoparticles were determined by dehydrogenase assay using 96-well microtiter plate. Bacterial inoculums were prepared by washing overnight grown culture twice with phosphate buffer saline (pH 7.4) and then diluted to yield a final concentration of 10^8 cfu mL⁻¹. 100 μ L of bacterial inoculum and 20 μ L of triphenyl tetrazolium chloride (TTC; 3 mg mL⁻¹ solution) were added in each microtiter well. Subsequently, 20 μ L of 50 μ g mL⁻¹ silver nanoparticle (bare or protein-capped) solution was added and microtiter plates were kept for incubation at 37 °C for 18 hours under dark conditions. The formazan production was determined by optical density measurement at 570 nm with an ELISA reader. The MIC measurement was done in triplicate and executed three times to confirm the MIC values for each tested bacteria.

5.2.4 Disk diffusion assay

Disk diffusion method was used to test the antibacterial efficacy of protein-capped and bare silver nanoparticles. Sterile Mueller-Hinton agar (HiMedia, India, pH 7.3) plates were prepared and separately swabbed with 100 μ L of bacterial suspension (10^8 cfu mL⁻¹) using spread plate method. Subsequently, four disks of 9 mm diameter were placed using sterile forceps and 50 μ L of equimolar amount (50 μ M) of protein-capped or bare silver nanoparticles solution was added. Similarly, disks were immersed with equivalent amount of fungal cell free filtrate and considered as control. After incubation at 37 °C for 15-18 hours under dark conditions, the zone of inhibition was measured. Percent increase in zone of inhibition was calculated using the formula $[(b-a)/a] \times 100$ where, a and b represent the values of inhibition zone for protein-capped and bare silver nanoparticles, respectively. The experiment was performed in triplicate.

5.2.5 Bacterial growth curve

To examine the bacterial growth rate in the presence of silver nanoparticles, the selected bacterial species were grown separately in 100 mL of liquid nutrient broth medium supplemented with 50 μ M of protein-capped or bare silver nanoparticles per mL of medium. The bacterial growth rates were determined by measuring the absorbance at 600 nm at different time intervals (0.1 absorbance corresponds to a concentration of 10^8 cells per mL). Media without nanoparticles and bacterial inoculation were used as positive and negative controls, respectively.

5.2.6 Reactive oxygen species formation

5.2.6.1 2',7'-dichlorofluorescein-diacetate quantitative assay

The generation of intracellular reactive oxygen species (ROS) in presence of protein-capped or bare silver nanoparticles was determined using an oxidation-sensitive fluorescent probe 2,7-dichlorofluorescein diacetate (DCFH-DA) (Wang and Joseph 1999). Briefly, the bacterial cells were grown overnight (10^8 cfu mL⁻¹), washed three times with phosphate-

buffered saline and further suspended in fresh nutrient broth medium. DCFH-DA (10 μM in phosphate-buffered saline) was mixed with washed cells at a ratio of 1:2000 and incubated for 30 min at 37 °C in dark to successfully load the DCFH-DA into the cells. Centrifugation was carried out to collect the DCFH-DA loaded cells from the free DCFH-DA molecules followed by a final wash with the phosphate-buffered saline. The cleaned cells were exposed to protein-capped or bare silver nanoparticles (50 μM) for 30 min at 37 °C as described in the previous section. In bacterial cells, intracellular esterases result in hydrolysis of DCFH-DA to non-fluorescent dichlorofluorescein (DCFH). In the presence of cellular oxidants, DCFH is further oxidized to fluorescent dichlorofluorescein (DCF). The fluorescent signal intensity of DCF was measured by VICTOR™ X Multilabel Plate Reader (Perkin Elmer) at an excitation and emission wavelength of 485 nm and 535 nm, respectively. Bacterial cells not incubated with DCFH-DA were used as negative control while cells incubated in 25 mM ascorbic acid for 1 h before DCFH-DA exposure were used as positive control (Rico et al. 2013). The experiment was performed in triplicate.

5.2.6.2 Anti-oxidative enzyme assay

For peroxidase enzyme assay, the reaction mixture was prepared by mixing 1 ml of 0.01 M pyrogallol in phosphate buffer, 2 ml of 0.1 M phosphate buffer, and 1 ml of 5 mM hydrogen peroxide as per the protocol of Hochman and Goldberg (1991). Bacterial culture was treated with either protein-capped or bare silver nanoparticles (50 μM) at 37 °C for 30 min and protein supernatant was collected. Bacterial culture without nanoparticle treatment served as control. The protein supernatant (1 ml) was added to the reaction mixture and incubated for 5 min at 25 °C. Subsequently, the reaction was terminated by addition of 2.5 N sulphuric acid (1 ml) and the absorbance at 420 nm was recorded using a UV-Visible spectrophotometer (JASCO V-630). Blank was prepared by adding sterile water instead of bacterial culture in reaction mixture. The enzyme activity was expressed in U mg^{-1} protein. One unit of peroxidase forms 1.0 milligram of purpurogallin from pyrogallol in 20 seconds at pH 6.0 and 20 °C. The experiment was performed in triplicate.

The activity of superoxide dismutase (SOD) in protein supernatant of bacterial cells was measured after exposure to protein-capped and bare silver nanoparticles (50 μM) for 30 min at 37 °C. Bacterial culture without nanoparticle treatment served as control. The protein supernatant (50 μl) was diluted to 500 μl with water and gently mixed with 1.5 ml of reaction buffer (13.0 mM methionine, 6.3 μM nitroblue tetrazolium, 6.5 μM riboflavin, 0.1 mM EDTA, 50 mM phosphate buffer, pH 7.8). The reaction mixture was incubated at 30°C for 10 min under 6000 lux and absorbance was measured at 560 nm on a UV-Visible spectrophotometer (JASCO V-630) using a quartz cuvette of 1 cm path length. Reaction mixture containing water (500 μl) instead of protein supernatant was also illuminated and served as blank. The non-irradiated reaction mixture which did not developed a colour, served as negative control. One unit of the SOD activity was defined as a 50% decrease in the

rate of nitroblue tetrazolium (NBT) reduction at 560 nm. The assay was performed in triplicate.

5.2.7 Effect on bacterial membrane integrity

5.2.7.1 Malondialdehyde content

The formation of malondialdehyde (MDA) was measured using thiobarbituric acid as a probe molecule. The assay is based on the level of unstable lipid peroxides which decompose to form more complex and reactive thiobarbituric acid reactive substances (TBARS) compounds such as MDA. These compounds react with thiobarbituric acid (TBA) reagent to form the MDA-TBA adduct that can be measured colorimetrically. The bacterial cells after the exposure to either protein-capped or bare silver nanoparticles (50 μM) were hydrated in 1 ml of 2.5% (w/v) TCA and subsequently centrifuged at 12000 g at 4 °C for 20 min. Then, 100 μl aliquots of the supernatant were mixed with 0.5% (w/v) TBA reagent containing 20% (w/v) TCA. The reaction mixture was heated in a water bath at 100 °C for 30 min and centrifuged at 12,000 g at 4 °C for 10 min. The absorbance values of the supernatants were measured at 532 nm using a UV-Visible spectrophotometer (JASCO V-630). MDA content was estimated as picomoles per milligram of protein using a molar extinction coefficient of $1.56 \text{ mM}^{-1} \text{ cm}^{-1}$ (Pandey et al. 2003).

5.2.7.2 Membrane leakage analysis

The extent of membrane leakage in bacterial cells after treatment with either protein-capped or bare silver nanoparticles (50 μM) was determined by quantification of protein, sugar and nucleic acid content in the culture supernatants. Protein content was measured using method of Bradford (1976) with BSA as a standard. Briefly, 200 μl of culture supernatant was mixed with 800 μl of Bradford reagent, incubated for 10 min in dark followed by measurement of absorbance at 595 nm. Amount of sugar leakage was quantified by the anthrone sulfuric acid method (Fales 1951). Culture supernatant (100 μl) was mixed with 5 ml of 2.5 N hydrochloric acid and heated in a water bath at 100 °C for 30 min. The solution was cooled, neutralized with solid sodium carbonate and transferred to a 100 ml measuring flask after filtration, followed by making up to a known volume with distilled water. A 0.5 ml of the prepared solution was aliquot and 4.5 ml of anthrone reagent was added, and the absorbance was measured at 630 nm. For nucleic acid leakage analysis, absorbance of culture supernatant was measured at 260 nm (1 OD unit = 50 $\mu\text{g mL}^{-1}$) using a UV-Visible spectrophotometer (JASCO V-630).

5.2.8 Silver ion measurement

The dissolution of silver ions from protein-capped or bare silver nanoparticles was measured for test duration in nutrient medium. After the test duration, the culture medium was dialyzed for 12 h using a 12 kDa cellulose membrane and the silver ion concentration in water (external medium) was measured using inductively coupled plasma - atomic emission spectrometry (ICP-AES; ICPS-7500, Shimadzu, Japan). The silver ion concentration in nutrient medium (without silver nanoparticles) was used as control.

5.2.9 Transmission electron microscopy

To prepare samples for transmission electron microscopy measurements, the bacterial solution exposed to silver nanoparticles (bare or protein-capped) was centrifuged at 5,000 rpm for 2 min. Subsequently, supernatant was discarded and the pellet was washed twice with 1X PBS buffer followed by a pre-fixation in 2.5% glutaraldehyde (prepared in 0.1 M cacodylate buffer) for 2 h at 4 °C. The bacterial cells were then rinsed three times with 0.1 M cacodylate buffer with an incubation period of 10 min between washing steps. Post-fixation of the bacterial cells was performed with 1% OsO₄ treatment for 1 h at 4 °C. The excess OsO₄ solution was removed by washing the bacterial cells two times with 0.1 M cacodylate buffer. The fixed bacterial cells were then stained with uranyl acetate and a drop of sample was placed on a carbon-coated copper grid and allowed to dry overnight in a vacuum desiccator. The grids were observed on a Hitachi transmission electron microscope operated at a constant voltage of 100kV.

5.3 Results and discussion

5.3.1 Bactericidal assay

The antibacterial activity was determined to compare the efficacy of protein-capped and bare silver nanoparticles against common pathogenic bacterial strains. Preliminary experiment was carried out by comparing the minimum inhibitory concentration (MIC) profiles of protein-capped and bare silver nanoparticles using dehydrogenase assay. As shown in Figure 5.1, a direct increase in the antibacterial activity was observed for both the tested silver nanoparticles (protein-capped and bare) with increase in concentration demonstrating the role of nanoparticles in determining antibacterial potential. The silver nanoparticles were found to be more effective against Gram negative bacteria as compared to Gram positive bacteria. The observed MIC values for protein-capped silver nanoparticles were 8 µg mL⁻¹ and 4-8 µg mL⁻¹ for Gram positive and Gram negative bacteria, respectively. On the other hand, MIC values for bare silver nanoparticles, without protein capping were found to be 2-4 µg mL⁻¹ and 2 µg mL⁻¹ for Gram positive and Gram negative bacteria, respectively.

To corroborate the increase in antimicrobial efficacy as observed from MIC experiments, disk diffusion studies were performed at an equimolar concentration (50 mM) of either protein-capped or bare silver nanoparticles (Table 5.1). Zone of inhibition values for Gram positive bacteria *B. cereus* and *S. aureus* in the presence of protein-capped silver nanoparticles were 11 mm and 10 mm, respectively which were increased to 14 mm and 12 mm in case of bare silver nanoparticles. Similarly, inhibition zones for Gram negative bacteria *E. coli* and *P. putida* were increased to 18 mm from 13 mm and 16 mm from 12 mm, respectively after the removal of capping proteins from the surface of nanoparticles. No antibacterial activity was observed in case of only capping proteins (control) validating the silver nanoparticles as solitary contributor for the observed bactericidal effects. These results clearly indicated that the presence of protein shell on nanoparticle surface acts as a barrier to

a certain extent for bactericidal effect of silver nanoparticles. The trend observed in the zone of inhibition was similar to that of the MIC values with higher bactericidal effects against Gram negative in comparison to Gram positive bacteria.

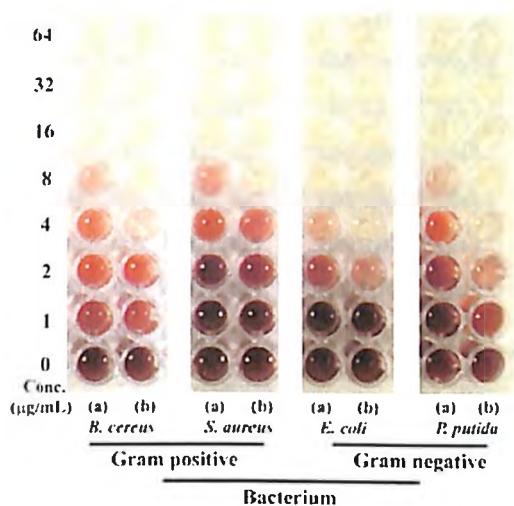


Figure 5.1 Dehydrogenase assay demonstrating MIC profiles of (a) protein-capped and (b) bare silver nanoparticles against selected Gram positive and Gram negative bacteria.

Table 5.1 Mean zone of inhibition (mm) of protein-capped and bare silver nanoparticles as determined using disk diffusion method.

Bacteria	Zone of Inhibition (Mean \pm SD)	
	Protein-capped silver nanoparticles	Bare silver nanoparticles
Gram positive		
<i>B. cereus</i>	11 \pm 0.8	14 \pm 1.1
<i>S. aureus</i>	10 \pm 0.4	12 \pm 0.7
Gram negative		
<i>E. coli</i>	13 \pm 0.7	18 \pm 0.8
<i>P. putida</i>	12 \pm 0.5	16 \pm 0.4

In addition to MIC and disk diffusion studies, we also investigated the effect of protein-capped and bare silver nanoparticles on bacterial growth dynamics. The time-dependent bacterial growth was monitored by measuring the absorbance at wavelength 600 nm which arises due to the scattering of light by bacterial cells. Subsequently, the bacterial counts were calculated by subtracting the background (LB medium) from each measurement. It is noteworthy that no absorbance of silver nanoparticles was observed at wavelength 600 nm which indicates no interference of nanoparticles while measuring the absorbance. Hence, OD₆₀₀ could be considered as an accurate method to measure the bacterial counts. Growth curve determination has also been previously demonstrated as the most appropriate method to determine the bacterial kinetics with minimal influence from silver nanoparticles (Zhou et al. 2012).

As illustrated in Figure 5.2, both the protein-capped as well as bare silver nanoparticles adversely affected the bacterial growth with major implications on exponential phase. The observation indicated that tested silver nanoparticles not only inhibited bacterial growth but also killed bacteria. Growth dynamics profile of both Gram positive bacteria (*B. cereus* and *S. aureus*) revealed that the protein-capped nanoparticles were more effective in controlling the bacterial growth as compared to bare silver nanoparticles. In contrast, bare nanoparticles were more effective than protein-capped nanoparticles in case of Gram negative bacteria (*E. coli* and *P. putida*). Moreover, a higher magnitude of toxicity was observed in case of Gram negative bacteria as compared to Gram positive bacteria which could be due to difference in cell wall composition of two classes.

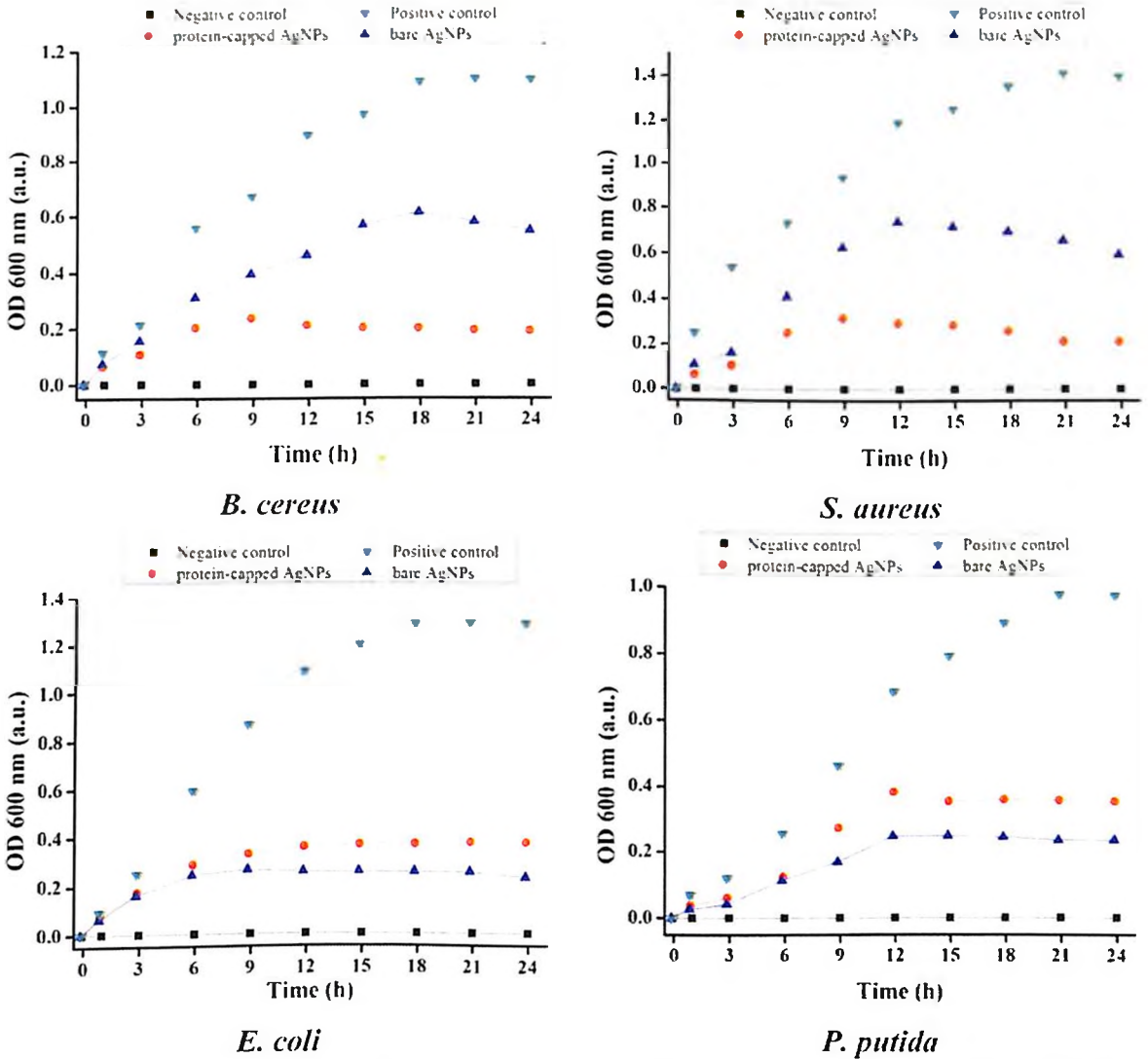


Figure 5.2 Growth dynamics of tested bacterial species in presence of protein-capped or bare silver nanoparticles as compared to controls. The nutrient medium with bacterial inoculation (no nanoparticles) and silver nanoparticles (no bacterial inoculation) were used as positive and negative control, respectively.

Collectively, bactericidal studies showed that the Gram negative bacteria were more sensitive than Gram positive bacteria which might be due to the difference in their cell wall

composition. Gram negative bacteria feature a thin (5-10 nm) peptidoglycan layer surrounded by an outer lipo-polysaccharide (LPS) membrane. The presence of porins (protein-channels) in LPS membrane can contribute to high susceptibility by facilitating the diffusion of silver nanoparticles. Conversely, Gram positive bacteria lack the LPS membrane and feature relatively thick (20-80 nm) and continuous peptidoglycan cell wall which can restrict the entry of silver nanoparticles. The greater efficacy of silver nanoparticles against Gram negative bacteria as compared to Gram positive bacteria observed during present study is in complete agreement with the previous reports (Feng et al. 2000, Fayaz et al. 2010, Amato et al. 2011). It is noteworthy to mention that the tested silver nanoparticles not only inhibited the bacterial growth but also possess “killing” potential, as inferred by the growth dynamic studies. The observed irreversible inhibition of growth i.e. “killing” potential is highly desirable for therapeutic and surgical devices, where bacterial killing potential is essential (Panáček et al. 2006). Interestingly, we observed that protein-capped silver nanoparticles were less effective as compared to bare silver nanoparticles which can be attributed to the presence of protein shell on the surface of silver nanoparticles. The observation is in complete agreement with results obtained during MIC and disk diffusion studies. Hence, it can be anticipated that the subtle changes on nanoparticle surface with protein shell can modulate their interactions with the bacterial surface, leading to different antibacterial profiles. To date, however, there is no clear understanding that surface modification of nanoparticles with protein shell controls the antibacterial properties of silver nanoparticles. The modulation of antibacterial profile due to presence of proteins on the nanoparticle surface makes it more interesting and motivated us to perform mechanistic studies to decipher the involved mechanism.

5.3.2 Bactericidal mechanism of protein-capped and bare silver nanoparticles

Presently, how silver nanoparticles confer bactericidal effects is not clear and is open to debate (Cui et al. 2013, Mijndonckx et al. 2013, Reidy et al. 2013). The most commonly reported mechanism is the generation of free radicals such as peroxide, superoxide and hydroxyl ions by silver nanoparticles which could play a key role in executing bactericidal effects. Therefore, we investigated the formation of free radicals in bacterial cells using a fluorescent probe, 2,7-dichlorofluorescein diacetate, which can enter inside the viable bacterial cell and is hydrolysed by the intracellular esterases to a non-fluorescent compound, dichlorofluorescein (DCFH). The cellular oxidants i.e. ROS molecules formed due to the exposure to silver nanoparticles oxidize DCFH to 2-electron fluorescent product 2',7' dichlorofluorescein (DCF) for which signal intensity can be measured using a spectrofluorometer. The method has been well established for studying ROS generation as a measure of nanoparticle toxicity (Wang and Joseph 1999, Lu et al. 2010).

Figure 5.3 depicts the magnitude of ROS species formation in bacterial cells exposed to the silver nanoparticles (protein-capped and bare) as compared to the control (without nanoparticle). We observed that for Gram positive bacteria (*B. cereus* and *S. aureus*),

magnitude of ROS species was approximately two fold higher for bare silver nanoparticles in comparison to the protein-capped silver nanoparticles. As expected, insignificant or no free radical generation was observed for bacterial cells grown in absence of silver nanoparticles (control). The observed low ROS production for protein-capped silver nanoparticles partly suggests that presence of protein shell on nanoparticles leads to non-specific interactions with peptidoglycan layer, thus halting their penetration. In contrast, absence of capping molecules (protein) on bare silver nanoparticles facilitates their easy penetration through peptidoglycan layer leading to high ROS production. Interestingly, for Gram negative bacteria (*E. coli* and *P. putida*), an almost similar magnitude of ROS species generation was observed for both protein-capped and bare silver nanoparticles. This observation can be explained by the fact that Gram negative bacteria possess thin peptidoglycan layer, hence, these nanoparticles, irrespective of capping molecules, could easily penetrate and generate ROS species.

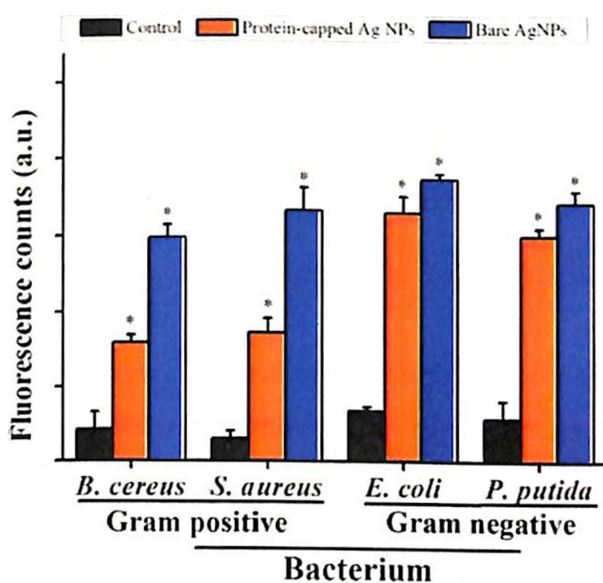


Figure 5.3 Relative fluorescence intensity (with respect to H_2O_2) showing the cellular ROS formation capability of protein-capped and bare silver nanoparticles as compare to control. Vertical bars represent standard errors. Significant differences from control ($p \leq 0.05$) are marked with asterisk.

It has been reported that silver ions catalyse the decomposition of H_2O_2 , thus resulting in the formation of free radicals (OH and/or O_2^-) (Chang et al. 2007) Hence, we evaluated the role of ROS generation and its consequences on antioxidant system by monitoring activities of two ROS related enzymes: peroxidase and superoxide dismutase (SOD). Peroxidase is a detoxifying enzyme having hydrogen peroxide as an optimal substrate, but shows more affinity towards organic hydroperoxides such as lipid peroxides. As illustrated in Figure 5.4a, the peroxidase activity in Gram positive bacteria was found to be increased by approximately 6-fold and 7-fold when cells were treated with protein-capped and bare silver nanoparticles, respectively. Similarly, the peroxidase activity was increased by approximately 5-fold and 6-fold for Gram negative bacteria after treatment with protein-capped and bare silver

nanoparticles, respectively. The observed high peroxidase activity in Gram positive bacteria in comparison to Gram negative bacteria when treated with protein-capped silver nanoparticles suggest high magnitude of lipid peroxides, a prominent indicator of membrane damage. In contrast, bare silver nanoparticle causes almost similar damage in both Gram negative and positive bacteria.

Similarly, we measured the activity of SOD enzyme, an important antioxidant defence enzyme which catalyses the dismutation of superoxide (O_2^-) into oxygen and hydrogen peroxide. We observed a similar magnitude of SOD and peroxidase activity in both Gram positive and Gram negative bacteria after treatment with protein-capped and bare silver nanoparticles indicated no accumulation of free radicals (Figure 5.4b). A related study on exposure of silver nanoparticles to bacterium *Pseudomonas chlororaphis* also observed no accumulation of intracellular hydroxyl radicals although cell count reduced from 10^8 to 10^3 cells/mL (Dimkpa et al. 2011). Hence, it can be inferred that the removal of protein corona not only generates enormous amount of ROS molecules but also leads to the formation of cellular oxidants which also interfere with the associated antioxidative system.

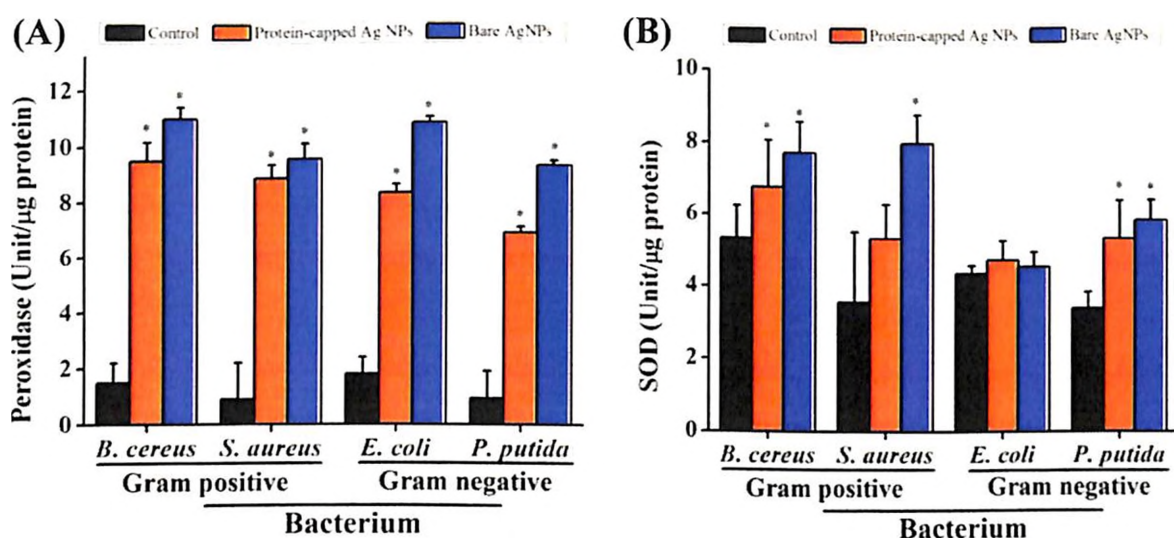


Figure 5.4 Levels of (a) peroxidase and (b) superoxide dismutase in untreated (control: not treated with silver nanoparticles) and treated (with protein-capped and bare silver nanoparticles) bacteria cells. The data are expressed as mean \pm standard error of three independent experiments ($p < 0.05$).

It is well evident that once ROS begins to accumulate, the oxidative stress in cells could confer damage to membrane integrity (Lima et al. 2012). Lipid peroxidation is a well-defined mechanism of cellular damage and is considered as a major indicator of oxidative stress in cells (Sayes et al. 2005, Farmer and Mueller 2013). Accordingly, we determined membrane damage by performing malondialdehyde (MDA) assay to support the ROS and antioxidant enzyme studies. Quantitative lipid peroxidation (TBARS) was measured after the exposure of bacterial cells to silver nanoparticles. In case of Gram positive bacterial species, TBARS values were almost similar when bacteria were treated with either protein-capped or

bare silver nanoparticles (Figure 5.5). A similar trend was observed in both tested Gram negative bacteria, however, the magnitude of TBARS value was found to be higher as compared to Gram positive bacterial species. The observation can be explained based on the interactions of protein with peptidoglycan cell wall of Gram positive bacteria, leading to greater damage. Related studies also demonstrated that silver nanoparticles may pass through the cell wall of bacteria to oxidize the surface proteins on plasma membrane and consequently disturb the cell homeostasis (Sondi and Salopek-Sondi 2004, Kong and Jang 2008). Moreover, the generation of free radicals such as peroxide, superoxide and hydroxyl ions by silver nanoparticles has been reported to exert lipid peroxidation and cause loss of membrane integrity (Morones et al. 2005). Furthermore, biochemical and proteomic studies strengthened the fact that silver nanoparticles resulted in an immediate dissipation of the proton motive force which causes de-energization of cell membrane and consequently cell death (Lok et al. 2006).

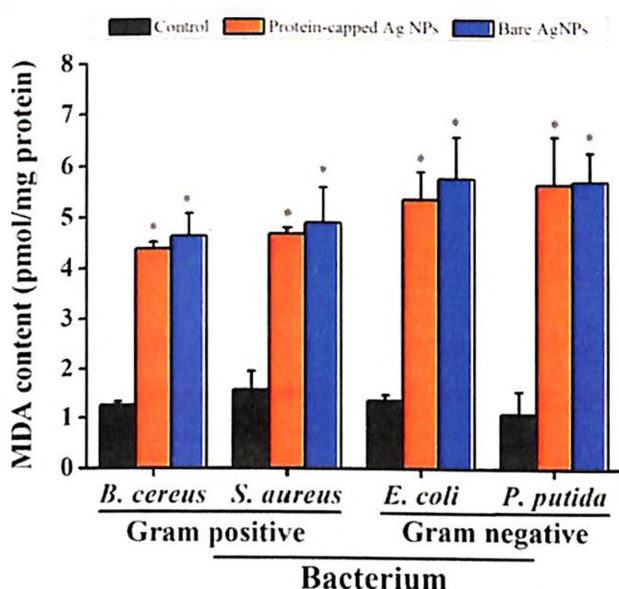


Figure 5.5 Malondialdehyde (MDA) assay demonstrating the difference in membrane damage capability of protein-capped and bare silver nanoparticles. Vertical bars represent standard errors. Significant differences from control ($p \leq 0.05$) are marked with asterisk.

To corroborate the membrane damage results, we further estimated the release of biomolecules from bacterial cells after the treatment of silver nanoparticles. As expected, higher amount of release of biomolecules was estimated for bacterial cells exposed to silver nanoparticles in comparison to bacterial cells grown without silver nanoparticles. Higher membrane leakage was observed in case of bare silver nanoparticles as compared to protein-capped silver nanoparticles (Table 5.2). Moreover, it was clearly evident that the bactericidal action of silver nanoparticles was more effective for Gram negative bacteria as compared to Gram positive bacteria. The trend in the magnitude of membrane leakage was approximately similar to that of MDA assay (Figure 5.5). It is well evident that damage to cell membrane leads to cell distortion which causes release of carbohydrates, proteins and nucleic acids (Choi et al. 2008, Travan et al. 2009).

Table 5.2 Magnitude of membrane leakage from bacterial cells after exposure to silver nanoparticles.

Bacteria	Protein content ($\mu\text{g ml}^{-1}$)			Carbohydrate content ($\mu\text{g ml}^{-1}$)			Nucleic acid content ($\mu\text{g ml}^{-1}$)		
	Control	Protein-capped silver nanoparticles	Bare silver nanoparticles	Control	Protein-capped silver nanoparticles	Bare silver nanoparticles	Control	Protein-capped silver nanoparticles	Bare silver nanoparticles
Gram positive									
<i>B. cereus</i>	3.99 \pm 0.1	99.54 \pm 9.4	108.33 \pm 14.7	2.19 \pm 0.5	88.13 \pm 3.5	97.28 \pm 6.3	0.98 \pm 0.09	7.74 \pm 0.5	9.43 \pm 0.6
<i>S. aureus</i>	4.78 \pm 0.1	88.34 \pm 14.9	94.86 \pm 9.6	6.42 \pm 1.0	93.86 \pm 5.3	105.47 \pm 9.9	0.75 \pm 0.13	8.73 \pm 0.4	8.92 \pm 0.3
Gram negative									
<i>E. coli</i>	8.33 \pm 0.6	134.38 \pm 9.6	154.72 \pm 12.2	6.28 \pm 1.3	128.41 \pm 9.9	144.49 \pm 5.4	0.35 \pm 0.07	10.45 \pm 0.2	11.73 \pm 0.7
<i>P. putida</i>	6.54 \pm 0.3	105.85 \pm 6.5	129.26 \pm 14.3	3.57 \pm 0.8	113.37 \pm 8.1	128.46 \pm 9.8	0.57 \pm 0.19	10.72 \pm 0.4	14.37 \pm 0.2

The release of silver ions liberated from the surface of silver nanoparticles has been found to be crucial in determining their antibacterial potential (Brett 2006, Arora et al. 2008, Chen and Schluesener 2008, Fayaz et al. 2010, Love et al. 2012, Cui et al. 2013, Reidy et al. 2013). It has been demonstrated that aerobic conditions can readily oxidized silver nanoparticles in aqueous solutions resulting in the release of silver ions (Liu et al. 2010). The positive charge generated due to release of Ag^+ ions from silver nanoparticles has also been involved in developing an electrostatic interaction with the negatively charged bacterial cell membrane (Kim et al. 2007). Moreover, the involvement of silver (I) ions generated from silver nanoparticles to further react with carbohydrates, hydroxyls and thiols of bacterial cell wall and nuclear membrane leading to cell distortion and finally death has also been well-documented (Feng et al. 2000, Hwang et al. 2008, Marambio-Jones and Hoek 2010). Hence, we measured the release of silver ions from protein-capped and bare silver nanoparticles. As expected, we did not detect presence of silver ions in nutrient medium without silver nanoparticles (control) (Figure 5.6). The dissolved silver ion concentrations for protein-capped and bare silver nanoparticles were measured as 15.8 and 27.5 $\mu\text{g L}^{-1}$, respectively. The observation clearly indicated that the presence of protein shell acts as a barrier for the release of silver ions from the surface of silver nanoparticles. Our results are in complete accordance with a previous study which demonstrated that surface coating plays a key role in dissolution of silver ions from nanoparticle surface (Yang et al. 2011). In fact, the study attributed the difference in toxicity to surface coating which is also similar to our observation.

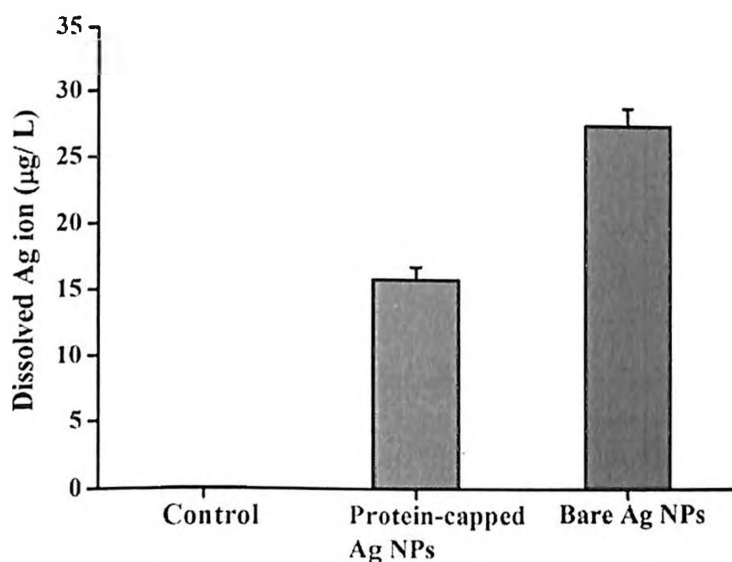
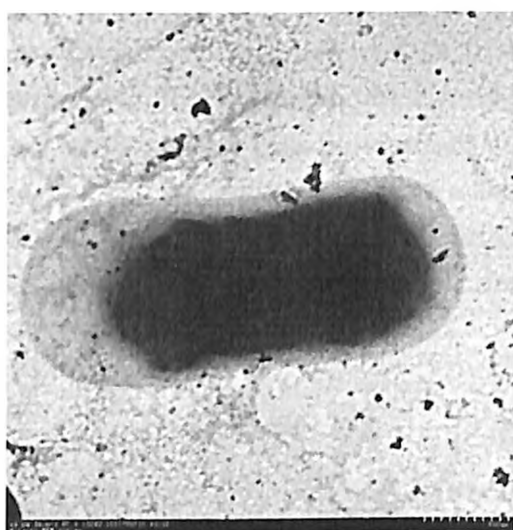


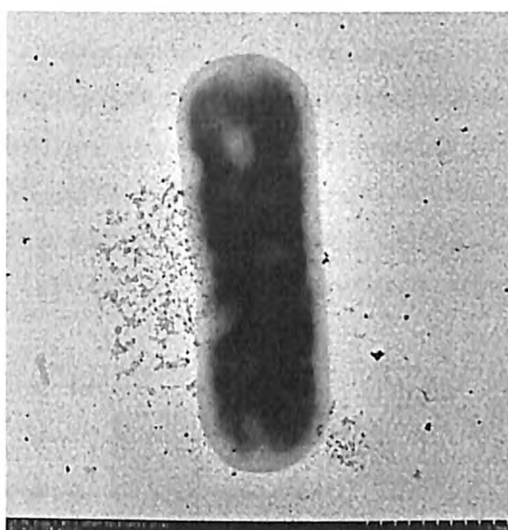
Figure 5.6 Silver dissolution profiles of protein-capped and bare silver nanoparticles.

Finally, transmission electron microscopy measurements were carried out to determine the distribution and location of the silver nanoparticles, as well as morphology of the bacteria after treatment with protein-capped or bare silver nanoparticles. Moreover, TEM observations could be helpful to determine the interactions between bacteria with protein-capped or bare silver nanoparticles. TEM micrographs of representative bacterial species after treatment are shown in Figure 5.7. For Gram positive bacterium *B. cereus*, protein-

capped silver nanoparticles were found deposited in the cytoplasm with minimal damage on membrane. Moreover, majority of nanoparticles were free in the medium or aggregated between bacteria. In contrast, treatment with bare silver nanoparticles showed significant membrane damage resulting in release of cytoplasm (Figure 5.7). In case of Gram negative bacterium (*E. coli*), the protein-capped nanoparticles were found to adhere at the surface of cell membrane as well as penetrated inside the bacterial cells. In comparison, bare silver nanoparticles accomplished the complete loss of membrane integrity in Gram negative bacterium and resulted in the release of cytoplasm (Figure 5.7).



Protein-capped

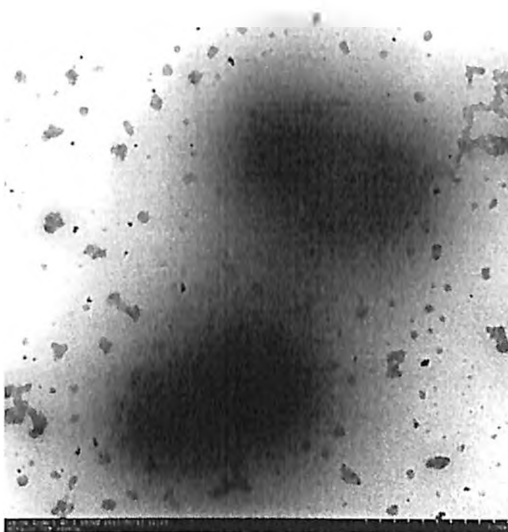


Bare silver nanoparticles

Gram positive *B. cereus*



Protein-capped



Bare silver nanoparticles

Gram negative *E. coli*

Figure 5.7 Transmission electron micrographs depicting the morphological changes in Gram positive *B. cereus* and Gram negative *E. coli* after exposure to protein-capped and bare silver nanoparticles.

5.4 Conclusions

The present study attempted to understand the role of protein shell on silver nanoparticles in determining their antibacterial potential. Bactericidal assays showed that Gram negative bacteria were more sensitive to silver nanoparticles as compared to Gram positive bacteria. Moreover, bare silver nanoparticles were found to be more effective bactericidal agents as compared to protein-capped silver nanoparticles. Further mechanistic studies indicated that the mode of action of silver nanoparticles is highly dependent on capping molecule (protein shell) and cell wall composition of bacteria. A higher extent of ROS formation was observed for Gram negative bacteria when treated with bare nanoparticles as compared to other treatments. Studies on antioxidant system and membrane damage further corroborate these results. A higher dissolution of silver ions from surface of bare nanoparticles than protein-capped nanoparticles was observed. In general, our results showed that the presence of protein shell on the surface of silver nanoparticles can decrease their bactericidal effects as illustrated through a cartoon representation (Figure 5.8). The present findings can contribute in designing rational antibacterial formulations of silver nanoparticles.

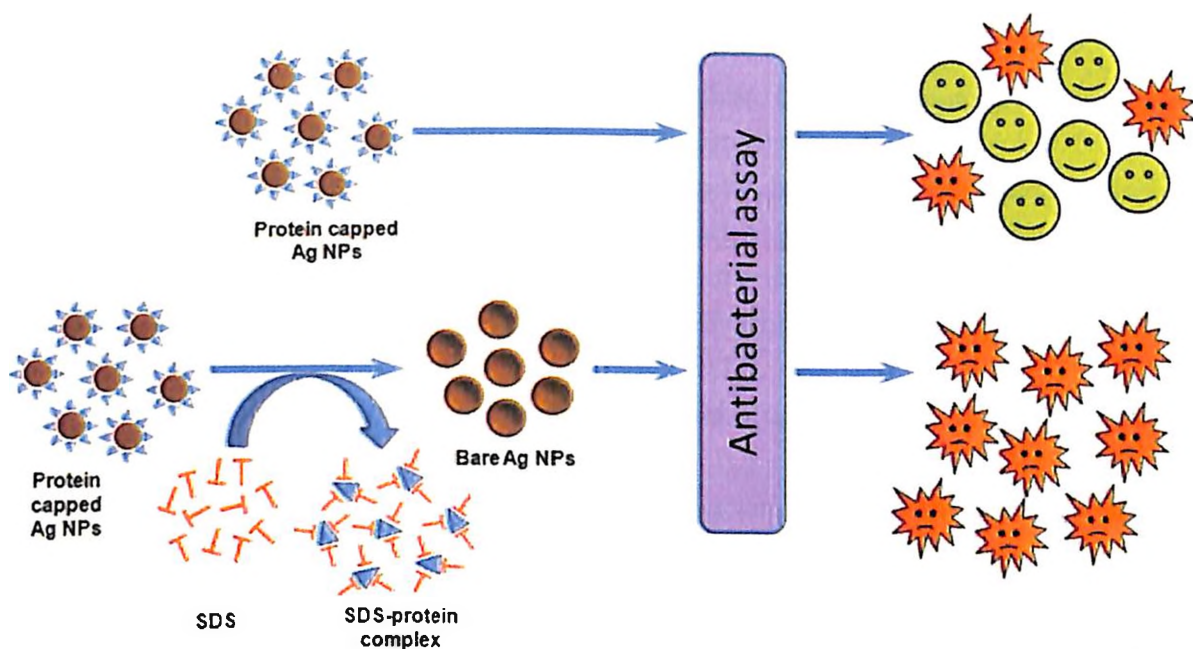


Figure 5.8 Cartoon representation of antibacterial potential of protein-capped and bare silver nanoparticles.

5.5 References

- Ahamed, M., Karns, M., Goodson, M., Rowe, J., Hussain, S. M., Schlager, J. J. and Hong, Y. (2008). DNA damage response to different surface chemistry of silver nanoparticles in mammalian cells. *Toxicology and Applied Pharmacology* **233**: 404-410.
- Alexander, J. W. (2009). History of the medical use of silver. *Surgical Infections* **10**: 289-292.
- Allen, H. K., Donato, J., Wang, H. H., Cloud-Hansen, K. A., Davies, J. and Handelsman, J. (2010). Call of the wild: Antibiotic resistance genes in natural environments. *Nature Reviews Microbiology* **8**: 251-259.
- Amato, E., Diaz-Fernandez, Y. A., Taglietti, A., Pallavicini, P., Pasotti, L., Cucca, L., Milanese, C., Grisoli, P., Dacarro, C., Fernandez-Hechavarria, J. M. and Necchi, V. (2011). Synthesis, characterization and antibacterial activity against Gram positive and Gram negative bacteria of biomimetically coated silver Nanoparticles. *Langmuir* **27**: 9165-9173.
- Andersson, D. I. and Hughes, D. (2010). Antibiotic resistance and its cost: is it possible to reverse resistance? *Nature Reviews Microbiology* **8**: 260-271.
- Andersson, D. I. and Hughes, D. (2011). Persistence of antibiotic resistance in bacterial populations. *FEMS Microbiology Reviews* **35**: 901-911.
- Arora, S., Jain, J., Rajwade, J. M. and Paknikar, K. M. (2008). Cellular responses induced by silver nanoparticles: *In vitro* studies. *Toxicology Letters* **179**: 93-100.
- Bartłomiejczyk, T., Lankoff, A., Kruszewski, M. and Szumiel, I. (2013). Silver nanoparticles- allies or adversaries? *Annals of Agricultural and Environmental Medicine* **20**: 48-54.
- Bradford, M. M. (1976). A rapid and sensitive method for the quantitation of microgram quantities of protein utilizing the principle of protein-dye binding. *Analytical Biochemistry* **72**: 248-254.
- Brett, D. W. (2006). A discussion of silver as an antimicrobial agent: Alleviating the confusion. *Ostomy Wound Management* **52**: 34-41.
- Chang, Q., Yan, L., Chen, M., He, H. and Qu, J. (2007). Bactericidal mechanism of Ag/Al₂O₃ against *Escherichia coli*. *Langmuir* **23**: 11197-11199.
- Chen, X. and Schluesener, H. (2008). Nanosilver: A nanoparticle in medical application. *Toxicology Letters* **176**: 1-12.
- Choi, O., Deng, K. K., Kim, N.-J., Ross Jr, L., Surampalli, R. Y. and Hu, Z. (2008). The inhibitory effects of silver nanoparticles, silver ions, and silver chloride colloids on microbial growth. *Water Research* **42**: 3066-3074.
- Cui, L., Chen, P., Chen, S., Yuan, Z., Yu, C. P., Ren, B. and Zhang, K. (2013). *In situ* study of the antibacterial activity and mechanism of action of silver nanoparticles by surface-enhanced raman spectroscopy. *Analytical Chemistry* **85**: 5436-5443.
- Curtis, A. and Wilkinson, C. (2001). Nanotechnology and approaches in biotechnology. *Trends in Biotechnology* **19**: 97-101.

- Dimkpa, C. O., Calder, A., Gajjar, P., Merugu, S., Huang, W., Britt, D. W., McLean, J. E., Johnson, W. P. and Anderson, A. J. (2011). Interaction of silver nanoparticles with an environmentally beneficial bacterium, *Pseudomonas chlororaphis*. *Journal of Hazardous Materials* **188**: 428-435.
- Fales, F. W. (1951). The assimilation and degradation of carbohydrates by yeast cells. *Journal of Biological Chemistry* **193**: 113-124.
- Farmer, E. E. and Mueller, M. J. (2013). ROS-mediated lipid peroxidation and RES-activated signaling. *Annual Review of Plant Biology* **64**: 429-450.
- Fayaz, A. M., Balaji, K., Girilal, M., Yadav, R., Kalaichelvan, P. T. and Venketesan, R. (2010). Biogenic synthesis of silver nanoparticles and their synergistic effect with antibiotics: A study against Gram-positive and Gram-negative bacteria. *Nanomedicine-Nanotechnology Biology and Medicine* **6**: 103-109.
- Feng, Q. L., Wu, J., Chen, G. Q., Cui, F. Z., Kim, T. N. and Kim, J. O. (2000). A mechanistic study of the antibacterial effect of silver ions on *Escherichia coli* and *Staphylococcus aureus*. *Journal of Biomedical Materials Research* **52**: 662-668.
- Hochman, A. and Goldberg, I. (1991). Purification and characterization of a catalase-peroxidase and a typical catalase from the bacterium *Klebsiella pneumoniae*. *Biochimica et Biophysica Acta -Protein Structure and Molecular Enzymology* **1077**: 299-307.
- Holt, K. B. and Bard, A. J. (2005). Interaction of silver(I) ions with the respiratory chain of *Escherichia coli*: an electrochemical and scanning electrochemical microscopy study of the antimicrobial mechanism of micromolar Ag. *Biochemistry* **44**: 13214-13223.
- Hwang, E. T., Lee, J. H., Chae, Y. J., Kim, Y. S., Kim, B. C., Sang, B. I. and Gu, M. B. (2008). Analysis of the toxic mode of action of silver nanoparticles using stress-specific bioluminescent bacteria. *Small* **4**: 746-750.
- Kim, J. S., Kuk, E., Yu, K. N., Kim, J. H., Park, S. J., Lee, H. J., Kim, S. H., Park, Y. K., Park, Y. H., Hwang, C. Y., Kim, Y. K., Lee, Y. S., Jeong, D. H. and Cho, M. H. (2007). Antimicrobial effects of silver nanoparticles. *Nanomedicine-Nanotechnology Biology and Medicine* **3**: 95-101.
- Kong, H. and Jang, J. (2008). Antibacterial properties of novel poly (methyl methacrylate) nanofiber containing silver nanoparticles. *Langmuir* **24**: 2051-2056.
- Kvitek, L., Panaček, A., Soukupova, J., Kolar, M., Večerova, R., Pucek, R., Holecova, M. and Zboril, R. (2008). Effect of surfactants and polymers on stability and antibacterial activity of silver nanoparticles. *Journal of Physical Chemistry C* **112**: 5825-5834.
- Lansdown, A. (2006). Silver in health care: Antimicrobial effects and safety in use. *Biofunctional Textiles and the Skin*. U. C. Hipler and P. Elsner. Basel, Karger. **33**: 17-34.
- Lansdown, A. B. G. (2002). Silver I: Its antibacterial properties and mechanism of action. *Journal of Wound Care* **11**: 125 - 130.

- Li, W.-R., Xie, X.-B., Shi, Q.-S., Zeng, H.-Y., You-Sheng, O.-Y. and Chen, Y.-B. (2010). Antibacterial activity and mechanism of silver nanoparticles on *Escherichia coli*. *Applied Microbiology and Biotechnology* **85**: 1115-1122.
- Li, Z., Greden, K., Alvarez, P. J., Gregory, K. B. and Lowry, G. V. (2010). Adsorbed polymer and NOM limits adhesion and toxicity of nano scale zerovalent iron to *E. coli*. *Environmental Science & Technology* **44**: 3462-3467.
- Lima, R., Seabra, A. B. and Durán, N. (2012). Silver nanoparticles: a brief review of cytotoxicity and genotoxicity of chemically and biogenically synthesized nanoparticles. *Journal of Applied Toxicology* **32**: 867-879.
- Liu, J., Sonshine, D. A., Shervani, S. and Hurt, R. H. (2010). Controlled release of biologically active silver from nanosilver surfaces. *ACS Nano* **4**: 6903-6913.
- Lok, C. N., Ho, C. M., Chen, R., He, Q. Y., Yu, W. Y., Sun, H. Z., Tam, P. K. H., Chiu, J. F. and Che, C. M. (2006). Proteomic analysis of the mode of antibacterial action of silver nanoparticles. *Journal of Proteome Research* **5**: 916-924.
- Love, S. A., Maurer-Jones, M. A., Thompson, J. W., Lin, Y. S. and Haynes, C. L. (2012). Assessing nanoparticle toxicity. *Annual Review of Analytical Chemistry* **5**: 181-205.
- Lu, W., Senapati, D., Wang, S., Tovmachenko, O., Singh, A. K., Yu, H. and Ray, P. C. (2010). Effect of surface coating on the toxicity of silver nanomaterials on human skin keratinocytes. *Chemical Physics Letters* **487**: 92-96.
- Marambio-Jones, C. and Hoek, E. M. V. (2010). A review of the antibacterial effects of silver nanomaterials and potential implications for human health and the environment. *Journal of Nanoparticle Research* **12**: 1531-1551.
- Mijnendonckx, K., Leys, N., Mahillon, J., Silver, S. and Van Houdt, R. (2013). Antimicrobial silver: uses, toxicity and potential for resistance. *BioMetals*: 1-13.
- Morones, J. R., Elechiguerra, J. L., Camacho, A., Holt, K., Kouri, J. B., Ramirez, J. T. and Yacaman, M. J. (2005). The bactericidal effect of silver nanoparticles. *Nanotechnology* **16**: 2346-2353.
- Neal, A. L. (2008). What can be inferred from bacterium–nanoparticle interactions about the potential consequences of environmental exposure to nanoparticles? *Ecotoxicology* **17**: 362-371.
- Neu, H. C. (1992). The crisis in antibiotic resistance. *Science* **257**: 1064-1073.
- Panáček, A., Kvítek, L., Pucek, R., Kolář, M., Večeřová, R., Pizúrová, N., Sharma, V. K., Nevěčná, T. j. and Zbořil, R. (2006). Silver colloid nanoparticles: Synthesis, characterization, and their antibacterial activity. *Journal of Physical Chemistry B* **110**: 16248-16253.
- Pandey, S., Parvez, S., Sayeed, I., Haque, R., Bin-Hafeez, B. and Raisuddin, S. (2003). Biomarkers of oxidative stress: a comparative study of river Yamuna fish *Wallago attu* (Bl. & Schn.). *Science of the Total Environment* **309**: 105-115.
- Pradeep, T. and Anshup (2009). Noble metal nanoparticles for water purification: A critical review. *Thin Solid Films* **517**: 6441-6478.

- Rai, M., Yadav, A. and Gade, A. (2009). Silver nanoparticles as a new generation of antimicrobials. *Biotechnology Advances* **27**: 76-83.
- Reidy, B., Haase, A., Luch, A., Dawson, K. A. and Lynch, I. (2013). Mechanisms of silver nanoparticle release, transformation and toxicity: A critical review of current knowledge and recommendations for future studies and applications. *Materials* **6**: 2295-2350.
- Rico, C., Hong, J., Morales, M. I., Zhao, L., Barrios, A. C., Zhang, J.-Y., Peralta-Videa, J. R. and Gardea-Torresdey, J. L. (2013). Effect of cerium oxide nanoparticles on rice: A study involving the antioxidant defense system and *in vivo* fluorescence imaging. *Environmental Science & Technology*.
- Ruden, S., Hilpert, K., Berditsch, M., Wadhwani, P. and Ulrich, A. S. (2009). Synergistic interaction between silver nanoparticles and membrane-permeabilizing antimicrobial peptides. *Antimicrobial Agents and Chemotherapy* **53**: 3538-3540.
- Russell, A. D. and Hugo, W. B. (1994). Antimicrobial activity and action of silver. *Progress in Medicinal Chemistry*. G. P. Ellis and D. K. Luscombe, Elsevier. **Volume 31**: 351-370.
- Sayes, C. M., Gobin, A. M., Ausman, K. D., Mendez, J., West, J. L. and Colvin, V. L. (2005). Nano-C₆₀ cytotoxicity is due to lipid peroxidation. *Biomaterials* **26**: 7587-7595.
- Shoults-Wilson, W. A., Reinsch, B. C., Tsyusko, O. V., Bertsch, P. M., Lowry, G. V. and Unrine, J. M. (2011). Effect of silver nanoparticle surface coating on bioaccumulation and reproductive toxicity in earthworms (*Eisenia fetida*). *Nanotoxicology* **5**: 432-444.
- Somasundaran, P., Chakraborty, S., Qiang, Q., Deo, P., Wang, J. and Zhang, R. (2004). Surfactants, polymers and their nanoparticles for personal care applications. *Journal of Cosmetic Science* **55**: S1-S18.
- Sondi, I. and Salopek-Sondi, B. (2004). Silver nanoparticles as antimicrobial agent: A case study on *E. coli* as a model for Gram-negative bacteria. *Journal of Colloid and Interface Science* **275**: 177-182.
- Stewart, P. S. and William Costerton, J. (2001). Antibiotic resistance of bacteria in biofilms. *The Lancet* **358**: 135-138.
- Travan, A., Pelillo, C., Donati, I., Marsich, E., Benincasa, M., Scarpa, T., Semeraro, S., Turco, G., Gennaro, R. and Paoletti, S. (2009). Non-cytotoxic silver nanoparticle-polysaccharide nanocomposites with antimicrobial activity. *Biomacromolecules* **10**: 1429-1435.
- Wang, H. and Joseph, J. A. (1999). Quantifying cellular oxidative stress by dichlorofluorescein assay using microplate reader. *Free Radical Biology and Medicine* **27**: 612-616.
- Xiu, Z.-m., Zhang, Q.-b., Puppala, H. L., Colvin, V. L. and Alvarez, P. J. (2012). Negligible particle-specific antibacterial activity of silver nanoparticles. *Nano Letters* **12**: 4271-4275.

- Xu, H., Qu, F., Xu, H., Lai, W., Wang, Y. A., Aguilar, Z. P. and Wei, H. (2012). Role of reactive oxygen species in the antibacterial mechanism of silver nanoparticles on *Escherichia coli* O157: H7. *BioMetals* **25**: 45-53.
- Yang, X., Gondikas, A. P., Marinakos, S. M., Auffan, M., Liu, J., Hsu-Kim, H. and Meyer, J. N. (2011). Mechanism of silver nanoparticle toxicity is dependent on dissolved silver and surface coating in *Caenorhabditis elegans*. *Environmental Science & Technology* **46**: 1119-1127.
- Zhou, Y., Kong, Y., Kundu, S., Cirillo, J. D. and Liang, H. (2012). Antibacterial activities of gold and silver nanoparticles against *Escherichia coli* and *Bacillus Calmette-Guérin*. *Journal of Nanobiotechnology* **10**: 1-9.

Chapter VI

Biosynthesis of Zinc Oxide Nanoparticles and their Photocatalysis Applications

This chapter demonstrates the potential of two indigenous fungi, *Aspergillus aeneus* isolate NJP12 and *Aspergillus* sp. isolate NJP02 for extracellular synthesis of ZnO nanoparticles under ambient conditions. The as-synthesized nanoparticles were spherical/quasi-spherical in shape with presence of proteins on the surface of individual nanoparticles. Various parameters such as reactant concentration (salt and proteins) and pH of the solution were found to influence the process of nanoparticle synthesis. Attempts toward understanding of the synthesis mechanism indicated that the process is non-enzymatic in nature but involves amino acids present in the protein chains. The low cost, simplicity and eco-friendly nature of the present protocol for “one-pot” synthesis and modification of ZnO nanoparticles could be extended to synthesize other metal nanoparticles thus expanding its applicability in various fields. The photocatalytic performance of protein-capped ZnO nanoparticles towards the degradation of methylene blue dye was also investigated. Owing to the presence of surface proteins, ZnO nanoparticles exhibited excellent enhancement of photocatalysis towards methylene blue dye suggesting their potential applications in catalysis, waste water treatment etc. The remarkable photocatalytic performance was attributed to the presence of surface proteins that act as effectual host for methylene blue dye and facilitates absorption of dye along with low recombination rate of the e^-/h^+ pairs.

Part of the work presented in this chapter have been published as per the following details:

- (a) Jain et al. (2013) *Appl. Microbiol. Biotechnol.* 97:859-869
- (b) Jain et al. (2013) Biosynthesis of ZnO nanoparticles. Indian patent office journal 20:11020
- (c) Jain et al. (2014) *Chem. Engg. Journal* 243:549-555

6.1 Introduction

Zinc oxide (ZnO) is a very well-known multifunctional wide and direct band gap semiconductor having excellent size dependent tunable optical properties. It is a representative compound of II–VI semiconductor oxides owing to its versatile and peculiar conducting, piezoelectric and pyroelectric properties. It has variety of applications in transparent electronics, ultraviolet (UV) light emitters, piezoelectric devices, chemical sensors, spin electronics, personal care products, coatings and paints (Wahab et al. 2010, Akhtar et al. 2011). However, the primary motivator of ZnO research is its great potential for a variety of commercial applications, such as in optoelectronic devices (light emitting diodes (LEDs), laser diodes, solar cells, photodetectors), energy harvesting devices, electronic devices (transistors), sensors, catalysts, active compounds in sunscreens etc. Moreover, ZnO nanoparticles are being increasingly used as photocatalysts to inactivate bacteria and viruses and for the degradation of environmental pollutants such as dyes, pesticides, and volatile organic compounds under appropriate light irradiation (Brayner et al. 2006, Liqiang et al. 2006, Meng et al. 2013).

ZnO nanoparticles have been considered as a material of choice for variety of biomedical and biolabeling applications. Recently, ZnO nanoparticles have also been considered to be a “GRAS” (Generally Recognized As Safe) substance by the Food and Drug Administration (FDA) agency, USA (Hong et al. 2013). An observation that a wide margin exists between the present intake levels of zinc oxide and those levels that have been reported to produce noticeably harmful effects support the fact. Hence, ZnO nanoparticles have been widely considered as biocompatible, biodegradable and biosafe for medical and environmental applications (Zhou et al. 2006). These properties make them a first choice candidate for drug delivery, bio-imaging and biomedical research. For example, ZnO nanoparticle based sensors have been developed for highly sensitive and selective real-time detection of a wide variety of biomolecules (Danielsson 2012, Willander et al. 2012). Another promising area of biomedical research using ZnO nanoparticles is development of effective drug delivery applications. It has been observed that ZnO nanoparticles induce toxicity in a cell-specific and proliferation-dependent manner with rapidly dividing cells being the most susceptible and quiescent cells being the least sensitive. Moreover, a marked difference between cancer cells and their normal counterparts, as well as differences between activated and resting T lymphocytes, suggests an exciting potential for ZnO nanoparticles as novel alternatives to cancer chemotherapy and radiation therapy as well as new approaches for treatment of autoimmunity (Hanley et al. 2008). Another interesting study by Taccola et al. (2010) reported that ZnO nanoparticles exhibit a strong preferential ability to kill cancerous T cells in comparison to normal cells. Mechanism of toxicity appears to involve the generation of reactive oxygen species (ROS), with cancerous T cells generating higher inducible levels than normal T cells. The selective toxicity of ZnO nanoparticles confers an immense potential for use in novel biomedical applications thus eliminating pathogenic cells while sparing healthy body tissues (Bao et al. 2013).

The tendency to induce generation of reactive oxygen species among cells by ZnO nanoparticles has been widely employed to formulate various antibacterial products. Antibacterial activity of ZnO was tested against the Gram-negative (*Escherichia coli* and *Pseudomonas aeruginosa*) and Gram-positive bacterium (*Staphylococcus aureus*) and the effect was more pronounced for Gram-positive bacteria (Premanathan et al. 2011). Enhanced synergistic activity of zinc oxide nanoparticles with β -lactam antibiotics was also investigated to use nanoparticles in a combination therapy to treat urinary tract infections. (Bhande et al. 2013) A panel of clinically isolated and extended spectrum β -lactamase producing microorganisms was selected and antimicrobial potency as well as minimum inhibitory concentration (MIC) was determined. The results demonstrated ZnO nanoparticles as a potentiator of β -lactam antibiotics and suggested their possibility to be used for combination therapies to treat urinary tract infections.

With the increase in demand of ZnO nanoparticles, research on development of protocols for their mass scale production has gained immense interest. Various physical and chemical methods have been reported to synthesize ZnO nanoparticles in a controlled and efficient manner such as sol-gel (Bahadur et al. 2007), hydrothermal growth (Baruah and Dutta 2009), template-assisted growth (Fan et al. 2006, Bechelany et al. 2012), wet chemical synthesis (Vayssieres 2003, Wang and Gao 2003), flame spray pyrolysis (Tani et al. 2002), chemical vapor deposition (Protasova et al. 2011), self-catalyzed vapor-liquid-solid growth (Song et al. 2013) and electro-spinning (Liu et al. 2008). However, majority of the methods are complicated, requiring drastic synthesis conditions (high temperature and pressure) and have a long reaction time. Apart from this, these methods utilize toxic reactants and require expensive experimental setup. To overcome these challenges, patterning methods have been employed which are based on self-assembly and have the advantage of being fast and simple. Patterning using self-assembled monolayer of polystyrene spheres has been successfully applied for the growth of ZnO nanorod arrays (Wang et al. 2004). Similarly, using DNA-capped gold nanoparticles as a model system, Cheng et al. (2008) have patterned nanoparticle super-lattices over large areas into a number of versatile structures with high degrees of internal order. Albeit rapid and simple, methods based on self-assembly inevitably contain defects when applied to large areas. Moreover, due to the need of sophisticated instrumentation set up, it is very expensive to scale the patterning methods for mass scale synthesis of nanoparticles.

The use of biological systems, especially biomolecules, has gained enormous attraction owing to their simplicity and economic nature (Raveendran et al. 2003, Narayanan and Sakthivel 2010, Duran et al. 2011). A novel, clean method utilizing immobilized *Rhodobacter sphaeroides* has been developed for the synthesis of zinc sulfide (ZnS) nanoparticles with an average diameter of 8 nm (Bai et al. 2006). Prasad and Jha (2009) hypothesized the role of pH-dependent membrane-localized oxido-reductases for synthesis of ZnO nanoparticles in their study using *Lactobacillus sporogens*. Labrenz et al. (2000) showed

synthesis of spherical aggregates of sphalerite (ZnS) particles (2-5 nm) within the natural biofilms dominated by sulphate-reducing bacteria of the family *Desulfobacteriaceae*. They reported that a combination of geo-chemical and microbial processes leads to ZnS biomineralization resulting in the formation of ZnS nanoparticles.

Even with these successes, ZnO nanoparticles are often obtained in agglomerated state and are poorly water dispersible. The major lacuna behind these shortcomings is the lack of stable capping agents. To overcome this limitation, a fully characterized biosurfactant (rhamnolipid) produced by *Pseudomonas aeruginosa* BS01 was used as a novel and green soft template to synthesize and stabilize size-tunable ZnS NPs in an aqueous medium with uniform dispersity and hydrophilicity (Hazra et al. 2012). Rhamnolipid (biosurfactant) served the dual role of capping as well as stabilizing agent and allowed formation of homogeneous, water soluble, stable and polydisperse ZnS NPs with a particle size of 10–15 nm.

As mentioned in Chapter IV, the nanoparticles synthesized using secretory fungal proteins are often capped with proteins. Previous studies have also reported the formation of protein-capped nanoparticles when synthesized via extracellular synthesis approach (Bhainsa and D'Souza 2006, Kalishwaralal et al. 2008, Parikh et al. 2008, Balaji et al. 2009, Duran et al. 2011). Moreover, it has been observed that the microorganisms from metal rich regions can confer high metal tolerance and could be an attractive source for nanoparticle synthesis (Jain et al. 2011, Jain et al. 2013). The sophistication and success of natural bottom-up fabrication processes inspired us to utilize zinc metal tolerant fungal isolates for the synthesis of ZnO nanoparticles.

This chapter demonstrates the potential of two indigenous high zinc tolerant fungal isolates *Aspergillus aeneus* isolate NJP12 and *Aspergillus* sp. isolate NJP02 (mentioned in Chapter II) for extracellular synthesis of ZnO nanoparticles. The present study also demonstrates a positive correlation between zinc metal tolerance ability of fungi and their potential for the synthesis of ZnO nanoparticles. Our eclectic approach holds promises to contribute significantly in the development of a low cost, clean and environmentally benign protocol for fabrication of metal nanoparticles. Moreover, advantages of biologically synthesized protein-capped ZnO nanoparticles in comparison to bare ZnO nanoparticles for photocatalytic decomposition of organic compounds were studied. The presence of proteins on the surface of ZnO nanoparticles makes them attractive in general and is expected to have great potential for various applications such as sensing, catalysis and delivery systems.

6.2 Materials and methods

6.2.1 Extracellular synthesis of ZnO nanoparticles

For extracellular synthesis of ZnO nanoparticles, the experimental fungal isolate (4 days old) was inoculated in 100 mL of MGY medium (0.3 % malt extract, 1.0 % glucose, 0.3 % yeast extract, 0.5 % peptone; pH 7.0) in 250 mL Erlenmeyer flasks. Inoculated flasks were incubated at 28 °C for 72 h on a rotary shaker (150 rpm) under dark conditions. Fungal mycelia were separated from the culture medium by centrifugation (8000 rpm, 10 min and

4 °C) and washed thrice with sterile water in order to remove all traces of media. Typically, 10 g of biomass (fresh weight) was re-suspended in 100 mL of sterile deionized Milli-Q water and further incubated for 72 h under the same conditions as described above. After incubation, biomass was separated by filtration using Whatman filter paper no. 1 (Whatman Inc., USA), and the fungal cell free filtrate containing extracellular secretions was collected. For synthesis of nanoparticles, aqueous zinc acetate solution (Sigma-Aldrich, USA) at a final concentration of 1.0 mM was added to flasks containing 100 mL of fungal cell free filtrate and incubated for 72 h under the same conditions as described above. Controls containing fungal cell free filtrate (without zinc acetate; positive control) and pure zinc acetate solution (without fungal cell free filtrate; negative control) were also run simultaneously along with experimental flasks in three replicates. Viability of the fungal cells after incubation in Milli-Q water for 72 h was also checked. For this, the fungal mycelia were inoculated on fresh PDA plates in triplicate and incubated for 4 days at 28 °C in dark conditions.

6.2.2 Characterization of ZnO nanoparticles

The synthesized nanoparticles were characterized using standard techniques as mentioned in the Chapter III, section 3.2.3.

6.2.3 Role of proteins in ZnO nanoparticle synthesis

To investigate the involvement of proteins in nanoparticle synthesis, proteins were precipitated from the fungal cell free filtrates using the standard trichloroacetic acid (TCA) method (Simpson 2004). 100 mL of supernatant fraction without proteins was used for synthesis of ZnO nanoparticles under the same conditions as mentioned above. In order to understand the nature of proteins present in the fungal cell free filtrate, a separate experiment was performed. Briefly, 100 mL of fungal cell free filtrate was boiled in a water bath for 20 min, cooled and used for synthesis of ZnO nanoparticles under the same conditions as described above. A flask containing 100 mL of fungal cell free filtrate without heat treatment was used as control. Systematic monitoring of pH of the reaction medium was also observed at different time intervals to understand the chemical nature of system.

6.2.4 Photocatalytic studies of ZnO nanoparticles

The photocatalytic performance of the biologically synthesized protein-capped ZnO nanoparticles and commercially available bare ZnO nanoparticles was evaluated by measuring the degradation of aqueous methylene blue (MB) solution under UV light irradiation. In a typical photocatalytic experiment, 10 mg of freeze-dried nanoparticles (photocatalyst) were added to 40 mL of aqueous MB solution (10 µM) in a 100 mL glass beaker. The suspension was vigorously stirred in the dark for 60 min to ensure the establishment of adsorption-desorption equilibrium of MB dye on the photocatalyst surfaces. Under ambient conditions and stirring, the beaker was exposed to UV irradiation generated by a high pressure mercury vapour lamp with the predominant wave crest at 365 nm. The distance between the beaker containing suspension and the irradiation source was optimized at 13 cm (data not shown) and kept constant for further studies. During illumination, 1 mL of

the suspension was withdrawn periodically and centrifuged to remove the catalyst. UV-visible spectra of the samples were recorded with a Jasco V-630 UV-visible spectrophotometer. Control experiment was repeated without the presence of photocatalyst in the MB solution. All recorded spectra were analysed using Spectra Manager software supplied by JASCO Corporation and plotted against the time of UV irradiation. The degree of photocatalytic degradation of MB dye as a function of time was calculated by the following equation (1) where C_0 represents the initial concentration of MB solution and C_t stands for the concentration of MB solution after UV irradiation at any time (t). The data were applied to pseudo-first-order kinetics using equation (2) given below and a graph was plotted against $\ln([C]_t)$ versus time to calculate rate constant and R^2 values.

$$X = \left[\frac{(C_0 - C_t)}{C_0} \right] \times 100 \% \quad \text{Eq. 1}$$

$$\ln([C]_t) = \ln([C]_0) - kt \quad \text{Eq. 2}$$

6.2.5 Optimization of ZnO nanoparticle synthesis

The details of optimization of ZnO nanoparticle synthesis are similar as mentioned in Chapter III, section 3.2.4.

6.3 Results and discussion

6.3.1 Synthesis of ZnO nanoparticles using *Aspergillus aeneus* isolate NJP12

6.3.1.1 Characterization of ZnO nanoparticles

UV-visible spectroscopy was used to monitor the synthesis of ZnO nanoparticles. Figure 6.1 shows a gradual increase in absorbance at ca. 375 nm with respect to time of reaction, representing the synthesis of ZnO nanoparticles. At initial time intervals (0, 6, 12 and 24 h), synthesis was relatively slow but at later time intervals (36, 48 and 72 h) significant changes in the magnitude of absorbance were observed. The observed absorption maxima at 375 nm can be attributed to a band-to-band emission of ZnO which represents a direct band gap of 3.3eV (Prasad et al. 2006, Sridevi and Rajendran 2009). pH values of 7.4 and 7.8 were observed at the start (0 h) and end (72 h) of the reaction, respectively. This minimal change in pH makes the present protocol “eco-friendly” which is highly advantageous as compared to chemical synthesis protocols which show high pH variations (Sharma et al. 2009). The stability of the nanoparticle solution stored at room temperature in dark conditions for more than three months after completion of reaction was determined by UV-visible spectroscopy measurements (data not shown).

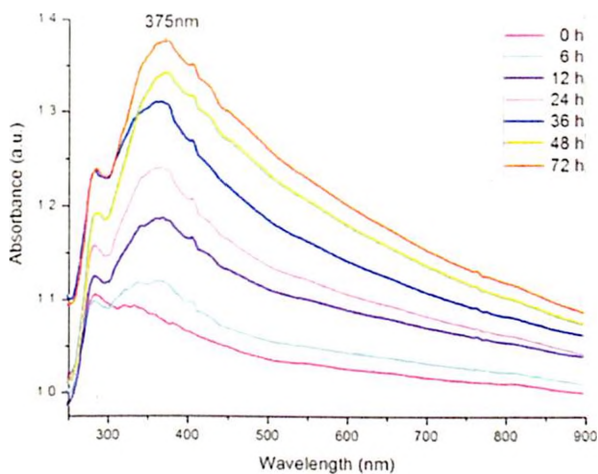


Figure 6.1 UV-visible spectrum representing gradual synthesis of ZnO nanoparticles with respect to time.

TEM measurements of samples were performed to visualize the size and morphology of ZnO nanoparticles. A TEM micrograph (Figure 6.2a) showed the well distributed spherical ZnO nanoparticles surrounded by a thin protein layer. The size distribution analysis showed that the particle size ranged from 100-140 nm. EDS analysis of drop coated grids of samples was performed to determine the elemental composition of nanoparticles (Figure 6.2b). EDS spectra showed strong peaks at 0.5, 1.1, 8.6 and 9.5 keV which are due to O K_{α} , Zn L_{α} , Zn K_{α} , and Zn K_{β} , respectively (Bahadur et al. 2007). The atomic percent values of Zn and O observed were 0.38 and 0.18, respectively. Other peaks observed for copper and carbon were due to the supporting carbon coated copper grid used for sample preparation.

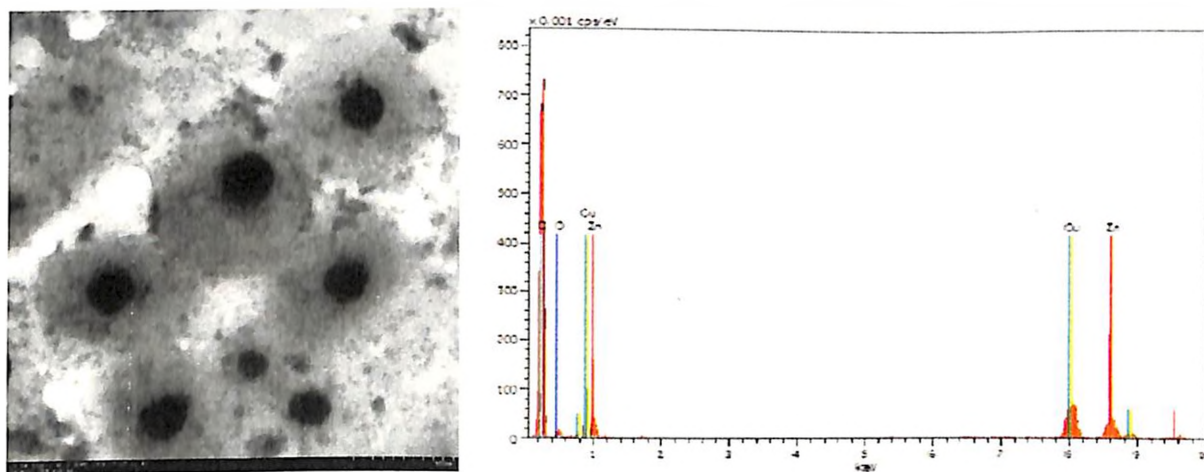


Figure 6.2 (a) A representative transmission electron micrograph showing the spherical shape of ZnO nanoparticles. (scale bar = 500 nm) (b) EDS spectrum representing the elemental composition of ZnO nanoparticles.

Figure 6.3 shows the XRD patterns of synthesized ZnO nanoparticles. Analysis of XRD spectra showed well-defined peaks at 2θ values of 32.05° , 34.69° and 36.53° which corresponds to (100), (002) and (101) planes of ZnO, respectively. The observed lattice

values were in agreement with the hexagonal phase of ZnO (PCPDF-WIN; JCPDS-ICDD 2008).

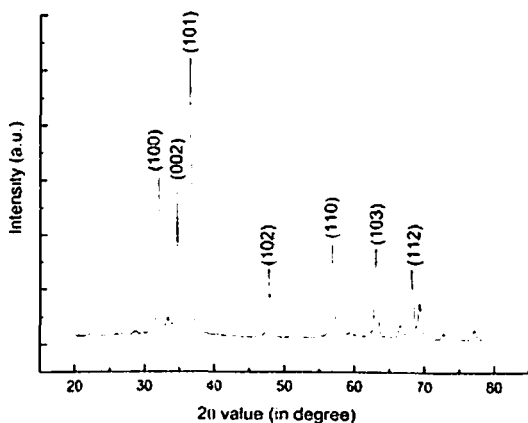


figure 6.3 X-ray diffraction spectrum of ZnO nanoparticles with Bragg's diffraction values shown in parentheses. The absorbance is expressed in terms of arbitrary unit (a.u.).

6.3.1.2 Characterization of capping molecule

FTIR measurements of freeze-dried ZnO nanoparticles were performed to characterize the surface molecules on as-synthesized ZnO nanoparticles. As shown in Figure 6.4, an intense band attributed to ZnO vibrations could be seen in the vicinity of wavenumbers 400-600 cm^{-1} that centered at wavenumber 430 cm^{-1} (Becheri et al. 2008). The presence of bands at wavenumbers 1625 and 1550 cm^{-1} corresponds to the bending vibrations of the amide I and amide II of proteins, respectively (Ahmad et al. 2003). The band at 3450 cm^{-1} has been reported to occur due to stretching vibrations of amide I superimposed on the side of hydroxyl group band (Saeed et al. 2009). Moreover, the bands at 2995 and 2350 cm^{-1} are due to the stretching vibrations of amide II and presence of atmospheric CO_2 , respectively (Becheri et al. 2008, Saeed et al. 2009).

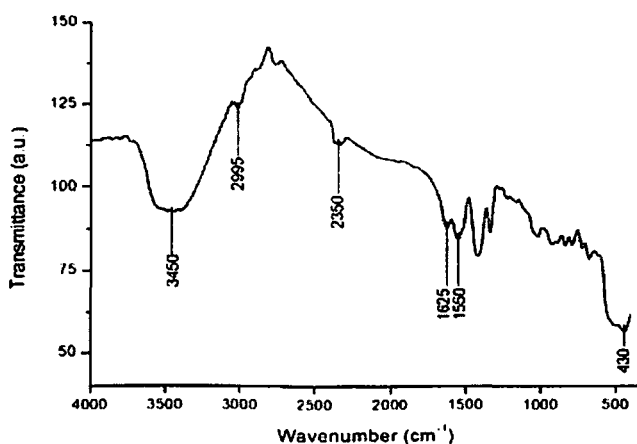


Figure 6.4 FTIR spectrum of freeze-dried samples of ZnO nanoparticles depicting the presence of proteins on the surface of ZnO nanoparticles. The absorbance is expressed in terms of arbitrary unit (a.u.).

6.3.1.3 Role of proteins in ZnO nanoparticle synthesis

An absorption peak at ca. 280 nm, observed in the UV-visible spectrum of fungal cell free filtrate, indicated the presence of proteins in the fungal cell free filtrate (data not shown). Concentration of proteins in the fungal cell free filtrate was determined to be $458.2 \pm 2.8 \mu\text{g mL}^{-1}$. Incubation of precursor zinc ions with a supernatant fraction without proteins (obtained by protein precipitation) showed no evidence of ZnO nanoparticle synthesis which indicates that proteins play an important role in the synthesis of ZnO nanoparticles. An experiment with incubation of denatured (heat treated) and native (untreated) proteins with precursor zinc ions resulted in the synthesis of ZnO nanoparticles in both cases. Interestingly, comparison of absorbance spectra indicates a higher rate of reaction in case of denatured proteins as compared to native proteins (Figure 6.5).

This result revealed that the native form of protein is not mandatory for nanoparticles synthesis. It can also be inferred that the nanoparticle synthesis process is non-enzymatic as the activity of enzymes depends on their structure which changes during denaturation. Hence, with the current experimental evidences, it can be concluded that the synthesis process depends on interaction with amino acids present in the proteins. The high reaction rate for ZnO nanoparticles synthesis as observed by absorption spectra (Figure 6.5) in case of denatured (heat treated) proteins further validates that the rate of synthesis depends on the interaction of amino acids with metal (Zn^{+2}) ions. Heating of protein molecules results in the breakdown of hydrogen bonds which allows dismantling the hydrophobic core which in turn enhances the interactions between amino acids and zinc ions. Our results substantiate the previous reports which demonstrate that interactions between amino acids and metal ions are responsible for synthesis of metal nanoparticles (Xie et al. 2007). However, the present findings are in disagreement with earlier reports which hypothesize the involvement of enzymes in synthesis of nanoparticles (Ahmad et al. 2003, Nangia et al. 2009). To the best of our knowledge, this is the first study which proposes the involvement of simply amino acids in the fungal mediated synthesis of metal nanoparticles.

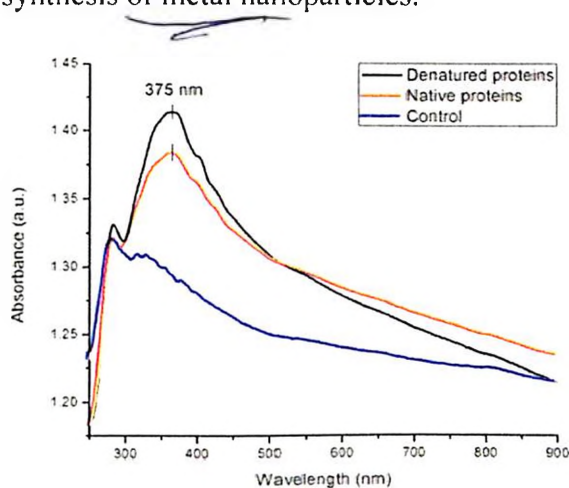


Figure 6.5 Effect of denaturation of proteins on synthesis of ZnO nanoparticles. The absorbance is expressed in terms of arbitrary unit (a.u.)

6.3.2 Optimization of ZnO nanoparticle synthesis using *Aspergillus aeneus* isolate NJP12

The essential feature of any nanoparticle synthesis protocol is to achieve a desirable particle size and distribution with high yield and low preparation cost. Although, extracellular biosynthesis of ZnO nanoparticles using secreted fungal proteins is economic and eco-friendly, yield of the nanoparticle formation is still a major concern. Many parameters such as reactants (precursor zinc ion and secreted protein), concentration and pH of the reaction medium are important to control the formation of zinc oxide nanoparticles. Herein, the influence of these parameters on the formation of ZnO nanoparticles using fungus *Aspergillus aeneus* isolate NJP12 has been investigated. As formation of ZnO nanoparticles is not evident visually, yield of the synthesized ZnO nanoparticles was monitored by critically assessing their absorbance at 375 nm (Kanade et al. 2006, Jain et al. 2013).

The effects of various parameters on the yield of ZnO nanoparticle synthesis have been shown in Figure 6.6. The effect of pH on ZnO nanoparticle synthesis was studied in the pH range of 2 to 10. As can be seen in Figure 6.6a, the formation of ZnO nanoparticles was found to be severely hampered at acidic conditions (pH 2-4). In contrast, alkaline conditions facilitated the formation of ZnO nanoparticles with maximum yield at pH 9 and 10. It is well known that the solution pH is one of the important factors influencing the synthesis of ZnO nanoparticles. In particular, pH affects the hydrolysis and condensation behaviour of the solution and therefore influences the morphology of the ZnO. The phenomenon is very well observed during sol-gel method of ZnO nanoparticle synthesis (Wahab et al. 2010). Li et al. (2003) also showed that the solution conditions have a particular effect on ZnO particle-size powders. The pH can also change the number of ZnO nuclei and growth units (Zhang et al. 2004). Alias et al. (2010) showed the formation of ZnO nanoparticles with high homogeneity when the pH was increased to alkaline conditions (pH 8 and 9). Moreover, presence of predominantly spherical shaped ZnO nanoparticles demonstrated a strict control over shape.

The other parameter that significantly determines the growth of nanoparticles thereafter influencing yield is the concentration of precursor zinc ions. Precursor zinc ions control the nanoparticle synthesis process by determining the magnitude of addition of reactive precursors available in solution to already existing particles. Extensive investigations have shown that the growth of nanoparticles proceeds by a surface reaction limited condensation of precursors. As shown in Figure 6.6b, precursor zinc (salt) concentration demonstrated a near bell-shaped response on the formation of ZnO nanoparticles. The maximum yield was observed in the range of 1.0 - 3.0 mM concentration of zinc ions with higher concentrations restricting the growth of ZnO nanoparticles.

The influence of varying concentration of fungal proteins (reactant) on formation of ZnO nanoparticles is illustrated in Figure 6.6c. The amount of fungal proteins was varied by suspending increasing quantity of fungal biomass in a constant reaction volume. It was observed that the amount of proteins secreted from the biomass up to the range of 4 to 6 g

/100 mL of reaction volume was insufficient to deliver high yield of ZnO nanoparticles. Increasing the fungal biomass in the range of 12-15 g /100 mL of reaction volume resulted in approximately 40% higher yield of ZnO nanoparticles. Moreover, no further increase in yield of nanoparticle synthesis was observed even the fungal biomass was placed up to 20 g /100 mL of reaction volume. These findings clearly suggest that the reactant concentration (fungal proteins) play a crucial role to achieve controlled synthesis of ZnO nanoparticles.

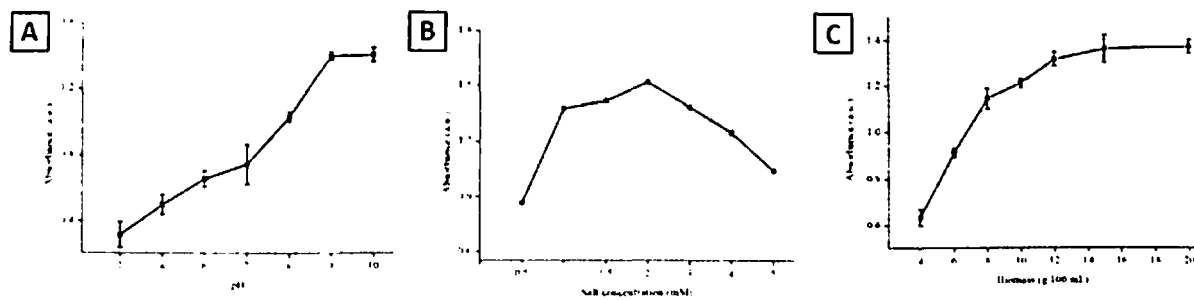


Figure 6.6 Optimization of process parameters for synthesis of ZnO nanoparticles using fungus *Aspergillus aeneus* isolate NJP12 with respect to (a) pH, (b) salt concentration and (c) biomass.

6.3.3 Synthesis of zinc oxide nanoparticles using *Aspergillus* sp. isolate NJP02

6.3.3.1 Characterization of zinc oxide nanoparticles

UV-Visible spectroscopy is often employed for the determination of absorption properties of nanoparticles and consistently used to monitor the nanoparticle synthesis. Figure 6.7 illustrates UV-visible spectra recorded at different time intervals to study the gradual change in light absorption profile of the reaction mixture containing fungal proteins and precursor zinc ions. Emergence of a strong narrow absorption peak with respect to time at ca. 371 nm embodies the gradual synthesis of ZnO nanoparticles. The observed absorption maxima can be attributed to the direct band gap of ZnO due to electron transitions from the valence band to the conduction band ($O_{2p} \rightarrow Zn3d$) (Ameen et al. 2013). At initial time intervals (0 and 12 h), synthesis was relatively slow but at later time intervals (36, 48 and 72 h) significant changes in the magnitude of absorbance values were observed. Additionally, another peak at 280 nm confirmed presence of proteins in the reaction mixture, which is characteristic to aromatic amino acids present in the proteins.

The crystalline nature and phase purity of the synthesized ZnO nanoparticles were evaluated using X-ray diffraction (XRD) measurements. As shown in Figure 6.8, XRD spectrum exhibited well-defined peaks at 2θ values of 31.83° , 34.50° , 36.32° and 47.62° corresponds to (100), (002), (101) and (102) planes of ZnO, respectively. The recorded XRD pattern was perfectly indexed with Joint Committee on Powder Diffraction Standard (JCPDS) card number 36-1451, confirming the existence of typical wurtzite crystal structure of ZnO nanoparticles. Noticeably, diffraction peaks related to any other phase of ZnO or impurities were not observed, which indicated the high purity of the synthesized ZnO nanoparticles.

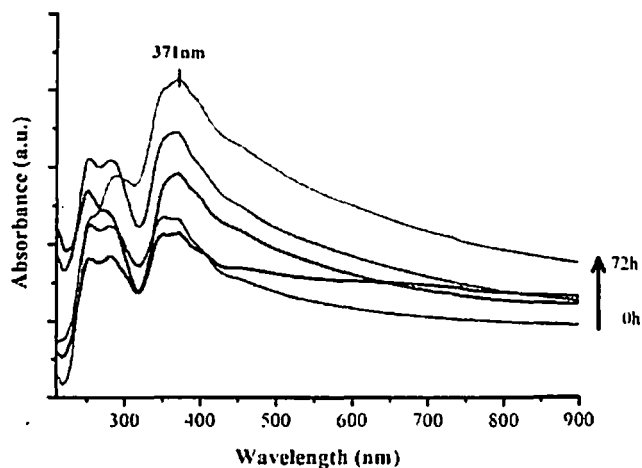


Figure 6.7 UV-visible spectra showing gradual synthesis of ZnO nanoparticles with respect to time.

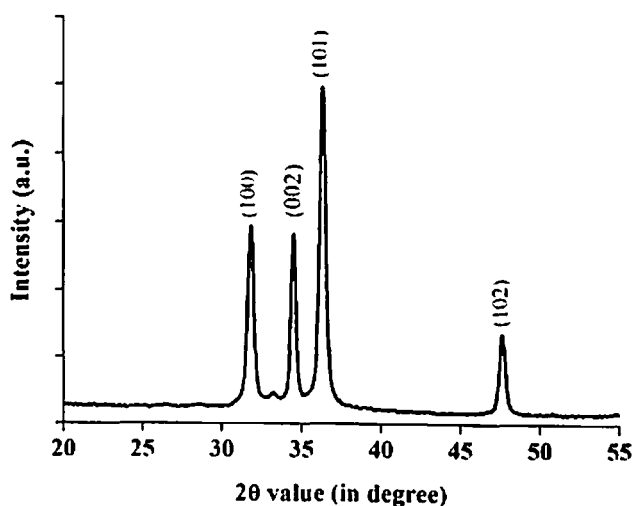


Figure 6.8 X-ray Diffraction pattern recorded for freeze-dried ZnO nanoparticles synthesized using fungus *Aspergillus* sp. isolate NJP02. Bragg's diffraction values are shown in parentheses.

The morphology and particle size of nanoparticles were determined using transmission electron microscopy measurements. A representative TEM micrograph (Figure 6.9a) shows that the synthesized particles were quasi-spherical, symmetrical, polydisperse and well distributed without any aggregation with size predominantly ranging between 80 to 120 nm (Figure 6.9b). The quasi-spherical shape of protein-capped nanoparticles has been found to be consistent with previous observation which postulates that presence of numerous sulphur containing cysteine residues at various locations of a protein essentially directs the shape of nanoparticles to be quasi-spherical (Makhal et al. 2012). Owing to the presence of protein capping on the surface, nanoparticles were steadily dispersed in water to form an optically transparent solution (Figure 6.9c). The elemental composition of nanoparticles has been confirmed using the energy dispersive X-ray spectroscopy measurements. An EDX

spectrum (Figure 6.9d) recorded from a single nanoparticle depicts three distinct peaks at 1.1 keV, 8.6 keV, and 9.5 keV which could be ascribed to Zn L_α, Zn K_α, and Zn K_β, respectively (Bahadur et al. 2007). Additional peaks observed for copper and carbon were due to the supporting carbon coated copper grid used for sample preparation.

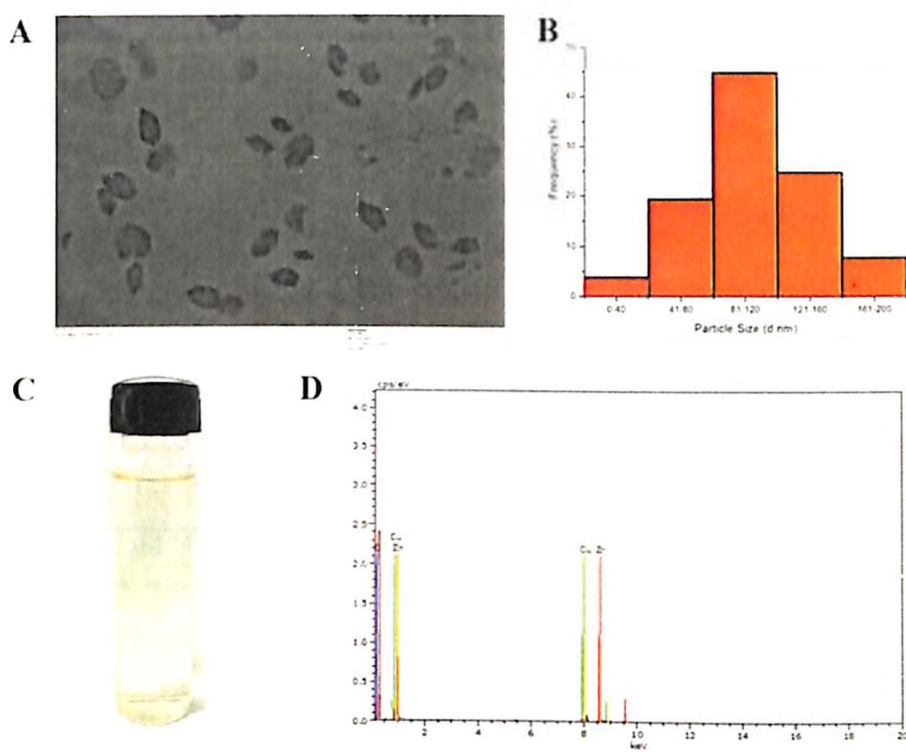


Figure 6.9 Characterization of as-synthesized “protein-capped” ZnO nanoparticles. (a) A representative TEM micrograph depicting quasi-spherical shape. (b) Histogram showing the size distribution analysis. (c) Optically transparent solution under daylight. (d) EDX spectrum showing elemental composition.

6.3.3.2 Characterization of capping molecule

In order to evaluate the presence of protein molecules on the surface of as-synthesized ZnO nanoparticles, the intrinsic fluorescence measurements were recorded. The nanoparticle suspension was excited at a wavelength of 280 nm and fluorescence emission spectrum was recorded between 300 and 400 nm (Figure 6.10a). A distinct emission peak at 340 nm was observed which arises due to the presence of tyrosine residues in the capping proteins (Fatima and Husain 2007). Furthermore, when excited with 325 nm wavelength, a distinct emission peak at 520 nm was observed which could be attributed to strong green emission band of ZnO nanoparticles. It has been well documented that fluorescence measurements of ZnO nanoparticles exhibit a green emission band which attributes to the transition of photo-generated electron from a dark level below the conduction band to a deeply trapped hole, induced by an oxygen vacancy (Kim et al. 2003, Vigneshwaran et al. 2006). Figure 6.10b shows a FTIR spectrum with an intense broad band in the vicinity of 400-600 cm^{-1} and centred around 480 cm^{-1} which can be associated with the Zn-O stretching mode (Becheri et

al. 2008). Presence of bands at wavenumbers 1641 and 1520 cm^{-1} correspond to the bending vibrations of the amide I and amide II of proteins, respectively (Ahmad et al. 2003). These experimental observations indicate successful synthesis of protein-capped ZnO nanoparticles. These results are consistent with the fact that nanoparticles synthesized through the biological approach are often capped with proteins. For example, studies on noble metal (Au and Ag) nanoparticle synthesis using microorganisms showed the presence of protein molecules on the surface of nanoparticles and have predicted their role in nanoparticle stability (He et al. 2007, Husseiny et al. 2007, Balaji et al. 2009, Duran et al. 2011, Jain et al. 2011).

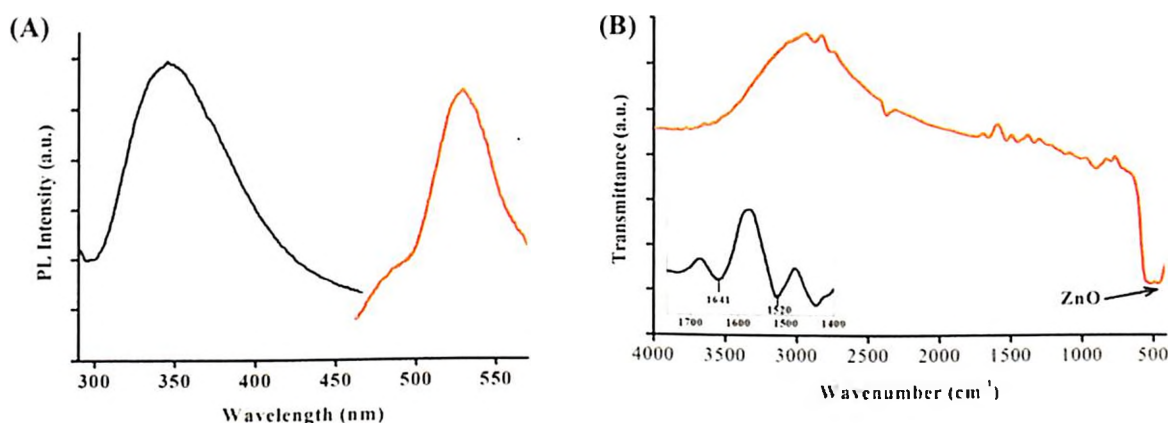


Figure 6.10 (a) Intrinsic fluorescence spectra of protein-capped ZnO nanoparticles excited at a wavelength of 280 nm (black) and 325 nm (red). (b) FTIR spectrum of freeze-dried ZnO nanoparticles with inset showing the amide I band of the proteins.

6.3.4 Optimization of ZnO nanoparticle synthesis using *Aspergillus* sp. isolate NJP02

Optimization of process parameters is an important step to achieve strict control over the process of ZnO nanoparticle synthesis. As mentioned in section 6.3.2, the reactants (precursor zinc ion and secreted protein) concentration and pH of the reaction medium are crucial to control the formation of zinc oxide nanoparticles. Moreover, in order to achieve control over shape and size, other parameters such as temperature, capping molecules, etc. can be varied. For instance, Wu et al. (2006) demonstrated that on increasing the reaction temperature, the morphology of particles seems to change from rod-like to short prism-like form. Herein, the influence of these parameters on the formation of ZnO nanoparticle synthesis using fungus *Aspergillus* sp. isolate NJP02 was investigated. The absorbance at 375 nm critically assessed to monitor the yield of the ZnO nanoparticle synthesis (Kanade et al. 2006, Jain et al. 2013).

Figure 6.11a shows the effect of increase in reaction medium pH on the formation of ZnO nanoparticle synthesis. It is apparent that the alkaline pH induces the nanoparticle formation in comparison to acidic pH. The highest rate of nanoparticle synthesis was observed at pH 9. These results are in complete agreement with the previous report which showed that the increase in pH (from acidic to alkaline) of the solution facilitates the formation of ZnO nanoparticles (Sagar et al. 2007). This observation can be described by

taking into account the fact that alkaline pH can increase the concentration of dissolved zinc ions and promotes their solubility in water (Meulenkamp 1998). Moreover, alkaline pH also affects the hydrolysis and condensation reactions (Wahab et al. 2010). Similar observations have been documented for synthesis processes for SiO₂ nanoparticles (Iler 1979).

The dependence of ZnO nanoparticle synthesis on the precursor zinc ion concentration has been illustrated in Figure 6.11b. The maximum yield of ZnO nanoparticle synthesis was observed at a zinc ion concentration of 2 mM. Further increase in concentration limited the nanoparticle synthesis that may be due to the formation of larger aggregates that are undetectable at absorbance 375 nm. These findings were similar to the results obtained during ZnO nanoparticle synthesis using fungus *Aspergillus aeneus* isolate NJP12 discussed in section 6.3.2.

Similarly, the effect of varying protein concentration on formation of ZnO nanoparticles was investigated by varying the amount of fungal biomass in the reaction medium. The maximum yield of ZnO nanoparticle synthesis was observed when 15 g fungal biomass was suspended in 100 mL reaction volume. The yield value was found to be lower as compared to the ZnO nanoparticle synthesis using fungus *Aspergillus aeneus* isolate NJP12.

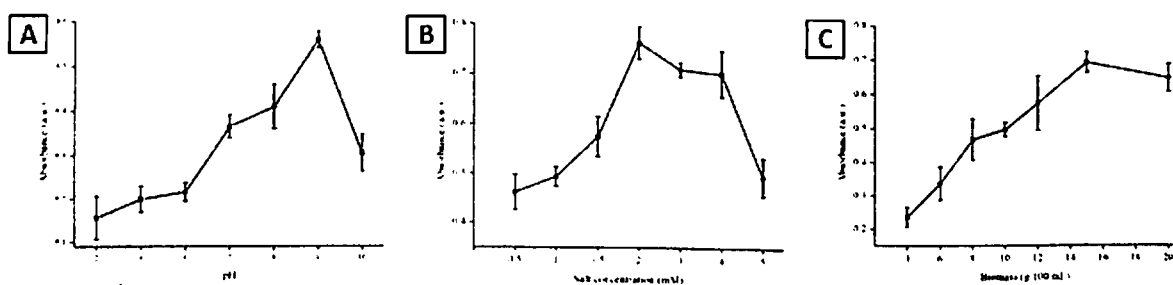


Figure 6.11 Optimization of various process parameters for synthesis of ZnO nanoparticles using fungus *Aspergillus* sp. isolate NJP02 (a) pH, (b) salt concentration and (c) biomass.

6.3.5 Photocatalytic activity of “protein-capped” ZnO nanoparticles

Industrial effluents have long been a major concern among the environmental protection issues and considered as a potential threat. Organic dyes have received particular attention as prominent environmental contaminants owing to their non-biodegradability and carcinogenic effects on humans. Moreover, they drastically affect the nature of water, inhibit sunlight penetration and reduce photosynthesis resulting in severe toxicity to aquatic creatures (Aksu 2005, Srinivasan and Viraraghavan 2010). Semiconductor based photocatalytic oxidation have attracted great attention for solving many current environmental issues especially removal of dye pollutants from water (Hoffmann et al. 1995, Rajeshwar et al. 2001). This approach is highly advantageous as it does not yield toxic intermediate products, making it suitable for cleaning polluted water bodies that contains low to medium concentration of contaminants. Various semiconductors such as TiO₂ (E_g = 3.2 eV), ZnO (E_g = 3.4 eV), ZnS (E_g = 3.6 eV), WO₃ (E_g = 2.8 eV), SrTiO₃ (E_g = 3.2 eV) etc.

have been widely implemented as promising candidates for the photocatalytic degradation reactions.

Although TiO_2 has been universally recognized as the most efficient photocatalyst, recent reports have highlighted the effectiveness of ZnO in removing organic compounds from water matrices (Sakthivel et al. 2003, Li et al. 2009). In particular, ZnO in nanoparticle regime has appeared to be catalyst that is more efficient than TiO_2 as it exhibits high reaction and mineralization rates with efficient generation of H_2O_2 . Furthermore, ZnO nanoparticles possess more number of active sites with high surface reactivity than bulk ZnO (Wang 2004, Ameen et al. 2013). Unfortunately, ZnO possesses the critical drawbacks of photocorrosion, quick recombination of charge carriers and poor response to visible light which significantly hampers its photocatalytic efficiency and stability, thus limiting its practical applications (Spathis and Poullos 1995, Zhang et al. 2009). Thus, substantial efforts have been devoted to overcome these problems such as depositing metals or coatings on ZnO surface, doping/hybridization with metals or metal ions and combining ZnO with another semiconductor (Bandara et al. 2002, Lahiri and Batzill 2008, Kochuveedu et al. 2013, Meng et al. 2013). Modifications of ZnO nanoparticles surface with organic molecules such as oleic acid, polydimethylsiloxane etc. have improved the photocatalytic performance upto a remarkable extent (Comparelli et al. 2005, Hong et al. 2006, Jeong et al. 2012). Surface modifications with proteins, organic molecules of the biological origin, can act as potential alternative because of high dye adsorption rate along with low recombination rate of the e^-/h^+ pairs. However, the use of protein molecules for surface modification of ZnO photocatalyst is still unexplored.

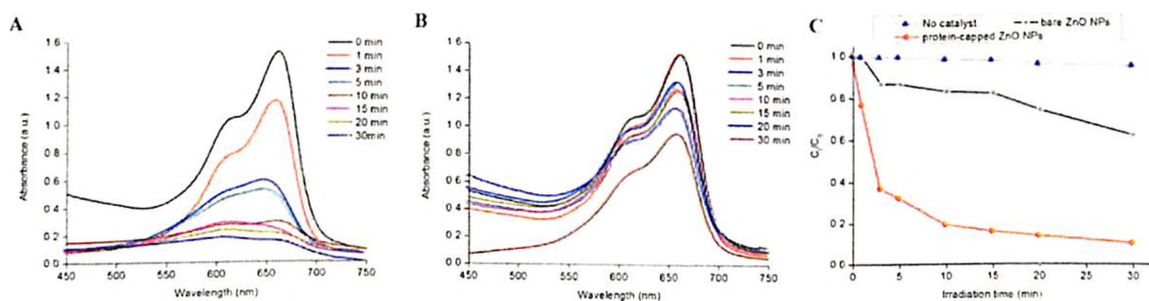


Figure 6.12 Photodegradation of methylene blue dye solution under UV-light irradiation by (a) as-prepared protein-capped ZnO nanoparticles and (b) bare ZnO nanoparticles. (c) The extent of MB dye decomposition with respect to time intervals over a period of 30 min UV irradiation. (catalyst concentration: 10 mg/mL; initial dye concentration: 10 μM).

The degradation of organic pollutants by ZnO photocatalysts has received immense attention due to environmental concerns. To determine the efficacy of the protein-capped ZnO nanoparticles as compared to commercially available bare ZnO nanoparticles, photocatalytic degradation of methylene blue dye was investigated. Methylene blue, a globally adopted representative organic pollutant of dye waste effluents was used as a probe

molecule to evaluate the performance of photocatalysts. The characteristic optical absorption maximum of MB at 665 nm was used to monitor the photocatalytic degradation process. Figure 6.12 (a and b) represents the UV-visible absorption spectra of MB dye solution by protein-capped ZnO nanoparticles and bare ZnO nanoparticles respectively, recorded within the time range of 30 min under UV light irradiation. In both cases, it was clearly evident that on increasing the exposure time, a noticeable decrease in the absorbance intensity of MB dye was observed which corresponds to the photocatalysis of MB dye. Albeit, the rate of degradation is being slower in case of bare ZnO nanoparticles. A systematic comparison of MB dye degradation in presence of protein-capped and bare ZnO nanoparticles under UV light irradiation is depicted in Figure 6.12c which clearly emphasize variation in the relative concentration (C_t/C_0) of MB dye solution. It was observed that the MB concentration was hardly reduced in absence of photocatalyst (control) validating the MB stability under UV light irradiation. The degradation rate of MB by protein-capped ZnO nanoparticles increased significantly with the increase of time period under UV light irradiation as compared to bare ZnO nanoparticles. Moreover, to evaluate the photocatalysis quantitatively, the kinetic parameters (reaction rate, % MB degradation and regression coefficient) of dye degradation were calculated and summarized in Table 6.1. It can be clearly observed that the reaction rate (k) is dramatically higher for protein capped ZnO nanoparticles ($3.27 \times 10^{-3} \text{ s}^{-1}$) as compared to bare ZnO nanoparticles ($5.99 \times 10^{-3} \text{ s}^{-1}$). Also, more than two fold increase in total amount of MB degradation was observed when protein molecules were present on the surface of ZnO nanoparticle as compared to bare ZnO signifying protein-capped ZnO nanoparticles as a superior photocatalyst.

Table 6.1 Kinetic parameters^a for the photocatalytic degradation of methylene blue (MB) dye with protein-capped and bare ZnO nanoparticles catalysts.

Sample	$k \text{ (s}^{-1}\text{)}$	Final MB degradation (A%) (in 30 min)	R^2
Protein-capped ZnO nanoparticles	3.27×10^{-3}	89.68	0.96
Bare ZnO nanoparticles	5.99×10^{-3}	38.08	0.89
No catalyst	7.00×10^{-3}	1.57	0.85

^areaction rate (k), percentage of MB degradation (A), and the regression coefficient (R)

It is generally accepted that the light absorption and transportation & separation of charge on the surface of catalyst are key parameters to determine photocatalytic performance (Basu et al. 2010). The high surface area attained due to the presence of protein molecules in case of protein-capped ZnO nanoparticles might have resulted in more unsaturated surface coordination sites exposed to the reactants thus facilitating the absorption of MB molecules. It has also been postulated that the presence of amino acids containing aromatic rings can create hydrophobic spaces which can enhance the efficient binding of MB dye molecules (Baruah et al. 2009). Alternatively, it may be possible that presence of protein molecules will

result in molecular recognition of MB molecules which can effectively facilitate the electron transfer process when electron donor and acceptor molecules come to a close proximity. Makhal et al. (2012) observed similar phenomenon while studying the photocatalysis of MB dye with chymotrypsin associated ZnS nanoparticles. Conclusively, the enhanced photocatalytic performance can be attributed to charge transfer from zinc oxide nanoparticles to the attached proteins, which effectively reduce the recombination of electrons and holes, leading to enhanced photocatalytic properties of protein-capped ZnO nanoparticles.

6.4 Conclusions

The present chapter establishes a positive correlation between zinc metal tolerance ability of tested soil fungi (*Aspergillus aeneus* isolate NJP12 and *Aspergillus* sp. isolate NJP02) with their potential for the synthesis of ZnO nanoparticles at ambient conditions. UV-visible Spectroscopy, Fourier Transform Infrared (FTIR) Spectroscopy, X-Ray Diffraction (XRD) analysis, Transmission Electron Microscopy (TEM) and Energy Dispersive Spectroscopy (EDS) studies further confirmed the crystallinity, morphology and composition of synthesized ZnO nanoparticles. In both the cases, it was observed that as-synthesized spherical/quasi-spherical nanoparticles were coated with protein molecules which may serve as stabilizing agents. Investigations on the role of fungal extracellular proteins in the synthesis of nanoparticles indicated that the process is non-enzymatic but involves amino acids present in the protein chains. Moreover, various parameters such as reactant concentration (salt and proteins) and pH of the solution were found to influence the process of nanoparticle synthesis. The photocatalytic performance of as-synthesized protein-capped ZnO nanoparticles towards MB degradation was compared with commercially available bare ZnO nanoparticles. Owing to the presence of surface proteins, ZnO nanoparticles exhibited enhanced photocatalysis towards methylene blue dye as compared to bare ZnO nanoparticles suggesting their potential applications in catalysis, waste water treatment etc. The remarkable photocatalytic performance originated mainly due to the presence of surface proteins which act as effectual host for methylene blue dye and facilitates absorption of dye along with low recombination rate of the e^-/h^+ pairs. The low cost, simplicity and eco-friendly nature of the present protocol for “one-pot” synthesis and modification of ZnO nanoparticles could be extended to synthesize other metal nanoparticle thus expanding its applicability in various fields.

6.5 References

- Ahmad, A., Mukherjee, P., Senapati, S., Mandal, D., Khan, M. I., Kumar, R. and Sastry, M. (2003). Extracellular biosynthesis of silver nanoparticles using the fungus *Fusarium oxysporum*. *Colloids and Surfaces, B: Biointerfaces* **28**: 313-318.
- Akhtar, M. S., Ameen, S., Ansari, S. A. and Yang, O. (2011). Synthesis and characterization of ZnO nanorods and balls nanomaterials for dye sensitized solar cells. *Journal of Nanoengineering and Nanomanufacturing* **1**: 71-76.

- Aksu, Z. (2005). Application of biosorption for the removal of organic pollutants: a review. *Process Biochemistry* **40**: 997-1026.
- Alias, S., Ismail, A. and Mohamad, A. (2010). Effect of pH on ZnO nanoparticle properties synthesized by sol-gel centrifugation. *Journal of Alloys and Compounds* **499**: 231-237.
- Ameen, S., Akhtar, M. S., Nazim, M. and Shin, H.-S. (2013). Rapid photocatalytic degradation of crystal violet dye over ZnO flower nanomaterials. *Materials Letters* **96**: 228-232.
- Bahadur, H., Srivastava, A. K., Sharma, R. K. and Chandra, S. (2007). Morphologies of sol-gel derived thin films of ZnO using different precursor materials and their nanostructures. *Nanoscale Research Letters* **2**: 469-475.
- Bai, H.-J., Zhang, Z.-M. and Gong, J. (2006). Biological synthesis of semiconductor zinc sulfide nanoparticles by immobilized *Rhodobacter sphaeroides*. *Biotechnology Letters* **28**: 1135-1139.
- Balaji, D. S., Basavaraja, S., Deshpande, R., Mahesh, D. B., Prabhakar, B. K. and Venkataraman, A. (2009). Extracellular biosynthesis of functionalized silver nanoparticles by strains of *Cladosporium cladosporioides* fungus. *Colloids and Surfaces, B: Biointerfaces* **68**: 88-92.
- Bandara, J., Tennakone, K. and Jayatilaka, P. P. B. (2002). Composite Tin and Zinc oxide nanocrystalline particles for enhanced charge separation in sensitized degradation of dyes. *Chemosphere* **49**: 439-445.
- Bao, G., Mitragotri, S. and Tong, S. (2013). Multifunctional nanoparticles for drug delivery and molecular imaging. *Annual Review of Biomedical Engineering* **15**: 253-282.
- Baruah, S. and Dutta, J. (2009). Hydrothermal growth of ZnO nanostructures. *Science and Technology of Advanced Materials* **10**: 013001.
- Baruah, S., Sinha, S. S., Ghosh, B., Pal, S. K., Raychaudhuri, A. K. and Dutta, J. (2009). Photoreactivity of ZnO nanoparticles in visible light: Effect of surface states on electron transfer reaction. *Journal of Applied Physics* **105**: 074308-074313.
- Basu, M., Sinha, A. K., Pradhan, M., Sarkar, S., Negishi, Y., Govind and Pal, T. (2010). Evolution of hierarchical hexagonal stacked plates of CuS from liquid-liquid interface and its photocatalytic application for oxidative degradation of different dyes under indoor lighting. *Environmental Science & Technology* **44**: 6313-6318.
- Bechelany, M., Amin, A., Brioude, A., Cornu, D. and Miele, P. (2012). ZnO nanotubes by template-assisted sol-gel route. *Journal of Nanoparticle Research* **14**: 1-7.
- Becheri, A., Dürr, M., Lo Nostro, P. and Baglioni, P. (2008). Synthesis and characterization of zinc oxide nanoparticles: application to textiles as UV-absorbers. *Journal of Nanoparticle Research* **10**: 679-689.
- Bhainsa, K. C. and D'Souza, S. (2006). Extracellular biosynthesis of silver nanoparticles using the fungus *Aspergillus fumigatus*. *Colloids and Surfaces B: Biointerfaces* **47**: 160-164.

- Bhande, R. M., Khobragade, C., Mane, R. and Bhande, S. (2013). Enhanced synergism of antibiotics with zinc oxide nanoparticles against extended spectrum β -lactamase producers implicated in urinary tract infections. *Journal of Nanoparticle Research* **15**: 1-13.
- Brayner, R., Ferrari-Iliou, R., Brivois, N., Djediat, S., Benedetti, M. F. and Fiévet, F. (2006). Toxicological impact studies based on *Escherichia coli* bacteria in ultrafine ZnO nanoparticles colloidal medium. *Nano Letters* **6**: 866-870.
- Cheng, W., Park, N., Walter, M. T., Hartman, M. R. and Luo, D. (2008). Nanopatterning self-assembled nanoparticle superlattices by moulding microdroplets. *Nature Nanotechnology* **3**: 682-690.
- Comparelli, R., Fanizza, E., Curri, M., Cozzoli, P., Mascolo, G. and Agostiano, A. (2005). UV-induced photocatalytic degradation of azo dyes by organic-capped ZnO nanocrystals immobilized onto substrates. *Applied Catalysis, B: Environmental* **60**: 1-11.
- Danielsson, B. (2012). Zinc oxide nanorods and their application to intracellular glucose measurements. *Nanotechnology and Nanomedicine in Diabetes*: 120.
- Duran, N., Marcato, P. D., Duran, M., Yadav, A., Gade, A. and Rai, M. (2011). Mechanistic aspects in the biogenic synthesis of extracellular metal nanoparticles by peptides, bacteria, fungi, and plants. *Applied Microbiology and Biotechnology* **90**: 1609-1624.
- Fan, H. J., Lee, W., Hauschild, R., Alexe, M., Le Rhun, G., Scholz, R., Dadgar, A., Nielsch, K., Kalt, H. and Krost, A. (2006). Template-assisted large-scale ordered arrays of ZnO pillars for optical and piezoelectric applications. *Small* **2**: 561-568.
- Fatima, A. and Husain, Q. (2007). A role of glycosyl moieties in the stabilization of bitter gourd *Momordica charantia* peroxidase. *International Journal of Biological Macromolecules* **41**: 56-63.
- Hanley, C., Layne, J., Punnoose, A., Reddy, K., Coombs, I., Coombs, A., Feris, K. and Wingett, D. (2008). Preferential killing of cancer cells and activated human T cells using ZnO nanoparticles. *Nanotechnology* **19**: 295103.
- Hazra, C., Kundu, D., Chaudhari, A. and Jana, T. (2012). Biogenic synthesis, characterization, toxicity and photocatalysis of zinc sulfide nanoparticles using rhamnolipids from *Pseudomonas aeruginosa* BS01 as capping and stabilizing agent. *Journal of Chemical Technology and Biotechnology* **88**: 1039-1048
- He, S. Y., Guo, Z. R., Zhang, Y., Zhang, S. and Gu, J. W. N. (2007). Biosynthesis of gold nanoparticles using the bacteria *Rhodospseudomonas capsulata*. *Materials Letters* **61**: 3984-3987.
- Hoffmann, M. R., Martin, S. T., Choi, W. and Bahnemann, D. W. (1995). Environmental applications of semiconductor photocatalysis. *Chemical Reviews* **95**: 69-96.
- Hong, R., Pan, T., Qian, J. and Li, H. (2006). Synthesis and surface modification of ZnO nanoparticles. *Chemical Engineering Journal* **119**: 71-81.

- Hong, T.-K., Tripathy, N., Son, H.-J., Ha, K.-T., Jeong, H.-S. and Hahn, Y.-B. (2013). A comprehensive in vitro and in vivo study of ZnO nanoparticles toxicity. *Journal of Materials Chemistry B* 1: 2985-2992.
- Husseiny, M. I., El-Aziz, M. A., Badr, Y. and Mahmoud, M. A. (2007). Biosynthesis of gold nanoparticles using *Pseudomonas aeruginosa*. *Spectrochim Acta A Mol Biomol Spectrosc* 67: 1003-1006.
- Iler, R. K. (1979). The chemistry of silicas solubility, polymerization, colloid and surface properties, and biochemistry New York, John Wiley & Sons.
- Jain, N., Bhargava, A., Majumdar, S., Tarafdar, J. C. and Panwar, J. (2011). Extracellular biosynthesis and characterization of silver nanoparticles using *Aspergillus flavus* NJP08: A mechanism perspective. *Nanoscale* 3: 635-641.
- Jain, N., Bhargava, A., Tarafdar, J. C., Singh, S. K. and Panwar, J. (2013). A biomimetic approach towards synthesis of zinc oxide nanoparticles. *Applied Microbiology and Biotechnology* 97: 859-869.
- JCPDS-ICDD (2008) PCDPF WIN, File no. 36-1451. JCPDS-ICDD, Swarthmore.
- Jeong, M.-G., Seo, H., Kim, K.-D., Kim, D., Kim, Y. and Lim, D. (2012). Quenching of photocatalytic activity and enhancement of photostability of ZnO particles by polydimethylsiloxane coating. *Journal of Materials Science* 47: 5190-5196.
- Kalishwaralal, K., Deepak, V., Ramkumarpandian, S., Nellaiah, H. and Sangiliyandi, G. (2008). Extracellular biosynthesis of silver nanoparticles by the culture supernatant of *Bacillus licheniformis*. *Materials Letters* 62: 4411-4413.
- Kanade, K. G., Kale, B. B., Aiyer, R. C. and Das, B. K. (2006). Effect of solvents on the synthesis of nano-size zinc oxide and its properties. *Materials Research Bulletin* 41: 590-600.
- Kim, C. G., Sung, K. W., Chung, T. M., Jung, D. Y. and Kim, Y. (2003). Monodispersed ZnO nanoparticles from a single molecular precursor. *Chemical Communications*: 2068-2069.
- Kochuveedu, S. T., Jang, Y. H., Jang, Y. J. and Kim, D. H. (2013). Visible light active photocatalysis on block copolymer induced strings of ZnO nanoparticles doped with carbon. *Journal of Materials Chemistry A* 1: 898-905.
- Labrenz, M., Druschel, G. K., Thomsen-Ebert, T., Gilbert, B., Welch, S. A., Kemner, K. M., Logan, G. A., Summons, R. E., Stasio, G. D., Bond, P. L., Lai, B., Kelly, S. D. and Banfield, J. F. (2000). Formation of sphalerite (ZnS) deposits in natural biofilms of sulfate-reducing bacteria. *Science* 290: 1744-1747.
- Lahiri, J. and Batzill, M. (2008). Surface functionalization of ZnO photocatalysts with monolayer ZnS. *Journal of Physical Chemistry C* 112: 4304-4307.
- Li, W. J., Shi, E. W. and Fukuda, T. (2003). Particle size of powders under hydrothermal conditions. *Crystal Research and Technology* 38: 847-858.

- Hong, T.-K., Tripathy, N., Son, H.-J., Ha, K.-T., Jeong, H.-S. and Hahn, Y.-B. (2013). A comprehensive in vitro and in vivo study of ZnO nanoparticles toxicity. *Journal of Materials Chemistry B* 1: 2985-2992.
- Husseiny, M. I., El-Aziz, M. A., Badr, Y. and Mahmoud, M. A. (2007). Biosynthesis of gold nanoparticles using *Pseudomonas aeruginosa*. *Spectrochim Acta A Mol Biomol Spectrosc* 67: 1003-1006.
- Iler, R. K. (1979). The chemistry of silicas solubility, polymerization, colloid and surface properties, and biochemistry New York, John Wiley & Sons.
- Jain, N., Bhargava, A., Majumdar, S., Tarafdar, J. C. and Panwar, J. (2011). Extracellular biosynthesis and characterization of silver nanoparticles using *Aspergillus flavus* NJP08: A mechanism perspective. *Nanoscale* 3: 635-641.
- Jain, N., Bhargava, A., Tarafdar, J. C., Singh, S. K. and Panwar, J. (2013). A biomimetic approach towards synthesis of zinc oxide nanoparticles. *Applied Microbiology and Biotechnology* 97: 859-869.
- JCPDS-ICDD (2008) PCDFP WIN, File no. 36-1451. JCPDS-ICDD, Swarthmore.
- Jeong, M.-G., Seo, H., Kim, K.-D., Kim, D., Kim, Y. and Lim, D. (2012). Quenching of photocatalytic activity and enhancement of photostability of ZnO particles by polydimethylsiloxane coating. *Journal of Materials Science* 47: 5190-5196.
- Kalishwaralal, K., Deepak, V., Ramkumarpandian, S., Nellaiah, H. and Sangiliyandi, G. (2008). Extracellular biosynthesis of silver nanoparticles by the culture supernatant of *Bacillus licheniformis*. *Materials Letters* 62: 4411-4413.
- Kanade, K. G., Kale, B. B., Aiyer, R. C. and Das, B. K. (2006). Effect of solvents on the synthesis of nano-size zinc oxide and its properties. *Materials Research Bulletin* 41: 590-600.
- Kim, C. G., Sung, K. W., Chung, T. M., Jung, D. Y. and Kim, Y. (2003). Monodispersed ZnO nanoparticles from a single molecular precursor. *Chemical Communications*: 2068-2069.
- Kochuveedu, S. T., Jang, Y. H., Jang, Y. J. and Kim, D. H. (2013). Visible light active photocatalysis on block copolymer induced strings of ZnO nanoparticles doped with carbon. *Journal of Materials Chemistry A* 1: 898-905.
- Labrenz, M., Druschel, G. K., Thomsen-Ebert, T., Gilbert, B., Welch, S. A., Kemner, K. M., Logan, G. A., Summons, R. E., Stasio, G. D., Bond, P. L., Lai, B., Kelly, S. D. and Banfield, J. F. (2000). Formation of sphalerite (ZnS) deposits in natural biofilms of sulfate-reducing bacteria. *Science* 290: 1744-1747.
- Lahiri, J. and Batzill, M. (2008). Surface functionalization of ZnO photocatalysts with monolayer ZnS. *Journal of Physical Chemistry C* 112: 4304-4307.
- Li, W. J., Shi, E. W. and Fukuda, T. (2003). Particle size of powders under hydrothermal conditions. *Crystal Research and Technology* 38: 847-858.

- Li, Y., Xie, W., Hu, X., Shen, G., Zhou, X., Xiang, Y., Zhao, X. and Fang, P. (2009). Comparison of dye photodegradation and its coupling with light-to-electricity conversion over TiO₂ and ZnO. *Langmuir* **26**: 591-597.
- Liqiang, J., Yichun, Q., Baiqi, W., Shudan, L., Baojiang, J., Libin, Y., Wei, F., Honggang, F. and Jiazhong, S. (2006). Review of photoluminescence performance of nano-sized semiconductor materials and its relationships with photocatalytic activity. *Solar Energy Materials and Solar Cells* **90**: 1773-1787.
- Liu, H., Yang, J., Liang, J., Huang, Y. and Tang, C. (2008). ZnO nanofiber and nanoparticle synthesized through electrospinning and their photocatalytic activity under visible light. *Journal of the American Ceramic Society* **91**: 1287-1291.
- Makhal, A., Sarkar, S. and Pal, S. K. (2012). Protein-mediated synthesis of nanosized Mn-doped ZnS: a multifunctional, UV-durable bio-nanocomposite. *Inorganic Chemistry* **51**: 10203-10210.
- Meng, S., Li, D., Zheng, X., Wang, J., Chen, J., Fang, J., Shao, Y. and Fu, X. (2013). ZnO photonic crystals with enhanced photocatalytic activity and photostability. *Journal of Materials Chemistry A* **1**: 2744-2747.
- Meulenkamp, E. A. (1998). Synthesis and growth of ZnO nanoparticles. *The Journal of Physical Chemistry B* **102**: 5566-5572.
- Nangia, Y., Wangoo, N., Sharma, S., Wu, J.-S., Dravid, V., Shekhawat, G. S. and Suri, C. R. (2009). Facile biosynthesis of phosphate capped gold nanoparticles by a bacterial isolate *Stenotrophomonas maltophilia*. *Applied Physics Letters* **94**: 233901-233903.
- Narayanan, K. B. and Sakthivel, N. (2010). Biological synthesis of metal nanoparticles by microbes. *Advances in Colloid and Interface Science* **156**: 1-13.
- Parikh, R. Y., Singh, S., Prasad, B. L. V., Patole, M. S., Sastry, M. and Shouche, Y. S. (2008). Extracellular synthesis of crystalline silver nanoparticles and molecular evidence of silver resistance from *Morganella* sp.: towards understanding biochemical synthesis mechanism. *ChemBioChem* **9**: 1415-1422.
- Prasad, K. and Jha, A. K. (2009). ZnO nanoparticles: synthesis and adsorption study. *Natural Sciences* **1**: 129-135.
- Prasad, V., D'Souza, C., Yadav, D., Shaikh, A. J. and Vigneshwaran, N. (2006). Spectroscopic characterization of zinc oxide nanorods synthesized by solid-state reaction. *Spectrochim Acta A Mol Biomol Spectrosc* **65**: 173-178.
- Premanathan, M., Karthikeyan, K., Jeyasubramanian, K. and Manivannan, G. (2011). Selective toxicity of ZnO nanoparticles toward Gram-positive bacteria and cancer cells by apoptosis through lipid peroxidation. *Nanomedicine: Nanotechnology, Biology and Medicine* **7**: 184-192.
- Protasova, L., Rebrov, E., Choy, K., Pung, S., Engels, V., Cabaj, M., Wheatley, A. and Schouten, J. (2011). ZnO based nanowires grown by chemical vapour deposition for selective hydrogenation of acetylene alcohols. *Catalysis Science & Technology* **1**: 768-777.

- Rajeshwar, K., de Tacconi, N. R. and Chenthamarakshan, C. R. (2001). Semiconductor-based composite materials: Preparation, properties, and performance. *Chemistry of Materials* **13**: 2765-2782.
- Raveendran, P., Fu, J. and Wallen, S. L. (2003). Completely “green” synthesis and stabilization of metal nanoparticles. *Journal of the American Chemical Society* **125**: 13940-13941.
- Saeed, A., Iqbal, M. and Zafar, S. I. (2009). Immobilization of *Trichoderma viride* for enhanced methylene blue biosorption: batch and column studies. *Journal of Hazardous Materials* **168**: 406-415.
- Sagar, P., Shishodia, P. and Mehra, R. (2007). Influence of pH value on the quality of sol-gel derived ZnO films. *Applied Surface Science* **253**: 5419-5424.
- Sakthivel, S., Neppolian, B., Shankar, M., Arabindoo, B., Palanichamy, M. and Murugesan, V. (2003). Solar photocatalytic degradation of azo dye: comparison of photocatalytic efficiency of ZnO and TiO₂. *Solar Energy Materials and Solar Cells* **77**: 65-82.
- Sharma, V. K., Yngard, R. A. and Lin, Y. (2009). Silver nanoparticles: green synthesis and their antimicrobial activities. *Advances in Colloid and Interface Science* **145**: 83-96.
- Simpson, R. J. (2004). Purifying Proteins for Proteomics: A Laboratory Manual, Cold Spring Harbor Laboratory Press.
- Song, Y., Yin, W., Fernandes, C. and Ruda, H. E. (2013). Fabrication of one-dimension ZnSe and ZnO nanostructures via anodic alumina template assisted vapor-liquid-solid growth process. *Thin Solid Films*.
- Spathis, P. and Poullos, I. (1995). The corrosion and photocorrosion of zinc and zinc oxide coatings. *Corrosion Science* **37**: 673-680.
- Sridevi, D. and Rajendran, K. V. (2009). Synthesis and optical characteristics of ZnO nanocrystals. *Bulletin of Materials Science* **32**: 165-168.
- Srinivasan, A. and Viraraghavan, T. (2010). Decolorization of dye wastewaters by biosorbents: a review. *Journal of Environmental Management* **91**: 1915-1929.
- Taccola, L., Raffa, V., Riggio, C., Vittorio, O., Iorio, M. C., Vanacore, R., Pietrabissa, A. and Cuschieri, A. (2010). Zinc oxide nanoparticles as selective killers of proliferating cells. *International Journal of Nanomedicine* **6**: 1129-1140.
- Tani, T., Mädler, L. and Pratsinis, S. E. (2002). Homogeneous ZnO nanoparticles by flame spray pyrolysis. *Journal of Nanoparticle Research* **4**: 337-343.
- Vayssieres, L. (2003). Growth of arrayed nanorods and nanowires of ZnO from aqueous solutions. *Advanced Materials* **15**: 464-466.
- Vigneshwaran, N., Kumar, S., Kathe, A. A., Varadarajan, P. V. and Prasad, V. (2006). Functional finishing of cotton fabrics using zinc oxide-soluble starch nanocomposites. *Nanotechnology* **17**: 5087-5095.
- Wahab, R., Kim, Y.-S., Lee, D. S., Seo, J.-M. and Shin, H.-S. (2010). Controlled synthesis of zinc oxide nanoneedles and their transformation to microflowers. *Science of Advanced Materials* **2**: 35-42.

- Wang, J. and Gao, L. (2003). Wet chemical synthesis of ultralong and straight single-crystalline ZnO nanowires and their excellent UV emission properties. *Journal of Materials Chemistry* **13**: 2551-2554.
- Wang, X., Wang, X., Summers, C. J. and Wang, Z. L. (2004). Large-scale hexagonal-patterned growth of aligned ZnO nanorods for nano-optoelectronics and nanosensor arrays. *Nano Letters* **4**: 423-426.
- Wang, Z. L. (2004). Nanostructures of zinc oxide. *Materials Today* **7**: 26-33.
- Willander, M., Nur, O. and Ali, S. M. U. (2012). Zinc oxide nanostructures based bio-and chemical extra-and intracellular sensors. *Portable Chemical Sensors*, Springer: 305-322.
- Wu, C., Qiao, X., Chen, J., Wang, H., Tan, F. and Li, S. (2006). A novel chemical route to prepare ZnO nanoparticles. *Materials Letters* **60**: 1828-1832.
- Xie, J., Lee, J. Y., Wang, D. I. C. and Ting, Y. P. (2007). Silver nanoplates: from biological to biomimetic synthesis. *ACS Nano* **1**: 429-439.
- Zhang, H., Yang, D., Ma, X., Ji, Y., Xu, J. and Que, D. (2004). Synthesis of flower-like ZnO nanostructures by an organic-free hydrothermal process. *Nanotechnology* **15**: 622.
- Zhang, H., Zong, R. L. and Zhu, Y. F. (2009). Photocorrosion inhibition and photoactivity enhancement for zinc oxide via hybridization with monolayer polyaniline. *Journal of Physical Chemistry C* **113**: 4605-4611.
- Zhou, J., Xu, N. S. and Wang, Z. L. (2006). Dissolving behavior and stability of ZnO wires in biofluids: a study on biodegradability and biocompatibility of ZnO nanostructures. *Advanced Materials* **18**: 2432-2435.

Chapter VII

Zinc Oxide Nanoparticles as Potential “Nano-fertilizers”

This chapter outlines the systematic comparison of chemically synthesized and biologically synthesized zinc oxide (ZnO) nanoparticles with Zn^{+2} ions and its bulk counterpart using chili plant as a model system. The physico-chemical characteristics of various zinc salts in aqueous medium were determined followed by their effect on chili plants in terms of plant growth and biomass. Studies on stress and zinc related enzymes were carried out to determine the extent of plant damage after zinc exposure. Lastly, we determined the plant zinc content to compare the efficacy of zinc salts to deliver zinc in plants.

7.1 Introduction

In the past decade, there has been an unprecedented expansion in the research and development of novel nanomaterials and nano-based commercial products. A myriad amount and variety of nanoparticles are being manufactured which are anticipated to foster many sectors such as healthcare, energy, electronics, transportation, agriculture, etc. (Nel et al. 2006, Jain et al. 2011). ZnO nanoparticles have received particular interest owing to their distinct applications ranging from catalytic, semiconductor, piezo-electric and pyro-electric properties. A variety of commercial products containing ZnO nanoparticles such as transparent electronics, ultraviolet (UV) light emitters, piezoelectric devices, chemical sensors, spin electronics, surface coatings and personal care products are being increasingly produced (Wang 2004, Jain et al. 2013). Recently, ZnO nanoparticles have been enormously incorporated in health-care products viz. sunscreens, creams, lotions etc. due to their high UV absorption efficiency and transparency towards visible light which leads to cosmetic clarity. The bio-compatibility nature of ZnO nanoparticles has made them a promising candidate for various applications in biological systems (Nohynek et al. 2007).

Inappropriate disposal of nanoparticle containing products could result in contamination of environment. Due to the extensive use of ZnO nanoparticles in daily life products, it is quite obvious that nanoparticles are being discharged into aquatic, terrestrial and atmospheric environments (Auffan et al. 2009, Rico et al. 2011). Overgrowing concerns regarding the potential harmful consequences of nanoparticles have stimulated the advent of nano-toxicology as a unique and indispensable research discipline (Nel et al. 2006). Determination of nanoparticles toxicity presents significant challenges as the minute differences among size, shape and formulation of nanoparticles could potentially represent a unique risk that must be critically understood and addressed. Systematic details of progress in the area of nano-toxicology can be obtained from various articles (Albrecht et al. 2006, Borm et al. 2006, Nowack and Bucheli 2007, Love et al. 2012). In case of metal oxide nanoparticles, toxicity is at least partly due to the specific properties related to the small size and consequent high surface activity of nanoparticles, while effects may be further enhanced by the release of free metal ions (Auffan et al. 2009). If the free ions are more toxic than the original particles, this process of dissolution is likely to lead to an increase of the overall toxicity (Kool et al. 2011). It was shown that the toxicity of nano-ZnO was mainly attributed to the dissolved metal ions (Zn^{+2}) in the aqueous solution (Franklin et al. 2007, Heinlaan et al. 2008, Wiench et al. 2009).

Unfortunately, very limited efforts have been made to assess the interactions between nanoparticles and plants; an integral component of all the ecosystems (Ju-Nam and Lead 2008, Ma et al. 2010, Manzo et al. 2011). Plants are particularly relevant in considerations of eco-nanotoxicity as they have direct interactions with air, soil, and water. In addition, being at the producer level in the ecosystem, penetration of nanoparticles into plant biomass may result in the incorporation of nanoparticles in food chain (Boonyanitipong et al. 2011). The

large surface area of leaf and root structures of many plant species mean that plants have ample opportunity to interact with nanoparticles. The possible routes of nanoparticle uptake include traversing the cuticle surface of leaves, the cuticle-free portions of the plant (e.g., flowers), suberin-coated roots, or regions of new root formation/injured areas (Maurer-Jones et al. 2013).

Seed germination assay is widely employed for developing data on the acute phytotoxicity of chemical substances to assess their potential hazards to the environment. A recent work reported that CNTs can penetrate tomato seed coat and remarkably increase the seed germination rate and seedling growth (Khodakovskaya et al. 2009). A stimulatory effect of alumina nanoparticles on growth of *Lemna minor* has also been observed (Juhel et al. 2011). Study on the impact of ZnO nanoparticles on soybean plants has revealed no effect on germination rate; however, a differential effect on plant growth and zinc uptake was observed (Lopez-Moreno et al. 2010a). On the other hand, majority of the reports available in the literature indicate negative effects of nanoparticles on plants. Lee et al. (2010) assessed the comparative toxicity of nanoparticles of Al, Si, Fe and Zn on *Arabidopsis thaliana* and reported that ZnO nanoparticles significantly inhibited the seed germination at a concentration of 400 mg L⁻¹. Another study reported ZnO nanoparticles as one of the most potential toxic nanoparticles that could cease root growth for most of the tested plants viz. radish, rape, ryegrass, lettuce, corn and cucumber (Lin and Xing 2007).

Little is known about the fate and behaviour of nanoparticles in plant system especially in food crops. It is very crucial to determine the possible consequences of nanoparticles in the food chain. It has been observed that the selective exposure of plants to nanoparticles will inevitably prompt their uptake and accumulation which could generate toxicological effects on plant system (Rico et al. 2011). The uptake, translocation and accumulation of nanoparticles were found to be dependent on the species of plant and the size, type, chemical composition, functionalization and stability of the nanoparticles. A study by Zhu et al. (2008) unambiguously showed that iron oxide nanoparticles (Fe₃O₄) were taken up by pumpkin (*Cucurbita maxima*) roots and translocated through the plant tissues. Similarly, Lin et al. (2009) studied the uptake, accumulation and translocation of NOM-suspended fullerene C₇₀ and carbon nanotubes in rice plants. They reported the presence of C₇₀ in the form of black aggregates that were more abundant in the seeds and roots, compared to the stems and leaves of rice seedlings. The presence of NOM-C₇₀ aggregates in leaves suggested the transmission of nanoparticles through xylem tissue along with water and nutrients. Dietz and Herth (2011) demonstrated that nanoparticles (<20 nm) are taken up by plant cells through plasmodesmata and endocytosis and can be further transported apoplastically or symplastically. Recently, the ability of nanoparticles to enter the nuclear envelope has evoked much interest in possible genotoxic effects of nanoparticles (Raghunathan et al. 2013).

Entry of nanoparticles in plants would allow their interaction with biomolecules such as proteins, lipids etc. present in the cell environment. These interactions result in interference with cellular processes which often causes redox imbalances and oxidative stress in metal-exposed plants (Ma et al. 2010). The possibility of interactions upsurge with the fact that potential dissolution of nanoparticles release metallic ions which can confer toxicity (Franklin et al. 2007). There is ample evidence that reactive oxygen species (ROS) are crucial second messengers involved in oxidative stress in plants and also participate as important signalling molecules for controlling plant programmed cell death (Apel and Hirt 2004, Karuppanapandian et al. 2011). In general, ROS include the superoxide radical ($O_2^{\cdot-}$), hydroxyl radical (OH^{\cdot}), hydroperoxyl radical (HO_2^{\cdot}), hydrogen peroxide (H_2O_2), alkoxy radical (RO^{\cdot}), peroxy radical (ROO^{\cdot}), singlet oxygen (1O_2) and excited carbonyl (RO^*), all of which are cytotoxic to plants (Faisal et al. 2013). ROS production is especially relevant in the case of nanoparticles with photocatalytic properties such as TiO_2 and ZnO nanoparticles (Song et al. 2012, Mukherjee et al. 2014). In living systems, the control of oxidative stress is achieved by the antioxidative systems. Thus, the involvement of ROS defence mechanisms to confer protection against ROS-mediated nanoparticle effects is highly expected. The most common defence system in plants is enzyme-mediated scavenging of ROS species which involves superoxide dismutase, peroxidase and catalase as major components (Arora et al. 2002, Love et al. 2012).

The aim of the present study was to assess the potential of ZnO nanoparticles as potential substitute for conventional zinc fertilizers. Initially, the physico-chemical characteristics of ZnO nanoparticles in aqueous medium were calculated to determine their stability and surface characteristics. Subsequently, a systematic comparison of chemically synthesized and biologically synthesized ZnO nanoparticles with Zn^{+2} ions and their bulk counterpart was performed using chili plant as a model system.

7.2 Materials and methods

7.2.1 Characterization of ZnO nanoparticles and their stability in aqueous solution

ZnO nanoparticles (<50 nm) were procured commercially from Sigma-Aldrich, USA while protein-capped ZnO nanoparticles were synthesized as per the method described in section 6.2.1 of chapter VI. Bulk ZnO and zinc sulphate were purchased from Merck Inc., India. Suspensions of ZnO nanoparticles and bulk ZnO were prepared by dispersing corresponding salts in sterile Milli-Q water through stirring for 3 h in dark conditions followed by ultrasonication using a high energy probe (100W, 40kHz) for 30 min and then filtered with 0.45 μ m sterilized filter (Whatman, UK) (Lin and Xing 2007). In contrast, zinc sulphate solution was prepared by dissolving appropriate amount of salt in sterile Milli-Q water. To determine the stability of suspensions, particle size distribution and zeta potential measurements were performed on a Zetasizer Nano system (Malvern Instruments, U.K.) using a 1 mL disposable cuvette. Each sample was measured at $25 \pm 1^\circ C$, in triplicates and each measurement was the average of 20 datasets acquired for 10 seconds each. The method

measures the Brownian movement of particles and relates it to the hydrodynamic particle size (defined as the diameter of a hypothetical sphere that diffuses in the same fashion as that of the particle being measured).

7.2.2 Effect of ZnO nanoparticles on chili plants (pot studies)

7.2.2.1 Site description and plant growth conditions

The experiment was conducted in the Green house facility of Agri Farms Samod, Jaipur, India (27°10'N 75°43'E) which experiences a tropical climate all over the year. Chili (*Capsicum annum*. L.) seeds were procured from the local market of Jaipur, Rajasthan, India. The seeds were hybrid in nature and claimed to possess >85% germination rate. Initially, the seedlings were raised by sowing seeds about 1 cm deep in soilrite and watered daily to field capacity. After one week, seedlings of uniform size (~5 cm shoot length) were selected and further transplanted into black polybags containing approximately 5 kg of soil. The soil used was general nursery soil mixture containing soil, pond silt and farm yard manure (3:1:1 w/w). After two weeks of transplantation, foliar spray was performed using four zinc salts namely bulk ZnO (ZB), chemically synthesized ZnO nanoparticles (cZN), biologically synthesized protein-capped ZnO nanoparticles (bZN) and zinc sulphate (ZS) with two different concentrations (50 and 100 mg L⁻¹). The concentrations of the salt were chosen based on the results obtained during seed germination assay with varying concentrations of zinc salts (0 - 1000 mg L⁻¹) (data not included in thesis). Seedling sprayed with distilled water served as control. The experiment was performed with 10 replicates per treatment using complete randomized design. The sprays were conducted for four times at an interval of two weeks during the months of July and August 2013. The plants were harvested at the end of the experiment and various parameters were determined.

7.2.2.2 Effect on plant growth

To determine the plant growth, three representative plants from the pots of each treatment were removed from the soil. The plants were washed under running tap water for three times to remove all the traces of zinc salts and soil adhered to the shoot and root surface, respectively. The length of shoots and roots were measured using standard procedures. Fresh weight of the plants was measured using a Denver TB-214 weighing balance (Denver Instruments, USA). Subsequently, plants were kept separately in paper bags, oven-dried at 60 °C for 72 h and dry wet was measured. The calculated values were expressed in terms of mean ± standard deviation (SD).

7.2.2.3 Effect on plant metabolism

Total carbohydrate content in plant sample was estimated according to the standard Anthrone method (Yemm and Willis 1954). Protein content of the plants was estimated according to Bradford method using bovine serum albumin as standard (Bradford 1976). For estimation of photosynthetic pigments (chlorophyll a and b), fresh leaves were homogenized in chilled 80% acetone in dark using TissueLyzer LT (Qiagen). After centrifugation of

homogenate at 10,000×g for 10 min at 4°C, absorbance of supernatant was taken at 645 and 663 nm. The calculations were done according to Arnon's Formula (Arnon 1949).

$$\text{Chl a} = 12.7 \times (\text{OD at 663}) - 2.69 \times (\text{OD at 645}) \times V/1000 \times 1/W$$

$$\text{Chl b} = 22.9 \times (\text{OD at 645}) - 4.68 \times (\text{OD at 663}) \times V/1000 \times 1/W$$

$$\text{Total Chlorophyll} = 20.2 \times (\text{OD at 645}) + 8.02 \times (\text{OD at 663}) \times V/1000 \times 1/W$$

where, OD = absorbance, V = final volume of 80% acetone-chlorophyll extract and W = fresh weight of the tissue taken. Chlorophyll content was estimated in terms of µg chlorophyll per g of fresh plant tissue.

7.2.2.4 Effect on stress related enzymes and plant damage

Plant leaves (100 mg) were homogenized with 1 mL of chilled phosphate buffer (0.1 M, pH 6.8) using TissueLyzer (Qiagen) for 30 min. Subsequently, tubes were centrifuged at 15,000 rpm for 15 min at 4 °C and the supernatant was collected. The volume of recovered crude enzyme extract was made up to 10 mL using the same buffer. The prepared enzyme extract was used for the analysis of superoxide dismutase, peroxidase and polyphenol oxidase activities:

Superoxide dismutase (SOD) assay was carried out by following the method of Beyer and Fridovich (1987) which is based on the reduction of nitroblue tetrazolium (NBT) to water insoluble blue formazan. The assay mixture consisted of 50 µL of enzyme extract, 1.232 mL of 50 mM phosphate buffer, 150 µL of 0.75 mM NBT, 38 µL of 55mM Methionine and 30 µL of 0.1 mM riboflavin. Blank was prepared by using 50 µL of distilled water instead of enzyme extract. The assay mixture was incubated at room temperature under two fluorescent tubes (6000 lux) for 10 minutes to allow the development of purple colour formazan which was then measured at 560 nm against the blank. Units of the SOD activity were expressed as the amount of enzyme required to inhibit the reduction of NBT by 50% and the enzyme activity was expressed as units per mg of protein.

Peroxidase (POD) activity was determined by Egley et al. (1983) with minor modifications. The assay mixture consisted of 2.0 mL of 0.1 M phosphate buffer, 1.0 mL of 0.001 M pyrogallol, 1.0 mL of 0.005 M H₂O₂ and 1.0 mL of crude enzyme extract. The assay mixture was incubated for 5 mins at 25 °C for reaction to proceed after which 1.0 mL of 2.5 N H₂SO₄ was added to stop the reaction. The absorbance of indigo colour formed was read at 420 nm against blank containing water instead of enzyme extract.

Polyphenol oxidase (PPO) activity was determined according to the standard method of Mayer and Harel (1979). The assay mixture consisted of 2.0 mL of 0.1 M phosphate buffer, 1.0 mL of 0.001 M pyrogallol and 1.0 mL of crude enzyme extract. The assay mixture was incubated for 5 mins at 25 °C for reaction to proceed after which 1.0 mL of 2.5 N H₂SO₄ was added to stop the reaction. The absorbance of indigo colour formed was read at 420 nm against black containing water instead of enzyme extract.

Lipid peroxidation was estimated by measuring the thiobarbituric acid reactive substances (TBARS) content as per the standard procedure (Heath and Packer 1968). Briefly, fresh leaf discs (100 mg) were homogenized in 1.0 ml of 2.5% (w/v) trichloroacetic acid (TCA) using TissueLyzer (Qiagen) followed by centrifugation for 20 min at 12000 g at 4 °C. The supernatant was collected and used as aliquot for further analysis. 100 µL aliquot was mixed with 0.5% (w/v) TBA solution containing 20% (w/v) TCA. The reaction mixture was heated at 100 °C for 30 min in a water bath followed by immediate cooling on ice. Samples were centrifuged at 12,000 g at 4 °C for 20 min and absorbance of the supernatant were measured at 532 nm using a UV-Visible spectrophotometer (JASCO V-630). MDA content was estimated as picomoles per milligram of protein using a molar extinction coefficient of $1.56 \text{ mM}^{-1} \text{ cm}^{-1}$ (Pandey et al. 2003).

7.2.2.5 Effect on zinc related enzymes

Carbonic anhydrase (CA) activity in leaves was determined using the standard method of Wilbur and Anderson (1948). The enzyme extract was prepared by grinding fresh leaf discs (100 mg) in 1.0 ml of extraction buffer [50 mM HEPES-NaOH, pH 8.3; 0.5 mM EDTA; 10 mM dithiothreitol (DTT) and 10% (v/v) glycerol] at 4 °C. Tubes were centrifuged at 5000 g for 10 min at 4 °C and the supernatant (enzyme extract) was collected. The volume of recovered crude enzyme extract was made up to 10 mL using the same buffer. CA activity was measured by preparing an assay mixture containing 4.5 mL of 20 mM Na-Barbital buffer (pH 8.3), 1.5 mL of CO₂ saturated water and 75 µL of enzyme extract. CA activity was obtained from the reaction time of pH change from 8.3 to 7.3. To express the value of CA-activity, Wilbur and Anderson units calculated per mg protein used. The calculations were performed according to the formula: $(t_0 - t)/(t.m)$, where t_0 and t are times for pH change from 8.3 to 7.8 in the control and in the sample, respectively; m is the amount of protein in milligrams added to the reaction mixture. The measurements were carried out at least three times using three biological replications. One Wilbur-Anderson (W-A) unit will change the pH of a 0.012 M Veronal buffer to drop from 8.3 to 6.3 per minute at 0 °C.

Acid phosphatase (AP) activity was measured in the roots by standard procedure (Tabatabai and Bremner 1969). The procedure is based on colorimetric estimation of the p-nitrophenol released by phosphatase activity when sample is incubated with buffered sodium p-nitrophenyl phosphate solution (pH 5.4). Briefly, plant roots (100 mg) were homogenized on ice with 1 mL of chilled sodium acetate buffer (0.1 M, pH 5.4) using TissueLyzer (Qiagen) for 60 min. Subsequently, tubes were centrifuged at 5000 rpm for 10 min at 4 °C and the supernatant containing enzyme extract was collected. The volume of recovered crude enzyme extract was made up to 10 mL with the same buffer. The assay mixture was prepared by adding 100 µL of enzyme extract to 4.0 mL of p-nitrophenyl phosphate (1 mg mL^{-1}) prepared freshly in Na-Acetate buffer (pH 5.4). The assay mixture was incubated for 60 min at 37 °C in a shaking incubator. Subsequently, filtration was done through Whatman no. 42 paper and absorbance of filtrate was measured at 420 nm against the blank containing water instead of enzyme extract.

7.2.2.6 Effect on zinc content

To investigate the efficacy of zinc delivery into plants, zinc content of chili plants was determined. For this, dried chili plant sample (1 g) was digested in 50 mL conical flasks with 10 mL of HNO₃: HClO₄ (3:1) until the formation of transparent solution. Following digestion, the samples were made up to constant volume (50 mL) using deionized water before analysis by atomic absorption spectrometry (AAS). Quality control measures included the use of procedural blanks and repeat analysis of a certified reference.

7.3 Results and discussion

7.3.1 Characterization of ZnO nanoparticles and their stability in aqueous solution

Systematic research on the phytotoxicity of nanoparticles requires appropriate physico-chemical characterization of nanoparticles in the aqueous environment. The major physico-chemical properties involved are size and distribution, hydrodynamic behaviour, composition, concentration, and their zeta potential values (Handy et al. 2008). The stability of nanoparticles (i.e. their dispersion and persistence) is considered as a key parameter for risk assessment of biological activity and toxic properties of nanoparticles (Oberdörster et al. 2005). The unexpected physico-chemical properties and complexity of nanoparticles in different environment makes the nanoparticle characterization a necessary pre-requisite step (Luyts et al. 2013). Moreover, it is well evident that agglomerated nanoparticles migrate very slowly in biological systems as compared to the dispersed nanoparticles (Franklin et al. 2007, Zhang et al. 2008). Due to the amphoteric nature of ZnO, it is highly essential to determine their stability (i.e. state of agglomeration) in the aqueous environment. Electron microscopy has been proved to be an excellent technique to determine the aggregation states as it allows direct imaging of size and morphology. Figure 7.1 shows the TEM micrographs of chemically synthesized ZnO nanoparticles depicting their spherical morphology with an approximate particle size of 50 nm. The discrepancy in the size of ZnO nanoparticles as determined through TEM measurements and manufacturer report could be attributed to their aggregation in aqueous suspensions.

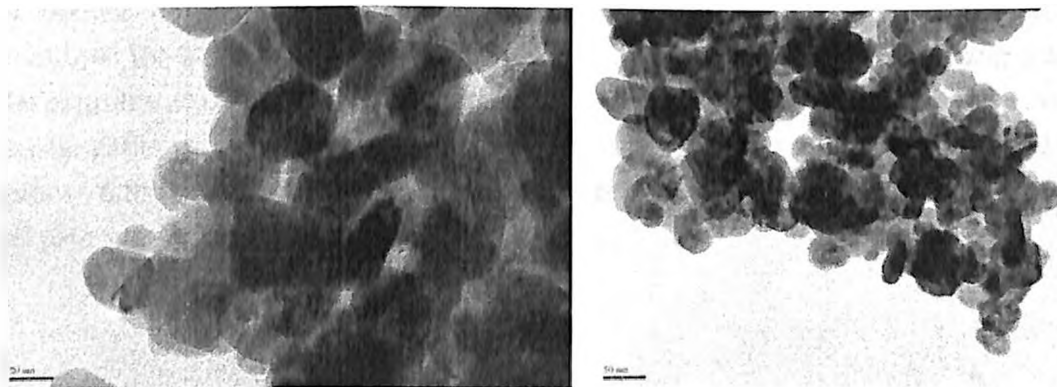


Figure 7.1 Transmission electron micrographs of ZnO nanoparticles depicting agglomeration in aqueous suspension. Bars show the scale in nanometers.

To corroborate the microscopy observations, dynamic light scattering (DLS) measurements were performed. DLS is a conventional method often employed to determine the size and agglomeration state of nanoparticles in aqueous solutions. DLS measurements of ZnO nanoparticle suspension showed an average particle diameter size of 303.5 nm (Table 7.1) which were much higher than the size reported by the manufacturer. For bulk ZnO suspension, the average particle diameter size was found to be 2112.0 nm and the results were unable to meet the quality criteria of the instrument. The observed high magnitude of agglomeration for aqueous suspensions of both bulk as well as ZnO nanoparticles was consistent with the previous findings stating agglomeration in environments varying from aqueous solution to complex biological media (Franklin et al. 2007). The agglomeration of nanoparticles is mainly caused by excess surface energy and high thermodynamic instability of nanoparticle surface (Olenin et al. 2008).

In order to segregate the agglomerates formed in both ZnO nanoparticles and bulk ZnO suspensions, high energy sonication was performed. The sonicated suspensions were immediately analysed by DLS measurements and average particle diameter sizes of 146.3 and 415.3 nm were obtained for sonicated ZnO nanoparticle and bulk ZnO suspensions, respectively. These results suggest that sonication was incapable to completely dissociate the formed aggregates which may be due to irreversible fusion, strong binding of the particles or rapid reformation of particles into aggregation after sonication. However, the low polydispersity index (PDI = 0.120) observed for sonicated ZnO nanoparticle suspension indicated the substantial monodispersity of nanoparticles which validated their use in further studies.

Zeta potential measurements were carried out to investigate the stability and nature of electrostatic potential on the surface of nanoparticles in aqueous suspensions. As zeta potential measures the magnitude of electrostatic repulsive interaction between nanoparticles, it is widely used as a superior index for representing nanoparticle stability (Oberdörster et al. 2005). Zeta potential values for aqueous suspensions of ZnO nanoparticles and bulk ZnO were found to be +42.4 and +33.7, respectively (Table 7.1). The observed positive charge on the surface of ZnO nanoparticles is in agreement with previous studies performed to investigate the stability of commercial metal oxide nanoparticles in water (Zhang et al. 2008). The plausible reason for positive charge on the surface of ZnO nanoparticles in pure water may be attributed to the higher isoelectric point of ZnO (~9.3) as compare to the pH of pure water (~ 6.8) (Zeng et al. 2005). For zinc sulphate solution, observed values for zeta potential and pH were -2.73 and 6.21, respectively.



?

Table 7.1 Selected physico-chemical characteristics of the ZnO nanoparticles, bulk ZnO and zinc sulphate at a concentration of 1000 mg L⁻¹.

Physico-chemical parameters		ZnO nanoparticles	bulk ZnO	Zinc sulphate
Purity (%)		99.50 ^a	99.99 ^a	99.80 ^a
pH		7.02 ± 0.09	7.06 ± 0.13	6.21 ± 0.04
Average particle size in powder (nm)		<50 ^a	820±8 ^a	NA
Average hydrodynamic particle size (nm)	Before sonication	303.5 ± 12.0 ^b (0.275)	2112.0 ± 37.2 ^b (0.173)	796.3 ± 5.6 ^b (0.695)
	After sonication	146.3 ± 5.6 ^b (0.120)	415.3 ± 11.0 ^b (0.178)	
Zeta potential (mV)		42.4 ± 4.38	33.7 ± 5.87	NA

values are listed as Mean ± SD; values in bracket indicates polydispersity index

^aprovided by the manufacturer; ^bmeasured by dynamic light scattering

7.3.2 Effect of ZnO nanoparticles on chili plants

7.3.2.1 Phenotypic assessment of plants

Zinc supplement is known to exhibit effects on plant morphology and physiology. Deficiency of zinc in plants results in a number of physiological impairments and results in inhibition of the growth, differentiation and development of plants (Cakmak 2000). Similarly, excess of zinc supplement causes stress-based physiological constraints leading to decreased plant vigour and growth (Van Steveninck et al. 1990). In present study, all the plants (control as well as treatments) appeared green and healthy indicating the used zinc supplement were in appropriate doses and do not have any toxic effects on chili plants (Figure 7.2). Comparison of chili plants sprayed with 50 mg L⁻¹ zinc (ZB, cZN, bZN and ZS) with chili plants sprayed with water (control) indicated that zinc supplement stimulated the plant growth. In contrast, similar comparison at higher zinc supplement (100 mg L⁻¹) indicated inhibition of growth in case of cZN and ZS salt solution treatments.



Figure 7.2 Comparative phenotypic assessment of chili plants sprayed with distilled water (control) and various zinc treatments. 50 and 100 represent mg L^{-1} concentrations of respective salt.

7.3.2.2 Effect on plant growth

Figure 7.3 shows the variation in length of chili plants with different zinc salt treatments. The minimum plant length was observed for the treatment of 100 mg L^{-1} cZN, which was significantly different from the control plants. On the other hand, maximum plant length was recorded in case of 50 mg L^{-1} bZN which was also significantly higher than control plants. However, the variation in plant length of other treatment was found to be non-significant as compared to control plants. The stimulation effects of zinc on vegetative

growth may be attributed to the well-known functions of zinc in plant life cycle. For instance, zinc is a major component of several dehydrogenases and auxin production enzymes which may enhance the elongation processes (Marschner and Marschner 2012). Interestingly, we observed that biologically synthesized zinc oxide nanoparticles (bZN) at 50 mg L⁻¹ resulted in higher plant growth zinc sulphate (ZS): which is a conventional zinc fertilizer. Previous report also indicated that metals in nanoparticle regime can exhibit fertilizing effects (Rico et al. 2013). Similarly, enhancement of growth in cucumber plants after exposure to CeO₂ NPs has been reported (Lopez-Moreno et al. 2010b).

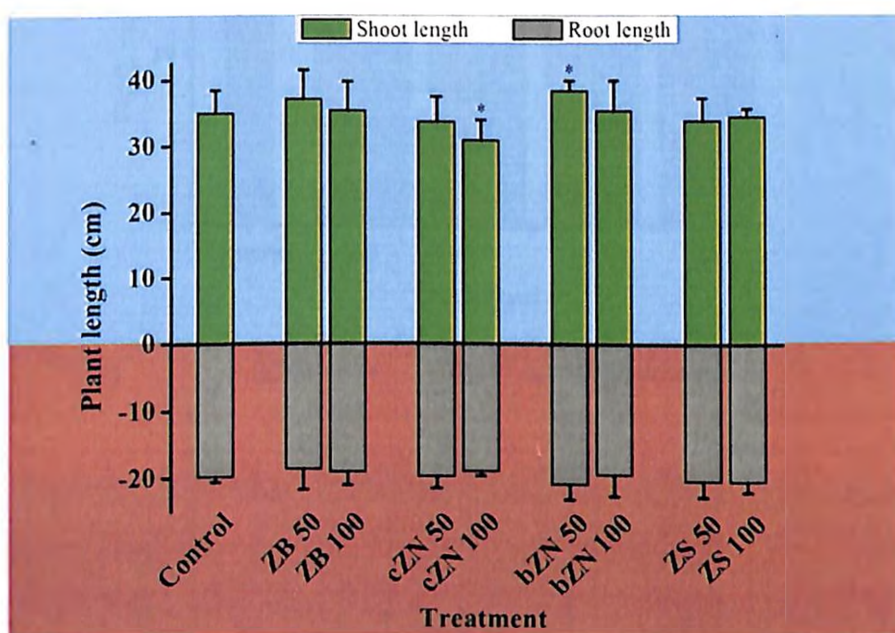


Figure 7.3 Variation in shoot and root length of chili plants sprayed with distilled water (control) and various zinc treatments. Vertical bars represent standard deviation. Significant differences from control ($p \leq 0.05$) are marked with asterisk.

7.3.2.3 Effect on plant biomass

Biomass production is usually considered as an indicator of plant health. Effect of tested concentrations of various zinc salts on biomass of chili plants is illustrated in Figure 7.4. Among all the treatments, ZB treatment resulted in reduced plant fresh weight at both concentrations as compared to the control plants. Plants treated with cZN, bZN and ZS exhibited higher fresh weight values than control plants (Figure 7.4a). This observation can be explained based on the fact that these salts can release high amount of zinc ions in aqueous suspensions as compared to bulk ZnO. Various enzymes involved in plant photosynthetic machinery are zinc-dependent and can utilize the available zinc which results in stimulated plant biomass. Similarly, carbonic anhydrase activity to perform CO₂ assimilation is known to get stimulated at higher zinc concentrations. The results for plant dry weight were in accordance to the fresh weight observations; however, no significant differences among the treatment and control plants were noticed (Figure 7.4b). Notably, plant biomass was affected by the type of zinc salt used as compared to the different zinc concentrations. These results

agree with previous report of zinc treatment on *Populus* plants in the concentration range of 1-1000 μ M (Di Baccio et al. 2003).

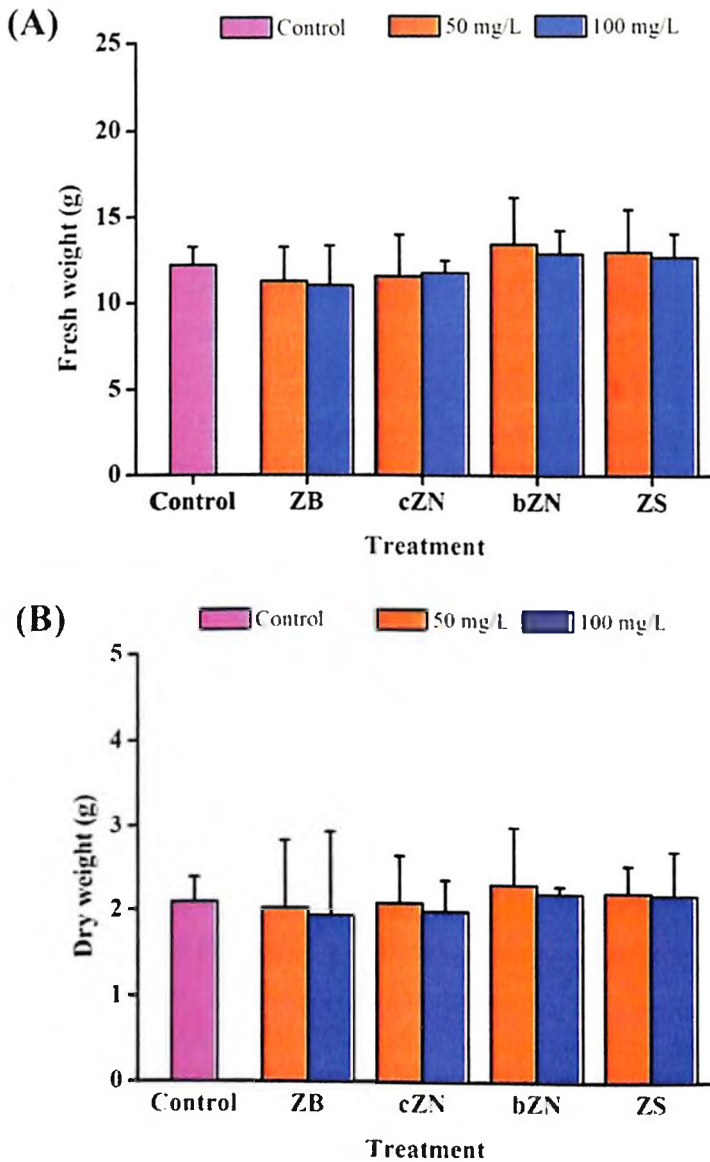


Figure 7.4 (a) Fresh weight and (b) dry weight of chili plants sprayed with distilled water (control) and various zinc treatments. Vertical bars represent standard deviation. No significant differences were observed between control and treatments ($p \leq 0.05$).

7.3.2.4 Effect on plant metabolism

With the well-defined role of zinc in various plant metabolic pathways, it was very important to determine the effect of various zinc treatments on the metabolism of chili plants. Carbohydrate and protein contents have been considered as an important indicator of plant metabolism. In the present study, both carbohydrate and protein contents of chili plants sprayed with various zinc salts were higher as compared to the control plants (Table 7.2). Among all treatments, bZN and cZN were found to promote protein and carbohydrate

contents as compared to control as well as ZB and ZS treatments. A similar stimulatory effect of zinc treatment was also demonstrated by numerous previous reports (Ahl and Omer 2009, Bairwa et al. 2013). In general, plants sprayed with low zinc concentration (50 mg L^{-1}) were found to be much superior to plants sprayed with higher zinc concentration (100 mg L^{-1}). In contrast, plants treated with ZB showed low protein and carbohydrate contents which could be due to feeble penetration of ZnO aggregates in plants.

Table 7.2 Effect on metabolism of chili plants sprayed with water (control) and various zinc salt treatments.

Treatment	Carbohydrate (mg g^{-1} FW)	Protein (mg g^{-1} FW)	Chlorophyll a ($\mu\text{g g}^{-1}$ FW)	Chlorophyll b ($\mu\text{g g}^{-1}$ FW)
Control	19.35 ± 2.21	9.35 ± 2.21	174.79 ± 22.48	52.33 ± 6.2
ZB 50	19.31 ± 0.61	9.31 ± 3.61	160.18 ± 17.32	56.03 ± 5.9
ZB 100	19.05 ± 2.67	9.12 ± 1.67	152.76 ± 14.72	66.20 ± 9.4
cZN 50	21.29 ± 4.29	12.85 ± 3.96	202.35 ± 13.67	65.84 ± 7.1
cZN 100	20.29 ± 4.06	12.30 ± 5.34	181.27 ± 14.51	61.27 ± 5.3
bZN 50	22.72 ± 3.32	13.13 ± 4.24	204.14 ± 28.53	60.50 ± 8.7
bZN 100	22.92 ± 4.55	12.93 ± 6.38	218.03 ± 16.93	64.64 ± 3.7
ZS 50	22.48 ± 2.62	12.48 ± 2.92	202.74 ± 31.13	59.27 ± 9.2
ZS 100	21.98 ± 3.13	11.98 ± 5.31	221.12 ± 13.81	69.10 ± 8.9
LSD ($p \leq 0.05$)	1.62	2.76	19.55	9.43

Chlorophyll a molecules are the chemically active pigment at the reaction center and take part in the photochemical reaction. Both chlorophyll (a and b) content were influenced by the tested zinc treatments (Table 7.2). The maximum increase in Chl a content was observed in bZN followed by ZS treatment as compared to control. In case of cZN, chl content was more at low concentration (50 mg L^{-1}) as compared to the higher concentration (100 mg L^{-1}). This observation can be explained based on the fact that excess Zn^{+2} becomes toxic as it binds to proteins, displacing other metal ions, such as Fe^{+2} , from their binding sites (Arrivault et al. 2006). Similarly, treatment of titanium dioxide (TiO_2) nanoparticles to spinach plants resulted in enhanced chlorophyll biosynthesis (Hong et al. 2005). In contrast, Hu et al. (2013) reported a decrease in chlorophyll content in plants exposed to ZnO nanoparticles.

7.3.2.5 Effect on plant defence

Under normal growth condition, reactive oxygen species (ROS) are generated as by-products of natural cell functions, and a delicate balance between their production and removal must be maintained to prevent oxidative stress (Mittler 2002). Superoxide dismutase (SOD, EC 1.15.1.1) enzyme plays an important role in maintaining the ROS levels through electron transfers in redox reactions. Foliar application of zinc in plants may probably cause oxidative stress resulting in an elevation of ROS levels and consequently requires higher

SOD activity. Accordingly, we measured the SOD activity in leaves of chili plants sprayed with different zinc salts in comparison to the control plants.

As compared to control plants, except ZS-50, all the zinc treatments exhibited a significant increase in the SOD activity (Figure 7.5). SOD activity was found to be increased by 51.2% and 71.2% for the plants treated with 50 and 100 mg L⁻¹ concentration of bulk ZnO, respectively. In comparison, the variation was much higher in case of cZn and bZn treatments with increase by 83.91 and 80.95% for 50 mg L⁻¹ and 116.78 and 109.18% for 100 mg L⁻¹ concentrations, respectively. Interestingly, no major change in the SOD activity was observed for the plants sprayed with 50 mg L⁻¹ ZS treatment, however, more pronounced change was observed in case of 100 mg L⁻¹ ZS treatment. The observed high magnitude of SOD activity for zinc salts in both the nanoparticle forms can be attributed to their superior penetration and reactivity which is highly expected owing to their high surface to volume ratio. The observed variation in SOD activity was not very surprising as earlier studies also reported an increase in SOD activity under excess Zn conditions (Wang et al. 2009, Ozdener and Aydin 2010). In contrast, few studies reported a decrease in SOD activity upon Zn treatment (Candan and Tarhan 2003, Panda and Khan 2004).

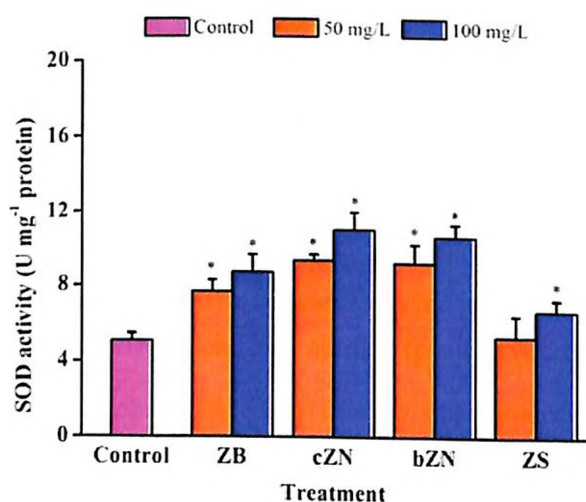


Figure 7.5 SOD activity in leaves of chili plants sprayed with distilled water (control) and various zinc treatments. Vertical bars represent standard errors. Significant differences from control ($p \leq 0.05$) are marked with asterisk.

There are many important ROS molecules in the cells (e.g. superoxide radicals, peroxide radicals, hydroxyl radicals, and singlet oxygen, among others) that could induce the oxidative stress and often detoxified by various antioxidant enzymes (Halliwell and Gutteridge 2007). Peroxidase (POD, EC 1.11.1.7) enzyme oxidizes different substrates in the presence of H₂O₂. The induction of peroxidase is a general phenomenon in higher plants in response to uptake of toxic amounts of metals (Assche and Clijsters 1990). Figure 7.6a represents the total peroxidase activity in leaves of chili plants for the various zinc treatments and concentrations used in this study. A significantly higher peroxidase activity was observed

in plants sprayed with ZB and cZN at both tested concentrations as compared to control. No significant induction of POD activity was observed for bZN and ZS treatments at both tested concentrations. Previous study on chick pea seedlings also demonstrated induction of peroxidase activity after the zinc treatments (Burman et al. 2013). However, our results are not in agreement with previous report indicating induced POD activity in detached rice leaves after ZS treatment (Fang and Kao 2000). Similar to peroxidase, polyphenol peroxidase (PPO, EC 1.10.3.1) is another important constituent of antioxidant system of plants (Vámos-Vigyázó and Haard 1981, Farmer and Mueller 2013). As shown in Figure 7.6b, the observed differences in PPO activity under various zinc treatments were in accordance to the POD activity. Previous study on mung bean plant also observed a variation in PPO activity after the exposure of manganese in bulk and nano regime (Pradhan et al. 2013).

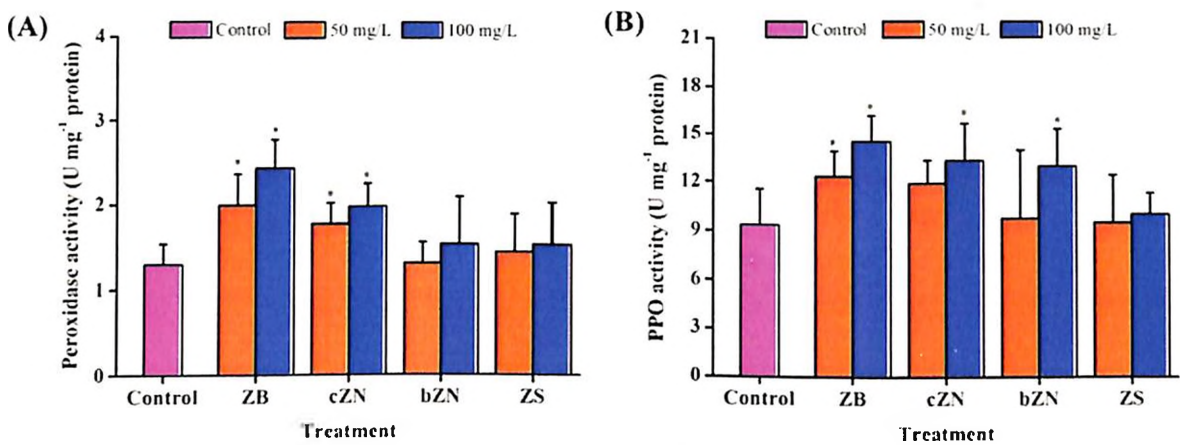


Figure 7.6 (a) Peroxidase and (b) Polyphenol oxidase activity in leaves of chili plants sprayed with distilled water (control) and various zinc treatments. Vertical bars represent standard errors. Significant differences from control ($p \leq 0.05$) are marked with asterisk.

In plants, oxidative stress generated due to imbalances in the accumulation and removal of ROS molecules results in oxidative damage to proteins, lipids and nucleic acids. Overproduction of ROS could convert fatty acids to toxic peroxides which results in the TBARS formation and consequently damage membrane permeability. TBARS is used as a general indicator to determine the extent of lipid peroxidation resulting from oxidative stress (Karuppanapandian et al. 2011). In the present study, magnitude of membrane damage and lipid peroxidation by various zinc treatments in leaves of chili plants was measured. As shown in Figure 7.7, the TBARS concentration in the leaves of chili plants treated with ZB salt was significantly higher than that of control and other zinc treatments. This result also supported the overproduction of ROS molecules by ZB treatment in leaves as observed during antioxidant enzyme assays. Previous studies also reported that excess of zinc stimulated MDA production in plants due to increased lipid peroxidation through excessive generation of free radicals (Prasad and Pardha Saradhi 1995, Wang et al. 2009).

A concentration-dependent formation of TBARS was noticed in case of cZN treated plants which may be due to the higher zinc ion dissolution rate with an increase in

concentration. Previous studies on pea plants also showed enormous TBARS production after the treatment with higher concentration of ZnO nanoparticles (500 mg kg^{-1}) (Mukherjee et al. 2014). Excessive generation of H_2O_2 and other ROS molecules such as superoxide radicals, peroxide radicals, hydroxyl radicals and singlet oxygen and the inhibition of antioxidant enzyme activity has been observed on the exposure of nanoparticle treatment in various organisms such as algae (Manzo et al. 2013), carp (Hao et al. 2013), zebra fish (Xiong et al. 2011) and mammalian cells (Bondarenko et al. 2013). Interestingly, no sign of lipid peroxidation was observed in case of bZN treated plants which signifies the importance of bio-compatibility nature of protein capping molecule which decrease the toxic effect of biologically synthesized nanoparticles (Figure 7.7). Capping agents are well known to provide electrostatic and steric stabilization effects for the dispersion of nanoparticles in suspensions (Raveendran et al. 2003, Li et al. 2012, Makhal et al. 2012). Organics molecules carrying functional groups such as proteins are reported to dominate the surface chemistries and activities of nanoparticles (Niemeyer 2001, Makhal et al. 2012).

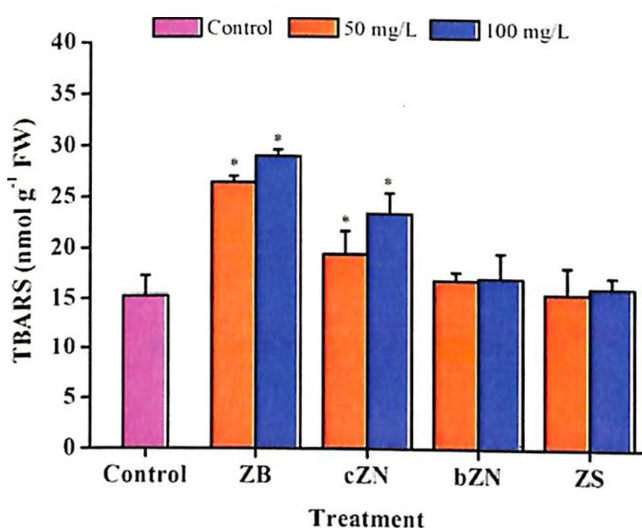


Figure 7.7 TBARS concentration in leaves of chili plants sprayed with distilled water (control) and various zinc treatments. Vertical bars represent standard errors. Significant differences from control ($p \leq 0.05$) are marked with asterisk.

7.3.2.6 Effect on zinc related enzymes

Zinc is an integral component of many enzyme structures and is the only metal to be represented in all six enzyme classes viz. oxido-reductases, transferases, hydrolases, lyases, isomerases and ligases (Auld 2001). Various forms of zinc have significant roles in a wide variety of processes ranging from metabolite synthesis to their degradation. It does this through a large mosaic of zinc binding motifs that can be structural, catalytic and co-catalytic in nature (Maret 2013). In order to assess the extent of zinc content in chili plants, we have determined the activity levels of two zinc-dependent enzymes namely, carbonic anhydrase and acid phosphatase for which activity is reported to be highly dependent on zinc availability (Pandey et al. 2002).

Carbonic anhydrase (CA; EC 4.2.1.1) catalyzes the rapid inter-conversion of carbon dioxide and water to bicarbonate and protons and play an important role in photosynthesis (Moroney et al. 2001). The active site of carbonic anhydrase enzyme contains a zinc ion which is coordinated in three positions by histidine side-chains. The interplay between carbonic anhydrase activity and zinc concentration has been known from many decades (Wood and Sibly 1952). A relationship between CA activity and photosynthesis by manipulating the zinc supply to the plant has also been demonstrated (Randall and Bouma 1973, Badger and Price 1994). As shown in Figure 7.8, CA activity varies significantly with type of zinc salt treatment at both the tested zinc concentrations. The minimum variation in CA activity was observed for ZB treatment with 20.39 and 25.24% change over control for 50 and 100 mg L⁻¹ concentrations, respectively. Treatment of chili plants with cZN showed a mixed response with higher CA activity in case of lower concentration (73.53%) as compared to higher concentration (25.87%). In comparison, bZN treatment stimulated the carbonic anhydrase activity rapidly with 50.18% over control for 50 mg L⁻¹ concentration which further increased to 79.29% at 100 mg L⁻¹ concentration. Similar results were observed for ZS treatment with significant differences in CA activity (47.35 and 73.46% over control for 50 and 100 mg L⁻¹ concentration, respectively). These results corroborate well with the published reports on variation in CA activity in various plants exposed to zinc treatments (Rengel 1995, Sagardoy et al. 2010, Tu et al. 2012). However, to the best of our knowledge, this is the first observation of variation in the CA activity of plants in response to ZnO nanoparticles.

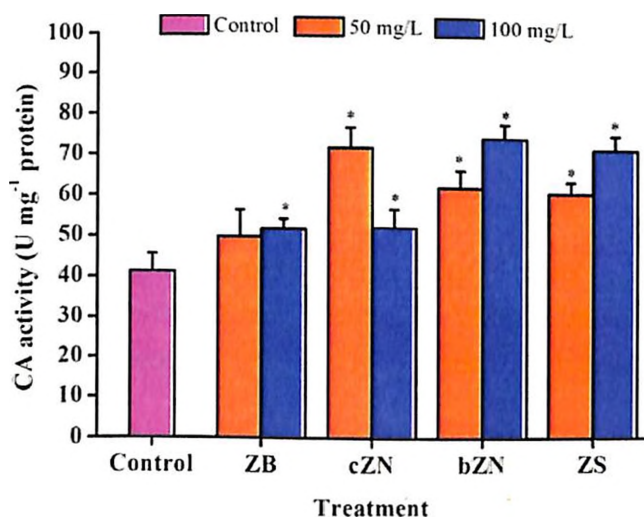


Figure 7.8 Carbonic anhydrase (CA) activity in leaves of chili plants sprayed with distilled water (control) and various zinc treatments. Vertical bars represent standard errors. Significant differences from control ($p \leq 0.05$) are marked with asterisk.

Acid phosphatase (AP, EC 3.1.3.2) is another zinc-dependent enzyme known to catalyse the hydrolysis of orthophosphate monoesters under acidic conditions (Bull et al. 2002). The enzyme comprised of two subunits with two domains in each of its subunit; a smaller N-terminal domain (about 120 residues) and a larger C-terminal domain (about 210

residues) with [Fe(III)-Zn(II)] metallic center. Zinc ion is co-ordinated with the N^ε-atom of His286, the N^δ-atom of His323 and amide oxygen of Asn201 residues of the AP enzyme (Vogel et al. 2002, Olczak et al. 2003). In the present study, variation in the AP activity in the roots of chili plants treated with various zinc treatments was observed (Figure 7.9). The data revealed no significant variation in AP activity for roots of plant treated with ZB and ZS at both the tested concentrations as compared to control. Significant difference was observed in case of cZN treatment as compared to control plants, however; no noticeable difference was observed among the tested concentrations (50 and 100 mg L⁻¹). A striking increase in AP activity was observed in case of plants treated with 100 mg L⁻¹ concentration of bZN. An increased AP activity in case of both types of ZnO nanoparticles indicates the higher penetration potential of nanoparticles in plants. Previous investigation on *Nicotiana tabacum* also demonstrated the capability of single-walled carbon nanotubes to penetrate the cell wall and cell membrane of intact plant cells (Liu et al. 2009).

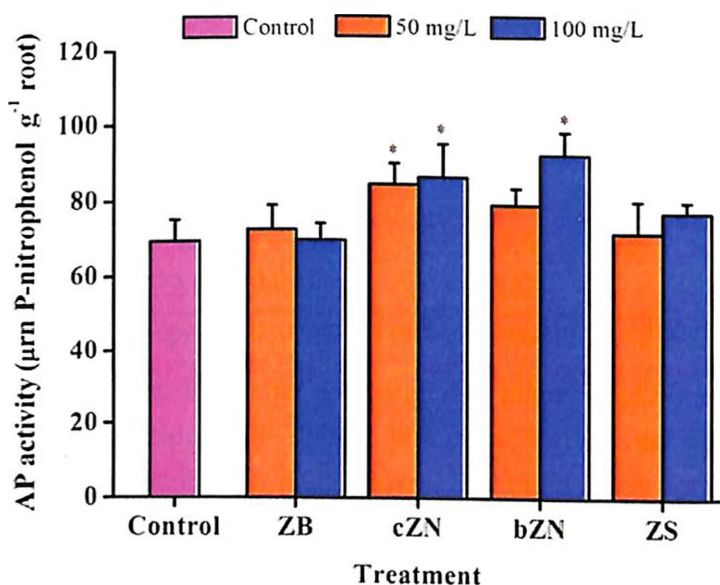


Figure 7.9 Changes in acid phosphatase (AP) activity in roots of chili plants sprayed with distilled water (control) and various zinc treatments. Vertical bars represent standard errors. Significant differences from control ($p \leq 0.05$) are marked with asterisk.

7.3.2.7 Effect on zinc content

At the end of experiment, harvested chili plants were thoroughly washed to remove all traces of zinc salts present on the leaf surface. The step was very crucial especially for treatments such as ZB which are often deposited on the plant surface due to lack of cell penetration potential and may generate erroneous results. Table 7.3 shows the concentration of zinc in chili plants sprayed with various zinc salts at both the tested concentrations. No significant change ($p < 0.05$) in zinc concentration was observed in case of ZB treatment as compared to control plants. Due to larger particle dimensions and high aggregation nature in aqueous solutions, bulk ZnO particles have found to possess less penetration potential in plants (Rico et al. 2011, Luyts et al. 2013). In contrast, significant increase in a dose-

dependent manner was observed in plants sprayed with cZn, bZn and ZS salts. These results are in agreement with previous studies which demonstrated a positive correlation between zinc concentration and uptake (Ahl and Omer 2009, Lopez-Moreno et al. 2010a, Mukherjee et al. 2014). Similar observation has also been reported with other metal oxide nanoparticles such as CeO₂, TiO₂, magnetite, etc (Ghafariyan et al. 2013, Morales et al. 2013, Servin et al. 2013, Trujillo-Reyes et al. 2013).

Table 7.3 Zinc concentration in chili plants sprayed with distilled water (control) and various zinc treatments.

Treatment	Zn concentration (mg kg ⁻¹ DW)
Control	49.57 ± 3.12
ZB 50	57.42 ± 7.61
ZB 100	69.64 ± 3.70
cZn 50	111.47 ± 6.51
cZn 100	213.91 ± 7.54
bZn 50	140.87 ± 5.42
bZn 100	299.62 ± 8.04
ZS 50	92.18 ± 5.96
ZS 100	201.65 ± 7.03
LSD (p ≤ 0.05)	38.13

± represents standard error of means (n = 3)

Our findings suggest that after entering the plants, ZnO nanoparticles undergo transformation to release zinc ions which promotes various enzymatic activities and consequently results in an increase in plant growth and biomass. A comparative assessment of translocation of CeO₂ nanoparticles between pumpkin (*Cucurbita maxima*) and wheat (*Triticum aestivum*) cultivated in hydroponic solution revealed that Ce was translocated to the pumpkin shoot but not to the wheat shoot (Schwabe et al. 2013). However, no evidence of nanoparticle translocation were observed in maize plants (Birbaum et al. 2010). A systematic assessment of chemical transformation of ZnO nanoparticles in plants is yet to be carried out to determine their fate and behaviour in the food chain.

7.4 Conclusions

The present chapter targeted to assess the potential of ZnO nanoparticles as potential substitute for conventional zinc fertilizers. A systematic comparison of chemically and biologically synthesized protein-capped ZnO nanoparticles with Zn⁺² ions and their bulk counterpart were performed using chili plant as a model system. Initially, physico-chemical characteristics of ZnO nanoparticles in aqueous medium were calculated to determine their stability and surface characteristics. The low polydispersity index (PDI = 0.120) observed for sonicated nano-ZnO suspension indicated the substantial monodispersity of nanoparticles which validated their use in further studies. The foliar spray studies on chili plants showed

that ZnO nanoparticles were more effective as compared to zinc sulphate and bulk ZnO indicating their potential scope as a promising alternative to conventional zinc fertilizers. Moreover, we noticed a superior growth response in case of biologically synthesized protein-capped ZnO nanoparticles as compared to commercial bare ZnO nanoparticles signifying the importance of surface modification with protein shell. These results indicate the significance of importance of nanoparticle surface modification and biocompatible nature of protein shell which decrease the toxic effects of biologically synthesized ZnO nanoparticles.

7.5 References

- Ahl, S.-A. and Omer, E. (2009). Effect of spraying with zinc and/or iron on growth and chemical composition of coriander (*Coriandrum sativum* L.) harvested at three stages of development. *Journal of Medicinal Food Plants* 1: 30-46.
- Albrecht, M. A., Evans, C. W. and Raston, C. L. (2006). Green chemistry and the health implications of nanoparticles. *Green Chemistry* 8: 417-432.
- Apel, K. and Hirt, H. (2004). Reactive oxygen species: metabolism, oxidative stress, and signal transduction. *Annual Review of Plant Biology* 55: 373-399.
- Arnon, D. I. (1949). Copper enzymes in isolated chloroplasts. Polyphenoloxidase in *Beta vulgaris*. *Plant Physiology* 24: 1.
- Arora, A., Sairam, R. and Srivastava, G. (2002). Oxidative stress and antioxidative system in plants. *Current Science* 82: 1227-1238.
- Arrivault, S., Senger, T. and Krämer, U. (2006). The Arabidopsis metal tolerance protein AtMTP3 maintains metal homeostasis by mediating Zn exclusion from the shoot under Fe deficiency and Zn oversupply. *The Plant Journal* 46: 861-879.
- Assche, F. V. and Clijsters, H. (1990). Effects of metals on enzyme activity in plants. *Plant, Cell & Environment* 13: 195-206.
- Auffan, M., Rose, J., Bottero, J. Y., Lowry, G. V., Jolivet, J. P. and Wiesner, M. R. (2009). Towards a definition of inorganic nanoparticles from an environmental, health and safety perspective. *Nature Nanotechnology* 4: 634-641.
- Auld, D. S. (2001). Zinc coordination sphere in biochemical zinc sites. *BioMetals* 14: 271-313.
- Badger, M. R. and Price, G. D. (1994). The role of carbonic anhydrase in photosynthesis. *Annual Review of Plant Biology* 45: 369-392.
- Bairwa, L., Khandelwal, S. and Verma, H. (2013). Effect of zinc on growth, seed yield and nutrient content of bottle gourd seeds [*Lagenaria siceraria* (Mol.) Standl.]. *Progressive Horticulture* 45: 218-221.
- Beyer, W. F. and Fridovich, I. (1987). Assaying for superoxide dismutase activity: some large consequences of minor changes in conditions. *Analytical Biochemistry* 161: 559-566.
- Birbaum, K., Brogioli, R., Schellenberg, M., Martinoia, E., Stark, W. J., Günther, D. and Limbach, L. K. (2010). No evidence for cerium dioxide nanoparticle translocation in maize plants. *Environmental Science & Technology* 44: 8718-8723.

- Bondarenko, O., Juganson, K., Ivask, A., Kasemets, K., Mortimer, M. and Kahru, A. (2013). Toxicity of Ag, CuO and ZnO nanoparticles to selected environmentally relevant test organisms and mammalian cells *in vitro*: a critical review. *Archives of Toxicology*: 1-20.
- Boonyanitipong, P., Kositsup, B., Kumar, P., Baruah, S. and Dutta, J. (2011). Toxicity of ZnO and TiO₂ nanoparticles on germinating rice seed *Oryza sativa* L. *International Journal of Bioscience, Biochemistry and Bioinformatics* 1: 282-285.
- Borm, P. J., Robbins, D., Haubold, S., Kuhlbusch, T., Fissan, H., Donaldson, K., Schins, R., Stone, V., Kreyling, W., Lademann, J., Krutmann, J., Warheit, D. and Oberdorster, E. (2006). The potential risks of nanomaterials: a review carried out for ECETOC. *Particle Fibre and Toxicology* 3: 11.
- Bradford, M. M. (1976). A rapid and sensitive method for the quantitation of microgram quantities of protein utilizing the principle of protein-dye binding. *Analytical Biochemistry* 72: 248-254.
- Bull, H., Murray, P. G., Thomas, D., Fraser, A. and Nelson, P. N. (2002). Acid phosphatases. *Molecular Pathology* 55: 65-72.
- Burman, U., Saini, M. and Praveen-Kumar (2013). Effect of zinc oxide nanoparticles on growth and antioxidant system of chickpea seedlings. *Toxicological and Environmental Chemistry* 95: 605-612.
- Cakmak, I. (2000). Tansley Review No. 111. Possible roles of zinc in protecting plant cells from damage by reactive oxygen species. *New Phytologist*: 185-205.
- Candan, N. and Tarhan, L. (2003). The correlation between antioxidant enzyme activities and lipid peroxidation levels in *Mentha pulegium* organs grown in Ca²⁺, Mg²⁺, Cu²⁺, Zn²⁺ and Mn²⁺ stress conditions. *Plant Science* 165: 769-776.
- Di Baccio, D., Tognetti, R., Sebastiani, L. and Vitagliano, C. (2003). Responses of *Populus deltoides* × *Populus nigra* (*Populus* × *euramericana*) clone I-214 to high zinc concentrations. *New Phytologist* 159: 443-452.
- Dietz, K.-J. and Herth, S. (2011). Plant nanotoxicology. *Trends in Plant Science* 16: 582-589.
- Egley, G., Paul Jr, R., Vaughn, K. and Duke, S. (1983). Role of peroxidase in the development of water-impermeable seed coats in *Sida spinosa* L. *Planta* 157: 224-232.
- Faisal, M., Saquib, Q., Alatar, A. A., Al-Khedhairi, A. A., Hegazy, A. K. and Musarrat, J. (2013). Phytotoxic hazards of NiO-nanoparticles in tomato: A study on mechanism of cell death. *Journal of Hazardous Materials* 250-251: 318-332.
- Fang, W.-C. and Kao, C. H. (2000). Enhanced peroxidase activity in rice leaves in response to excess iron, copper and zinc. *Plant Science* 158: 71-76.
- Farmer, E. E. and Mueller, M. J. (2013). ROS-mediated lipid peroxidation and RES-activated signaling. *Annual Review of Plant Biology* 64: 429-450.
- Franklin, N. M., Rogers, N. J., Apte, S. C., Batley, G. E., Gadd, G. E. and Casey, P. S. (2007). Comparative toxicity of nanoparticulate ZnO, bulk ZnO, and ZnCl₂ to a

freshwater microalga (*Pseudokirchneriella subcapitata*): the importance of particle solubility. *Environmental Science & Technology* 41: 8484-8490.

Ghafariyan, M. H., Malakouti, M. J., Dadpour, M. R., Stroeve, P. and Mahmoudi, M. (2013). Effects of magnetite nanoparticles on soybean chlorophyll. *Environmental Science & Technology* 47: 10645-10652.

Halliwell, B. and Gutteridge, J. M. (2007). *Free Radicals in Biology and Medicine*. London, Oxford university press.

Handy, R. D., Owen, R. and Valsami-Jones, E. (2008). The ecotoxicology of nanoparticles and nanomaterials: current status, knowledge gaps, challenges, and future needs. *Ecotoxicology* 17: 315-325.

Hao, L., Chen, L., Hao, J. and Zhong, N. (2013). Bioaccumulation and sub-acute toxicity of zinc oxide nanoparticles in juvenile carp (*Cyprinus carpio*): A comparative study with its bulk counterparts. *Ecotoxicology and Environmental Safety*.

Heath, R. L. and Packer, L. (1968). Photoperoxidation in isolated chloroplasts: I. Kinetics and stoichiometry of fatty acid peroxidation. *Archives of Biochemistry and Biophysics* 125: 189-198.

Heinlaan, M., Ivask, A., Blinova, I., Dubourguier, H.-C. and Kahru, A. (2008). Toxicity of nanosized and bulk ZnO, CuO and TiO₂ to bacteria *Vibrio fischeri* and crustaceans *Daphnia magna* and *Thamnocephalus platyurus*. *Chemosphere* 71: 1308-1316.

Hong, F. H., Zhou, J., Liu, C., Yang, F., Wu, C., Zheng, L. and Yang, P. (2005). Effect of nano-TiO₂ on photochemical reaction of chloroplasts of spinach. *Biological Trace Element Research* 105: 269-279.

Hu, C., Liu, X., Li, X. and Zhao, Y. (2013). Evaluation of growth and biochemical indicators of *Salvinia natans* exposed to zinc oxide nanoparticles and zinc accumulation in plants. *Environmental Science and Pollution Research*: 1-8.

Jain, N., Bhargava, A., Majumdar, S., Tarafdar, J. C. and Panwar, J. (2011). Extracellular biosynthesis and characterization of silver nanoparticles using *Aspergillus flavus* NJP08: A mechanism perspective. *Nanoscale* 3: 635-641.

Jain, N., Bhargava, A., Tarafdar, J. C., Singh, S. K. and Panwar, J. (2013). A biomimetic approach towards synthesis of zinc oxide nanoparticles. *Applied Microbiology and Biotechnology* 97: 859-869.

Ju-Nam, Y. and Lead, J. R. (2008). Manufactured nanoparticles: an overview of their chemistry, interactions and potential environmental implications. *Science of the Total Environment* 400: 396-414.

Juhel, G., Batisse, E., Hugues, Q., Daly, D., Pelt, F. N. A. M. v., O'Halloran, J. and Jansen, M. A. K. (2011). Alumina nanoparticles enhance growth of *Lemna minor*. *Aquatic Toxicology* 105: 328-336.

Karuppanapandian, T., Moon, J.-C., Kim, C., Manoharan, K. and Kim, W. (2011). Reactive oxygen species in plants: their generation, signal transduction, and scavenging mechanisms. *Aust J Crop Sci* 5: 709-725.

- Khodakovskaya, M., Dervishi, E., Mahmood, M., Xu, Y., Li, Z., Watanabe, F. and Biris, A. S. (2009). Carbon nanotubes are able to penetrate plant seed coat and dramatically affect seed germination and plant growth. *ACS Nano* **3**: 3221-3227.
- Kool, P. L., Ortiz, M. D. and van Gestel, C. A. (2011). Chronic toxicity of ZnO nanoparticles, non-nano ZnO and ZnCl₂ to *Folsomia candida*(Collembola) in relation to bioavailability in soil. *Environmental Pollution* **159**: 2713-2719.
- Lee, C. W., Mahendra, S., Zodrow, K., Li, D., Tsai, Y. C., Braam, J. and Alvarez, P. J. (2010). Developmental phytotoxicity of metal oxide nanoparticles to *Arabidopsis thaliana*. *Environmental Toxicology and Chemistry* **29**: 669-675.
- Li, C.-C., Chang, S.-J., Su, F.-J., Lin, S.-W. and Chou, Y.-C. (2012). Effects of capping agents on the dispersion of silver nanoparticles. *Colloids and Surfaces A: Physicochemical and Engineering Aspects*.
- Lin, D. and Xing, B. (2007). Phytotoxicity of nanoparticles: Inhibition of seed germination and root growth. *Environmental Pollution* **150**: 243-250.
- Lin, S., Reppert, J., Hu, Q., Hudson, J. S., Reid, M. L., Ratnikova, T. A., Rao, A. M., Luo, H. and Ke, P. C. (2009). Uptake, translocation, and transmission of carbon nanomaterials in rice plants. *Small* **5**: 1128-1132.
- Liu, Q., Chen, B., Wang, Q., Shi, X., Xiao, Z., Lin, J. and Fang, X. (2009). Carbon nanotubes as molecular transporters for walled plant cells. *Nano Letters* **9**: 1007-1010.
- Lopez-Moreno, M. L., de la Rosa, G., Hernandez-Viezcas, J. A., Castillo-Michel, H., Botez, C. E., Peralta-Videa, J. R. and Gardea-Torresdey, J. L. (2010a). Evidence of the differential biotransformation and genotoxicity of ZnO and CeO₂ nanoparticles on soybean (*Glycine max*) plants. *Environmental Science & Technology* **44**: 7315-7320.
- Lopez-Moreno, M. L., de la Rosa, G., Hernandez-Viezcas, J. A., Peralta-Videa, J. R. and Gardea-Torresdey, J. L. (2010b). X-ray absorption spectroscopy (XAS) corroboration of the uptake and storage of CeO(2) nanoparticles and assessment of their differential toxicity in four edible plant species. *Journal of Agricultural and Food Chemistry* **58**: 3689-3693.
- Love, S. A., Maurer-Jones, M. A., Thompson, J. W., Lin, Y. S. and Haynes, C. L. (2012). Assessing nanoparticle toxicity. *Annual Review of Analytical Chemistry* **5**: 181-205.
- Luyts, K., Napierska, D., Nemery, B. and Hoet, P. H. M. (2013). How physico-chemical characteristics of nanoparticles cause their toxicity: complex and unresolved interrelations. *Environmental Science-Processes & Impacts* **15**: 23-38.
- Ma, X., Geiser-Lee, J., Deng, Y. and Kolmakov, A. (2010). Interactions between engineered nanoparticles (ENPs) and plants: phytotoxicity, uptake and accumulation. *Science of the Total Environment* **408**: 3053-3061.
- Makhal, A., Sarkar, S. and Pal, S. K. (2012). Protein-mediated synthesis of nanosized Mn-doped ZnS: a multifunctional, UV-durable bio-nanocomposite. *Inorganic Chemistry* **51**: 10203-10210.

- Manzo, S., Miglietta, M. L., Rametta, G., Buono, S. and Di Francia, G. (2013). Toxic effects of ZnO nanoparticles towards marine algae *Dunaliella tertiolecta*. *Science of the Total Environment* **445**: 371-376.
- Manzo, S., Rocco, A., Carotenuto, R., Picione Fde, L., Miglietta, M. L., Rametta, G. and Di Francia, G. (2011). Investigation of ZnO nanoparticles ecotoxicological effects towards different soil organisms. *Environmental Science and Pollution Research International* **18**: 756-763.
- Maret, W. (2013). Zinc biochemistry: From a single zinc enzyme to a key element of life. *Advances in Nutrition: An International Review Journal* **4**: 82-91.
- Marschner, H. and Marschner, P. (2012). Marschner's mineral nutrition of higher plants, Academic press.
- Maurer-Jones, M. A., Gunsolus, I. L., Murphy, C. J. and Haynes, C. L. (2013). Toxicity of engineered nanoparticles in the environment. *Analytical Chemistry* **85**: 3036-3049.
- Mayer, A. M. and Harel, E. (1979). Polyphenol oxidases in plants. *Phytochemistry* **18**: 193-215.
- Mittler, R. (2002). Oxidative stress, antioxidants and stress tolerance. *Trends in Plant Science* **7**: 405-410.
- Morales, M. I., Rico, C. M., Hernandez-Viezcas, J. A., Nunez, J. E., Barrios, A. C., Tafoya, A., Flores-Marges, J. P., Peralta-Videa, J. R. and Gardea-Torresdey, J. L. (2013). Toxicity assessment of cerium oxide nanoparticles in cilantro (*Coriandrum sativum* L.) plants grown in organic soil. *Journal of Agricultural and Food Chemistry* **61**: 6224-6230.
- Moroney, J., Bartlett, S. and Samuelsson, G. (2001). Carbonic anhydrases in plants and algae. *Plant, Cell & Environment* **24**: 141-153.
- Mukherjee, A., Peralta-Videa, J. R., Bandyopadhyay, S., Rico, C. M., Zhao, L. and Gardea-Torresdey, J. L. (2014). Physiological effects of nanoparticulate ZnO in green peas (*Pisum sativum* L.) cultivated in soil. *Metallomics* **6**: 132-138.
- Nel, A., Xia, T., Madler, L. and Li, N. (2006). Toxic potential of materials at the nanolevel. *Science* **311**: 622-627.
- Niemeyer, C. M. (2001). Nanoparticles, proteins, and nucleic acids: biotechnology meets materials science. *Angewandte Chemie, International Edition* **40**: 4128-4158.
- Nohynek, G. J., Lademann, J., Ribaud, C. and Roberts, M. S. (2007). Grey goo on the skin? Nanotechnology, cosmetic and sunscreen safety. *Critical Reviews in Toxicology* **37**: 251-277.
- Nowack, B. and Bucheli, T. D. (2007). Occurrence, behavior and effects of nanoparticles in the environment. *Environmental Pollution* **150**: 5-22.
- Oberdörster, G., Maynard, A., Donaldson, K., Castranova, V., Fitzpatrick, J., Ausman, K., Carter, J., Karn, B., Kreyling, W. and Lai, D. (2005). Principles for characterizing the potential human health effects from exposure to nanomaterials: elements of a screening strategy. *Particle and fibre toxicology* **2**: 8.

- Olczak, M., Morawiecka, B. and Watorek, W. (2003). Plant purple acid phosphatases-genes, structures and biological function. *Acta Biochimica Polonica-English Edition* **50**: 1245-1256.
- Olenin, A. Y., Krutyakov, Y. A., Kudrinskii, A. A. and Lisichkin, G. V. (2008). Formation of surface layers on silver nanoparticles in aqueous and water-organic media. *Colloid Journal* **70**: 71-76.
- Ozdener, Y. and Aydin, B. K. (2010). The effect of zinc on the growth and physiological and biochemical parameters in seedlings of *Eruca sativa* (L.)(Rocket). *Acta Physiologiae Plantarum* **32**: 469-476.
- Panda, S. K. and Khan, M. H. (2004). Changes in growth and superoxide dismutase activity in *Hydrilla verticillata* L. under abiotic stress. *Brazilian Journal of Plant Physiology* **16**: 115-118.
- Pandey, N., Pathak, G. C., Singh, A. K. and Sharma, C. P. (2002). Enzymic changes in response to zinc nutrition. *Journal of Plant Physiology* **159**: 1151-1153.
- Pandey, S., Parvez, S., Sayeed, I., Haque, R., Bin-Hafeez, B. and Raisuddin, S. (2003). Biomarkers of oxidative stress: a comparative study of river Yamuna fish *Wallago attu* (Bl. & Schn.). *Science of the Total Environment* **309**: 105-115.
- Pradhan, S., Patra, P., Das, S., Chandra, S., Mitra, S., Dey, K. K., Akbar, S., Palit, P. and Goswami, A. (2013). Photochemical modulation of biosafe manganese nanoparticles on *Vigna radiata*: a detailed molecular, biochemical, and biophysical study. *Environmental Science & Technology* **47**: 13122-13131.
- Prasad, K. and Pardha Saradhi, P. (1995). Effect of zinc on free radicals and proline in *Brassica* and *Cajanus*. *Phytochemistry* **39**: 45-47.
- Raghunathan, V. K., Devey, M., Hawkins, S., Hails, L., Davis, S. A., Mann, S., Chang, I. T., Ingham, E., Malhas, A. and Vaux, D. J. (2013). Influence of particle size and reactive oxygen species on cobalt chrome nanoparticle-mediated genotoxicity. *Biomaterials* **34**: 3559-3570.
- Randall, P. and Bouma, D. (1973). Zinc deficiency, carbonic anhydrase, and photosynthesis in leaves of spinach. *Plant Physiology* **52**: 229-232.
- Raveendran, P., Fu, J. and Wallen, S. L. (2003). Completely “green” synthesis and stabilization of metal nanoparticles. *Journal of the American Chemical Society* **125**: 13940-13941.
- Rengel, Z. (1995). Carbonic anhydrase activity in leaves of wheat genotypes differing in Zn efficiency. *Journal of Plant Physiology* **147**: 251-256.
- Rico, C., Hong, J., Morales, M. I., Zhao, L., Barrios, A. C., Zhang, J.-Y., Peralta-Videa, J. R. and Gardea-Torresdey, J. L. (2013). Effect of cerium oxide nanoparticles on rice: A study involving the antioxidant defense system and *in vivo* fluorescence imaging. *Environmental Science & Technology*.
- Rico, C. M., Majumdar, S., Duarte-Gardea, M., Peralta-Videa, J. R. and Gardea-Torresdey, J. L. (2011). Interaction of nanoparticles with edible plants and their possible

implications in the food chain. *Journal of Agricultural and Food Chemistry* **59**: 3485-3498.

- Sagardoy, R., Vázquez, S., Florez-Sarasa, I., Albacete, A., Ribas-Carbó, M., Flexas, J., Abadía, J. and Morales, F. (2010). Stomatal and mesophyll conductances to CO₂ are the main limitations to photosynthesis in sugar beet (*Beta vulgaris*) plants grown with excess zinc. *New Phytologist* **187**: 145-158.
- Schwabe, F., Schulin, R., Limbach, L. K., Stark, W., Bürge, D. and Nowack, B. (2013). Influence of two types of organic matter on interaction of CeO₂ nanoparticles with plants in hydroponic culture. *Chemosphere* **91**: 512-520.
- Servin, A. D., Morales, M. I., Castillo-Michel, H., Hernandez-Viezcas, J. A., Munoz, B., Zhao, L., Nunez, J. E., Peralta-Videa, J. R. and Gardea-Torresdey, J. L. (2013). Synchrotron verification of TiO₂ accumulation in cucumber fruit: a possible pathway of TiO₂ nanoparticle transfer from soil into the food chain. *Environmental Science & Technology* **47**: 11592-11598.
- Song, G., Gao, Y., Wu, H., Hou, W., Zhang, C. and Ma, H. (2012). Physiological effect of anatase TiO₂ nanoparticles on *Lemna minor*. *Environmental Toxicology and Chemistry* **31**: 2147-2152.
- Tabatabai, M. and Bremner, J. (1969). Use of *p*-nitrophenyl phosphate for assay of soil phosphatase activity. *Soil biology and biochemistry* **1**: 301-307.
- Trujillo-Reyes, J., Vilchis-Nestor, A., Majumdar, S., Peralta-Videa, J. and Gardea-Torresdey, J. (2013). Citric acid modifies surface properties of commercial CeO₂ nanoparticles reducing their toxicity and cerium uptake in radish *Raphanus sativus* seedlings. *Journal of Hazardous Materials* **263**: 677-684.
- Tu, C., Foster, L., Alvarado, A., McKenna, R., Silverman, D. N. and Frost, S. C. (2012). Role of zinc in catalytic activity of carbonic anhydrase IX. *Archives of Biochemistry and Biophysics* **521**: 90-94.
- Vámos-Vigyázó, L. and Haard, N. F. (1981). Polyphenol oxidases and peroxidases in fruits and vegetables. *Critical Reviews in Food Science & Nutrition* **15**: 49-127.
- Van Steveninck, R., Van Steveninck, M., Wells, A. and Fernando, D. (1990). Zinc tolerance and the binding of zinc as zinc phytate in *Lemna minor*. X-ray microanalytical evidence. *Journal of Plant Physiology* **137**: 140-146.
- Vogel, A., Borchers, T., Marcus, K., Meyer, H. E., Krebs, B. and Spener, F. (2002). Heterologous expression and characterization of recombinant purple acid phosphatase from red kidney bean. *Archives of Biochemistry and Biophysics* **401**: 164-172.
- Wang, C., Zhang, S. H., Wang, P. F., Hou, J., Zhang, W. J., Li, W. and Lin, Z. P. (2009). The effect of excess Zn on mineral nutrition and antioxidative response in rapeseed seedlings. *Chemosphere* **75**: 1468-1476.
- Wang, C., Zhang, S. H., Wang, P. F., Hou, J., Zhang, W. J., Li, W. and Lin, Z. P. (2009). The effect of excess Zn on mineral nutrition and antioxidative response in rapeseed seedlings. *Chemosphere* **75**: 1468-1476.

- Wang, Z. L. (2004). Zinc oxide nanostructures: growth, properties and applications. *Journal of Physics: Condensed Matter* **16**: 829-858.
- Wiench, K., Wohlleben, W., Hisgen, V., Radke, K., Salinas, E., Zok, S. and Landsiedel, R. (2009). Acute and chronic effects of nano- and non-nano-scale TiO₂ and ZnO particles on mobility and reproduction of the freshwater invertebrate *Daphnia magna*. *Chemosphere* **76**: 1356-1365.
- Wilbur, K. M. and Anderson, N. G. (1948). Electrometric and colorimetric determination of carbonic anhydrase. *Journal of Biological Chemistry* **176**: 147-154.
- Wood, J. and Sibly, P. M. (1952). Carbonic anhydrase activity in plants in relation to zinc content. *Australian Journal of Biological Sciences* **5**: 244-255.
- Xiong, D., Fang, T., Yu, L., Sima, X. and Zhu, W. (2011). Effects of nano-scale TiO₂, ZnO and their bulk counterparts on zebrafish: Acute toxicity, oxidative stress and oxidative damage. *Science of the Total Environment* **409**: 1444-1452.
- Yemm, E. and Willis, A. (1954). The estimation of carbohydrates in plant extracts by anthrone. *Biochemical Journal* **57**: 508.
- Zeng, H., Cai, W., Li, Y., Hu, J. and Liu, P. (2005). Composition/structural evolution and optical properties of ZnO/Zn nanoparticles by laser ablation in liquid media. *Journal of Physical Chemistry B* **109**: 18260-18266.
- Zhang, Y., Chen, Y., Westerhoff, P., Hristovski, K. and Crittenden, J. C. (2008). Stability of commercial metal oxide nanoparticles in water. *Water Research* **42**: 2204-2212.
- Zhu, H., Han, J., Xiao, J. Q. and Jin, Y. (2008). Uptake, translocation, and accumulation of manufactured iron oxide nanoparticles by pumpkin plants. *Journal of Environmental Monitoring* **10**: 713-717.

Chapter VIII

Summary and Future Scope

This chapter summarizes the significant features of the work presented in this thesis and emphasizes on potential avenues for future endeavours.

8.1. Summary of accomplished work

Biology is considered as the master of so-called ‘bottom-up’ fabrication which includes building up nanostructures starting from basic atoms or molecules. Since several decades, biological systems serve as a prominent source of inspiration for materials science due to their remarkable variety of complex structures and functions. Some examples of natural amalgams include crustacean’s carapaces, mollusk shells, bone and tooth tissues in vertebrates. A number of single-celled organisms are known to produce inorganic materials of nanometer range intra- and/or extra-cellularly. Common examples include magnetotactic bacteria which synthesize magnetite; diatoms which synthesize siliceous materials, S-layer forming bacteria, etc.

Recently, taking inspiration from these natural biological systems, the importance of microorganisms as a potential template for nanoparticle synthesis has been established. The present thesis addresses an important aspect towards selection of an efficient microbial isolate for nanoparticle synthesis. Our results substantiate that well adapted microbes isolated from native metal rich soil conditions can serve as a better source for bio-inspired synthesis of metal nanoparticles. In fact, a positive correlation between metal tolerance ability of fungi and their potential for nanoparticle synthesis was established. Two indigenous fungi, *Aspergillus flavus* isolate NJP08 and *Aspergillus* sp. isolate NJP02 were utilized to develop an eco-friendly and low cost protocol for the extracellular synthesis of silver nanoparticles. Optimization of various process factors (pH, salt concentration and biomass) to achieve control over particle size of silver nanoparticles was also attempted. The simplicity and versatility of our approach makes it attractive and could be implemented for various metal nanoparticles synthesis leading to future “nano-factories”.

The underlying mechanism involved in synthesis of silver nanoparticles by *Aspergillus flavus* isolate NJP08 was also deciphered. Using protein depletion studies, a protein with a molecular mass of ca. 33kDa was found to execute the “dual function” of silver reduction as well as stabilization and further identified as “alkaline protease”. The effect of silver nanoparticle binding on the structure and function of this protein was also investigated. Using *in silico* tools, we identifies a structural motif containing Tyr59, Ser107, Asp111 and Asn118 which is highly specific to binding of silver nanoparticles. The identification of a protein possessing “dual function” is surprising and intriguing as well as will open up new exciting avenues for large-scale eco-friendly synthesis of nanomaterials. Moreover, the obtained knowledge of protein-nanoparticle interactions can be exploited for the design and development of future bio-scaffolds to achieve mass scale production of nanoparticles.

Synthesis of nanoparticle is of no significance unless it makes some applications. The antibacterial studies of silver nanoparticles with emphasis to the role of protein shell were investigated. We observed that presence of protein shell on the surface of silver nanoparticles can decrease their bactericidal effects. This observation clearly indicated that surface

modifications of nanoparticles with proteins allow modulation of their functional properties. The present findings can significantly contribute in designing rational antibacterial formulations of silver nanoparticles.

Similar to synthesis of silver nanoparticles, two indigenous fungi, *Aspergillus aeneus* isolate NJP12 and *Aspergillus* sp. isolate NJP02 were utilized for extracellular synthesis of ZnO nanoparticles under ambient conditions. Attempts toward understanding of the synthesis mechanism indicated that the process is non-enzymatic in nature but involves amino acids present in the protein chains. The photocatalytic performance of protein-capped ZnO nanoparticles towards the degradation of methylene blue dye was also investigated. Owing to the presence of surface proteins, ZnO nanoparticles exhibited excellent enhancement of photocatalysis towards methylene blue dye suggesting their potential applications in catalysis, waste water treatment etc.

The potential of ZnO nanoparticles as future “nano-fertilizers” was also investigated. A systematic comparison of chemically synthesized and biologically synthesized zinc oxide (ZnO) nanoparticles with Zn^{+2} ions and its bulk counterpart was carried out using chili plant as a model system. The physico-chemical characteristics of various zinc salts in aqueous medium were determined followed by their effect on chili plants in terms of plant growth and biomass. Studies on stress and zinc related enzymes were carried out to determine the extent of plant damage after zinc exposure. We also determined the plant zinc content to compare the efficacy of zinc salts to deliver zinc in plants.

8.2. Potential for future work

The simplicity and versatility of present “biomimetic” protocol for nanoparticle synthesis allows its utilization for synthesis of various other metal and metal oxide nanoparticles. Moreover, sincere efforts are still required to achieve strict control over size, shape and composition of nanoparticles. Additionally, the knowledge obtained for mechanism involved in nanoparticle synthesis in the present thesis offers exciting possibilities to achieve mass scale production of nanoparticles. Thus, studies will be targeted to accomplish cloning and expression of alkaline protease gene from fungus *Aspergillus flavus* isolate NJP08. This is a pre-necessitate step to produce higher amount of proteins which is an essential step to decipher the protein structure. Also, it will be of particular interest to utilize the site-directed mutagenesis methods to enhance the nanoparticle binding affinity of alkaline protease and understanding protein-nanoparticle interactions. In future, it will be interesting to evaluate the potential of other metal binding proteins to achieve efficient production of nanoparticles.

The observed variation in antibacterial and photocatalytic properties of nanoparticles by protein shell excites us to utilize surface modification strategies for various other applications. For instance, protein shell (corona) on the surface of nanoparticles can be tailored to create novel biomaterials with wide range of controlled toxicities and biomedical applications. Modulation of nanoparticles with protein shell can be utilized to improve the uptake and penetration of nanoparticles within biological systems such as bacteria, cancer

and mammalian cells. Further, protein-capped nanoparticles can be conjugated with various fluorochromes for applications in the area of diagnostics and detection systems.

Another future prospect of the present thesis is to utilize nanoparticles as an alternative to conventional fertilizers for efficient nutrient delivery to plant systems. The observed superior plant growth response in case of zinc oxide nanoparticles than zinc sulphate motivates us to validate these findings in other plant models as well as farm levels. Moreover, further studies can be targeted to implement this approach for various other micronutrients.

Appendices

List of Publications

Patent:-

Jain N, Bhargava A, Panwar J. Biosynthesis of zinc oxide nanoparticles. Indian patent application No. 1439/DEL/2011, *Patent Office Journal*, Issue No. 20/2013, Page 11020.

Research Articles (published):-

Jain N, Bhargava A, Majumdar S, Tarafdar JC, Panwar J. 2011. Extracellular biosynthesis and characterization of silver nanoparticles using *Aspergillus flavus* NJP08: a mechanism perspective. *Nanoscale* 3:635-641.

Rao VK, Rao MS, **Jain N**, Panwar J, Kumar A. 2011. Silver triflate catalyzed synthesis of 3-aminoalkylated indoles and evaluation of their antibacterial activities. *Organic and Medicinal Chemistry Letters* 1:10-17.

Khungar B, Rao MS, Pericherla K, Nehra P, **Jain N**, Panwar J, Kumar A. 2012. Synthesis, characterization and microbiocidal studies of novel ionic liquid tagged Schiff bases. *Comptes Rendus Chimie* 15:669-674.

Jain N., Bhargava A., Tarafdar J. C., Singh S. K. and Panwar J. 2013. A biomimetic approach towards synthesis of zinc oxide nanoparticles. *Applied Microbiology and Biotechnology* 97: 859-869.

Bhargava A, **Jain N**, Barathi ML, Akhtar MS, Yun Y-S, Panwar J. 2013. Synthesis, characterization and mechanistic insights of mycogenic iron oxide nanoparticles. *Journal of Nanoparticle Research* 15:2031-2042.

Jain N, Bhargava A, Panwar J. 2013. Enhanced photocatalytic degradation of methylene blue using biologically synthesized "protein-capped" ZnO nanoparticles. *Chemical Engineering Journal* 243:549-555.

Research Articles (communicated/ under preparation):-

Jain N, Bhargava A, Sabat D, Panwar J. Unveiling the potential of metal-tolerant fungal isolate for efficient enzyme production. *Process Biochemistry* (under review)

Jain N, Bhargava A, Panwar J. Protease-assisted one-pot synthesis and stabilization of spherical silver nanoparticles: a novel template to study protein-nanoparticle interactions.

Jain N, Bhargava A, Rathi M, Panwar J. Removal of protein corona enhances the antibacterial efficiency of biogenic silver nanoparticles.

Jain N, Bhargava A, Panwar J. Comparative phytotoxicity assessment of ZnO nanoparticles with bulk ZnO and Zn (II) ions: role of seed size and anatomy.

Jain N, Bhargava A, Panwar J. *In vitro* assessment of toxicity of ZnO nanoparticles and bulk ZnO on tomato seedlings.

Jain N, Bhargava A, Panwar J. ZnO nanoparticles induced changes in chili plants at biochemical and gene expression levels.

Book Chapters:-

Bhargava A, **Jain N**, Panwar J. 2011. Synthesis and applications of magnetic nanoparticles: A biological perspective. In: *Current Topics in Biotechnology and Microbiology*. Eds. Dhingra H, Jha PN, Lambert Academic Publications, Germany.

Solanki P, Bhargava A, Chhipa HR, **Jain N**, Panwar J. 2014. Nanoparticles for sustainable agriculture. In: *Emerging Nanotechnologies in Agriculture*. Eds Rai M, Ribeiro C, Mattoso L, Duran N, Springer, Germany. (In press)

Invited Lecture:-

Jain N, Bhargava A, Panwar J. 2013. Biomimetics @ nanoscale. Punjab Agricultural University, Ludhiana, India.

Conferences:-

Oral Presentations:-

Jain N, Bhargava A, Panwar J. 2013. Biomimetics at nanoscale: Utilizing metal tolerant fungal isolate to fabricate ZnO nanoparticles. In: Asian Congress on Biotechnology, New Delhi, India.

Jain N, Bhargava A, Panwar J. 2014. Protease-assisted synthesis and stabilization of spherical silver nanoparticles: a novel template to study protein-nanoparticle interactions. In: NanoScitech, Punjab University, Chandigarh, India.

Poster Presentations:-

Jain N, Bhargava A, Panwar J. 2010. Biosynthesis of silver nanoparticles: a green chemistry approach. In: *National Conference on Green and Sustainable Chemistry*, BITS, Pilani, India.

Jain N, Panwar J. 2011. Elucidation of mechanism for extracellular biosynthesis of silver nanoparticles using fungi. In: *4th Congress of European Microbiologists (FEMS)*, Geneva, Switzerland.

Jain N, Bhargava A, Panwar J. 2011. Improved antimicrobial efficacy of biogenic silver nanoparticles. In: *International Conference on Nanomaterials and Nanotechnology*, Delhi, India.

Jain N, Bhargava A, Akhtar MS, Yun Y-S, Panwar J. 2012. Positive effect of zinc oxide nanoparticles on tomato plants: a step towards developing “Nanofertilizers”. In: *International Conference on Nanoscience and Technology*, Hyderabad, India.

Dey D, Bhargava A, **Jain N**, Panwar J. 2012. Phytosynthesis of silver nanoparticles from *Prosopis cineraria* leaf extract and evaluation of their antimicrobial activity. In: *International Conference on Industrial Biotechnology*, Patiala, India.

Biography of Prof. Jitendra Panwar

Prof. Jitendra Panwar completed his Master's degree in Botany with specialization in Microbiology in the year 1997 and Doctoral degree in the area of Mycorrhizal Biotechnology in the year 2000 from Jai Narain Vyas University, Jodhpur. During his at Division of Soil-Water-Plant Relationship, Central Arid Zone Research Institute (ICAR), Jodhpur, he worked in the area of soil fertility, microbiology and plant physiology. In the year 2003, he was awarded Young Scientist Project by Department of Science & Technology, New Delhi, India. Subsequently, in October 2005, he joined Department of Biological Sciences, BITS Pilani, Pilani Campus as Assistant Professor. He has been promoted to Head of the Department in September 2012 and Associate Professor in February 2013. He has 16 years of teaching and research experience as in the year 2014.

Prof. Panwar is also a recipient of "Visiting Professor Fellowship" to visit South Korea for a period of three months under INSA-NRF International Bilateral Exchange/ Collaboration Programme 2011-12. He has successfully completed three research projects funded by Department of Science & Technology (DST), New Delhi, Aditya Birla Group, Mumbai and Indian Council of Agricultural Research (ICAR), New Delhi. Currently, he is working on a research project funded by Department of Science & Technology (DST), New Delhi under its Nano-Mission programme. As a result of his research accomplishments, he has published more than 40 research papers in peer reviewed journals. In addition, he has presented papers and delivered lectures in several National & International conferences and organizations. His current research interest lies in the area of nano-biotechnology, nano-fertilizers and protein-nanoparticle interactions.

Biography of Mr. Navin Jain

Mr. Navin Jain has qualified Combined Entrance Examination for Biotechnology (CEEB) in the year 2006 and joined DBT-sponsored M.Sc. Biotechnology programme at Rajiv Gandhi Biotechnology Centre, Nagpur. He did his M.Sc. dissertation at Cadila Pharmaceuticals Ltd., Ahmedabad. Subsequently, he worked as a Lecturer at Department of Biotechnology, Shree Krishn College, Udaipur. He joined Birla Institute of Technology and Science, Pilani in a World Bank funded NAIP-ICAR project in the year 2009. Later, he joined Ph.D. program and awarded Council Scientific and Industrial Research (CSIR) research fellowship. He possesses an active research interest in the area of bio-nanotechnology with major emphasis on understanding nanoparticle interactions at bio-molecular level. He has published several research articles in renowned journals and also presented his research findings in various National and International conferences. He has also been consistently involved in the teaching programme of Department of Biological Sciences, BITS Pilani, Pilani Campus.

MTCC Certificate for Culture Deposition



प्रतिकल्प-मानक सूक्ष्मजीव संग्रहण एव जीन बैंक
MICROBIAL TYPE CULTURE COLLECTION & GENE BANK

सूक्ष्मजीव प्रौद्योगिकी संस्थान
INSTITUTE OF MICROBIAL TECHNOLOGY

Plot No. 1, Sector-8, Gandhinagar, Gurgaon
Sector-8, Gandhinagar, Gurgaon, Haryana



Dr. Belle D. Shenoy
Scientist

24th March 2011

Dr. Jitendra Panwar
Biological Sciences Group,
Birla Institute of Technology and Science,
Pilana-333 031, Rajasthan, India

Dear Dr. Panwar,

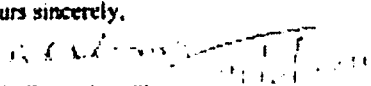
Subject: Deposition of fungal isolates in MTCC – reg.

Please be informed that the following fungal isolates have been deposited in MTCC under general category deposition

1. Strain no. NJP02 : *Aspergillus* sp (MTCC No. 10740)
2. Strain no. NJP08 : *Aspergillus* sp (MTCC No. 10829)
3. Strain no. NJP12 : *Aspergillus* sp (MTCC No. 10830)

Thank you for your interest in MTCC

Yours sincerely,


Belle Damodaru Shenoy
E-mail: shenoy@imtech.res.in
Cell Number: 098888 15846

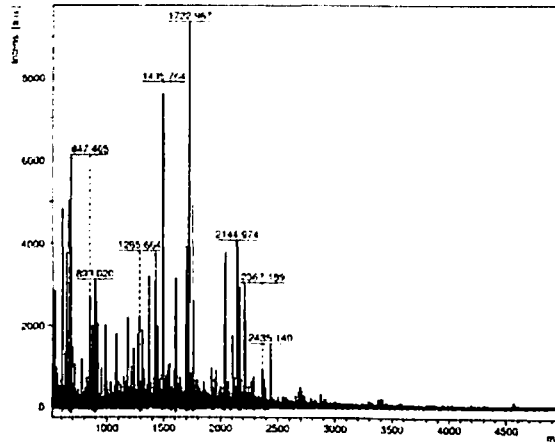
Phones
दूरभाष
+91 172 2680562 2695215
2685216 2695219
2685225 2695226
2685227 2695228

Fax
फैक्स
+91 172 2690632
2690585
Gurgaon, Haryana, INDIA

E-mail: curator@imtech.res.in
Web: <http://web01.imtech.res.in>

Supplementary Data

(A)



(B)

Mr(expt) ^a (Da)	Mr(cale) ^b (Da)	ppm ^c	Start	End	Peptide
778.347	778.343	5.5	287	292	K.NPDFMR.Q
846.457	846.460	-2.7	132	138	K.ETPVFVR.F
851.439	851.429	12.8	453	460	K.GFFTAPGR.E
901.459	901.441	21.4	154	161	R.DVHGFATR.F
1082.616	1082.620	-3.52	514	522	R.NNVIIQLNR.V
1183.591	1183.573	14.8	90	98	R.FDHERVPR.A
1284.657	1284.636	16.2	241	251	R.HVDGFGIHTFR.F
1306.677	1306.692	-11.3	74	84	R.GPTLLEDIFR.Q
1368.707	1368.704	2.6	385	395	R.LFSYLDTQLNR.H
1445.719	1445.715	2.5	372	384	R.GVDFTEDPLLQGR.L
1549.795	1549.810	-9.9	699	713	K.SVTSGFVDGIKDGLR.T
1603.759	1603.763	-2.3	469	482	R.AVSPSFEDVWSQPR.L
1613.803	1613.826	-14.5	591	605	K.QLSEGDVDDVVVAER.L
1702.840	1702.854	-8.4	396	410	R.HGGPNFEQLPINQPR.V
2165.000	2165.036	-17.0	354	371	R.NYFAETEQQVMFQPGHIVR.G
2210.089	2210.137	-21.8	483	501	R.LFYNSLTPAEQQFVVDAIR.F

^aMr (expt) is the observed experimental molecular mass of the peptide^bMr (cale) is the calculated molecular mass of the peptide from the proteom database^cerror on the experimental peptide mass values

*indicates Oxidation (M)

(C)

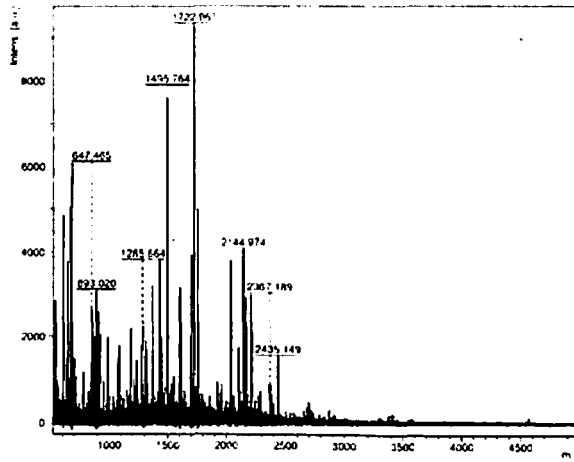
```

1 MRALSLASLI GIASAACPYM TGELERRDTG TDDATAATEE FLSQYYMADN DTFLTSDVGG PIEDQNSLQV GDRGPTLLED
81 FIFRQKIQRF DHERVPERAV HARGVGANGV FTSYGDYSNI TAASFLGAEK KETPVFVRFS TVAGSRGSSD LARDVHGPFAT
161 RFYTDEGNFD IVGNINPVFF IQDAILFPDL IHAVKPRGDN EIPQAATAHD SAWDFFSQQP SSLHTLLWAM SGHGIPRSLR
241 HVDGFGIETF RFVTDNGDSK LVKFHWKSLQ GKASMVWEEA QQVSGKNPDF MRQDLFEAIE AGRYPWEWELG VQIMDEEDQL
321 KFGFDLDFPT KIVPEEYVPI TKLKGMTLNR NFRNYFAETE QVMFQPGHIV RGVDFTEDFL LQGLRFSYLD TQLNRHGGEN
401 FEQLPINQFR VPVHNNNRDG AGQMFILNPN NAYSPTLNK GSPKQANQTV GKGFFTAPGR ESTGRFTRAV SPSFEDVWSQ
481 RRLFYNSLTP AEQQFVVDIAI RFENSNVKSS VVRNNVITQL NRVSNDLARR VARAIGVEEP EADPTYHHNN KTTDVGTFGQ
561 KLKLLDGLKV GFLASVETPA SIEAAEELSK QLSEGDVDDV VVAERLSDGV DQYTSGSDAI QFDAVIVAPG AEGLFSTFSF
641 TAPSNATSSS TLFPAGRPLQ IVIDGFRFGK PVGAVGSAAT ALKNAGIQTS RDGVYVDKSV TSGFVDGIKD GLRTFKFLDR
721 FKLDDH

```

Figure A4.1 Peptide mass fingerprinting of catalase protein of fungus *Aspergillus flavus* isolate NJP08.

(A)



(B)

Mr(expt) ^a (Da)	Mr(calc) ^b (Da)	ppm ^c	Start	End	Peptide
636.297	636.3231	-40.9	545	549	K.DYIAR.W
919.490	919.4763	15.1	610	617	K.YGVPLDTR.H
1272.674	1272.671	1.7	123	133	K.FLSPITPDDL.R
1428.770	1428.773	-1.5	123	134	K.FLSPITPDDLRR.Q
1494.756	1494.762	-3.7	251	263	R.AISTNWPVFAFSR.D
1750.834	1750.853	-10.8	623	638	K.ADWELFTA AVASESVR.D
2037.987	2038.022	-17.2	337	355	K.DSIDAAGQDYLTITSLTVR.Q
2102.948	2102.966	-8.6	153	171	K.AHDIQVYADISAEWASGDR.N
2143.967	2144.011	-20.6	639	656	R.DMFHQALATWINETPTNR.A
2366.182	2366.233	-21.5	334	355	R.ISKDSIDAAGQDYLTITSLTVR.Q
2382.986	2383.141	-65.0	447	467	K.MPLEECGNMVMALAYAQKAK.D

^aMr (expt) is the observed experimental molecular mass of the peptide

^bMr (calc) is the calculated molecular mass of the peptide from the protein database

^cerror on the experimental peptide mass values

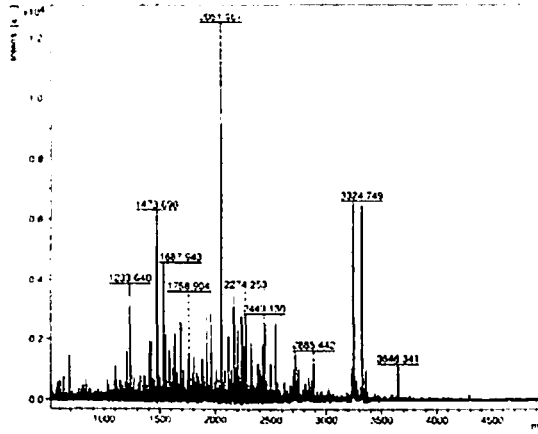
*indicates Oxidation (N)

(C)

1 MMHLSFCLS VASLVSYAGA ASTFSPARPP ALPLAVKSPY LSTWLSAGTD GGNGGYLAGQ WPTFWFGQVT GHAGQIRVDN
81 STYTWGAIP NTPTVNQTSF EYTSTSSVFT MRVGMVEMK VKFLSPITPD DLRRQSLVFS YLDVDVESID GKARDIQVYA
161 DISAEWASGD RNAIAQWDYG VTDDGVAYHK VYRQTQLFS ENTEQAWEGE WYWATDDQDG LSYQSGPVDV VRGAFKNGK
241 LANSDDKNYR AISTNWPVFA FSRDLGSVKT SAGTLFSIGL AQDSAIQYSG KPEGTTVMPS LWKSYFSTAT AALEFFHHDY
321 AAAAALSKDL DDRISKSDID AAGQDYLTIT SLTVRQVFAA VQLTGTPEDP YIFMKEISSN GNMNTVDVIF PAHPFLYTN
401 PELLKLIKPK IYEIQENKGY PNTYAMHDIG THYPNATGHP KGDDEKMLE ECGNMVIMAL AYAQRKAKND YLSQHYPILN
481 KWTTYLVEDS IYPANQISTD DFAGSLANQT NLALKGIIIGI QAMAVISNTT GHPDDASNHS SIAKDYIARW QTLGVAHDAN
561 PPHTTLYSGA NETHGLLYNL YADRELGLNL VPQSVYDMQN TFYPTVKEKY GVPLDTRVY TKADWELFTA AVASESVRDM
641 FQALATWIN ZPTNRAFTD LYDTQTGNYP AGITFIARPV MGGAFALLIL

Figure A4.2 Peptide mass fingerprinting of glutaminase protein of fungus *Aspergillus flavus* isolate NJP08.

(A)



(B)

Mr(expt) ^a (Da)	Mr(calc) ^b (Da)	ppm ^c	Start	End	Peptide
1119.582	1119.556	22.8	148	157	R.DYTDPAALR.G
1203.633	1203.588	36.9	310	319	K.NYRPDSPDLK.F
1245.566	1245.574	-6.4	611	622	R.GLGEAEYHASR.R
1472.689	1472.676	9.1	408	418	R.MYIWTESQPYR.D
2201.086	2201.050	16.1	419	438	R.DGSFEAGIVIHEYTHGLSNRL
2442.122	2442.077	18.7	448	470	R.CLNALESGGMGEGWGFMAAIR.
3234.595	3234.489	32.5	235	263	K.DVHGVVDYVAEADYQVYAWGIND
3244.798	3244.477	99.0	373	405	K.GGAGNDYVILNAQDGSQTNNANF

^aMr (expt) is the observed experimental molecular mass of the peptide

^bMr (calc) is the calculated molecular mass of the peptide from the protein database

^cerror on the experimental peptide mass values

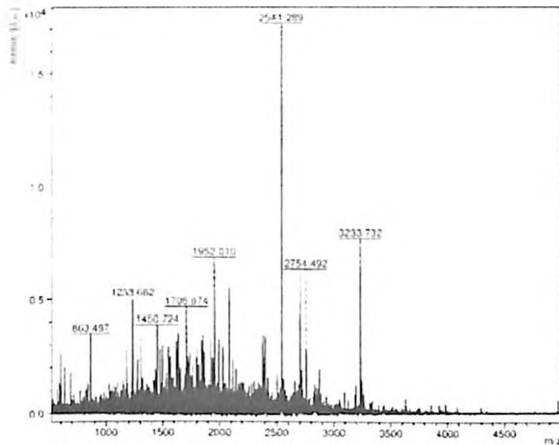
*indicates Oxidation (M)

(C)

1 MRGLLAGAL GLPLAVLAHP THHAHGLQRR TVDLNSFRLH QAQYINATE SSSDVSSSFS PFTEQSYVET ATQLVKNILP
 81 DATFRVVKDH YIGSNGVAHV NFRQTAHGLD IDNADFNVV GKNKIFSYG HSFYTGKIPD ANPLTKRDT DPVAALRGTN
 161 EALQLSITLD QVSTEATEDK ESFNFKGVSG TVSDPKAQLV YLVKEDGSLA LTWKVETDID SNWLLTYIDA NTGKDVVEGVV
 241 DYVAEADYQV YAWGINDPTE GPRTVISDFW DSSASAFTWI SDGENNYTTT RGNNGIAQSN PTGGSQYLKN YRPDSPDLKF
 321 QYPYSLNATP PESYIDASIT QLFYANTYH DLLYTLGFNE EAGNFQYDNN GKGGAGNDYV ILNAQDGSST NNANFATPPD
 401 GQPGRMRYI WTESQPYRDS SPEAGIVIE YTHGLSNRLT GGPANSRCLN ALESGGMGEG WGFMAAIR LKAGDTHSTD
 481 YTMGEWANR KGGIRAYPFS TSLETNPLTY TSLNELDEVH AIGAVWANVL YELLWNLIDK HGKNDGPKPE FKDGVPTDGR
 561 YLAMKLVIDG MALQPCNPNC VQARDAILDA DKALTDGANK CEIWKAFKR GLGEAEYHA SRRVGSDRVP SDAC

Figure A4.3 Peptide mass fingerprinting of elastinolytic metalloproteinase protein of fungus *Aspergillus flavus* isolate NJP08.

(A)



(B)

Mr(expt) ^a (Da)	Mr(calc) ^b (Da)	ppm ^c	Start	End	Peptide
862.489	862.422	78.2	203	209	K.TLLDDMR.E
1061.567	1061.529	35.5	243	251	K.TSNLLMNNR.G
1306.691	1306.670	15.6	252	263	R.GEIKIADFGMAR.Y
1433.756	1433.730	18.6	240	251	R.DLKTSNLLMNNR.G*
1614.872	1614.742	80.4	418	431	K.EMFPTFPSKAGMEK.R*
1735.922	1735.947	-14.6	354	371	R.LPPTSSSSGSGALPLI.PR.S
1750.871	1750.892	-12.4	147	162	K.LKMETATDGGFPVTGLR.E*
1919.020	1918.971	25.5	203	218	K.TLLDDMREPFPLPSEIK.T*
1951.003	1951.074	-36.2	354	373	R.LPPTSSSSGSGALPLI.PRSK.F
2030.074	2030.030	22.0	410	426	K.EDPRPKPKEMFPTFPSK.A
2038.032	2038.132	-49.3	163	179	R.EIQTLLEARHANIVYL.R.E
2500.300	2500.405	-41.9	372	394	R.SKFPFLTNAGLELLSSLLALNPR.A
2688.367	2688.256	41.1	71	94	R.RFANQQPQQQMEQEAVSAAAAEEK.E
2842.498	2842.323	61.8	187	209	K.MDDVFLVMDLEHDLK.TLLDDMR.E**
2871.537	2871.558	-7.32	219	242	K.TLLLQVLSGLDFLHSHWIMHRDLK.T

^aMr (expt) is the observed experimental molecular mass of the peptide

^bMr (calc) is the calculated molecular mass of the peptide from the protein database

^cerror on the experimental peptide mass values

*indicates Oxidation (M)

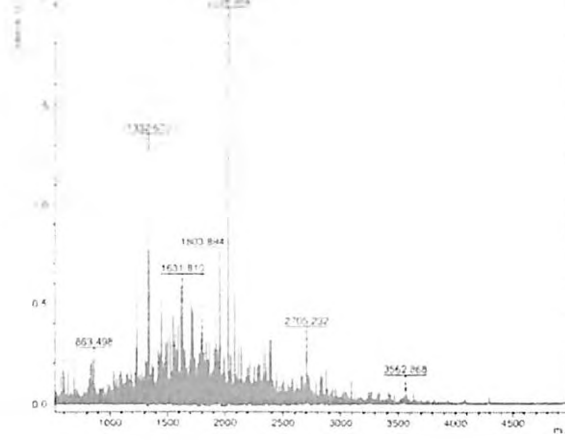
(C)

```

1 MSAPSKSSRW AASDPEEEAL LAQRKPEKEE KKRKAAKQR QLDEQTQAS VSHAHDEPNG DADEPPPKRR RFANQQPQQQ
81 MEQEAVSAAA AEEREKPLLF FPPGQAWGPC RHVDNFERLN HIEEGAYGWV SRAKDIMTGE VVALKKLME TATDGFVVTG
161 LREIQTLEA RHANIVYLRE VVMGSKDDV FLVMDLEHD LKTLDDMRE PFLPSEIKTL LLQVLSGLDF LSHWIMHRD
241 LKTSNLLMN RGEIKIADFG MARYYGDPPP KLTQLVVTW YRAPELLGA EKYPPEIDMW SIGCVLGELL TKEPLLQGKN
321 EVDQVSKIFA LTGPPTQQNW PGFRSLPNAK SLRLPPTSS SSGALPLP RSKFPFLTNA GLELLSLLA LNFRRPSTQ
401 QCLSHKYFKE DPRPKPKEMF PTFPSKAGME KRRRRETPEA PKRGQEAPSL DFASVFGGQS GGDTEAGAG FTLLRLG

```

Figure A4.4 Peptide mass fingerprinting of protein kinase of fungus *Aspergillus flavus* isolate NJP08.



(B)

Mr(expt) ^a (Da)	Mr(calc) ^b (Da)	ppm ^c	Start	End	Peptide
1449.690	1449.634	38.6	64	75	K.CPACRSSDQELK.L
1549.815	1549.837	-13.9	286	297	K.RELLHELAVWER.T
1630.802	1630.707	58.4	124	139	K.VDQEDGPDASGSEG
1706.809	1706.841	-19.0	204	219	K.QASFGSLQPMSPAS
1950.941	1950.850	46.7	316	332	R.KDFDAAAWSNNHG
2027.977	2027.928	24.0	147	165	R.GNSQAEPPVVDAIE
2382.979	2383.166	-78.6	183	203	R.MKNEAVQHLDICT

^aMr (expt) is the observed experimental molecular mass of the peptide

^bMr (calc) is the calculated molecular mass of the peptide from the protein database

^cerror on the experimental peptide mass values

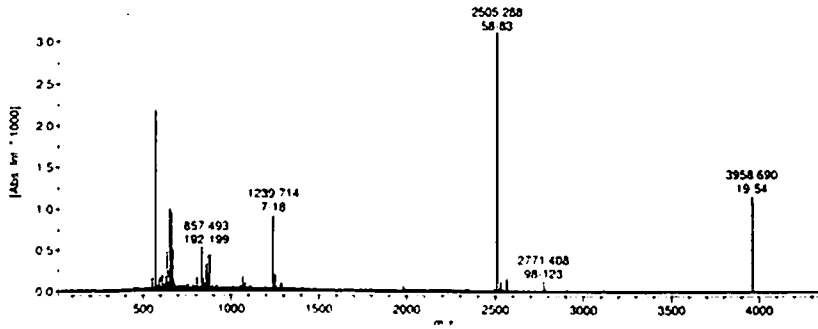
*indicates Oxidation (M)

(C)

1 MEQTFDLPDS TDWLETPLSL VSPLESSLRC QVCKDFFDNP VITSCSHTFC SLCIRRCCLST EGKCFACRSS DQELKLRNK
81 AVQELVEAFQ NARPSMLELA RKAANSRLDG GYVTGQPAK KRKVDQEDGP DASGSEGIRT RSQSRRGNSQ AEPVVVDAIE
161 DDQDKEYIPE DGLVACPICG R**MKNEAVFQ** HLDICTGDPA PLR**QASFGSL** QPMSPASRKS KDVTDKPPER LPTINYSLLK
241 DNVLRKKLKD LGIPNWGPRP LLQRRHTEWM NLWNANCDISK APKSKRELLH ELAVWERTQG GHAAPSESS NTVMRKDFDA
321 **AAWSNNHGDE** FKRLIANARK RKDAVIRTTI PQAAPARDGT STASAPEQST EMSTPPEVAE RLQTQTVPEG TSVATIAENE
401 TGTIQTPNIT QVVSSPPE

Figure A4.5 Peptide mass fingerprinting of DNA repair protein of fungus *Aspergillus flavus* isolate NJP08.

(A)



(B)

Mr(expt) ^a (Da)	Mr(calc) ^b (Da)	ppm ^c	Start	End	Peptide
856.4853	856.4079	90.4	192	199	R.ASFSNFGK.V
1238.707	1238.641	53.6	7	18	K.SAPWGLGSISHK.G
2504.281	2504.216	26.1	58	83	K.AYNAAGGQHVDLSIGHGTHVSGTIAGK.T
2770.401	2770.345	20.2	98	123	K.VFQGESSTSVILDGFNWAANDIVSK.K
3957.683	3957.709	-6.66	19	54	K.GQSTDIYDTSAGEGTYAYVVDSGVNVNDHEEFEGR.A

^aMr (expt) is the observed experimental molecular mass of the peptide

^bMr (calc) is the calculated molecular mass of the peptide from the protein database

^cerror on the experimental peptide mass values

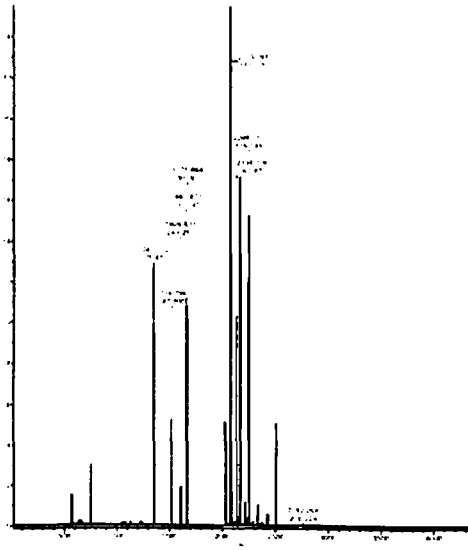
*indicates Oxidation (M)

(C)

1 GLTTQKSAPW GLGSISHERGQ QSTDYIYDTS AGEPTYAYVV DSGVNVDBEE FEGRASKAYN AAGGQHVDLSI GEGTEVSGTI
81 AGKTYGIACK ASILSVKVPQ GESSTSVIL DGFNWAANDI VSKRRTSKAA INMSLGGYS KAFNDAVENA FEQGVLSVVA
161 AGNENS DAGQ TSPASAPDAI TVAAIQSNN RASFSNFGKV VDFVAPGQDI LSAWIGSSSA TNTISGTSMA TPHIVGLSLY
241 LAALENLDP AAVTKRIKEL ATRDVKVDK GSPNLLAYNG NA

Figure A4.6 Peptide mass fingerprinting of alkaline protease protein of fungus *Aspergillus flavus* isolate NJP08.

(A)



(B)

Mr(expt) ^a (Da)	Mr(calc) ^b (Da)	ppm ^c	Start	End	Peptide
1344.725	1344.679	34.6	75	87	R.VEVHIASGSSGFR.T
1515.789	1515.743	30.2	187	200	K.VEVHVASGASNYQR.R
1605.824	1605.775	30.5	243	257	K.VEVHVASGSSTYNTR.V
1660.865	1660.817	29.1	131	145	R.VEVHIASASSNYQTR.I
1670.856	1670.822	20.3	291	307	K.TQNTGTGSVEVHVASGK.S
2074.059	2074.019	19.0	181	200	R.NTGTGKVEVHVASGASNYQR.R
2133.098	2133.056	19.7	67	87	K.TTNTGTGRVEVHIASGSSGFR.T
2247.143	2247.099	19.3	125	145	R.NTGTGRVEVHIASASSNYQTR.I
2761.261	2761.233	10.2	202	224	R.IQEVGTTFPEDNGVWQMVD ^d FDR.D*

^aMr (expt) is the observed experimental molecular mass of the peptide

^bMr (calc) is the calculated molecular mass of the peptide from the protein database

^cerror on the experimental peptide mass values

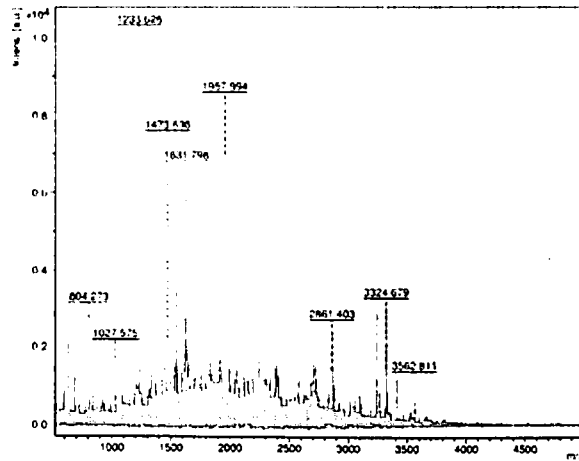
^dindicates Oxidation (M)

(C)

1 MEAFNLHNFLL SLYILLPFV ILANPVHAAP YQNRILETGS TFGAPDPYGP WQMIPSIPTD DLTYYIKTTNT GTGRVEVHLA
 81 SSSGFRTRS LEVGTTFVSE DNGTWQLIDA DGDGRPDLYV IKTRNTGTGR VEVHIASASS NYQTRILETG TTFYPEDNGV
 161 WQMAFDHHDG KLDLVYIKTR NTGTGKVEVH VASGASNYQR RIQEVGTTFY PEDNGVWQMV DFDRDGKLDL AYIKTRNTGT
 241 GKVEVHIASG SSTYNTRVQE VGTTFYPESN GFWELSDFNH DGVLDLVYIK TQNTGTGSVE VEVASGKS

Figure A4.7 Peptide mass fingerprinting of FG-GAP repeat protein of fungus *Aspergillus flavus* isolate NJP08.

(A)



(B)

Mr(expt) ^a (Da)	Mr(calc) ^b (Da)	ppm ^c	Start	End	Peptide
1099.673	1099.603	64.1	259	267	K.NVKEPSWIK.G
1232.619	1232.593	20.9	356	365	K.ESPVIKMPWM.-
1306.648	1306.663	-11.1	149	160	R.ICMVTEAGIIGK.I
1494.770	1494.775	-3.5	327	339	R.TSTLFNIVMNLDK.Q
1533.770	1533.826	-36.8	276	289	R.AQQLAHELVNNGIK.G
1630.791	1630.923	-80.8	1	14	.MHVEAPELPKLVLR.G
1674.813	1674.837	-14.3	121	134	R.VLAQNWDWTTTSVQK.N
1802.878	1803.030	-84.7	177	192	K.ARPCVSSKVPPIHALR.L
1837.882	1837.844	20.5	34	48	K.SQLGIYEEMFEYTTK.M
2860.396	2860.486	-31.6	135	160	K.NLALMDIEISGPRICMV

^aMr (expt) is the observed experimental molecular mass of the peptide

^bMr (calc) is the calculated molecular mass of the peptide from the protein database

^cerror on the experimental peptide mass values

*indicates Oxidation (M)

(C)

1 MHVEAPELPK LVLRGTPKEI GLQHG YRLQE QIKSQLGIYE EMFEYTTKMD WPTVLKLAEE FRASLERKTP SLYLEMQGIA
 81 EGAGVGILDI VALNCRSEIS FGSFSDGCTS LSWKKNENAR VLAQNWDWTT SVQKNLALMD IEISGKPRIC MVTEAGIIGK
 161 IGENSAGVGT CLNAIKARPC VSSKVPPIHIA LRLCLESTSV ASALQTIASL GGVASSQHIL IADSTSLGL ELSPLGDVHL
 241 KEDEDFIMH TNHFIEKNV KEPSWIKGSP ARLEAAQQLA HELVNNGIIGK DLITPSLLRE QVFSOTCNAP QSICAQEDPS
 321 THHTRRTSTL FNIVMNLDRQ DLGAEVVVVGQ PGSGKESFVI KMPWM

Figure A4.8 Peptide mass fingerprinting of acyl-CoA:6-aminopenicillanic-acid-acyltransferase protein of fungus *Aspergillus flavus* isolate NJP08.

```

TARGET      1      LTTQKSA PWGLGSISHK GQSTDIYD TSAGEGYAY VVDSGVNVDH
3f7oB      1      a--ytqqpga pwglgrishr skgsttyeyd tsgsgtccay vidtgveash

TARGET      sssss  hhhh      sssss      ssss sss
3f7oB      s ssssss  hhhh      ssssss s      ssss sss

TARGET      48      EEFEGRASKA YNAAGQHV D SIGHGTHVSG TIAGKTYGIA KKASILSVKV
3f7oB      49      pefegrasqi ksfisgqntd gngghthcag tigshtygya kktkiygvkv

TARGET      sssss      hhhhhhh hh      ssssss
3f7oB      sssss sss      hhhhhhh hh      ssssss

TARGET      98      FQG-ESSSTS VILDGFNWAA NDIVSKKRTS KAAINMSLGG GYSKAFNDAV
3f7oB      99      ldnsqsgsys giisgmdfav qdsksrscpk gvvanmslgg gkaqsvndga

TARGET      hh hhhhhhhhhh hhhh      ssssss s ss hhhhhhh
3f7oB      hh hhhhhhhhhh hhhh      ssssss s ss hhhhhhh

TARGET      147     ENAFEQGVLS VVAAGNENS D AGQTSPASAP DAITVAAIQK SNNRASFSNF
3f7oB      149     aamiragvfl avaagndnan aanyspasep tvctvgatts sdarssfsny

TARGET      hhhhhh ss sssssss      sss      ssssss      sss sss
3f7oB      hhhhhh ss sssssss      sss      ssssss      sss sss

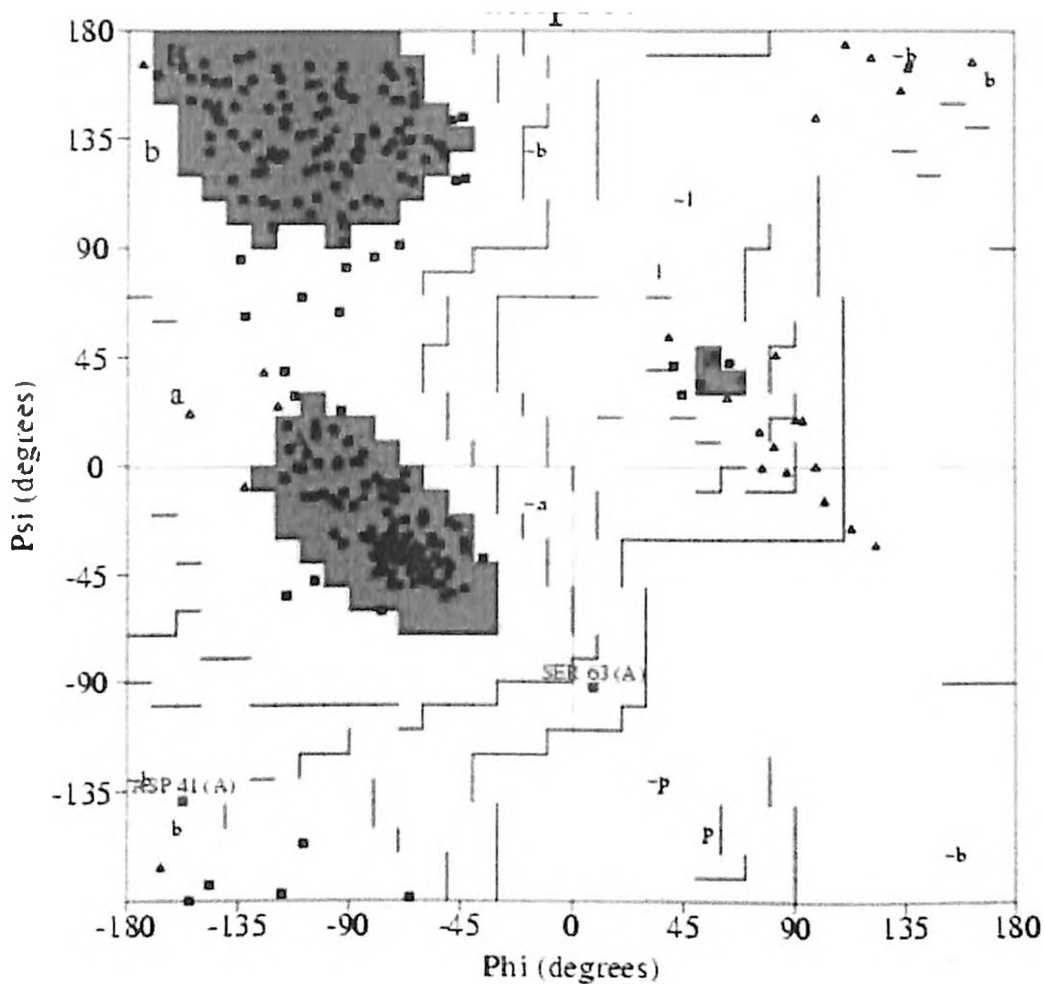
TARGET      197     GKVVDVFAPG QDILSAWIGS SSATNTISGT SMATPHIVGL SLYLALENL
3f7oB      199     gnlvdifapg snilstwigg --ttntisgt smatphivgl gaylaglegf

TARGET      sssss  sssss  sssss  hhhhhhhhhh hhhhhhh
3f7oB      sssss  sssss  sssss  hhhhhhhhhh hhhhhhh

TARGET      247     DGPAAVTKRI KELATKDVVK -DVKGSPNLL AYNGNA -

```

Figure A4.9 Pairwise alignment of the amino acid sequences of the target with those of template. Predicted protein secondary structures are also shown for each sequence (h for α -helices and s for β -sheets). (E-value: 6e-85; bit-score: 259; aligned-length: 98%; sequence identity: 53%)

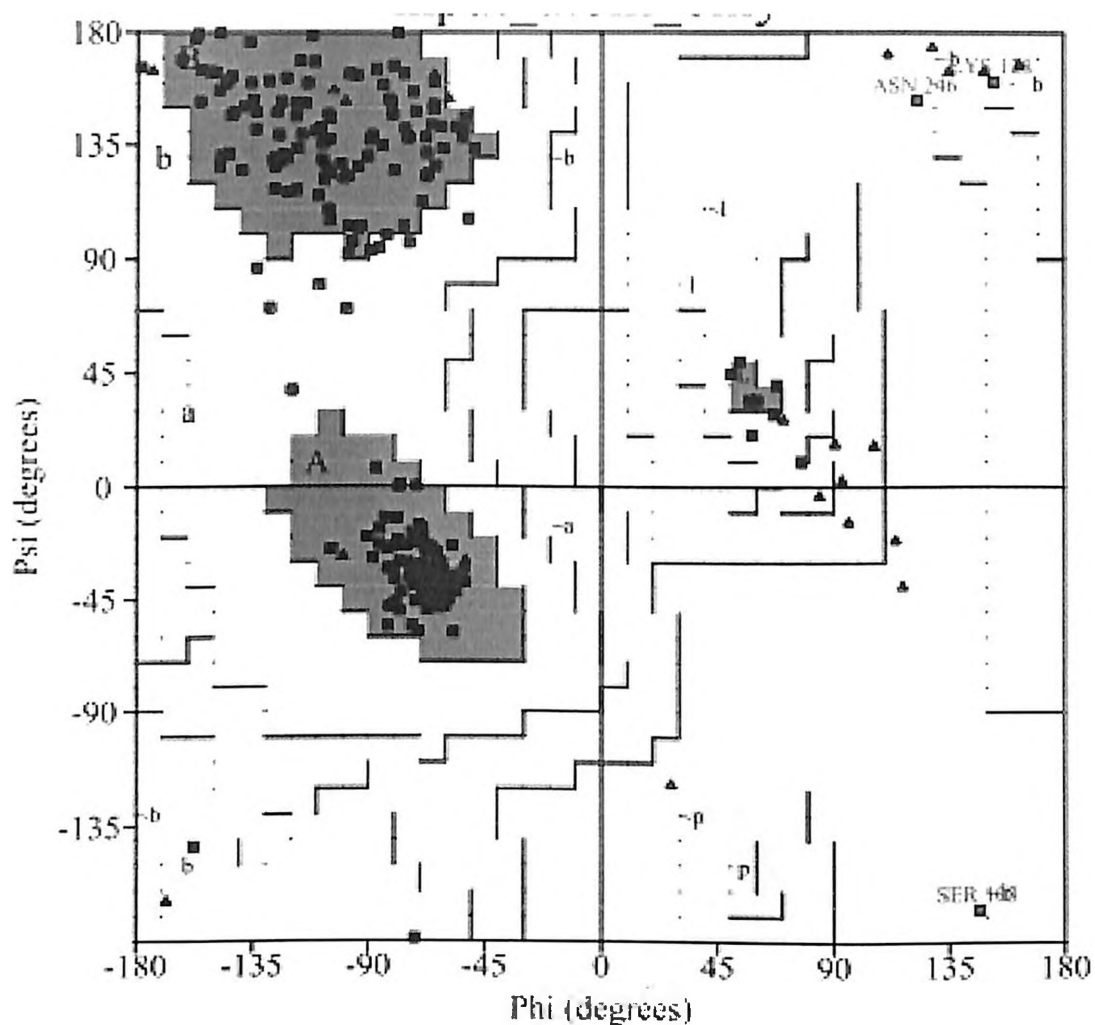


Plot statistics

Residues in most favoured regions [A,B,L]	202	88.2%
Residues in additional allowed regions [a,b,l,p]	25	10.9%
Residues in generously allowed regions [-a,-b,-l,-p]	2	0.9%
Residues in disallowed regions	0	0.0%
<hr/>		
Number of non-glycine and non-proline residues	229	100.0%
Number of end-residues (excl Gly and Pro)	3	
Number of glycine residues (shown as triangles)	43	
Number of proline residues	11	
<hr/>		
Total number of residues	256	

Based on an analysis of 115 structures of resolution of at least 2.0 Angstroms and R-factor no greater than 20%, a good quality model would be expected to have over 90% in the most favoured regions

Figure A4.10 Ramachandran plot for experimentally derived template structure (PDB ID:3F7O)



Plot statistics

Residues in most favoured regions [A,B,L]	224	92.2%
Residues in additional allowed regions [a,b,p]	16	6.6%
Residues in generously allowed regions [-a, -b, -l, -p]	1	0.4%
Residues in disallowed regions	2	0.8%
Number of non-glycine and non-proline residues	243	100.0%
Number of end-residues (e.g. Gly and Pro)	1	
Number of glycine residues (shown as triangles)	31	
Number of proline residues	7	
Total number of residues	282	

Based on an analysis of 114 structures of resolution of at least 2.0 Angstroms and R-factor no greater than 20% a good quality model would be expected to have over 90% in the most favoured regions.

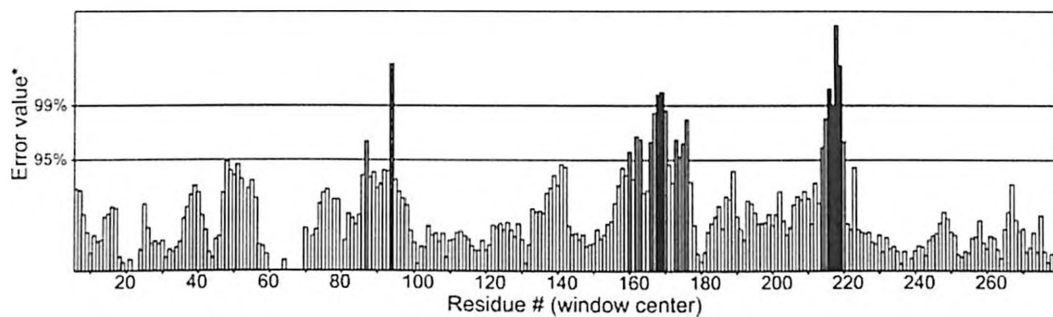
Figure A4.11 Ramachandran plot for protein model before minimization.

(a)

Program: ERRAT2

Chain#: 1

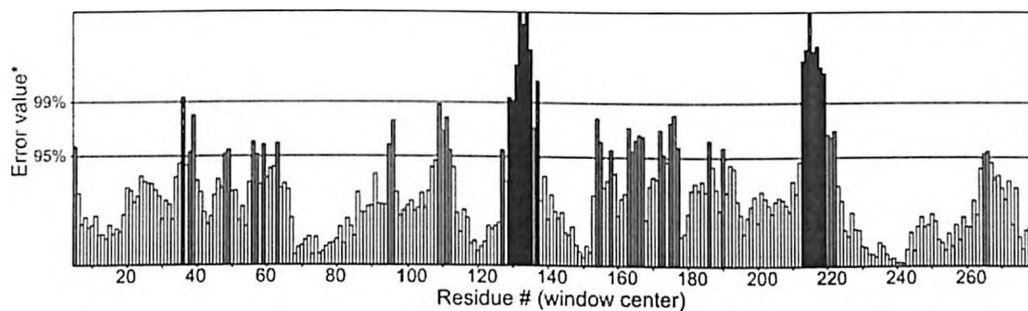
Overall quality factor**: 91.829



(b)

* Chain#: 1

Overall quality factor**: 80.657



(c)

Chain#: 1

Overall quality factor**: 92.754

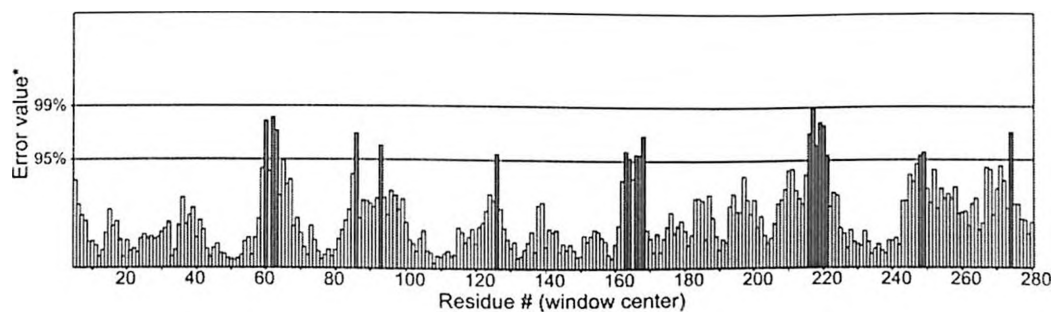


Figure A4.12 ERRAT score of (a) template; (b) before minimization and (c) after minimization.

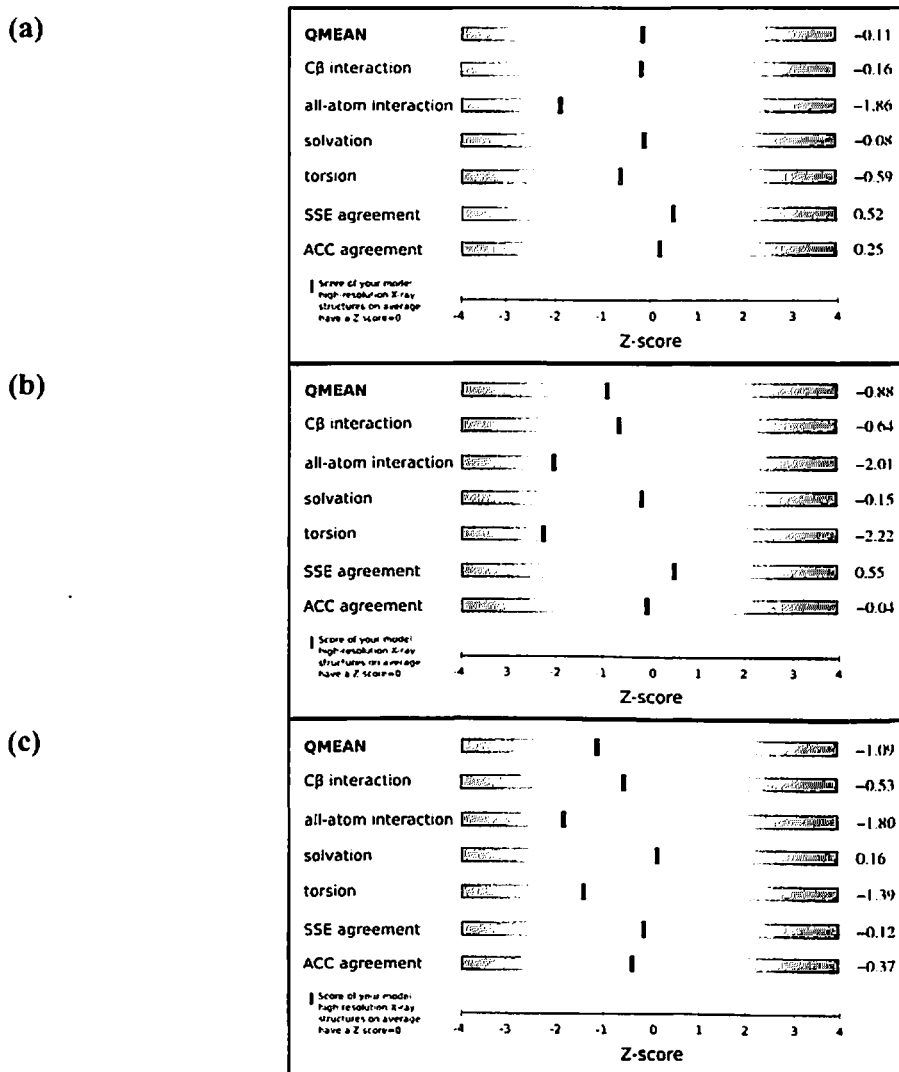
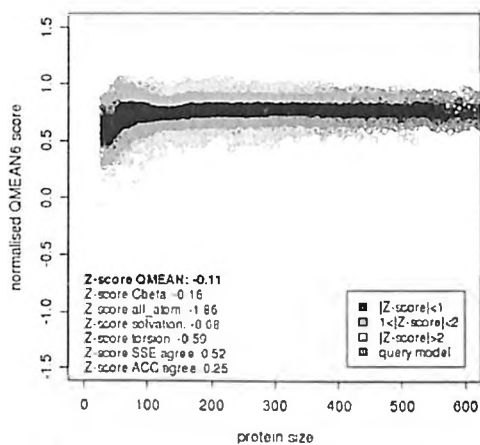
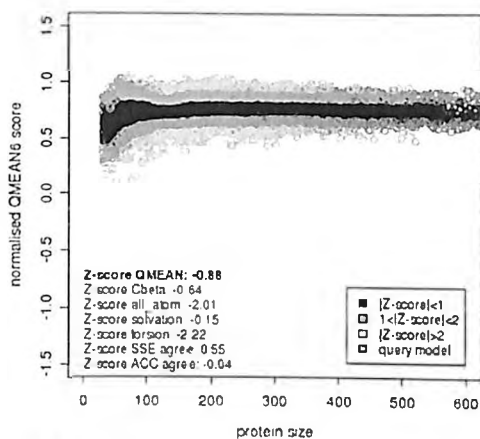


Figure A4.13 Plot showing Q-mean scores of (a) template; (b) before minimization and (c) after minimization. The calculations were carried out using structure assessment tool of Swiss-Model workspace.

(a)



(b)



(c)

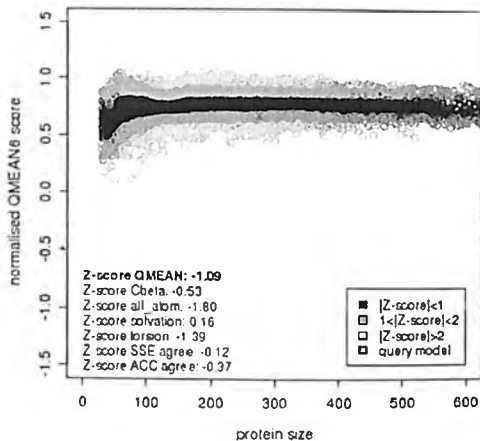


Figure A4.14 Z-scores of (a) template; (b) before minimization and (c) after minimization. The calculations were carried out using structure assessment tool of Swiss-Model workspace.

पेटेंट कार्यालय
का
शासकीय जर्नल

**OFFICIAL JOURNAL
OF
THE PATENT OFFICE**

निर्गमन सं. 20/2013
ISSUE NO. 20/2013

शुक्रवार
FRIDAY

दिनांक: 17/05/2013
DATE: 17/05/2013

पेटेंट कार्यालय का एक प्रकाशन
PUBLICATION OF THE PATENT OFFICE

Publication After 18 Months:

The following Patent Applications have been published under Section 11A (3) of The Patents (Amendment) Act, 2005. Any Person may file representation by way of opposition to the Controller of Patents at the appropriate office against the grant of the patent in the prescribed manner under section 25(1) of the Patents (Amendment) Act, 2005 read with the rule 55 of The Patents (Amendment) Rules, 2006:

(12) PATENT APPLICATION PUBLICATION (21) Application No.1439/DEL/2011 A
(19) INDIA
(22) Date of filing of Application :19/05/2011 (43) Publication Date : 17/05/2013

(54) Title of the invention : BIOSYNTHESIS OF ZINC OXIDE NANOPARTICLES

(51) International classification	:A61K	(71)Name of Applicant :
(31) Priority Document No	:NA	1)INDIAN COUNCIL OF AGRICULTURAL RESEARCH
(32) Priority Date	:NA	Address of Applicant :KRISHI BHAWAN, DR. RAJENDRA
(33) Name of priority country	:NA	PRASAD ROAD, NEW DELHI-110001 India
(86) International Application No	:NA	(72)Name of Inventor :
Filing Date	:NA	1)NAVIN JAIN
(87) International Publication No	:NA	2)ARPIT BHARGAVA
(61) Patent of Addition to Application Number	:NA	3)JITENDRA PANWAR
Filing Date	:NA	
(62) Divisional to Application Number	:NA	
Filing Date	:NA	

(57) Abstract :

The invention provides a low cost and eco-friendly method for synthesis of zinc oxide nanoparticles. The method comprises incubation of cell-free filtrate of fungus with an aqueous solution comprises of precursor zinc ions.

No. of Pages : 17 No. of Claims : 17

Extracellular biosynthesis and characterization of silver nanoparticles using *Aspergillus flavus* NJP08: A mechanism perspective

Navin Jain,^a Arpit Bhargava,^a Sonali Majumdar,^a J. C. Tarafdar^b and Jitendra Panwar^{*a}

Received 7th September 2010, Accepted 9th October 2010

DOI: 10.1039/c0nr00656d

The present study demonstrates an eco-friendly and low cost protocol for synthesis of silver nanoparticles using the cell-free filtrate of *Aspergillus flavus* NJP08 when supplied with aqueous silver (Ag⁺) ions. Identification of the fungal isolate was based on nuclear ribosomal DNA internal transcribed spacer (ITS) identities. Transmission electron microscopy (TEM) and energy dispersive spectroscopy (EDS) revealed the formation of spherical metallic silver nanoparticles. The average particle size calculated using Dynamic Light Scattering measurements (DLS) was found to be 17 ± 5.9 nm. UV-Visible and Fourier transform infrared (FTIR) spectroscopy confirmed the presence of extracellular proteins. SDS-PAGE profiles of the extracellular proteins showed the presence of two intense bands of 32 and 35 kDa, responsible for the synthesis and stability of silver nanoparticles, respectively. A probable mechanism behind the biosynthesis is discussed, which leads to the possibility of using the present protocol in future “nano-factories”.

Introduction

Nanotechnology has now started leaving the confines of laboratories; and conquering new applications to change our lives. Nanoparticles possess increased structural integrity as well as unique chemical, optical, mechanical, electronic and magnetic properties compared to large particles of bulk materials.¹ These unique properties are derived due to variations in specific characteristics such as size, distribution and structure of particles. Due to these incredible properties, nanoparticles have become significant in recent years and nano-products are coming to the market rapidly. The fast growing field of nanotechnology presents great potential to influence various sectors in the areas of energy, environment, agriculture, healthcare and consumer goods. Therefore, it has built great expectations not only in the academic community but also among the investors, governments, and industries. According to estimates, the worldwide nano product market is estimated to reach \$1 trillion by the year 2015.² To compete with this tremendous demand, the synthesis of nanomaterials of specific composition, shape and size is a burgeoning area of research in the field of nanotechnology.

Among various metals, silver has been known since ancient times as effective antimicrobial agent for the treatment of diseases, for food preservation and to keep water safe.³ With the recent advancements in the field of nanotechnology, silver nanoparticles have been widely used as a novel therapeutic agent extending their use as antibacterial, antifungal, antiviral, anti-inflammatory and anti-cancerous agents. The broad-spectrum antimicrobial properties of silver nanoparticles encourage its use in a large number of biomedical and environmental applications

as well as in growing list of cosmetics, clothing and numerous consumer products.^{4,5}

Conventional synthesis of silver nanoparticles involves a number of chemical and physical methods including chemical reduction in aqueous or non-aqueous solution,⁶ microemulsion,⁷ template,⁸ sonochemical,⁹ and microwave-assisted¹⁰ methods. However, all these methods are energy and capital intensive, employ toxic chemicals, and often yield particles in non-polar organic solutions, thus precluding their biomedical applications. Thus the need for the development of clean, reliable, biocompatible and benign processes to synthesize nanoparticles leads to turning of more and more researchers to exploit biological systems as possible eco-friendly “nano-factories”.

It is well known that the biological systems can provide a number of metal or metal-containing particles in the nanometre range. Thus, they can be seen as a nanophase system in their own right and as the starting point for producing other novel nanophase systems. Biological methods for nanoparticle synthesis would help circumvent many of the detrimental features by enabling synthesis at mild pH, pressure and temperature and at a substantially lower cost. A number of micro-organisms have been found to be capable of synthesizing inorganic nanocomposites either intra- or extracellularly. These include magnetotactic bacteria,^{11,12} silica deposits by diatoms,¹³ and gypsum and calcium layers by S-layer bacteria.¹⁴ The secrets gleaned from nature combined with academic and scientific curiosity have led to the development of biomimetic approaches for the synthesis of nanoparticles.

Whilst various studies have been commenced on identification of microorganisms as possible nanofactories,¹⁵ very little work has been conducted on the actual mechanisms of nanoparticle formation in microorganisms. The defensive mechanism of cells for silver detoxification has been suggested as a biological pathway for the synthesis of silver nanoparticles.¹⁶ Ahmad *et al.* had shown that NADH-dependent enzymes are responsible for the biosynthesis of nanoparticles.¹⁷ The reduction mechanism

^aCentre for Biotechnology, Department of Biological Sciences, Birla Institute of Technology and Science, Pilani, Rajasthan, 333031, India. E-mail: drjitendrapanwar@yahoo.co.in; Fax: +911596244183; Tel: +919414411654

^bCentral Arid Zone Research Institute, Jodhpur, Rajasthan, 342003, India

seems to be initiated by electron transfer from the NADH by NADH-dependent reductase as electron carrier.

Recent studies demonstrated that the nitrate reductase enzyme system can be responsible for the bioreduction which leads to formation of silver nanoparticles.¹⁸ Similarly, studies with *Fusarium oxysporum* has shown that the reduction of silver ions occurs by a nitrate-dependent reductase and a shuttle quinone extracellular process.¹⁹ However, the exact mechanism of the formation of silver nanoparticles is yet to be elucidated.

In the present study, learning from nature's own sustainable way of bioremediation of the metal ions, we have utilized a soil fungal isolate *Aspergillus flavus* NJP08 to develop an eco-friendly and low cost protocol for the extracellular synthesis of silver nanoparticles. The plausible mechanism behind the synthesis of silver nanoparticles and their subsequent stabilization via capping proteins is discussed.

Experimental

Materials

All chemicals were of analytical grade and procured from Sigma Aldrich (India) or Merck (India) unless otherwise stated. All culture media were purchased from HiMedia (India). Standard protein molecular weight marker (SM-0431) was obtained from MBI Fermentas, USA.

Isolation and identification of fungal isolate

The fungal isolate was isolated from metal-rich regions of Udaipur, Rajasthan, India (24°21'35"N and 73°44'15"E). Soil samples were used as inoculums for serial dilution technique and plated on Martin Rose Bengal Agar media. The plates were incubated at 28 °C for 4 days. Individual fungal colonies were picked and further purified by sub-culturing on Potato Dextrose Agar (PDA) media.

The identification of the fungal isolate was carried out by morphological and microscopic observations (such as color, texture of the mycelia, spore formation pattern, etc.) followed by nuclear ribosomal DNA internal transcribed spacer (ITS) sequencing. The genomic DNA was isolated by CTAB extraction method using standard protocols.²⁰ Internal transcribed spacer (ITS) regions were amplified using primers ITS1 and ITS4 with 5'-TCCGTAGGTGAACCTGCGG and 5'-TCCTCCGC-TTATTGATATGC sequences respectively.²¹ PCR amplified products were sequenced using ABI prism DNA sequencer by BigDye terminator method. The resulting sequence was entered into the BLAST algorithm of National Centre of Biological Information (NCBI) database to obtain closely related phylogenetic sequences. The phylogenetic tree was constructed using Neighbor Joining method in Mega 4.0 software.²² The substitution model was based on Jukes and Cantor.²³

Extracellular biosynthesis of silver nanoparticles

The fungal isolate was maintained on PDA slants (pH 5.6) at 28 °C with regular sub-culturing on fresh media. The stock culture (4 days old) was inoculated in 100ml of MGYP medium (0.3% malt extract, 1.0% glucose, 0.3% yeast extract, 0.5% peptone; pH 7.0) in 250 ml Erlenmeyer flasks. The inoculated

flasks were then incubated at 28 °C for 4 days on a rotary shaker (150 rpm). Fungal mycelium were separated from the culture medium by centrifugation (8000 rpm, 10 min, and 4 °C) and washed thrice with sterile water. Typically, 10 g of biomass (fresh weight) was resuspended in 100 ml of sterile deionized Milli-Q water and further incubated for 72 h in an Erlenmeyer flask and agitated in similar conditions as described earlier. After incubation, biomass was separated by filtration using Whatman filter paper no. 1 and the cell-free filtrate was obtained. For synthesis of silver nanoparticles, aqueous silver nitrate solution at a final concentration of 1.0 mM was added to the reaction vessels containing cell-free filtrate and incubated at 28 °C on a rotary shaker (150 rpm) without light. Controls containing cell-free filtrate (without silver nitrate) as positive and pure silver nitrate solution (without cell-free filtrate) as negative controls were also run simultaneously along with the experimental flask in three replicates.

Characterization of silver nanoparticles

UV-Visible spectroscopy analysis. Change in color was visually observed in the silver nitrate solution incubated with *Aspergillus flavus* NJP08. The bioreduction of precursor silver ions was monitored by sampling of aliquots (1 ml) at different time intervals. Absorption measurements were carried out on Jasco V-630 UV-Visible Spectrophotometer at a resolution of 1 nm. UV-Vis. analysis of several weeks old samples was also carried out to check the stability of silver nanoparticles.

FTIR spectroscopy analysis. For Fourier transform infrared (FTIR) spectroscopy measurements, the bio-transformed products present in cell-free filtrate were freeze-dried and diluted with potassium bromide in the ratio of 1 : 100. FTIR spectrum of samples was recorded on Shimadzu IR Prestige-21 FTIR instrument with a diffuse reflectance mode (DRS-8000) attachment. All measurements were carried out in the range of 400–4000 cm⁻¹ at a resolution of 4 cm⁻¹.

TEM, HR-TEM and SAED analysis. For transmission electron microscope (TEM) measurements, a drop of solution containing as-synthesized silver nanoparticles was placed on the carbon coated copper grids and kept under vacuum desiccation for overnight before loading them onto a specimen holder. TEM micrographs were taken by analyzing the prepared grids on Hitachi H-7650 TEM instrument using low voltage (100 kV).

High-resolution transmission electron microscope (HR-TEM) micrographs of the sample were taken using the JEOL-2100 TEM instrument having selected area electron diffraction (SAED) attachment. The instrument was operated at an accelerating voltage of 200 kV.

EDS analysis. For energy dispersive spectroscopy (EDS) samples were prepared on a copper substrate by drop coating of silver nanoparticles. Elemental analysis on single particles was carried out using Thermo Noran EDS attachment equipped with TEM.

Particle size (DLS) analysis. The particle size distribution of silver nanoparticles was evaluated using dynamic light scattering

(DLS) measurements conducted with a Malvern Zetasizer Nanoseries compact scattering spectrometer (Malvern Instruments Ltd, Malvern, UK). Data obtained were analyzed using Zetasizer software.

Protein purification and one dimensional gel electrophoresis

For the purification of proteins from aqueous cell-free filtrate, solid ammonium sulfate was added slowly to control solutions containing extracellular proteins at a final concentration of 80% (w/v). The mixture was gently stirred for overnight at 4 °C. The resulting precipitate was subsequently collected by centrifugation at 12 000 rpm for 10 min at 4 °C. The protein obtained thereafter were resuspended in copious amount of water and dialyzed using a 12-kDa cut off dialysis bag made up of cellulose acetate membrane. The dialysis bag was pre-treated as per the manufacturer's instructions. The bag was then suspended in dialysis buffer (50 mM phosphate buffer, pH 7.2) and stirred slowly. The dialysis buffer was changed 3–4 times over a 24 h period. The dialyzed protein fraction was further analyzed by one dimensional SDS-PAGE (sodium dodecyl sulfate–polyacrylamide gel electrophoresis) as per standard procedure with adequate modifications.²⁴ All samples were denatured in sample buffer containing 60 mM Tris (pH 6.8), 25% glycerol, 2% SDS, 14.4 mM 2-mercaptoethanol, 0.1% bromophenol blue and boiled for 5 min, followed by centrifugation at 8000 rpm for 1 min at 4 °C. Stained molecular weight marker was run along with samples. Electrophoresis was performed using Bio-Rad Mini Protean gel system at a constant voltage of 100 kV for 120 min. After electrophoresis, the gel was stained with Coomassie Brilliant Blue dye and was observed in a gel imaging system (Bio-Rad, USA).

In order to investigate the proteins which are bound to the surface of silver nanoparticles, samples were boiled with 1% SDS solution for 10 min followed by centrifugation at 8000 rpm for 10 min for collection of supernatant. The SDS- treated and untreated samples were further analyzed by the 12% SDS-PAGE as described earlier.

Results and discussion

Identification of fungal isolate

It is pre-requisite to identify the fungal isolate up to the species level in order to fully understand its nanoparticle synthesis mechanism. Amplification and sequencing of fungal rRNA gene resulted in 564 bp long nucleotide sequence, which has been deposited in NCBI GenBank (Accession Number: HM222933). The sequence was compared using BLAST algorithm and the closely related sequences were selected followed by their analysis using molecular evolutionary computing software MEGA 4.0. The phylogenetic tree was constructed which confirms that strain NJP08 exhibited 100% similarity with *Aspergillus flavus* (Fig. 1).

Characterization of silver nanoparticles

Fig. 2 shows Erlenmeyer flasks containing the cell-free filtrate of *Aspergillus flavus* NJP08 without (A) and with silver nitrate (B) after completion of reaction at 72 h. The flask containing silver nitrate solution showed gradual change in color of reaction

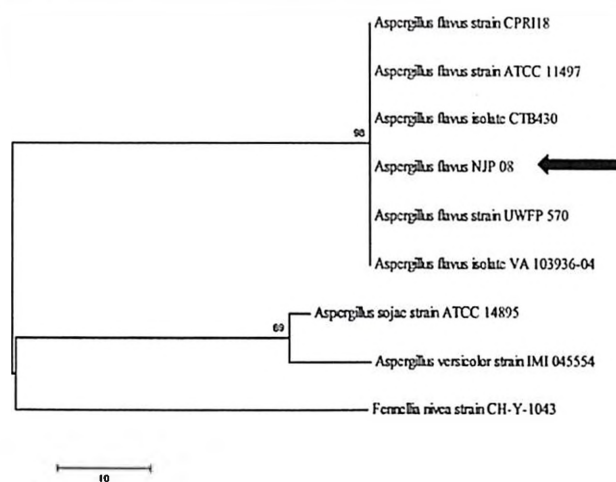


Fig. 1 Phylogenetic tree showing genetic relationship between the isolate *Aspergillus flavus* NJP08 and other closely related reference microorganisms. Scale bar represents 10 nucleotide substitutions.

mixture from colorless to brown with intensity increasing during the incubation period. The negative control (pure silver nitrate solution without cell-free filtrate) did not show the characteristic change in color indicating that the synthesis is not a thermal and temporal process.

UV-visible spectroscopy is one of the most widely used techniques for structural characterization of silver nanoparticles. The bio-transformed products were simultaneously characterized by UV-Vis. spectroscopy measurements performed at different time intervals to study the change in light absorption profile of the solution and increase in intensity. The absorption spectra of nanoparticles showed highly symmetric single-band absorption with peak maximum at ca. 421 nm with steadily increased in intensity as a function of time of reaction without any shift in the peak (Fig. 3). This indicates the presence of silver nanoparticles which is due to the excitation of surface plasmons; typical of silver nanoparticles.²⁵ Inset to Fig. 3 represents the plot of absorbance at 420 nm at different time intervals of reaction. After 72 h of incubation, no further increase in intensity was recorded indicating complete reduction of precursor silver ions.

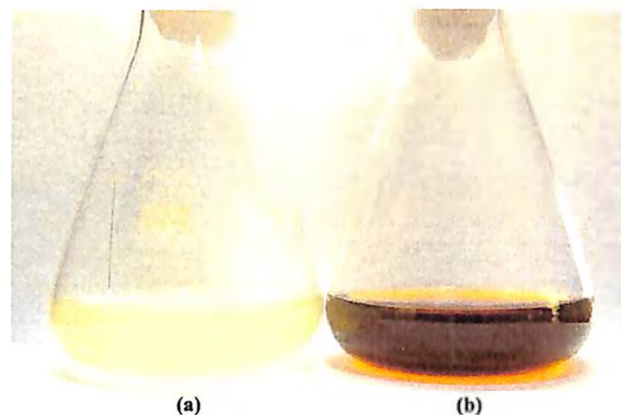


Fig. 2 Erlenmeyer flask containing cell-free filtrate of *Aspergillus flavus* NJP08 without (a) and with (b) silver nitrate solution (1 mM) after 72 h of reaction.

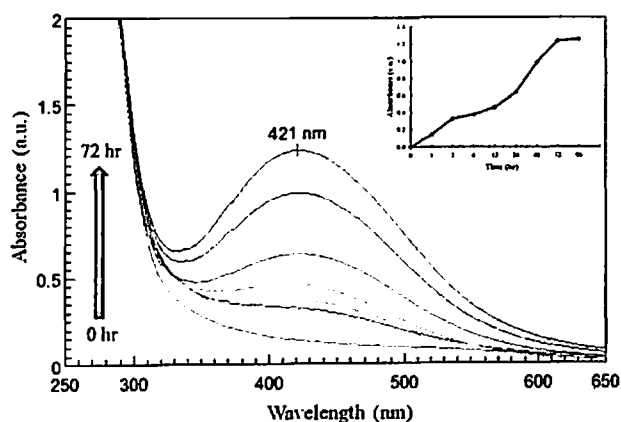


Fig. 3 UV-Vis. spectra of cell free filtrate as a function of time. Arrow represents time of reaction (0, 3, 6, 12, 24, 48 and 72 h) with respective curves. Inset graph shows reaction saturation curve.

It is observed that the graph follows the sigmoid kinetics which is characteristic of enzyme catalysis reactions. The kinetics of silver nanoparticles formation showed that more than 85% of the particles were formed within the 48 h of the reaction which suggests that the formation of silver nanoparticles is exponential in nature.

Fig. 4 shows the UV-Vis. spectrum recorded from the reaction vessel after 72 h of reaction. An absorption peak at *ca.* 280 nm was observed which corresponds to aromatic amino acids of proteins (Fig. 4). It is well known that the absorbance peak at 280 nm arises due to electronic excitations in tyrosine and tryptophan residues of the protein.^{26,27} This observation indicates the presence of proteins secreted by fungus in the cell-free filtrate. The particles in the solution are thus stabilized by the capping agent that is likely to be proteins present in the cell-free filtrate.

Stability of as-synthesized silver nanoparticles was monitored regularly for more than four months of completion of reaction. It was observed that the nanoparticle solution was extremely stable at room temperature, with no evidence of flocculation of particles as determined by UV-Vis. spectroscopy measurements. This indicates that the nanoparticles were well dispersed in the solution without aggregation. Monodispersity and chemical stability

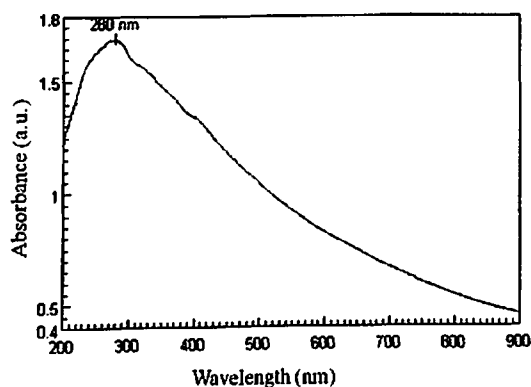


Fig. 4 UV-Vis. spectra of cell-free filtrate showing presence of proteins. The absorption maxima at 280 nm arise due to electronic excitations in tyrosine and tryptophan residues of proteins.

are highly desirable characteristics of the nanoparticles.²⁸ This is an important aspect of synthesis of nanoparticles, since the lack of sufficient stability of many nanoparticles preparation has to some extent impeded the development of the real world applications of nanomaterials.²⁹

FTIR measurements of the freeze-dried samples were carried out to identify the possible interactions between silver and bioactive molecules, which may be responsible for synthesis and stabilization (capping material) of silver nanoparticles. The amide linkages between amino acid residues in proteins give rise to well known signatures in the infrared region of the electromagnetic spectrum. FTIR spectrum reveals two bands at 1647 and 1543 cm^{-1} that corresponds to the bending vibrations of the amide I and amide II bands of the proteins respectively; while their corresponding stretching vibrations were seen at 3302 and 2926 cm^{-1} respectively (Fig. 5). The presence of the signature peaks of amino acids supports the presence of proteins in cell-free filtrate as observed in UV-Vis. spectra.

It is well known that protein-nanoparticle interactions can occur either through free amine groups or cysteine residues in proteins and *via* the electrostatic attraction of negatively charged carboxylate groups in enzymes.³⁰ The two bands observed at 1381 and 1032 cm^{-1} can be assigned to the C-N stretching vibrations of the aromatic and aliphatic amines, respectively.³¹ These observations indicate the presence and binding of proteins with silver nanoparticles which can lead to their possible stabilization. FTIR results revealed that secondary structure of proteins have not been affected as a consequence of reaction with silver ions or binding with silver nanoparticles. It is important to understand though, that it is not just the size and shape of proteins, but the conformation of protein molecules that plays an important role.

TEM measurements were used to determine the morphology and shape of nanoparticles. Low magnification TEM micrographs (Fig. 6a) revealed that the particles are spherical in shape and uniformly distributed (monodispersed) without significant agglomeration. The particle size histogram (Fig. 7a) of silver nanoparticles shows that the particle size ranges from 10 to 35 nm and possess an average size of 17 ± 5.9 nm, although very tiny particles (*ca.* 5–10 nm) have also been observed that may be due to vigorous shaking. The frequency distribution observed from the histogram shows that almost 80% of the particles are in the 10- to 25-nm range. These results are in agreement with the values obtained by DLS measurements as shown in Fig. 7b.

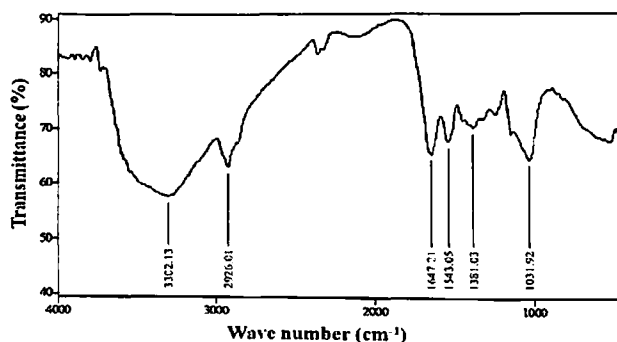
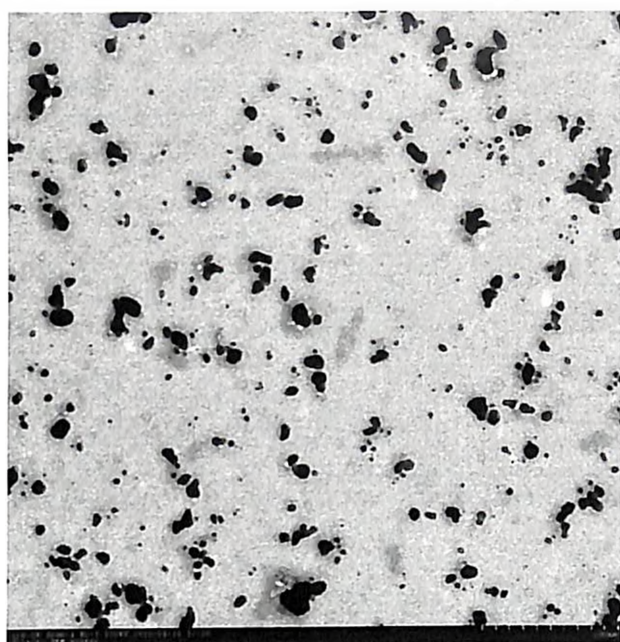
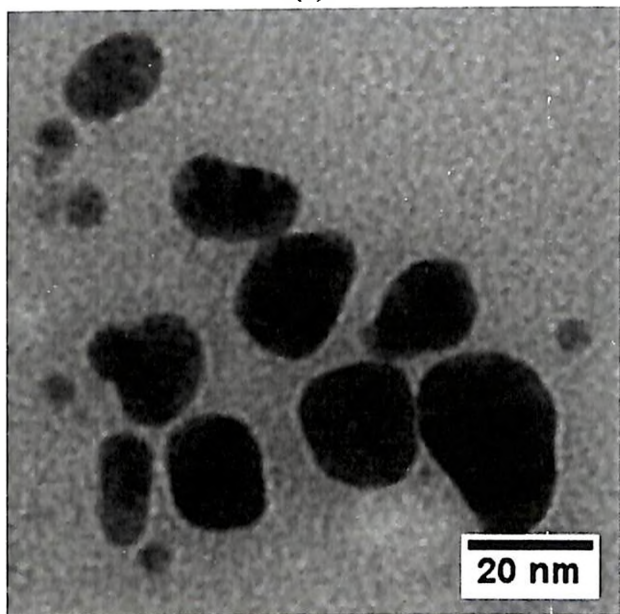


Fig. 5 FTIR spectra of freeze-dried powder of silver nanoparticles.



(a)



(b)

Fig. 6 TEM micrographs showing uniformly distributed silver nanoparticles. (a) Low magnification image and (b) high magnification image.

The structural features of the individual silver nanoparticles can be observed more clearly in the HR-TEM images (Fig. 8). The particles are predominantly spherical with round edges and no sign of crystal defects. The inset to Fig. 8 shows the selected area electron diffraction (SAED) pattern from one of the silver nanoparticles which confirms the plane (111) of silver nanoparticles. The lattice fringes observed in micrograph also supports the crystalline nature of silver nanoparticles.

An EDS spectrum of drop coated film of silver nanoparticles is shown in Fig. 9. The presence of an optical absorption band at

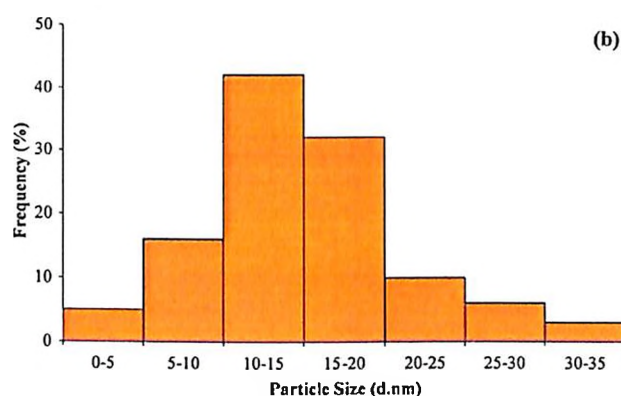
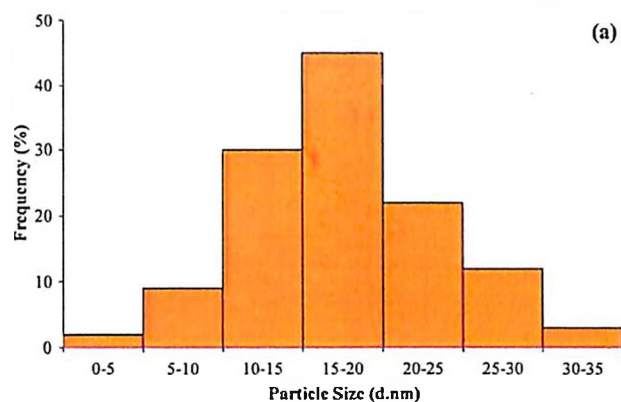


Fig. 7 Particle size distribution histogram of silver nanoparticles from (a) transmission electron microscope (TEM) analysis and (b) particle size (DLS) analysis.

~ 3 eV reveals the presence of pure metallic silver nanoparticles.³² The spectrum shows mainly Ag (59 atom%) and only minor amounts of other elements with Nb (8.99 atom%) being the largest. Apart from this, the signals for C, N and O indicate the presence of proteins as a capping material on the surface of silver nanoparticles.

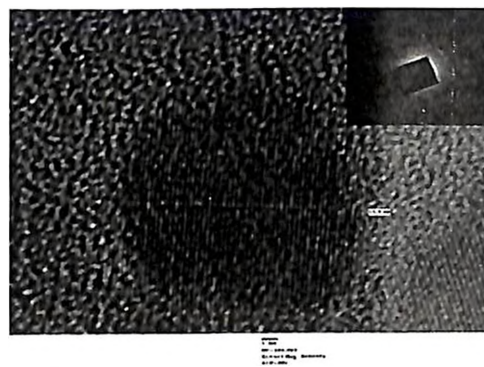


Fig. 8 HR-TEM micrograph showing spherical shape of silver nanoparticle. Inset showing SAED pattern recorded from silver nanoparticle; the spot array is from [111] beam direction for a fcc crystal.

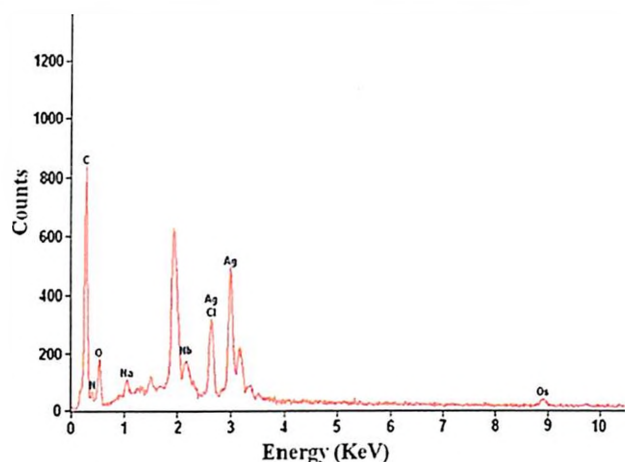


Fig. 9 EDS spectrum showing the presence of elemental silver.

Role of fungal proteins

Fungi are very well known to secrete large amount of proteins which play a major role in their life cycle. The majority of these proteins include hydrolytic enzymes such as amylases, cellulases and proteases.³³ Most of the proteomic studies have focused on the proteins involved in the metabolic pathways, however, other proteins and their role still remains unknown.

To identify the fungal proteins responsible for synthesis of silver nanoparticles, the cell-free filtrate was salted out overnight at 4 °C using ammonium sulfate precipitation method followed by centrifugation. The pellet fraction was subsequently dialyzed using a 12-kDa cut-off membrane. The protein profiles were compared by one dimensional SDS-PAGE followed by Coomassie Brilliant Blue staining (Fig. 10). The protein fraction clearly showed presence of two intense bands of 35 and 32 kDa (bands highlighted by arrows in Fig. 10, lane 2). These proteins

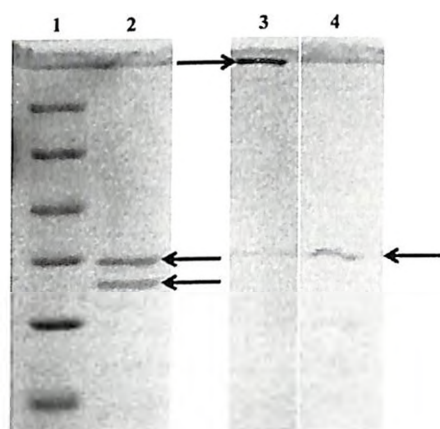


Fig. 10 SDS-PAGE analysis of purified extracellular proteins secreted from *Aspergillus flavus* NJP08. Lane 1, molecular size marker (116.0 kDa β -galactosidase; 66.2 kDa, bovine serum albumin; 45 kDa, ovalbumin; 35 kDa, lactate dehydrogenase; 25 kDa, REase Bsp 98I; 18.4 kDa, β -lactoglobulin; 14.4 kDa, lysozyme). Lane 2, purified extracellular proteins. The arrows highlighted in Lane 2 indicate two intense bands of 35 and 32 kDa proteins. Protein profile bound to silver nanoparticles before (Lane 3) and after (Lane 4) boiling in 1% SDS solution.

can be responsible for the synthesis as well as stability of silver nanoparticles. Similarly, studies with *Fusarium oxysporum* showed presence of two extracellular proteins having molecular weight of 24 and 28 kDa responsible for the synthesis of zirconia nanoparticles.³⁴

In order to identify the proteins bound to the surface of silver nanoparticles, the as-synthesized silver nanoparticles were treated with 1% SDS solution in boiling water bath for 10 min. SDS act as a denaturing agent and its treatment results in detachment of the surface bounded proteins from nanoparticles. The treated and un-treated samples were analyzed by 12% SDS-PAGE as described earlier. An intense band was observed at the transition of the stacking and resolving gel containing un-treated samples showing silver deposition (Fig. 10, lane 3). It can be predicted that the strong interactions between protein and nanoparticles prevent the migration of proteins into the resolving gel. Interestingly, the SDS treated samples showed the presence of a single intense band of ca. 35 kDa which is similar to the protein band present in lane 1 (Fig. 10, lane 4). Thus, it can be proposed that this 35 kDa protein acts as a capping material and confers stability to the silver nanoparticles. Further studies are in progress to understand the actual mechanism behind the synthesis and stability of silver nanoparticles. Efforts are underway in our laboratory to purify and characterize these two proteins.

Based on these experimental findings, a schematic presentation of the possible mechanism for synthesis of silver nanoparticles is speculated (Fig. 11). The synthesis process occurs in two steps: firstly, reduction of bulk silver ions into silver nanoparticles and, secondly, capping of the as-synthesized nanoparticles. The first step involves a 32 kDa protein which may be a reductase secreted by the fungal isolate, which may be specific for reduction of silver ions into silver nanoparticles. The second step involves 35 kDa proteins which bind with nanoparticles and confer stability. The protein-nanoparticle interactions can play a very significant role in providing stability to nanoparticles. Previous studies had also shown that the proteins bound to nanoparticle surface

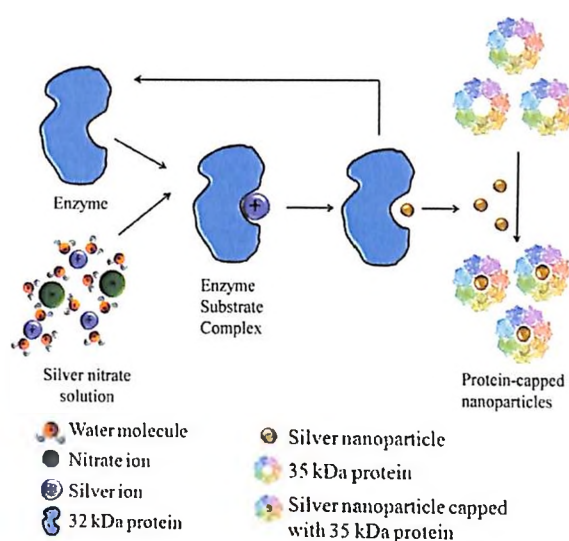


Fig. 11 Mechanism showing the role of extracellular proteins in the synthesis of silver nanoparticles.

immediately upon contact with the nanoparticles.³⁵ The protein adsorption has been widely studied and it has been found that protein adsorption depends on various factors such as electrostatic, hydrophobic and specific chemical interactions between the protein and the adsorbent.³⁶ FTIR results obtained during the present study also revealed that the carbonyl groups from amino acid residues and peptides of proteins have strong affinity to bind metal. However, the interaction between protein and nanoparticles is still not completely understood.

This is the first report showing an immense study on the proteins responsible for the synthesis and stability (capping agent) of silver nanoparticles using the fungus *Aspergillus flavus* NJP08. The present study suggests that a protein with a molecular weight of 32 kDa may be responsible for the synthesis and one of 35 kDa is responsible for the stability of silver nanoparticles.

Conclusion

An eco-friendly and low cost protocol for biosynthesis of silver nanoparticles using cell-free filtrate of *Aspergillus flavus* NJP08 has been demonstrated. The formation of silver nanoparticles in extracellular secretion at room temperature can be easily handled during downstream processing. Since, the nanoparticles formed outside the cell are devoid of unnecessary cellular components, they can be directly used in various biomedical applications. The possibility of proteins as a stabilizing agent in silver nanoparticles is revealed by UV-Vis. spectroscopy and FTIR analysis. As a step towards understanding the mechanism of silver nanoparticles, the protein profile of the cell-free filtrate was analyzed. SDS-PAGE profiles of the extracellular proteins showed the presence of two intense bands of 32 and 35 kDa which are responsible for the synthesis and stability of silver nanoparticles, respectively. Efforts are underway in our laboratory to purify and characterize these two proteins to understand their mode of action and possible interactions with silver nanoparticles. Understanding the protein-nanoparticle interactions during the synthesis mechanism will lead to the possibility of using present system as future "nano-factories". The possibility of rational use of this fungal strain isolated from metal-rich soils in synthesis of other important metal nanoparticles is an exciting and enormous future possibility.

Acknowledgements

This research work was financially supported by the Indian Council of Agricultural Research, Government of India under the National Agricultural Innovation Project scheme (NAIP/C4/C-2032). Facilities provided by the Electron Microscopy & Nanoscience Laboratory, Punjab Agricultural University, Ludhiana are gratefully acknowledged. Navin Jain thanks the Council of Scientific and Industrial Research, Government of India for providing a research fellowship.

Notes and references

- B. Bhushan, in *Springer Handbook of Nanotechnology*, Springer-Verlag Berlin, Heidelberg, 2004.
- M. C. Roco, *J. Nanopart. Res.*, 2005, **7**, 707–712.
- S. Silver, *FEMS Microbiol. Rev.*, 2003, **27**, 341–353.
- M. Rai, A. Yadav and A. Gade, *Biotechnol. Adv.*, 2009, **27**, 76–83.
- C. Marambio-Jones and E. Hoek, *J. Nanopart. Res.*, 2010, **12**, 1531–1551.
- C. Petit, P. Lixon and M. P. Pileni, *J. Phys. Chem.*, 1993, **97**, 12974–12983.
- J. N. Solanki and Z. V. P. Murthy, *Colloids Surf., A*, 2010, **359**, 31–38.
- S. Chen and D. L. Carroll, *Nano Lett.*, 2002, **2**, 1003–1007.
- V. G. Pol, D. N. Srivastava, O. Palchik, V. Palchik, M. A. Slifkin, A. M. Weiss and A. Gedanken, *Langmuir*, 2002, **18**, 3352–3357.
- X. Li, L. Wang and X. Lu, *J. Hazard. Mater.*, 2010, **177**, 639–647.
- D. R. Loveley, J. F. Stolz, G. L. Nord and E. J. P. Phillips, *Nature*, 1987, **330**, 252–254.
- D. P. E. Dickson, *J. Magn. Magn. Mater.*, 1999, **203**, 46–49.
- N. Kroger, R. Deutzmann and M. Sumper, *Science*, 1999, **286**, 1129–1132.
- D. Pum and U. B. Sleytr, *Trends Biotechnol.*, 1999, **17**, 8–12.
- K. N. Thakkar, S. S. Mhatre, Y. Rasesh and R. Y. Parikh, *Nanomed.: Nanotechnol., Biol. Med.*, 2010, **6**, 257–262.
- T. Klaus, R. Joerger, E. Olsson and C. G. Granqvist, *Proc. Natl. Acad. Sci. U. S. A.*, 1999, **96**, 13611–13614.
- A. Ahmad, P. Mukherjee, S. Senapati, D. Mandal, M. I. Khan, R. Kumar and M. Sastry, *Colloids Surf., B*, 2003, **28**, 313–318.
- S. Anil Kumar, M. K. Abyaneh, S. W. Gosavi, S. K. Kulkarni, R. Pasricha, A. Ahmad and M. I. Khan, *Biotechnol. Lett.*, 2007, **29**, 439–445.
- N. Duran, P. D. Marcato, O. L. Alves, G. I. De Souza and E. Esposito, *J. Nanobiotechnol.*, 2005, **3**, 8.
- J. Sambrook, E. F. Fritsch and T. Maniatis, *Molecular Cloning: A Laboratory Manual*, Cold Spring Harbour Laboratory Press, New York, 1989.
- T. White, T. Bruns, S. Lee and J. Taylor, *PCR Protocols: A Guide to Methods and Applications*, ed. M. A. Innis, D. H. Gelfand, J. J. Shinsky, T. J. White, Academic Press, San Diego, 1990, pp. 315–322.
- S. Kumar, J. Dudley, M. Nei and K. Tamura, *Briefings Bioinf.*, 2008, **9**, 299–306.
- T. H. Jukes and C. R. Cantor, in *Mammalian Protein Metabolism*, ed. H. N. Munro, Academic Press, New York, 1969, pp. 121–123.
- U. K. Laemmli, *Nature*, 1970, **227**, 680–685.
- S. Gurunathan, K. Kalishwaralal, R. Vaidyanathan, D. Venkataraman, S. R. K. Pandian, J. Muniyandi, N. Hariharan and S. H. Eom, *Colloids Surf., B*, 2009, **74**, 328–335.
- J. Xie, J. Y. Lee, D. I. C. Wang and Y. P. Ting, *ACS Nano*, 2007, **1**, 429–439.
- N. Saifuddin, C. W. Wong and A. A. Nur Yasumira, *E-J. Chem.*, 2009, **6**, 61–70.
- K. C. Bhainsa and S. F. D'Souza, *Colloids Surf., B*, 2006, **47**, 160–164.
- S. S. Shankar, A. Ahmad, R. Pasricha and M. Sastry, *J. Mater. Chem.*, 2003, **13**, 1822–1826.
- A. Gole, C. Dash, V. Ramakrishnan, S. R. Sainkar, A. B. Mandale, M. Rao and M. Sastry, *Langmuir*, 2001, **17**, 1674–1679.
- N. Vigneshwaran, A. A. Katha, P. V. Varadarajan, R. P. Nachane and R. H. Balasubramanya, *Langmuir*, 2007, **23**, 7113–7117.
- P. Magudapathy, P. Gangopadhyay, B. K. Panigrahi, K. G. M. Nair and S. Dhara, *Phys. B*, 2001, **299**, 142–146.
- J. F. Peberdy, *Trends Biotechnol.*, 1994, **12**, 50–57.
- V. Bansal, D. Rautaray, A. Ahmad and M. Sastry, *J. Mater. Chem.*, 2004, **14**, 3303–3305.
- J. L. Elechiguerra, J. L. Burt, J. R. Morones, A. Camacho-Bragado, X. Gao, H. H. Lara and M. J. Yacaman, *J. Nanobiotechnol.*, 2005, **3**, 6.
- Lynch and K. A. Dawson, *Nano Today*, 2008, **3**, 40–47.

A biomimetic approach towards synthesis of zinc oxide nanoparticles

Navin Jain · Arpit Bhargava · Jagadish C. Tarafdar ·
Sunil K. Singh · Jitendra Panwar

Received: 7 October 2011 / Revised: 30 January 2012 / Accepted: 30 January 2012 / Published online: 1 March 2012
© Springer-Verlag 2012

Abstract Using natural processes as inspiration, the present study demonstrates a positive correlation between zinc metal tolerance ability of a soil fungus and its potential for the synthesis of zinc oxide (ZnO) nanoparticles. A total of 19 fungal cultures were isolated from the rhizospheric soils of plants naturally growing at a zinc mine area in India and identified on the genus, respectively the species level. *Aspergillus aeneus* isolate NJP12 has been shown to have a high zinc metal tolerance ability and a potential for extracellular synthesis of ZnO nanoparticles under ambient conditions. UV–visible spectroscopy, Fourier transform infrared spectroscopy, X-ray diffraction analysis, transmission electron microscopy, and energy dispersive spectroscopy studies further confirmed the crystallinity, morphology, and composition of synthesized ZnO nanoparticles. The results revealed the synthesis of spherical nanoparticles coated with protein molecules which served as stabilizing agents. Investigations on the role of fungal extracellular proteins in the synthesis of nanoparticles indicated that the process is nonenzymatic but involves amino acids present in the protein chains.

Keywords Biomimetics · ZnO nanoparticles · Rhizosphere · Soil fungi · Metal tolerance · *Aspergillus*

Introduction

Nature is considered as a school for material science and its associated disciplines such as chemistry, biology, physics, or engineering (Bensaude-Vincent et al. 2002). An assortment of biological entities serves as the fundamental base for solving a variety of challenges in the field of architecture, aerodynamics, and mechanical engineering, as well as in material science (Fratzl 2007). Biology is considered as the master of so-called bottom-up fabrication which includes building up nanostructures starting from basic atoms or molecules (Naik and Stone 2005). Biological systems serve as prominent source of inspiration due to their remarkable variety of complex structures and functions which confer a huge impact on material science since several decades. Some examples of natural amalgams include crustacean's carapaces, mollusk shells, bone, and tooth tissues in vertebrates (Sanchez et al. 2005). A number of single-celled organisms also produce inorganic materials of nanometer range intra- and/or extracellularly. Common examples include magnetotactic bacteria which synthesize magnetite (Lovley et al. 1987); diatoms which synthesize siliceous materials (Kröger et al. 1999), S-layer forming bacteria (Pum and Sleytr 1999), etc. These structures are highly controlled, range from macroscopic to nanometer scale, and result in intricate architectures that provide multifunctional properties.

Taking inspiration from these natural biological systems, recently, biologists were able to develop an alternative strategy for nanoparticle synthesis using microorganisms. A landmark study by Klaus et al. (1999) established an interface between material science and biological systems. They reported the synthesis of crystalline silver nanoparticles of well-defined composition and shapes using *Pseudomonas stutzeri* isolated from a silver mine. The nanoparticles were

N. Jain · A. Bhargava · J. Panwar (✉)
Centre for Biotechnology, Department of Biological Sciences,
Birla Institute of Technology and Science,
Pilani, India
e-mail: drjitendrapanwar@yahoo.co.in

J. C. Tarafdar · S. K. Singh
Central Arid Zone Research Institute,
Jodhpur, India

observed on the surface of bacterium with sizes ranging from a few to 200 nm. A similar approach used by Nangia et al. (2009) demonstrated the intracellular synthesis of gold nanoparticles by *Stenotrophomonas maltophilia* isolated from soil samples of the Singhbhum gold mines, India. The study also proposed a mechanism of production which suggests the involvement of a NADPH-dependent enzyme that reduces Au^{3+} to Au^0 through an electron shuttle pathway for the synthesis of gold nanoparticles. In contrast, Prasad and Jha (2009) hypothesized the role of pH-dependent membrane-localized oxidoreductases for synthesis of ZnO nanoparticles in their study using *Lactobacillus sporogenes*. Labrenz et al. (2000) had shown the synthesis of spherical aggregates of sphalerite particles (2–5 nm) within the natural biofilms dominated by sulfate-reducing bacteria of the family *Desulfobacteraceae*. These observations lead to the emergence of a new branch of science called “Biomimetics,” which is defined as application of biological principles for material synthesis (Sarıkaya et al. 2003). Biomimetics is sometimes also coined as material bionics or bio-inspired material research (Fratzl 2007). The subject is not just a consequence of an observation of naturally occurring structures but also involves complex biochemical and physiological processes which are still not properly understood and might play an important role in the formation of structures in nanometer range.

Microorganisms present in metal-rich regions exhibit high metal resistance which is mostly due to absorption or adsorption of metals and their chelation by extra- or intracellular proteins (Pócsi 2011). It is well demonstrated that high metal stress may lead to affect the various microbial activities (Giller et al. 2009). Well-adapted microbes isolated from native metal-rich soil conditions can be a better source for bio-inspired synthesis of metal nanoparticles as an indigenous microbial ecotype results from the long-term adaptation to soil with extreme properties.

The sophistication and success of natural bottom-up fabrication processes inspired the present attempt of creating a biomimetic approach using a zinc metal-tolerant fungal isolate for the synthesis of zinc oxide (ZnO) nanoparticles. ZnO is a unique material that exhibits semiconducting, piezoelectric, and pyroelectric properties and has versatile applications in transparent electronics, ultraviolet (UV) light emitters, piezoelectric devices, chemical sensors, spin electronics, personal care products, and coating and paints (Wang 2004; Wahab et al. 2010; Akhtar et al. 2011). In biological systems, various forms of zinc have significant roles in a wide variety of metabolic processes such as carbohydrate, lipid, nucleic acid, and protein synthesis as well as their degradation. In addition, zinc is an integral component of many enzyme structures and is the only metal to be represented in all six enzyme classes viz. oxidoreductases, transferases, hydrolases, lyases, isomerases, and ligases (Auld 2001).

With the objective of developing an eco-friendly and low-cost protocol for synthesis of ZnO nanoparticles, the present study investigates the relationship between the metal tolerance ability of soil fungi and their potential towards synthesis of ZnO nanoparticles. The study was carried out in two phases. The first was to investigate the metal tolerance profile of fungi isolated from a zinc-rich region and the second was to examine the potential of a fungal isolate exhibiting maximum metal tolerance towards synthesizing ZnO nanoparticles. Attempts were also made to investigate the role of fungal extracellular proteins in the nanoparticle synthesis process. The present study shows that the fungus *Aspergillus aeneus* isolate NJP12 exhibited maximum metal tolerance as well as that it has the potential of ZnO nanoparticle synthesis. We substantiate that our eclectic approach promises to yield revolutionary advances in the development of a low-cost, clean, and environmentally benign protocol for fabrication of metal nanoparticles. To the best of our knowledge, the present study is the first report on synthesis of ZnO nanoparticles using a fungus as a model organism.

Materials and methods

Sampling site and isolation of fungi

Soil samples were collected in February and July 2009 from the Zawar mines area (24°21' N, 73°44' E) which is located on the bank of the River Tiri, about 38 km south of Udaipur town in the Aravalli hill regions of Rajasthan, India. The mine is historically well known for zinc deposits and is owned by Hindustan Zinc Limited, Udaipur, India, the world's second largest producer of zinc. The deposits have estimated ore reserves of 28.7 million tons (Mt) containing 4.76% zinc with an annual ore production capacity of 1.20 Mt as in the year 2010 (<http://www.hzlandia.com/zawar.aspx>). The region has a seasonally tropical climate and minimum and maximum temperatures of 5.0 and 38.4 °C, respectively, with a total annual rainfall of 637 mm as recorded by the Agro-Meteorological Department, Udaipur, India.

A total of five sampling sites have been studied. Soil samples were collected from naturally grown plants (*Calotropis procera* and *Tephrosia purpurea*) from three spatially separated points at each site, with a minimum of 5-m distance between each sampling point. The upper layers of soil were scrapped off to remove foreign particles and litter before taking samples. Soil firmly adhering to the root, designated as rhizosphere soil, was collected by brushing the root part of the plants. The soil samples were stored in self-sealing polyethylene bags, placed in an insulated carrier for transport, and then immediately refrigerated at 4 °C. Before processing (in most cases within 2 days), soil samples were passed through a sieve (2-mm mesh

size) to remove stones and coarse roots. A subsample of each soil was air dried and used for estimation of various physico-chemical properties. In order to rule out the possibility of seasonal variation, an additional set of soil samples was also collected after a 6-month interval from the subsets of sites and processed separately.

Isolation of fungi was carried out for each sampling site by plating the inoculum on Martin Rose Bengal Agar medium (HiMedia, Mumbai, India, pH 7.2) after serial dilutions of pooled soil samples (homogenized soils of three samples taken per sampling site) during both first and second collection of soils. Bacterial contamination was inhibited by supplementing the medium with chloramphenicol (Sigma-Aldrich, St. Louis, MO, USA) at a concentration of $10 \mu\text{g mL}^{-1}$ after autoclaving. Petri plates were incubated at 28°C for 4 days under dark conditions. Individual fungal colonies were selected and further purified by repeated subculturing on Potato Dextrose Agar (PDA) medium (HiMedia, Mumbai, India, pH 5.6). Preliminary identification of fungal isolates was performed on the basis of morphological characteristics.

Physicochemical characteristics of rhizosphere soil

Rhizospheric soil samples were analyzed for pH and electrical conductivity (EC) on an 1:2.5 soil/water suspension using digital pH and EC meter, respectively. Organic carbon was estimated by the method of Walkley and Black (1934) using 1.0 N potassium dichromate for titration and 0.5 N ferrous ammonium sulfate for back titration. Available phosphorus (Olsen P) in soil samples was determined by chlorostannous-reduced molybdophosphoric blue color method (Olsen et al. 1954) after extraction with 0.5 M sodium bicarbonate for 30 min. Available N, K, and micronutrients (Cu, Fe, Pb, and Zn) in soil samples were estimated as described by Jackson (1967).

Molecular characterization of fungal isolates

Liquid cultures of fungal isolates were prepared using 25 mL of mineralic Czapek's Dox Broth medium (HiMedia, Mumbai, India, pH 7.3) in 100-mL Erlenmeyer flasks to obtain fresh mycelia for DNA extraction. Separation of mycelia was carried out by centrifugation at 8,000 rpm at 4°C for 10 min. The obtained mycelia were mechanically crushed in liquid nitrogen. The genomic DNA was extracted from 100 mg of fungal mycelia using HiPurA Plant Genomic DNA Miniprep Purification Kit (HiMedia, Mumbai, India) according to the manufacturer's instructions.

Polymerase chain reaction (PCR) primers namely ITS-1 (5' TCC GTA GGT GAA CCT GCG G 3') and ITS-4 (5' TCC TCC GCT TAT TGA TAT GC 3') developed by White et al. (1990) were used to amplify the internal transcribed space (ITS) region of ribosomal DNA, which encompasses the 5.8S gene

and the ITS1 and ITS2 regions. PCR amplification was performed in a total volume of 50 μL containing: 1 U Taq DNA polymerase (Promega, Mannheim, Germany), 2.5 mM MgCl_2 , 160 μM dNTP mix (MBI Fermentas, St. Leon-Rot, Germany), 50 pmol of each of the ITS-1 and ITS-4 primers (Sigma-Aldrich, St. Louis, MO, USA), and 50 ng genomic DNA in dH_2O . The reactions were performed in a gradient thermal cycler with the following conditions: 1 min denaturation at 95°C , 30 s annealing at 50°C , 90 s elongation at 72°C , for 34 cycles with a final elongation step of 72°C for 10 min.

Amplified ITS regions were sequenced with an ABI Prism DNA sequencer (Applied Biosystems, Carlsbad, CA, USA) using either the ITS-1 and/or the ITS-4 primer for DNA labeling by the BigDye terminator method (Applied Biosystems, Foster City, CA, USA). The sequenced data obtained from the ITS-4 primer were inversed using Gene Doc software (Nicholas et al. 1997) and clubbed with the sequence data obtained with the ITS-1 primer, to obtain the complete sequence of the ITS region. Comparison of nucleotide sequences was performed using the Basic Local Alignment Search Tool (BLAST) network services of the National Centre for Biotechnology Information (NCBI) database (<http://www.ncbi.nlm.nih.gov>). Molecular characterization of fungal isolates was done on the basis of similarity with the best aligned sequence of BLAST search.

Accession numbers

The ITS1-5.8S-ITS2 gene complex sequences of obtained fungal isolates were submitted to the GenBank database of NCBI with the following accession numbers: HM222932–34, HQ710532–46, and JF298825 (Table 2). *A. aeneus* isolate NJP12 has been deposited in the Microbial Type Culture Collection and Gene Bank at the Institute of Microbial Technology, Chandigarh, India with the MTCC number 10830 and available at public domain.

Metal tolerance profiles of fungal isolates

A maximum tolerable concentration (MTC) assay was performed to determine the zinc metal tolerance ability of fungal isolates. The experimental plates were prepared by supplementing PDA medium with varying amounts of zinc sulfate to obtain final concentrations of Zn^{+2} ions in the ranges of 200, 400, 800, 1,600, and 3,200 $\mu\text{g mL}^{-1}$. Plates without Zn^{+2} ions were used as control. Each plate was subdivided into four equal sectors and an inoculum of test fungi (10^6 cfu mL^{-1}) was spotted on the media surface. After inoculation, the plates were incubated at 28°C for 4 days under dark conditions to examine the fungal growth. The experiment was done in triplicate. The maximum concentration of Zn^{+2} ions in the medium which allowed the growth of a fungus was taken as MTC.

Extracellular biosynthesis of zinc oxide nanoparticles

The fungal isolate showing the highest MTC value was selected for extracellular synthesis of ZnO nanoparticles. For this, the fungal isolate was maintained at 28 °C by regular subculturing on fresh PDA medium slants. The stock culture (4 days old) was inoculated in 100 mL of MGY medium (0.3% malt extract, 1.0% glucose, 0.3% yeast extract, 0.5% peptone; pH 7.0) in 250-mL Erlenmeyer flasks. Inoculated flasks were incubated at 28 °C for 72 h on a rotary shaker (150 rpm) under dark conditions. Fungal mycelia were separated from the culture medium by centrifugation (8,000 rpm, 10 min, and 4 °C) and washed thrice with sterile water in order to remove all traces of media. Typically, 10 g of biomass (fresh weight) was resuspended in 100 mL of sterile deionized Milli-Q water and further incubated for 72 h under the same conditions as described above. After incubation, biomass was separated by filtration using Whatman filter paper no. 1 (Whatman Inc., Florham Park, NJ, USA), and the fungal cell-free filtrate containing extracellular secretions was collected. For synthesis of nanoparticles, aqueous zinc acetate solution (Sigma-Aldrich, St. Louis, MO, USA) at a final concentration of 1.0 mM was added to flasks containing 100 mL of fungal cell-free filtrate and incubated for 72 h under the same conditions as described above. Controls containing fungal cell-free filtrate (without zinc acetate; positive control) and pure zinc acetate solution (without fungal cell-free filtrate; negative control) were also run simultaneously along with experimental flasks in three replicates. Viability of the fungal cells after incubation in Milli-Q water for 72 h was also checked. For this, the fungal mycelia were inoculated on fresh PDA plates in triplicate and incubated for 4 days at 28 °C in dark conditions.

Characterization of zinc oxide nanoparticles

Synthesis of nanoparticles was monitored using UV–visible spectroscopy by sampling of aliquots (1 mL) at different time intervals. Absorption spectra were measured using a Jasco V-630 UV–visible spectrophotometer (Jasco Corporation, Tokyo, Japan) operated within the range of 200–900 nm at a resolution of 1 nm.

For Fourier transform infrared (FTIR) spectroscopy measurements, biotransformed products present in the fungal cell-free filtrate were freeze-dried and diluted with potassium bromide in a ratio of 1:100. FTIR spectra of samples were recorded on a Shimadzu IR Prestige-21 FTIR spectrometer (Shimadzu, Nakagyo-ku, Japan) with a diffuse reflectance mode (DRS-8000) attachment (Shimadzu Corporation, Nakagyo-ku, Japan). All measurements were carried out in the range of wavenumbers 400–4,000 cm^{-1} at a resolution of 4 cm^{-1} .

Samples for transmission electron microscopy (TEM) were prepared by drop coating the as-synthesized nanoparticle

solution onto carbon-coated copper grids. After about a minute, extra solution was removed using a blotting paper, and the grids were kept in a vacuum desiccator, prior to measurement. TEM micrographs were taken by analyzing the prepared grids on a Hitachi H-7650 TEM instrument (Hitachi High-Technologies Corporation, Tokyo, Japan) at an acceleration voltage of 100 kV. Energy dispersive spectroscopy (EDS) of drop coated grids of samples was carried out using Bruker attachment (Bruker AXS Ltd., Coventry, UK) with TEM instrument.

X-ray diffraction (XRD) measurements of the freeze-dried samples were carried out using a Rigaku MiniFlex II Benchtop XRD System (Rigaku Company, Texas, USA) operated at a voltage of 20 kV and current of 15 mA with CuK_α radiation. Phase analysis was carried out by comparing the calculated values of interplanar spacing and corresponding intensities of diffraction peaks with theoretical values from the Powder Diffraction File database (PCPDF-WIN; JCPDS-ICDD 2008).

Analysis of fungal cell-free filtrate

UV–visible spectra of fungal cell-free filtrates were recorded to confirm the presence of proteins. The total protein concentration in the fungal cell-free filtrates was determined by the method of Lowry et al. (1951) using bovine serum albumin as standard. To investigate the involvement of proteins in nanoparticle synthesis, proteins were precipitated from the fungal cell-free filtrates using the standard trichloroacetic acid method (Simpson 2004). One hundred milliliters of supernatant fraction without proteins was used for synthesis of ZnO nanoparticles under the same conditions as mentioned above. In order to understand the nature of proteins present in the fungal cell-free filtrate, a separate experiment was performed. Briefly, 100 mL of fungal cell-free filtrate was boiled in a water bath for 20 min, cooled, and used for synthesis of ZnO nanoparticles under the same conditions as described above. A flask containing 100 mL of fungal cell-free filtrate without heat treatment was used as control. Systematic monitoring of pH

Table 1 Physicochemical characteristics of rhizospheric soil samples collected from the Zawar mines, Udaipur, India

Parameter	Value
pH	7.72±0.02
EC	0.48±0.01 dS m^{-1}
Available N	63.39±4.5 mg kg^{-1}
Available P	30.0±1.2 mg kg^{-1}
Available K	150.0±10.9 mg kg^{-1}
Zn	121.0±14.3 mg kg^{-1}
Cu	0.02±0.001 mg kg^{-1}
Fe	10.0±0.61 mg kg^{-1}
Pb	3.4±0.08 mg kg^{-1}

n=30; 15 samples from the first and 15 samples from the second collection of soils

Table 2 Sequence analysis of fungal isolates with their reference organisms

Fungus	Isolate	Accession number	Sequence length			BLAST results				
			ITS1	5.8S	ITS2	Maximum score	Query coverage (%)	Maximum identity (%)	Closest match	Reference
<i>Aspergillus aeneus</i>	NJP12	HM222934	152	157	164	891	100	99	EF652474 ^T	Peterson (2008)
<i>Aspergillus flavus</i>	NJP08	HM222933	180	158	168	1,037	100	99	AF027863 ^T	Haugland et al. (2004)
<i>Aspergillus niger</i>	NJP09	HQ710538	185	157	170	1,018	94	99	EF661191 ^T	Peterson (2008)
<i>Aspergillus ochraceus</i>	NJP04	HQ710534	169	157	100 ^a	837	98	100	AY373856 ^T	Haugland et al. (2004)
<i>Aspergillus ochraceus</i>	NJP13	HQ710541	142 ^a	157	176	957	100	100	EF661419 ^T	Peterson (2008)
<i>Aspergillus oryzae</i>	NJP01	HQ710532	181	157	170	1,061	98	99	AY373857 ^T	Haugland et al. (2004)
<i>Aspergillus oryzae</i>	NJP06	HQ710536	181	157	170	1,053	98	99	AY373857 ^T	Haugland et al. (2004)
<i>Aspergillus oryzae</i>	NJP10	HQ710539	183	157	169	1,051	99	99	AY373857 ^T	Haugland et al. (2004)
<i>Aspergillus oryzae</i>	NJP15	HQ710543	181	157	168	1,064	100	99	AY373857 ^T	Haugland et al. (2004)
<i>Aspergillus oryzae</i>	NJP18	HQ710546	181	157	170	1,077	99	99	AY373857 ^T	Haugland et al. (2004)
<i>Aspergillus</i> sp.	NJP02	HM222932	154	156	170	983	99	99	EF652481	Peterson (2008)
<i>Cladosporium</i> sp.	NJP19	JF298825	154	157	152	952	97	99	FJ936159	Schubert et al. (2009)
<i>Cladosporium</i> sp.	NJP05	HQ710535	157	157	148 ^a	845	99	95	EU167574	Simon et al. (2009)
<i>Eupenicillium javanicum</i>	NJP17	HQ710545	175	157	169	931	94	97	GU981613 ^T	Houbraken et al. (2011)
<i>Mortierella</i> sp.	NJP14	HQ710542	173	158	258	1,000	100	96	HQ630345	Nagy et al. (2011)
<i>Penicillium commune</i>	NJP11	HQ710540	175	156	168	1,051	100	99	AY373905 ^T	Haugland et al. (2004)
<i>Penicillium commune</i>	NJP07	HQ710537	175	156	168	1,029	100	99	AY373905 ^T	Haugland et al. (2004)
<i>Penicillium commune</i>	NJP03	HQ710533	175	156	169	1,044	100	99	AY373905 ^T	Haugland et al. (2004)
<i>Penicillium crustosum</i>	NJP16	HQ710544	175	156	168	1,035	99	99	AY373907 ^T	Haugland et al. (2004)

^a Incomplete ITS sequence^T Type strain

of the reaction medium was also observed at different time intervals to understand the chemical nature of system.

(in total 11 isolates from 7 different species representing 58% of all isolated species) was observed.

Results

Physicochemical characteristics of rhizosphere soil

Physicochemical characteristics of rhizospheric soils of naturally grown plants collected from the Zawar mines, Udaipur, India are shown in Table 1. In general, the soil was slightly alkaline in nature. Nitrogen, phosphorus, and potassium contents of the soil samples were calculated as 63.4, 30.0, and 150.0 mg kg⁻¹, respectively. Determination of micronutrient content revealed the abundance of Zn in the rhizosphere soil with a mean value of 121.0 mg kg⁻¹ along with moderate concentrations of Cu, Fe, and Pb.

Identification of fungal isolates

Preliminary identification of fungi was performed on the basis of morphological parameters such as color, spore shape, arrangement, and hyphal branching pattern after staining with cotton blue. Molecular characterization of fungi was carried out using the universal primers for the amplification of the internal transcribed spacer (ITS) regions of the fungal rRNA operon as described by White et al. (1990).

A total of 19 fungal isolates were observed on the basis of distinct morphological parameters. However, molecular characterization has revealed the presence of fungal isolates of 13 different species from five different genera (Table 2). All detected fungal isolates belong to the phylum *Ascomycota* except *Mortierella* sp. isolate NJP14 which belongs to the phylum *Zygomycota*. An abundance of the genus *Aspergillus*

Metal tolerance profile of fungal isolates

All the 19 fungal isolates were subjected to a screening for metal tolerance towards zinc, and the results were expressed in terms of MTC. A higher proportion (90%) of fungal isolates showed significant tolerance with a varying degree of magnitude. The genus *Aspergillus* exhibited a more prominent level of zinc metal tolerance as compared to other fungal isolates. It is evident from the results that *A. aeneus* isolate NJP12 and *Aspergillus* sp. isolate NJP02 have tremendous zinc metal tolerances with a MTC value of 2,800 and 2,400 µg mL⁻¹ respectively (Fig. 1). Due to its maximum MTC value, *A. aeneus* isolate NJP12 was selected for further studies on extracellular synthesis of ZnO nanoparticles.

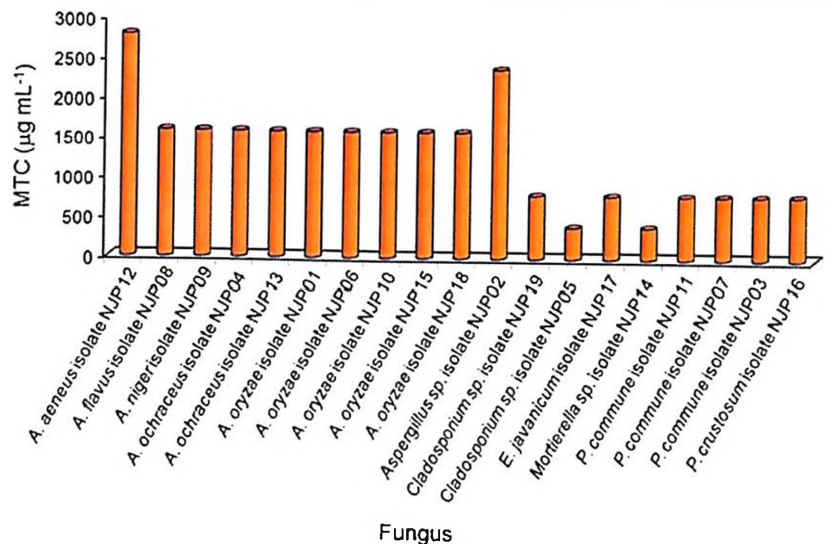
Extracellular biosynthesis of zinc oxide nanoparticles

The extracellular synthesis of ZnO nanoparticles was carried out by exposure of a precursor salt solution (Zn⁺² ions; 0.65 mM) to fungal cell-free filtrate obtained by incubating the fungus NJP12 in an aqueous solution. The viability experiment results showed that fungal cells were viable till the end of reaction (72 h).

Characterization of zinc oxide nanoparticles

UV–visible spectroscopy was used to monitor the synthesis of ZnO nanoparticles. Figure 2a showed a gradual increase in absorbance at ca. 375 nm with respect to time of reaction, representing the synthesis of ZnO nanoparticles. At initial time intervals (0, 6, 12, and 24 h), synthesis was relatively slow, but at later time intervals (36, 48, and 72 h), significant

Fig. 1 Zinc metal tolerance profile of fungal isolates



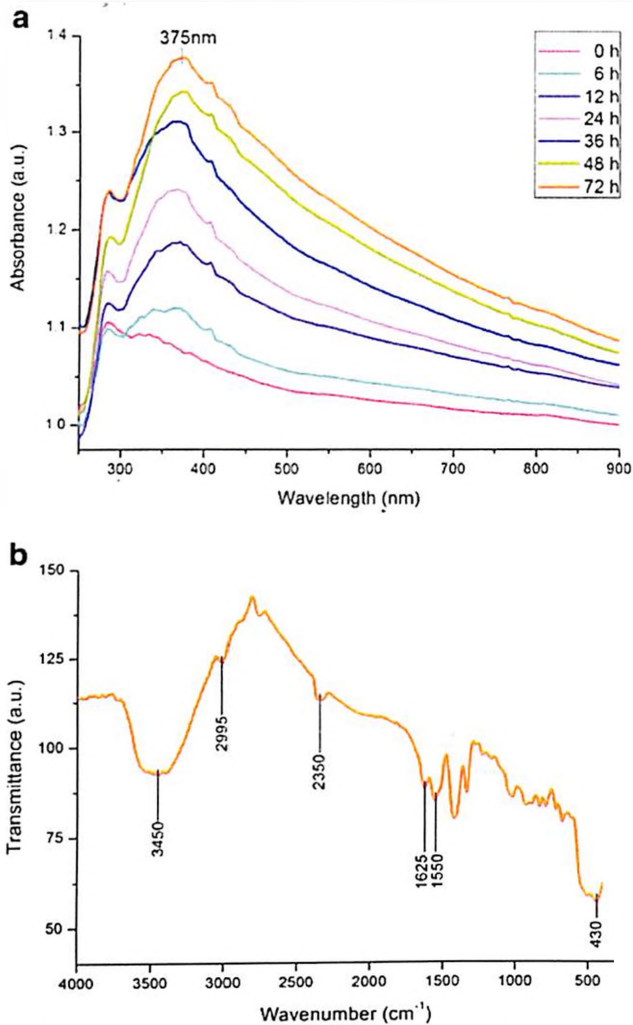


Fig. 2 a UV–visible spectrum representing gradual synthesis of ZnO nanoparticles with respect to time. The absorbance is expressed in terms of arbitrary unit (a.u.) b FTIR spectrum of freeze-dried samples of ZnO nanoparticles. The absorbance is expressed in terms of arbitrary unit (a.u.)

changes in the magnitude of absorbance were observed. pH values of 7.4 and 7.8 were observed at the start (0 h) and end (72 h) of the reaction, respectively. This minimal change in pH makes the present protocol “eco-friendly” which is highly advantageous as compared to chemical synthesis protocols which show high pH variations (Sharma et al. 2009). The stability of the nanoparticle solution stored at room temperature in dark conditions for more than 3 months after completion of reaction was determined by UV–visible spectroscopy measurements.

FTIR analysis of freeze-dried samples showed an intense band in the vicinity of wavenumbers 400–600 cm^{-1} that centered around wavenumber 430 cm^{-1} and is attributed to ZnO vibrations (Fig. 2b; Becheri et al. 2008). The presence of bands at wavenumbers 1,625 and 1,550 cm^{-1}

corresponds to the bending vibrations of the amide I and amide II of proteins, respectively (Ahmad et al. 2003). The band at wavenumber 3,450 cm^{-1} has been reported to occur due to stretching vibrations of amide I superimposed on the side of hydroxyl group band (Saeeda et al. 2009). Moreover, the bands at wavenumbers 2,995 and 2,350 cm^{-1} (Fig. 2b) are due to the stretching vibrations of amide II and presence of atmospheric CO_2 , respectively (Saeeda et al. 2009; Becheri et al. 2008).

TEM measurements of the samples were performed to visualize the size and morphology of ZnO nanoparticles. A TEM micrograph (Fig. 3a) showed the well-distributed spherical ZnO nanoparticles surrounded by a thin protein layer. The size distribution analysis showed that the particle size ranged from 100–140 nm. EDS analysis of drop coated grids of samples was performed to determine the elemental composition of nanoparticles (Fig. 3b). EDS spectra showed strong peaks at 0.5, 1.1, 8.6, and 9.5 keV which are due to O K_{α} , Zn L_{α} , Zn K_{α} , and Zn K_{β} , respectively (Bahadur et al. 2008). The atomic percent values of Zn and O observed were 0.38 and 0.18, respectively. Other peaks observed for copper and carbon were due to the supporting carbon-coated copper grid used for sample preparation.

Figure 4 shows the XRD pattern of synthesized ZnO nanoparticles. Analysis of XRD spectra showed well-defined peaks at 2θ values of 32.05°, 34.69°, and 36.53° which correspond to (100), (002), and (101) planes of ZnO, respectively. The observed lattice values were in agreement with the hexagonal phase of ZnO (PCPDF-WIN; JCPDS-ICDD 2008).

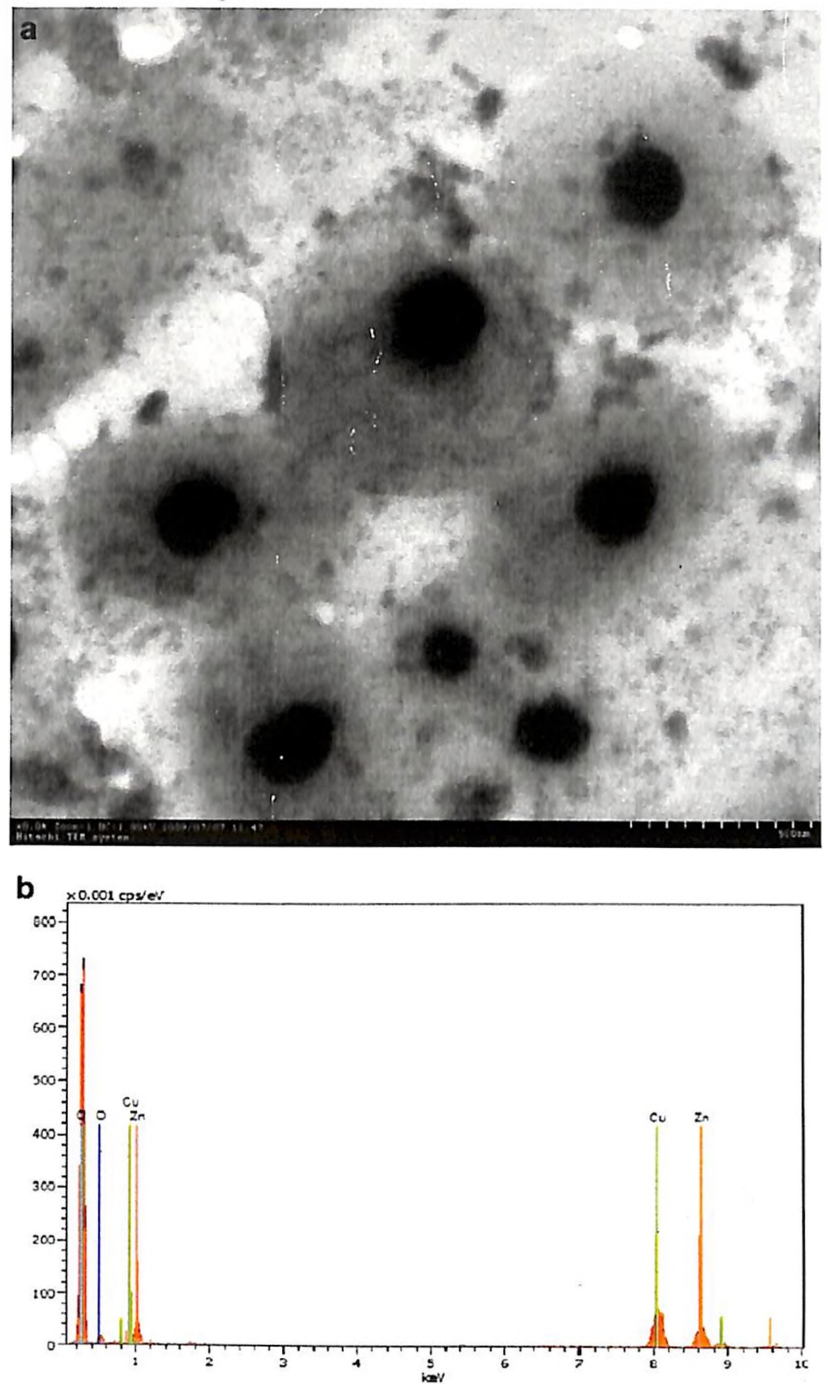
Analysis of fungal cell-free filtrate

An absorption peak at ca. 280 nm observed in the UV–visible spectrum of fungal cell-free filtrate indicated the presence of proteins in the fungal cell-free filtrate (not shown). Concentration of protein in the fungal cell-free filtrates was determined as $458.2 \pm 2.8 \mu\text{g mL}^{-1}$. Incubation of precursor zinc ions with a supernatant fraction without proteins (obtained by protein precipitation) showed no evidence of ZnO nanoparticle synthesis which indicates that proteins play an important role in the synthesis of ZnO nanoparticles. An experiment with incubation of denatured (heat treated) and native (untreated) proteins with precursor zinc ions resulted in the synthesis of ZnO nanoparticles in both cases. Interestingly, comparison of absorbance spectra indicates a higher rate of reaction in case of denatured proteins as compared to native proteins (Fig. 5).

Discussion

The present study approaches to establish the relationship between metal tolerance ability of a soil fungus and its

Fig. 3 a TEM micrograph showing the spherical shape of ZnO nanoparticles b EDS spectrum representing the elemental composition of ZnO nanoparticles



potential for synthesis of ZnO nanoparticles. The Zawar mines, Udaipur, India were opted as sample collection site which is a natural zinc metal-enriched region. The rhizospheric soil samples of naturally growing plants were used as a source for isolation of fungi. It is well known that rhizosphere regions exhibit high microbial populations due to presence of more organic contents (Griffiths et al. 2001). Analysis of physicochemical properties of soil samples is a prerequisite for a better understanding of microbial

population. Physicochemical analysis of collected rhizospheric soil samples showed the alkaline nature of the soil with abundant zinc concentration.

Selection of well-adapted fungi was performed by investigating the metal tolerance profile of obtained fungal isolates. Due to its high zinc metal tolerance ability, *A. aeneus* isolate NJP12 was selected for further studies on synthesis of ZnO nanoparticles. The protocol employed for nanoparticle synthesis was similar to our earlier study for synthesis

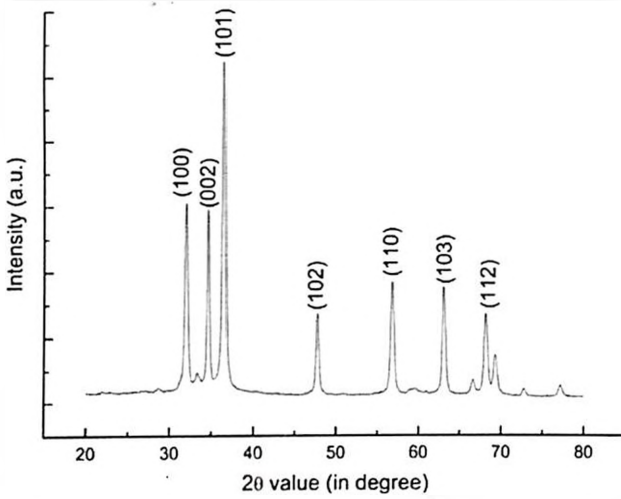


Fig. 4 XRD spectrum of ZnO nanoparticles with Bragg's diffraction values shown in *parentheses*. The absorbance is expressed in terms of arbitrary unit (a.u.)

of silver nanoparticles which involves exposure of precursor ions to proteins present in the fungal cell-free filtrate (Jain et al. 2011). The absorption maxima at 375 nm observed in UV–visible spectra of forming ZnO nanoparticles (Fig. 2a) can be attributed to a band-to-band emission of ZnO which represents a direct band gap of 3.3 eV (Prasad et al. 2006; Sridevi and Rajendran 2009). The presence of a broad absorption peak in FTIR spectra (Fig. 2b) indicates the synthesis of ZnO nanoparticles of varying sizes. TEM analysis of drop coated grids further confirmed the presence of ZnO nanoparticles of various sizes with proteins as capping molecule on individual ZnO nanoparticles (Fig. 3a). Previous studies on biosynthesis of silver nanoparticles using

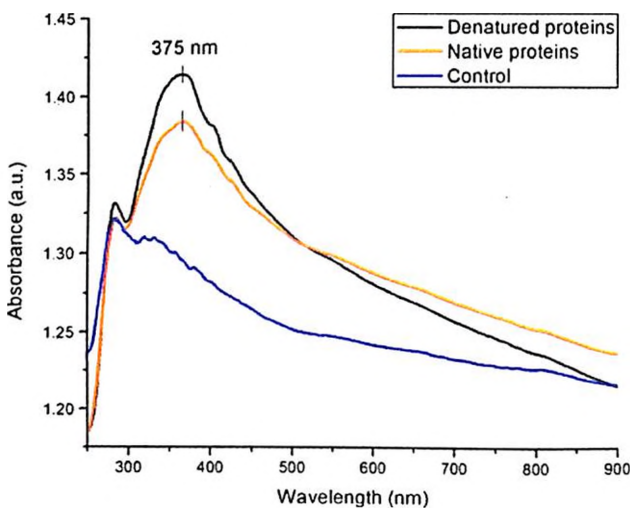


Fig. 5 Effect of denaturation of proteins on synthesis of ZnO nanoparticles. The absorbance is expressed in terms of arbitrary unit (a.u.)

fungal cell-free filtrate also showed the presence of proteins on the surface of individual nanoparticles which conferred their stability (Balaji et al. 2009; Jain et al. 2011). EDS and XRD analysis in this study further confirmed the composition and crystallinity of the obtained ZnO nanoparticles, respectively (Fig. 3b and 4).

The understanding of a plausible mechanism involved in biosynthesis of nanoparticles is a key step to scale-up the process for mass level production. Few studies have shown the role of proteins present in fungal cell-free filtrates for nanoparticle synthesis. In a previous study, we demonstrated the presence of two proteins (32 and 35 kDa) in a fungal cell-free filtrate and their involvement in silver nanoparticle synthesis (Jain et al. 2011). Ahmad et al. (2003) proposed the involvement of NADH-dependent reductases present in a cell-free filtrate of *Fusarium oxysporum* for the synthesis of silver nanoparticles. In the present study, efforts were made to investigate the role of fungal extracellular proteins towards synthesis of ZnO nanoparticles. No evidence of nanoparticle synthesis was observed in reaction medium lacking proteins which further confirm the involvement of proteins in the synthesis of ZnO nanoparticles.

Denaturation of proteins present in the fungal cell-free filtrate was performed to understand the nature of proteins. Synthesis of ZnO nanoparticles by both denatured (heat treated) and native (untreated) proteins revealed that the native form of proteins is not mandatory for nanoparticle synthesis. It can also be inferred that the nanoparticle synthesis process is nonenzymatic as the activity of enzymes depends on their structure which changes during denaturation. Hence, with the current experimental evidences, it can be concluded that the synthesis process depends on interaction with amino acids present in the proteins. The high reaction rate for ZnO nanoparticles synthesis as observed by absorption spectra (Fig. 5) in case of denatured (heat treated) proteins further validates that the rate of synthesis depends on the interaction of amino acids with metal (Zn^{+2}) ions. Heating of protein molecules results in the breakdown of hydrogen bonds which allows dismantling the hydrophobic core which in turn enhances the interactions between amino acids and zinc ions. Our results substantiate the previous reports which demonstrate that interactions between amino acids and metal ions are responsible for synthesis of metal nanoparticles (Xie et al. 2007). However, the present findings are in disagreement with earlier reports which hypothesize the involvement of enzymes in the synthesis of nanoparticles (Ahmad et al. 2003; Nangia et al. 2009). To the best of our knowledge, this is the first study which proposes the involvement of simply amino acids in the fungal-mediated synthesis of metal nanoparticles. Further investigations including isolation, purification, and characterization of proteins along with their possible interactions with zinc ions are in progress in our laboratory.

Acknowledgments This research was supported by the National Agricultural Innovation Project (NAIP), Indian Council of Agricultural Research (ICAR) through its sub-project entitled “Nano-technology for Enhanced Utilization of Native Phosphorus by Plants and Higher Moisture Retention in Arid Soils” Code number “NAIP/C4/C-2032.” Facilities provided by Electron Microscopy & Nanoscience Laboratory, Punjab Agricultural University, Ludhiana are gratefully acknowledged. Navin Jain thanks the Council of Scientific and Industrial Research, Government of India for providing a research fellowship. The authors are thankful to Dr. Ursula Kües for constructive and meaningful suggestions, which helped us to improve the manuscript up to the desired level.

Conflicts of interest The authors declare that they have no conflicts of interest.

References

- Auld DS (2001) Zinc coordination sphere in biochemical zinc sites. *BioMetals* 14:271–313
- Ahmad A, Mukherjee P, Senapati S, Mandal D, Khan MI, Kumar R, Sastry M (2003) Extracellular biosynthesis of silver nanoparticles using the fungus *Fusarium oxysporum*. *Colloids Surf B* 28:313–318
- Akhtar MS, Ameen S, Ansari SA, Yang O (2011) Synthesis and characterization of ZnO nanorods and balls nanomaterials for dye sensitized solar cells. *J Nanoeng Nanomanuf* 1:71–76
- Bahadur H, Srivastava AK, Sharma RK, Chandra S (2008) Morphologies of sol–gel derived thin films of ZnO using different precursor materials and their nanostructures. *Nano Res Lett* 2:469–475
- Balaji DS, Basavaraja S, Deshpande R, Mahesh DB, Prabhakar BK, Venkataraman A (2009) Extracellular biosynthesis of functionalized silver nanoparticles by strains of *Cladosporium cladosporioides* fungus. *Colloids Surf B* 68:88–92
- Becheri A, Dürr M, Lo Nostro P, Baglioni P (2008) Synthesis and characterization of zinc oxide nanoparticles: application to textiles as UV-absorbers. *J Nanopart Res* 10:679–689
- Bensaude-Vincent B, Arribart H, Bouligand Y, Sanchez C (2002) Chemists and the school of nature. *New J Chem* 26:1–5
- Fratzl P (2007) Biomimetic materials research: what can we really learn from nature’s structural materials? *J R Soc Interface* 4: 637–642
- Giller KE, Witter E, McGrath SP (2009) Heavy metals and soil microbes. *Soil Biol Biochem* 41:2031–2037
- Griffiths BS, Ritz K, Wheatley R, Kuan HL, Boag B, Christensen S, Ekelund F, Sørensen SJ, Muller S, Bloem J (2001) An examination of the biodiversity-ecosystem function relationship in arable soil microbial communities. *Soil Biol Biochem* 33:1713–1722
- Haugland R, Varma M, Wymer L, Vesper S (2004) Quantitative PCR analysis of selected *Aspergillus*, *Penicillium* and *Paecilomyces* species. *Syst Appl Microbiol* 27:198–210
- Houbraken J, Lopez-Quintero CA, Frisvad JC, Boekhout T, Theelen B, Franco-Molano AE, Samson RA (2011) *Penicillium araracuarense* sp. nov., *Penicillium elleniae* sp. nov., *Penicillium penaroenjense* sp. nov., *Penicillium vanderhammenii* sp. nov. and *Penicillium wotroi* sp. nov., isolated from leaf litter. *Int J Syst Evol Microbiol* 61:1462–1475
- Jackson ML (1967) Soil chemical analysis. Prentice Hall of Indian Private Limited, New Delhi
- Jain N, Bhargava A, Majumdar S, Tarafdar JC, Panwar J (2011) Extracellular biosynthesis and characterization of silver nanoparticles using *Aspergillus flavus* NJP08: a mechanism perspective. *Nanoscale* 3:635–641
- JCPDS-ICDD (2008) PCPDF WIN, File no. 36-1451. JCPDS-ICDD, Swarthmore
- Klaus T, Joergers R, Olsson E, Granqvist CG (1999) Silver-based crystalline nanoparticles microbially fabricated. *Proc Natl Acad Sci USA* 96:13611–13614
- Kröger N, Deutzmann R, Sumper M (1999) Polycationic peptides from diatom biosilica that direct silica nanosphere formation. *Science* 286:1129–1132
- Labrenz M, Druschel GK, Thomsen-Ebert T, Gilbert B, Welch SA, Kemner KM, Logan GA, Summons RE, Stasio GD, Bond PL, Lai B, Kelly SD, Banfield JF (2000) Formation of sphalerite (ZnS) deposits in natural biofilms of sulfate-reducing bacteria. *Science* 290:1744–1747
- Lovley DR, Stolz JF, Nord GL, Phillips EJP (1987) Anaerobic production of magnetite by a dissimilatory iron-reducing microorganism. *Nature* 330:252–254
- Lowry OH, Rosebrough NJ, Farr AL, Randall RJ (1951) Protein measurement with the Folin phenol reagent. *J Biol Chem* 193:265–275
- Nagy LG, Petkovits T, Kovács GM, Voigt K, Vágvölgyi C, Papp T (2011) Where is the unseen fungal diversity hidden? A study of *Mortierella* reveals a large contribution of reference collections to the identification of fungal environmental sequences. *New Phytol* 191:789–794
- Naik RR, Stone MO (2005) Integrating biomimetics. *Mater Today* 8:18–26
- Nangia Y, Wangoo N, Sharma S, Wu JS, Dravid V, Shekhawat GS, Suri CR (2009) Facile biosynthesis of phosphate capped gold nanoparticles by a bacterial isolate *Stenotrophomonas maltophilia*. *Appl Phys Lett* 94:233901–233903
- Nicholas KB, Nicholas HB, Deerfield DW (1997) GeneDoc: analysis and visualization of genetic variation. *EMBNEW.NEWS* 4:14
- Olsen SR, Cole CV, Watanabe FS, Dean LA (1954) Estimation of available phosphorus in soils by extraction with sodium bicarbonate. Circular 939 US Department of Agriculture, Washington DC, USA
- Peterson SW (2008) Phylogenetic analysis of *Aspergillus* species using DNA sequences from four loci. *Mycologia* 100:205–226
- Pócsi I (2011) Toxic metal/metalloid tolerance in fungi—a biotechnology-oriented approach. In: Bánfalvi G (ed) Cellular effects of heavy metals. Springer, Dordrecht, pp 31–58
- Prasad K, Jha AK (2009) ZnO nanoparticles: synthesis and adsorption study. *Nat Sci* 1:129–135
- Prasad V, D’Souza C, Yadav D, Shaikh AJ, Vigneshwaran N (2006) Spectroscopic characterization of zinc oxide nanorods synthesized by solid-state reaction. *Spectrochim Acta Part A* 65:173–178
- Pum D, Sleytr UB (1999) The application of bacterial S-layers in molecular nanotechnology. *Trends Biotechnol* 17:8–12
- Saeeda A, Iqbal M, Zafar SI (2009) Immobilization of *Trichoderma viride* for enhanced methylene blue biosorption: batch and column studies. *J Hazard Mater* 168:406–415
- Sarikaya M, Tamerler C, Jen AKY, Schulten K, Baneyx F (2003) Molecular biomimetics: nanotechnology through biology. *Nat Mater* 2:577–585
- Sanchez C, Arribart H, Giraud Guille M (2005) Biomimeticism and bioinspiration as tools for the design of innovative materials and systems. *Nat Mater* 4:277–288
- Schubert K, Greslebin A, Groenewald JZ, Crous PW (2009) New foliicolous species of *Cladosporium* from South America. *Persoonia* 22:111–122
- Sharma VK, Yugard RA, Lin Y (2009) Silver nanoparticles: green synthesis and their antimicrobial activities. *Adv Colloid Interface Sci* 145:83–96
- Simon UK, Groenewald JZ, Crous PW (2009) *Cymadothea trifolii*, an obligate biotrophic leaf parasite of *Trifolium*, belongs to *Mycosphaerellaceae* as shown by nuclear ribosomal DNA analyses. *Persoonia* 22:49–55

- Simpson RJ (2004) Purifying proteins for proteomics: a laboratory manual. Cold Spring Harbor Laboratory Press, Cold Spring Harbor
- Sridevi D, Rajendran KV (2009) Synthesis and optical characteristics of ZnO nanocrystals. *Bull Mater Sci* 32:165–168
- Wahab R, Kim YS, Lee DS, Seo JM, Shin HS (2010) Controlled synthesis of zinc oxide nanoneedles and their transformation to microflowers. *Sci Adv Mater* 2:35–42
- Walkley AJ, Black IA (1934) Estimation of soil organic carbon by the chromic acid titration method. *Soil Sci* 37:29–38
- Wang ZL (2004) Nanostructures of zinc oxide. *Mater Today* 7:26–33
- White T, Bruns T, Lee S, Taylor J (1990) Amplification and direct sequencing of fungal ribosomal RNA genes for phylogenetics. In: Innis MA, Gelfand DH, Sninsky JJ, White TJ (eds) *PCR protocols: a guide to methods and applications*. Academic, San Diego, pp 315–322
- Xie J, Lee JY, Wang DIC, Ting YP (2007) Silver nanoplates: from biological to biomimetic synthesis. *ACS Nano* 1:429–439



Enhanced photocatalytic degradation of methylene blue using biologically synthesized “protein-capped” ZnO nanoparticles

Navin Jain, Aprit Bhargava, Jitendra Panwar*

Centre for Biotechnology, Department of Biological Sciences, Birla Institute of Technology and Science, Pilani 333 031, India

HIGHLIGHTS

- One pot synthesis & surface modification of ZnO nanoparticles at ambient conditions.
- Simple, low-cost & eco-friendly protocol with potential for mass scale production.
- Superior photocatalytic performance of protein-capped ZnO nanoparticles.
- Surface proteins act as an effectual host and facilitates dye absorption.
- Low recombination rate of the e^-/h^+ pairs.

ARTICLE INFO

Article history:

Received 3 October 2013

Received in revised form 26 November 2013

Accepted 28 November 2013

Available online 4 December 2013

Keywords:

Photocatalysis

Aspergillus

Protein-capped

ZnO nanoparticles

Methylene blue

ABSTRACT

Using the extracellular fungal proteins, a low cost and eco-friendly synthesis of zinc oxide nanoparticles has been demonstrated in aqueous solvent system. The obtained nanoparticles were characterized by transmission electron microscopy (TEM), energy dispersive X-ray spectroscopy (EDS), UV-visible spectroscopy and powder X-ray diffraction (XRD) measurements. The as-synthesized particles were quasi-spherical, symmetrical, polydisperse and well distributed without any aggregation with size predominantly ranging between 80 and 120 nm. Photoluminescence (PL) and fourier-transform infrared (FT-IR) spectroscopy studies revealed that nanoparticles were individually coated with protein molecules that may act as stabilizing agents. Photocatalytic studies for the degradation of methylene blue dye under UV irradiation revealed extremely high photocatalytic activity of protein-capped ZnO nanoparticles (nearly 90% degradation in 30 min) which clearly outperformed commercial bare ZnO nanoparticles (nearly 40% degradation in 30 min) under the same conditions. The remarkable photocatalytic performance originated mainly due to the presence of surface proteins which act as an effectual host for methylene blue dye and facilitates absorption of dye along with low recombination rate of the e^-/h^+ pairs. The low cost, simplicity and eco-friendly nature of the present protocol for “one-pot” synthesis and modification of ZnO nanoparticles could be extended to synthesize other metal nanoparticles thus expanding its applicability in various fields.

© 2013 Elsevier B.V. All rights reserved.

1. Introduction

Industrial effluents have long been a major concern among the environmental protection issues and considered as a potential threat. Organic dyes have received particular attention as prominent environmental contaminants owing to their non-biodegradability and carcinogenic effects on humans. Moreover, they drastically affect the nature of water, inhibit sunlight penetration and reduce photosynthesis resulting in severe toxicity to aquatic creatures [1,2]. Semiconductor based photocatalytic oxidation

have attracted great attention for solving many current environmental issues especially removal of dye pollutants from water [3–6]. The approach is highly advantageous as it does not yield toxic intermediate products, making it suitable for cleaning polluted water bodies that contains low to medium concentration of contaminants. Various semiconductors such as TiO_2 ($E_g = 3.2$ eV), ZnO ($E_g = 3.4$ eV), ZnS ($E_g = 3.6$ eV), WO_3 ($E_g = 2.8$ eV) and $SrTiO_3$ ($E_g = 3.2$ eV) have been widely implemented as promising candidates for the photocatalytic degradation reactions.

Although TiO_2 has been universally recognized as the most efficient photocatalyst, recent reports have highlighted the effectiveness of ZnO in removing organic compounds from water matrices [7,8]. In particular, ZnO in nanoparticle regime has appeared to

* Corresponding author. Tel.: +91 1596 515250; fax: +91 1596 244183.

E-mail address: dtjitendrapanwar@yahoo.co.in (J. Panwar).

be more efficient catalyst than TiO_2 as it exhibits high reaction and mineralization rates with efficient generation of H_2O_2 . Furthermore, ZnO nanoparticles possess more numbers of active sites with high surface reactivity than bulk ZnO [9–11]. A plethora of studies have successfully demonstrated ZnO nanoparticles as a potential photocatalyst for degradation of broad range of organic pollutants. For instance, Ameen et al. formulated an effective ZnO/polyaniline nanocomposite for the photocatalytic degradation of methylene blue dye [12]. Another study by Rahman et al. reported rapid and effective photocatalytic degradation of rhodamine B dye by ZnO nanoparticles [13]. Similarly, Kansal et al. studied the de-coloration of pararosaniline chloride and alizarin red S dyes using ZnO nanostructure as a photocatalyst under UV irradiation [14,15]. Although ZnO nanoparticles have been targeted as a potential photocatalyst against various organic pollutants, they possess the critical drawbacks of photocorrosion, quick recombination of charge carriers and poor response to visible light which significantly hampers its photocatalytic efficiency and stability limiting its practical applications [16,17]. Thus, substantial efforts have been devoted to overcome these problems such as depositing metals or coatings on ZnO surface, doping/hybridization with metals or metal ions and combining ZnO with another semiconductor [18–21]. Modifications of ZnO nanoparticles surface with organic molecules such as oleic acid and polydimethylsiloxane have improved the photocatalytic performance to a remarkable extent [22–24]. Surface modifications with proteins, organic molecules of the biological origin, can act as potential alternative because of high dye adsorption rate along with low recombination rate of the e^-/h^+ pairs. However, the use of protein molecules for surface modification of ZnO photocatalyst is still unexplored.

With the overgrowing demand of ZnO nanoparticles for photocatalysis and other applications, there is a constant need to develop new synthesis methods which can confer controlled synthesis. Moreover, development of new strategies that could surpass conventional approaches especially in terms of speed and cost is a major concern. Numerous methods based on both “top-down” and “bottom-up” synthesis approaches are well documented. Conventional methods include sol-gel [25], hydrothermal growth [26], template-assisted growth [27], wet chemical synthesis [28,29] and flame spray pyrolysis [30]. These methods involve several processing steps, expensive equipments, toxic chemicals and drastic reaction conditions (pH, temperature, pressure etc.). In addition, such methods often yield particles in non-polar organic solutions and generate several by-products which are hazardous to the environment. Moreover, achieving controlled growth is often inconvenient which is vital to attain desirable size, shape and monodispersity [9,31]. So, there is a substantial need to develop an eco-friendly and low cost protocol for nanoparticle synthesis.

In recent years, taking inspiration from biological systems, researchers have been able to develop an alternative approach for nanoparticle synthesis using microorganisms. A plethora of microorganisms ranging from bacteria, virus and fungi have been well documented for nanoparticle synthesis [32–34]. However, most of the studies have been carried out on identification of microorganisms as possible alternative; finding a microbe capable of efficient synthesis of nanoparticles of various sizes, shapes and compositions along with high yield is a challenging task and is not given much attention yet. Recently, our research group has demonstrated the utilization of well adapted metal tolerant fungal isolates for synthesis of metal nanoparticles [35]. The rationale of using fungi as model organism is its economical cultivation, ease in handling and secretion of enormous amount of proteins [36]. Furthermore, extracellular protein-mediated synthesis of nanoparticles allows controlled manipulation of the method which is enviable to achieve high efficiency and desirable properties. Continuing our previous efforts [35,36], attempts were performed to synthesize

size ZnO nanoparticles using a well-adapted metal tolerant fungus *Aspergillus* sp. NJP02 and characterized using various standard analytical techniques. The photocatalytic performance of ZnO nanoparticles towards the degradation of methylene blue dye as representative organic pollutant has also been investigated. Owing to the presence of surface proteins, ZnO nanoparticles exhibited excellent enhancement of photocatalysis towards methylene blue dye suggesting their potential applications in catalysis, waste water treatment etc.

2. Materials and methods

2.1. Materials

High purity zinc acetate (Merck Inc.) was used for the biological synthesis of ZnO nanoparticles. Methylene blue dye and bare zinc oxide nanoparticles were purchased from Sigma Aldrich (India). The morphology of ZnO particles have been claimed to be spherical with a density of 1.7 ± 0.1 g/mL at 25 °C. The particle size has been reported to be <100 nm as calculated by dynamic light scattering (DLS) measurements and an average particle size of <35 nm measured using an aerodynamic particle sizer (APS) spectrometer. All other reagents used were of analytical grade and procured from Merck Inc. unless otherwise stated. De-ionized water was used throughout the experimental work. Components of culture medium routinely used for the growth and maintenance of the fungus were purchased from HiMedia laboratories (India) and used as per the manufacturer's instructions.

2.2. Fungal isolate and growth conditions

A soil-borne zinc tolerant fungus *Aspergillus* sp. NJP02 was used in the present study. The complete details of isolation and molecular characterization of the fungal isolate can be obtained from our previous study [35]. The fungal isolate has been submitted to the Microbial Type Culture Collection (MTCC), Institute of Microbial Technology, India and is available at public domain. The nucleotide sequence of the internal transcribed spacer (ITS) regions of ribosomal gene is also available at National Centre of Biological Information database (Accession number HM222932).

Stock cultures of the fungal isolate were maintained on Potato dextrose agar (PDA) medium slants at 28 °C under dark conditions. The periodic sub-culturing of the fungal isolate was performed at a regular interval of 4 weeks to replenish the nutrients.

2.3. Extracellular synthesis of ZnO nanoparticles

The experimental fungal isolate was grown in 100 mL of sterile MGY medium (0.3% malt extract, 1.0% glucose, 0.3% yeast extract, 0.5% peptone; pH 7.0) in a 250 mL Erlenmeyer flask with continuous shaking on a rotary shaker (150 rpm) at 28 °C for 72 h under dark conditions. After the incubation period, fungal biomass was separated from the culture medium by centrifugation (8000 rpm, 10 min, 4 °C) and was washed thoroughly (3–4 times) using sterile de-ionized water to remove medium components adhered to the biomass surface. Typically, 10 g (wet weight) of biomass was re-suspended in 100 mL of sterile Milli-Q water and incubated for 72 h in a 250 mL Erlenmeyer flask under the similar conditions described above. Subsequently, fungal biomass was separated by filtration using Whatman filter paper no. 1 and the fungal cell-free filtrate containing secreted extracellular proteins was collected. For the synthesis of nanoparticles, aqueous zinc acetate solution at a final concentration of 1.0 mM was added to 100 mL of fungal cell free filtrate in a 250 mL Erlenmeyer flask and agitated for 72 h under the similar conditions as described above. Controls

containing only fungal cell-free filtrate (without zinc acetate) and pure zinc acetate solution (without fungal cell free filtrate) were also run simultaneously along with experimental flasks in three replicates.

2.4. Characterization of ZnO nanoparticles

Synthesis of nanoparticles was monitored using UV–visible spectroscopy by sampling of aliquots (1 mL) at different time intervals. Absorption spectra were measured using a Jasco V-630 UV–visible spectrophotometer operated within the range of 200–900 nm at a resolution of 1 nm. For fourier transform infrared (FTIR) spectroscopy measurements, the synthesized nanoparticles were freeze-dried and mixed with potassium bromide in a ratio of 1:100. FTIR spectra of samples were recorded on a Shimadzu IR Prestige-21 FTIR spectrometer with a diffuse reflectance mode (DRS-8000) attachment in the range of 400–4000 cm^{-1} at a resolution of 4 cm^{-1} . Photoluminescence (PL) spectroscopy measurements were recorded on a Horiba spectrofluorometer using 90° illuminations with a scanning speed of 100 nm min^{-1} . The excitation and emission slit width values were attuned to 2.5 and 3.0 nm, respectively in order to achieve maximal signal-to-noise ratio.

Samples for transmission electron microscopy (TEM) were prepared by placing a drop of as-synthesized nanoparticle solution on to carbon coated copper grids. The extra solution was removed using an absorbent paper and the grids were kept in a vacuum desiccator, prior to measurement. TEM micrographs were captured by analyzing the prepared grids on a Hitachi H-7650 TEM instrument at an operating voltage of 200 kV. Energy dispersive spectroscopy (EDS) measurements of prepared grids were carried out using a Bruker attachment with TEM instrument. The thickness of protein layer was determined by performing the dynamic light scattering (DLS) measurements of ZnO nanoparticle before and after the incubation with sodium dodecyl sulphate solution in a water bath for 30 min. The method is well-demonstrated to remove the proteins from the nanoparticle surface [36]. DLS measurements were performed on a Malvern Zetasizer Nano-ZS spectrometer. X-ray diffraction (XRD) measurements of the freeze dried samples were carried out using a Rigaku MiniFlex II Bench top XRD System operated at a voltage of 20 kV and current of 15 mA with Cu K α radiation. Phase analysis was performed by comparing the calculated values of inter-planar spacing and corresponding intensities of diffraction peaks with theoretical values from the Powder Diffraction File database (PCPDF-WIN; JCPDS-ICDD 2008).

2.5. Photocatalytic activity of ZnO nanoparticles

The photocatalytic performance of the biologically synthesized protein-capped ZnO nanoparticles and commercially available bare ZnO nanoparticles was compared by measuring the degradation of aqueous methylene blue (MB) solution under UV light irradiation. In a typical photocatalytic experiment, 10 mg of freeze-dried nanoparticles (photocatalyst) were added to 40 mL of aqueous MB solution (10 μM) in a 100 mL glass beaker. The suspension was strongly magnetically stirred in the dark for 60 min to ensure the establishment of adsorption–desorption equilibrium of MB dye on the photocatalyst surfaces. Under ambient conditions and stirring, the beaker was exposed to UV irradiation generated by a high pressure mercury vapor lamp with the predominant wave crest at 365 nm. The distance between the beaker containing suspension and the irradiation source was optimized at 13 cm (data not shown) and kept constant for further studies. During illumination, 1 mL of the suspension was withdrawn periodically and centrifuged to remove the catalyst. UV–visible spectra of the samples were recorded with a Jasco V-630 UV–visible spectrophotometer. Control experiment was repeated without the presence of photocatalyst

in the MB solution. All the recorded spectra were analysed using Spectra Manager software supplied by JASCO Corporation and plotted against the time of UV irradiation. The degree of photocatalytic degradation of MB dye as a function of time was calculated by the following Eq. (1) where C_0 represents the initial concentration of MB solution and C_t stands for the concentration of MB solution after UV irradiation at any time (t). The data were applied to pseudo-first-order kinetics using Eq. (2) given below and a graph was plotted against $\ln([C]_t)$ versus time to calculate rate constant and R^2 values.

$$X = \left[\frac{C_0 - C_t}{C_0} \right] \times 100\% \quad (1)$$

$$\ln([C]_t) = \ln([C]_0) - kt \quad (2)$$

3. Results and discussion

The fungus was isolated as a part of our previous study carried out to investigate the zinc metal tolerance ability and potential of nanoparticle synthesis among fungi [35]. A total of 19 fungal isolates were screened for zinc metal tolerance and the nanoparticle synthesis was carried out using an indigenous protocol established in our laboratory [35,36]. Isolate *Aspergillus* sp. NJP02 demonstrated tremendous ability to tolerate zinc (Zn^{+2} ions in form of zinc sulphate) with metal tolerance concentration of 2400 $\mu\text{g mL}^{-1}$ [35]. Due to its high zinc metal tolerance potential, fungus *Aspergillus* sp. NJP02 was selected for the present study on extracellular synthesis of ZnO nanoparticles.

3.1. Synthesis and characterization of "protein-capped" ZnO nanoparticles

The morphology and particle size of "protein-capped" ZnO nanoparticles was determined using transmission electron microscopy measurements. A representative TEM micrograph (Fig. 1a) shows that the synthesized particles were quasi-spherical, symmetrical, polydisperse and well distributed without any aggregation with size predominantly ranging between 80 and 120 nm (Fig. 1b). The quasi-spherical shape of protein-capped nanoparticles has been found to be consistent with previous observation which postulated that the presence of numerous sulphur containing cysteine residues at various locations of a protein essentially directs the shape of nanoparticles to be quasi-spherical [37]. Owing to the presence of protein capping on the surface, nanoparticles are steadily dispersed in water to form an optically transparent solution (Fig. 1c). The thickness of ZnO core and protein shell were calculated as 5.7 ± 2.6 and 90.5 ± 23.8 nm, respectively based on dynamic light scattering measurements. The elemental composition of nanoparticles has been confirmed using the energy dispersive X-ray spectroscopy measurements. An EDX spectrum (Fig. 1d) recorded from a single nanoparticle depicts three distinct peaks at 1.1 keV, 8.6 keV, and 9.5 keV which could be ascribed to Zn L α , Zn K α , and Zn K β , respectively [25]. Additional peaks observed for copper and carbon were due to the supporting carbon coated copper grid used for sample preparation.

UV–visible spectroscopy is often employed for the determination of absorption properties of nanoparticles and consistently employed to monitor the nanoparticle synthesis. Fig. 2 represents UV–visible spectra recorded at different time intervals to study the gradual change in light absorption profile of the reaction mixture containing fungal proteins and precursor zinc ions. Emergence of a strong narrow absorption peak with respect to time at ca. 371 nm embodies the gradual synthesis of ZnO nanoparticles with a band gap value of 3.34 eV. The observed absorption maxima can

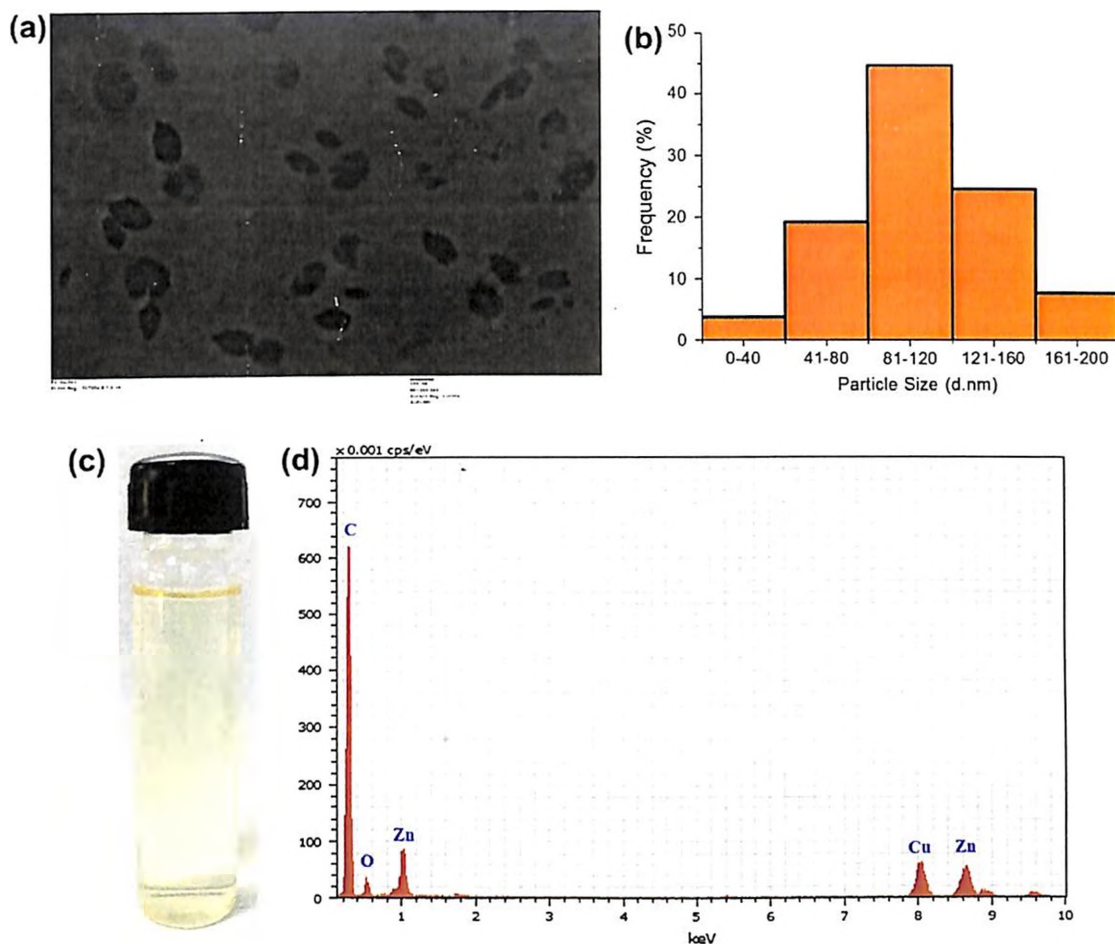


Fig. 1. Characterization of as-synthesized "protein-capped" ZnO nanoparticles. (a) A representative TEM micrograph depicting quasi-spherical shape; (b) histogram showing the size distribution analysis; (c) optically transparent solution under daylight and (d) EDX spectrum showing elemental composition.

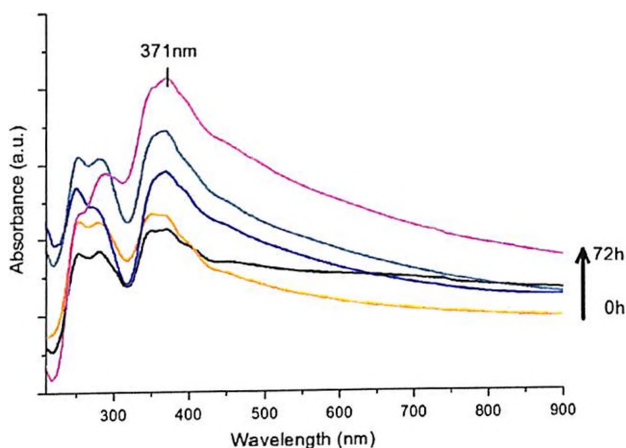


Fig. 2. UV-visible spectra showing gradual synthesis of ZnO nanoparticles with respect to time.

be attributed to the direct band gap of ZnO due to electron transitions from the valence band to the conduction band ($O_{2p} \rightarrow Zn3d$) [10]. At initial time intervals (0 and 12 h), synthesis was relatively slow but at later time intervals (36, 48 and 72 h) significant changes in the magnitude of absorbance values was observed. Additionally, another peak at 280 nm confirmed the presence of proteins in the reaction mixture, which is characteristic to

aromatic amino acids present in the proteins. The crystalline nature and phase purity of the synthesized ZnO nanoparticles were evaluated using X-ray diffraction (XRD) measurements. XRD spectrum (Fig. 3) exhibited well-defined peaks at 2θ values of 31.83° , 34.50° , 36.32° and 47.62° corresponds to (100), (002), (101) and (102) planes of ZnO, respectively. The recorded XRD pattern was perfectly indexed with Joint Committee on Powder Diffraction Standard (JCPDS) card number 36-1451, confirming the existence of typical wurtzite crystal structure of ZnO nanoparticles. Noticeably, diffraction peaks related to any other phase of ZnO or impurities were not observed, which indicated the high purity of the synthesized ZnO nanoparticles.

In order to confirm the presence of protein molecules on the surface of as-synthesized protein-capped ZnO nanoparticles, the intrinsic fluorescence measurements were recorded. The nanoparticle suspension was excited at a wavelength of 280 nm and fluorescence emission spectrum was recorded between 300 and 400 nm (Fig. 4a). A distinct emission peak at 340 nm was observed which arises due to the presence of tyrosine residues in the capping proteins [35,38]. Furthermore, when excited with 325 nm wavelength, a distinct emission peak at 520 nm was observed which could be attributed to strong green emission band of ZnO nanoparticles. It has been well documented that fluorescence measurements of ZnO nanoparticles exhibit a green emission band which attributes to the transition of photo-generated electron from a dark level below the conduction band to a deeply trapped hole, induced by an oxygen vacancy [39,40]. Fig. 4b shows a FTIR

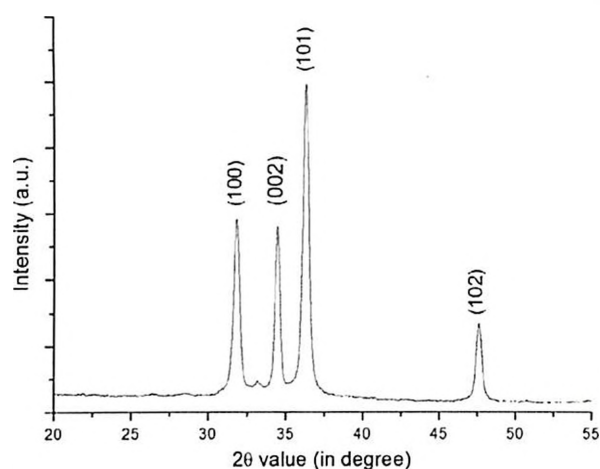


Fig. 3. XRD pattern recorded for freeze-dried ZnO nanoparticles. Bragg's diffraction values are shown in parentheses.

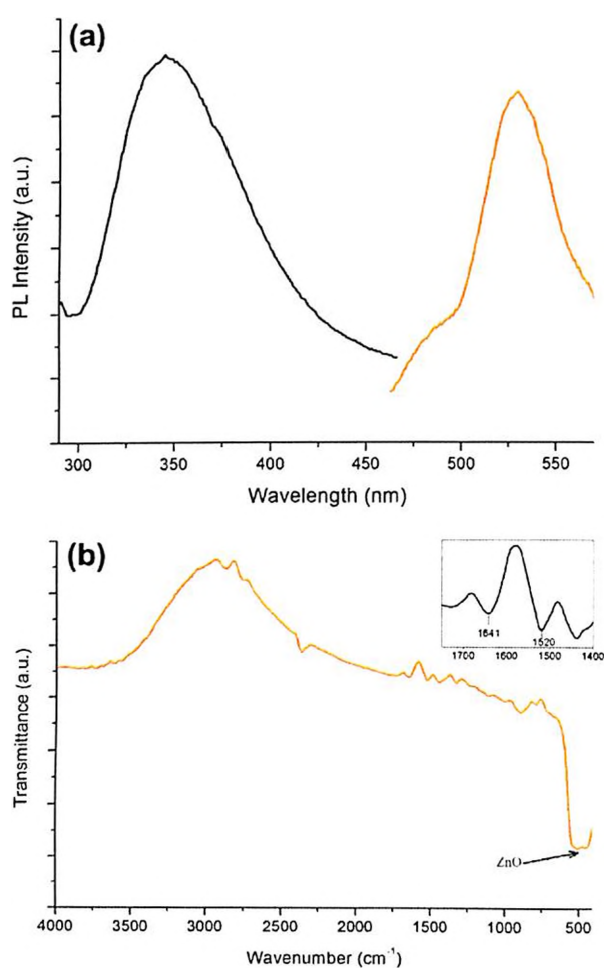


Fig. 4. (a) Intrinsic fluorescence spectra of protein-capped ZnO nanoparticles excited at a wavelength of 280 nm (black) and 325 nm (red) and (b) FTIR spectrum of freeze-dried ZnO nanoparticles with inset showing the amide I band of the proteins. (For interpretation of the references to color in this figure legend, the reader is referred to the web version of this article.)

spectrum with an intense broad band in the vicinity of 400–600 cm⁻¹ and centered around 480 cm⁻¹ which can be associated

with the Zn–O stretching mode [41]. Presence of bands at wavenumbers 1641 and 1520 cm⁻¹ correspond to the bending vibrations of the amide I and amide II of proteins, respectively [42]. These experimental observations indicate successful synthesis of protein-capped ZnO nanoparticles. These results are consistent with the fact that nanoparticles synthesized through the biological approach are often capped with the proteins. For example, studies on noble metal (Au and Ag) nanoparticle synthesis using microorganisms observed the presence of protein molecules on the surface of nanoparticles and have predicted their role in nanoparticle stability [36,43–47]. However, serious efforts have been lacking to attain profound understanding of protein binding to nanoparticles and to determine the plausible phenomenon. Efforts are going on in our laboratory for purification and characterization of capping proteins to resolve structural and functional properties which may contribute significantly in better understanding of protein-nanoparticle interactions [48].

3.2. Photocatalytic degradation of MB dye

The degradation of organic pollutants by ZnO photocatalysts has received immense attention due to environment concerns. To determine the efficacy of the protein-capped ZnO nanoparticles as compared to commercially available bare ZnO nanoparticles, photocatalytic degradation of methylene blue dye was investigated. Methylene blue, globally adopted as a representative organic pollutant of dye waste effluents was used as a probe molecule to evaluate the performance of photocatalysts. The characteristic optical absorption maximum of MB at 665 nm was used to monitor the photocatalytic degradation process. Fig. 5a and b represent the UV–visible absorption spectra of MB dye degradation by protein-capped ZnO nanoparticles and bare ZnO nanoparticles respectively, recorded within the time range of 30 min under UV light irradiation. In both cases, it was clearly evident that on increasing the exposure time, a noticeable decrease in the absorbance intensity of MB dye was observed, which corresponds to the photocatalysis of MB dye. Albeit, the rate of degradation is being slower in case of bare ZnO nanoparticles. A systematic comparison of MB dye degradation in presence of protein-capped and bare ZnO nanoparticles under UV light irradiation is depicted in Fig. 5c which clearly emphasize variation in the relative concentration (C_t/C_0) of MB dye solution. It was observed that the MB concentration was hardly reduced in absence of photocatalyst (control) validating the MB stability under UV light irradiation. The degradation rate of MB by protein-capped ZnO nanoparticles increased significantly with the increase of time period under UV light irradiation as compared to bare ZnO nanoparticles. Moreover, to evaluate the photocatalysis quantitatively, the kinetic parameters (reaction rate, % MB degradation and regression coefficient) of dye degradation were calculated and summarized in Table 1. It can be clearly observed that the reaction rate (k) is dramatically higher for protein capped ZnO nanoparticles ($3.27 \times 10^{-3} \text{ s}^{-1}$) as compared to bare ZnO nanoparticles ($5.99 \times 10^{-3} \text{ s}^{-1}$). Also, more than two fold increase in total amount of MB degradation was observed when protein molecules were present on the surface of ZnO nanoparticle as compared to bare ZnO, indicating protein-capped ZnO nanoparticles as superior photocatalyst.

The rapid degradation of MB dye by protein-capped ZnO nanoparticles in comparison to bare ZnO nanoparticles could be explained as follows. In case of protein-capped ZnO nanoparticles, the proteins may serve as an effectual host for dye adsorption allowing the electron donor and acceptor molecules to come in a close proximity. Indeed, it has been postulated that the presence of amino acids containing aromatic rings can create hydrophobic spaces which can enhance the efficient binding of MB dye molecules [49]. The intimacy between ZnO nanoparticles and MB dye

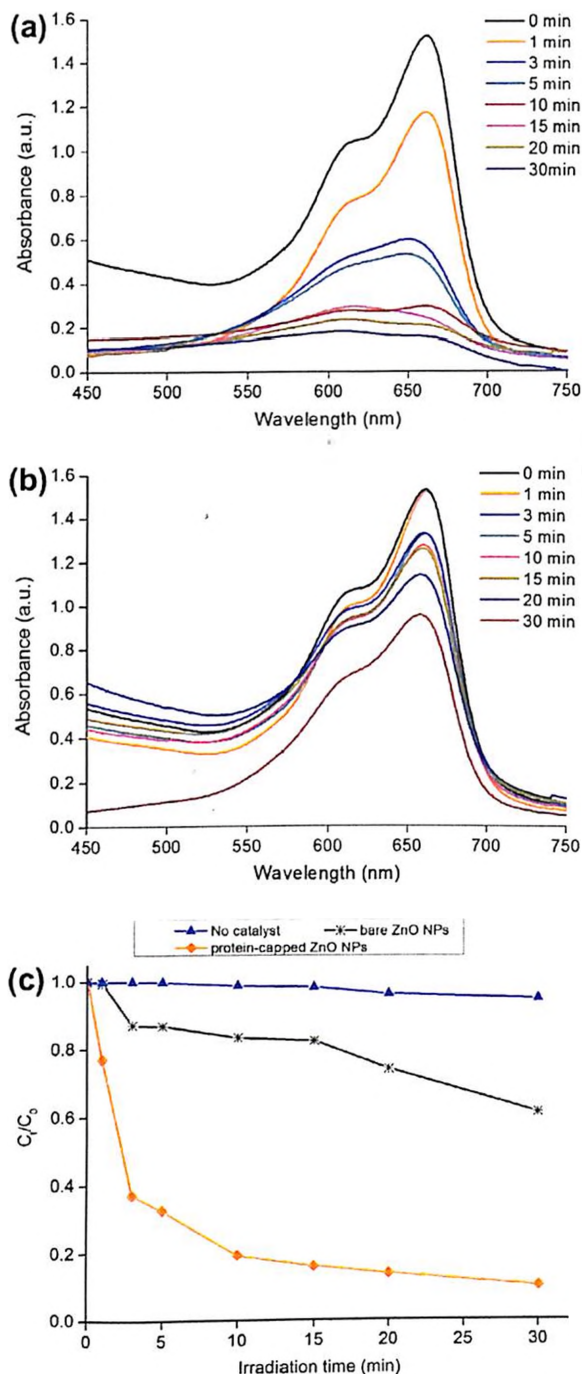


Fig. 5. Photodegradation of methylene blue dye solution under UV-light irradiation by (a) as-prepared protein-capped ZnO nanoparticles; (b) bare ZnO nanoparticles and (c) the extent of MB dye decomposition with respect to time intervals over a period of 30 min UV irradiation (catalyst concentration: 10 mg/mL; initial dye concentration: 10 μ M).

in turn facilitates the electron transfer process and showed enhanced photocatalytic activity. Makhal et al. [37] observed similar phenomenon while studying the photocatalysis of MB dye with chymotrypsin associated ZnS nanoparticles. In contrast, bare ZnO nanoparticles lack the capping molecules which provide efficient binding of MB molecules instigating inaccessibility between MB dye and ZnO nanoparticles. This inaccessibility prevents the excited electrons generated from ZnO nanoparticles to migrate and perform the reduction of MB dye. Moreover, the high surface area

Table 1
Kinetic parameters^a for the photocatalytic degradation of MB dye with protein-capped and bare ZnO nanoparticles catalysts.

Sample	k (s^{-1})	Final MB degradation (A%) (in 30 min)	R^2
Protein-capped ZnO nanoparticles	3.27×10^{-3}	89.68	0.96
Bare ZnO nanoparticles	5.99×10^{-3}	38.08	0.89
No catalyst	7.00×10^{-3}	1.57	0.85

^a Reaction rate (k), percentage of MB degradation (A), and the regression coefficient (R).

attained due to the presence of protein molecules in case of protein-capped ZnO nanoparticles might result in more unsaturated surface coordination sites exposed to the reactants thus facilitating the absorption of MB molecules. It is generally accepted that light absorption, charge transportation and separation on the surface of catalyst are key parameters to determine their photocatalytic performance [50]. Conclusively, the enhanced photocatalytic performance can be attributed to charge transfer from zinc oxide nanoparticles to the attached proteins, which effectively reduce the recombination of electrons and holes, leading to enhancement of photocatalytic properties of protein-capped ZnO nanoparticles. Further studies targeted to decipher the involved mechanism including protein characterization and subsequent protein-nanoparticle interactions are in progress.

4. Conclusions

In the present study, protein-capped ZnO nanoparticles were synthesized using secreted fungal proteins in aqueous system under ambient conditions. The physico-chemical characteristics of the as-synthesized nanoparticles were determined using various standard characterization techniques viz. TEM, UV-visible spectroscopy, XRD. The presence of proteins on the surface of as-synthesized nanoparticles was confirmed with FTIR and PL measurements. The photocatalytic performance of as-synthesized protein-capped ZnO nanoparticles towards MB dye degradation was compared with commercially available bare ZnO nanoparticles. A remarkable increase in photocatalytic activity was observed which mainly originated due to facilitation of dye absorption and low recombination rate of the e^-/h^+ pairs by the protein molecules present on the surface of synthesized ZnO nanoparticles. We believe that low cost, simplicity and eco-friendly nature of the present protocol for "one-pot" synthesis and modification of ZnO nanoparticles could significantly expand its applicability in various fields.

Acknowledgements

This research work was financially supported by the Indian Council of Agricultural Research, Government of India under the National Agricultural Innovation Project scheme (NAIP/C4/C-2032). Facilities provided by Birla Institute of Technology and Science, Pilani are gratefully acknowledged. Navin Jain and Arpit Bhargava are thankful to Council of Scientific and Industrial Research and Indian Council of Agricultural Research, Government of India, respectively for providing research fellowship.

References

- [1] Z. Aksu, *Process Biochem.* 40 (2005) 997–1026.
- [2] A. Srinivasan, T. Viraraghavan, *J. Environ. Manage.* 91 (2010) 1915–1929.
- [3] M.R. Hoffmann, S.T. Martin, W. Choi, D.W. Bahnemann, *Chem. Rev.* 95 (1995) 69–96.

- [4] K. Rajeshwar, N.R. de Tacconi, C.R. Chenthamarakshan, *Chem. Mater.* 13 (2001) 2765–2782.
- [5] S. Cao, K.L. Yeung, J.K. Kwan, P.M. To, S.C. Yu, *Appl. Catal. B: Environ.* 86 (2009) 127–136.
- [6] S. Cao, K.L. Yeung, P.-L. Yue, *Appl. Catal. B: Environ.* 76 (2007) 64–72.
- [7] Y. Li, W. Xie, X. Hu, G. Shen, X. Zhou, Y. Xiang, X. Zhao, P. Fang, *Langmuir* 26 (2009) 591–597.
- [8] S. Sakthivel, B. Neppolian, M. Shankar, B. Arabindoo, M. Palanichamy, V. Murugesan, *Sol. Energy Mater. Sol. Cells* 77 (2003) 65–82.
- [9] Z.L. Wang, *Mater. Today* 7 (2004) 26–33.
- [10] S. Ameen, M.S. Akhtar, M. Nazim, H.-S. Shin, *Mater. Lett.* 96 (2013) 228–232.
- [11] S. Liu, H. Sun, A. Suvorova, S. Wang, *Chem. Eng. J.* 229 (2013) 533–539.
- [12] S. Ameen, M.S. Akhtar, Y.S. Kim, O.-B. Yang, H.-S. Shin, *Colloid Polym. Sci.* 289 (2011) 415–421.
- [13] Q.I. Rahman, M. Ahmad, S.K. Misra, M. Lohani, *Mater. Lett.* 91 (2012) 170–174.
- [14] S. Kumar Kansal, R. Lamba, S. Mehta, A. Umar, *Mater. Lett.* 106 (2013) 385–389.
- [15] S.K. Kansal, A.H. Ali, S. Kapoor, D.W. Bahnemann, *Sep. Purif. Technol.* 80 (2011) 125–130.
- [16] P. Spathis, I. Poulos, *Corros. Sci.* 37 (1995) 673–680.
- [17] H. Zhang, R.L. Zong, Y.F. Zhu, *J. Phys. Chem. C* 113 (2009) 4605–4611.
- [18] J. Bandara, K. Tennakone, P.P.B. Jayatilaka, *Chemosphere* 49 (2002) 439–445.
- [19] J. Lahiri, M. Batzill, *J. Phys. Chem. C* 112 (2008) 4304–4307.
- [20] S. Meng, D. Li, X. Zheng, J. Wang, J. Chen, J. Fang, Y. Shao, X. Fu, *J. Mater. Chem. A* 1 (2013) 2744–2747.
- [21] S.T. Kochuveedu, Y.H. Jang, Y.J. Jang, D.H. Kim, *J. Mater. Chem. A* 1 (2013) 898–905.
- [22] R. Hong, T. Pan, J. Qian, H. Li, *Chem. Eng. J.* 119 (2006) 71–81.
- [23] M.-G. Jeong, H. Seo, K.-D. Kim, D. Kim, Y. Kim, D. Lim, *J. Mater. Sci.* 47 (2012) 5190–5196.
- [24] R. Comparelli, E. Fanizza, M. Curri, P. Cozzoli, G. Mascolo, A. Agostiano, *Appl. Catal. B* 60 (2005) 1–11.
- [25] H. Bahadur, A.K. Srivastava, R.K. Sharma, S. Chandra, *Nanoscale Res. Lett.* 2 (2007) 469–475.
- [26] S. Baruah, J. Dutta, *Sci. Technol. Adv. Mater.* 10 (2009) 013001.
- [27] H.J. Fan, W. Lee, R. Hauschild, M. Alexe, G. Le Rhun, R. Scholz, A. Dadgar, K. Nielsch, H. Kalt, A. Krost, *Small* 2 (2006) 561–568.
- [28] J. Wang, L. Gao, *J. Mater. Chem.* 13 (2003) 2551–2554.
- [29] L. Vayssieres, *Adv. Mater.* 15 (2003) 464–466.
- [30] T. Tani, L. Mädler, S.E. Pratsinis, *J. Nanopart. Res.* 4 (2002) 337–343.
- [31] Z.L. Wang, *J. Phys.: Condens. Matter* 16 (2004) 829–858.
- [32] K.B. Narayanan, N. Sakthivel, *Mater. Lett.* 62 (2008) 4588–4590.
- [33] A.S. Blum, C.M. Soto, C.D. Wilson, J.D. Cole, M. Kim, B. Gnade, A. Chatterji, W.F. Ochoa, T. Lin, J.E. Johnson, *Nano Lett.* 4 (2004) 867–870.
- [34] K.N. Thakkar, S.S. Mhatre, R.Y. Parikh, *Nanomed. Nanotechnol. Biol. Med.* 6 (2010) 257–262.
- [35] N. Jain, A. Bhargava, J.C. Tarafdar, S.K. Singh, J. Panwar, *Appl. Microbiol. Biotechnol.* 97 (2013) 859–869.
- [36] N. Jain, A. Bhargava, S. Majumdar, J.C. Tarafdar, J. Panwar, *Nanoscale* 3 (2011) 635–641.
- [37] A. Makhil, S. Sarkar, S.K. Pal, *Inorg. Chem.* 51 (2012) 10203–10210.
- [38] A. Fatima, Q. Husain, *Int. J. Biol. Macromol.* 41 (2007) 56–63.
- [39] N. Vigneshwaran, S. Kumar, A.A. Kathe, P.V. Varadarajan, V. Prasad, *Nanotechnology* 17 (2006) 5087–5095.
- [40] C.G. Kim, K.W. Sung, T.M. Chung, D.Y. Jung, Y. Kim, *Chem. Commun.* (2003) 2068–2069.
- [41] A. Becheri, M. Dürr, P. Lo Nostro, P. Baglioni, *J. Nanopart. Res.* 10 (2008) 679–689.
- [42] A. Ahmad, S. Senapati, M.I. Khan, R. Kumar, R. Ramani, V. Srinivas, M. Sastry, *Nanotechnology* 14 (2003) 824.
- [43] A. Ahmad, P. Mukherjee, S. Senapati, D. Mandal, M.I. Khan, R. Kumar, M. Sastry, *Colloids Surf. B* 28 (2003) 313–318.
- [44] D.S. Balaji, S. Basavaraja, R. Deshpande, D.B. Mahesh, B.K. Prabhakar, A. Venkataraman, *Colloids Surf. B* 68 (2009) 88–92.
- [45] N. Duran, P. Marcato, M. Duran, A. Yadav, A. Gade, M. Rai, *Appl. Microbiol. Biotechnol.* 90 (2011) 1609–1624.
- [46] S.Y. He, Z.R. Guo, Y. Zhang, S. Zhang, J.W.N. Gu, *Mater. Lett.* 61 (2007) 3984–3987.
- [47] M.I. Husseiny, M.A. El-Aziz, Y. Badr, M.A. Mahmoud, *Spectrochim. Acta Part A* 67 (2007) 1003–1006.
- [48] M. Mahmoudi, I. Lynch, M.R. Eftehadi, M.P. Monopoli, F.B. Bombelli, S. Laurent, *Chem. Rev.* 111 (2011) 5610–5637.
- [49] S. Baruah, S.S. Sinha, B. Ghosh, S.K. Pal, A.K. Raychaudhuri, J. Dutta, *J. Appl. Phys.* 105 (2009) 074308–074313.
- [50] M. Basu, A.K. Sinha, M. Pradhan, S. Sarkar, Y. Negishi, Govind, T. Pal, *Environ. Sci. Technol.* 44 (2010) 6313–6318.